The Geological Society of America
Special Paper 459
2009

Hydrothermal processes above the Yellowstone magma chamber: Large hydrothermal systems and large hydrothermal explosions

Lisa A. Morgan
W.C. Pat Shanks, III
U.S. Geological Survey, M.S. 973, Denver Federal Center, P.O. Box 25046, Denver, Colorado 80225-0046, USA

Kenneth L. Pierce
U.S. Geological Survey, Northern Rocky Mountain Center, P.O. Box 173492, Bozeman, Montana 59717-3492, USA

"The pool was considerably enlarged, its immediate borders swept entirely clear of all movable rock, enough of which had been hurled or forced back to form a ridge from knee to breast high at a distance of from 20 to 50 feet (6 to 15 m) from the ragged edges of the yawning chase." (C.H. Wyman to Colonel Philetus W. Norris, second superintendent of Yellowstone National Park, upon witnessing the 1881 hydrothermal explosion at Excelsior Geyser in the Midway Geyser Basin. From Norris, 1881, p. 60.)

ABSTRACT

Hydrothermal explosions are violent and dramatic events resulting in the rapid ejection of boiling water, steam, mud, and rock fragments from source craters that range from a few meters up to more than 2 km in diameter; associated breccia can be emplaced as much as 3 to 4 km from the largest craters. Hydrothermal explosions occur where shallow interconnected reservoirs of steam- and liquid-saturated fluids with temperatures at or near the boiling curve underlie thermal fields. Sudden reduction in confining pressure causes fluids to flash to steam, resulting in significant expansion, rock fragmentation, and debris ejection.

In Yellowstone, hydrothermal explosions are a potentially significant hazard for visitors and facilities and can damage or even destroy thermal features. The breccia deposits and associated craters formed from hydrothermal explosions are mapped as mostly Holocene (the Mary Bay deposit is older) units throughout Yellowstone National Park (YNP) and are spatially related to within the 0.64-Ma Yellowstone caldera and along the active Norris-Mammoth tectonic corridor.

In Yellowstone, at least 20 large (>100 m in diameter) hydrothermal explosion craters have been identified; the scale of the individual associated events dwarfs similar features in geothermal areas elsewhere in the world. Large hydrothermal explosions in Yellowstone have occurred over the past 16 ka averaging ~1 every 700 yr; similar events are likely in the future. Our studies of large hydrothermal explosion events indicate: (1) none are directly associated with eruptive volcanic or shallow intrusive events; (2) several historical explosions have been triggered by seismic

Morgan, L.A., Shanks, W.C., III, and Pierce, K.L., Hydrothermal processes above the Yellowstone magma chamber: Large hydrothermal systems and large hydrothermal explosions: Geological Society of America Special Paper 459, p. 1–95, doi: 10.1130/2009.2459. For permission to copy, contact editing@geosociety.org.

events; (3) lithic clasts and comingled matrix material that form hydrothermal explosion deposits are extensively altered, indicating that explosions occur in areas subjected to intense hydrothermal processes; (4) many lithic clasts contained in explosion breccia deposits preserve evidence of repeated fracturing and vein-filling; and (5) areal dimensions of many large hydrothermal explosion craters in Yellowstone are similar to those of its active geyser basins and thermal areas. For Yellowstone, our knowledge of hydrothermal craters and ejecta is generally limited to after the Yellowstone Plateau emerged from beneath a late Pleistocene icecap that was roughly a kilometer thick. Large hydrothermal explosions may have occurred earlier as indicated by multiple episodes of cementation and brecciation commonly observed in hydrothermal ejecta clasts.

Critical components for large, explosive hydrothermal systems include a water-saturated system at or near boiling temperatures and an interconnected system of well-developed joints and fractures along which hydrothermal fluids flow. Active deformation of the Yellowstone caldera, active faulting and moderate local seismicity, high heat flow, rapid changes in climate, and regional stresses are factors that have strong influences on the type of hydrothermal system developed. Ascending hydrothermal fluids flow along fractures that have developed in response to active caldera deformation and along edges of low-permeability rhyolitic lava flows. Alteration of the area affected, self-sealing leading to development of a caprock for the hydrothermal system, and dissolution of silica-rich rocks are additional factors that may constrain the distribution and development of hydrothermal fields. A partial low-permeability layer that acts as a cap to the hydrothermal system may produce some over-pressurization, thought to be small in most systems. Any abrupt drop in pressure initiates steam flashing and is rapidly transmitted through interconnected fractures that result in a series of multiple large-scale explosions contributing to the excavation of a larger explosion crater. Similarities between the size and dimensions of large hydrothermal explosion craters and thermal fields in Yellowstone may indicate that catastrophic events which result in large hydrothermal explosions are an end phase in geyser basin evolution.

The Mary Bay hydrothermal explosion crater complex is the largest such complex in Yellowstone, and possibly in the world, with a diameter of 2.8 km in length and 2.4 km in width. It is nested in Mary Bay in the northern basin of Yellowstone Lake, an area of high heat flow and active deformation within the Yellowstone caldera. A sedimentary sequence exposed in wave-cut cliffs between Storm Point and Mary Bay gives insight into the geologic history of the Mary Bay hydrothermal explosion event. The Mary Bay explosion breccia deposits overlie sand above varved lake sediments and are separated locally into an upper and lower unit. The sand unit contains numerous small normal faults and is coextensive with the Mary Bay breccia in its northern extent. This sand may represent deposits of an earthquake-generated wave. Seismicity associated with the earthquake may have triggered the hydrothermal explosion responsible for development of the Mary Bay crater complex. Large hydrothermal explosions are rare events on a human time scale; however, the potential for additional future events of the sort in Yellowstone National Park is not insignificant. Based on the occurrence of large hydrothermal explosion events over the past 16,000 yr, an explosion large enough to create a 100-m-wide crater might be expected every 200 yr.

INTRODUCTION

Regional Geology

The Yellowstone Plateau (Fig. 1) has been the site of three catastrophic caldera-forming eruptions occurring at 2.05, 1.3, and 0.64 Ma (Christiansen, 2001) and constitute some of the largest volcanic eruptions ever documented (Mason et al., 2004). The volcanic field originally covered an area of nearly 17,000 km^2 and has erupted more than 3700 km^3 of pyroclastic flows during the three cataclysmic eruptions (Christiansen, 2001). The magma chamber associated with the most recent 0.64-Ma-caldera-forming eruption is estimated to be ~25,000 km^3 (Miller and Smith, 1999; Husen et al., 2004a), has temperatures that may be in excess of 800 °C (Christiansen, 2001), and generates heat-flow values that are 30 times above average for the northern Rocky Mountains (Fournier et al., 1976; Fournier, 1989; Morgan et al., 1977). Heated from the crystallizing magma chamber below, groundwater in the upper crust circulates along fractures (White, 1957) kept open by high regional seismicity and active deformation of the Yellowstone caldera creating the extensive hydrothermal system host to more than 10,000 active hot springs, geysers, fumeroles, and mud pots (Fig. 2). Hydrothermal activity associated with this heat source has been intense over the past 15 ka (Fournier, 1999). U-series ages of travertine deposits near Mammoth indicate a long span of hydrothermal activity, with deposits dating at 375, 134, 50, 20, and 15 ka to present (Pierce et al., 1991; Sturchio et al., 1992, 1994).

The majority of hydrothermal features, including hydrothermal explosion craters, are clustered within or along the topographic margin of the 45-km × 85-km Yellowstone caldera or along N-S–trending structural zones north and south of the caldera (Figs. 1 and 2). Partially molten magma is present at <10 km depth (Miller and Smith, 1999) and possibly as shallow as 6–8 km (Husen et al., 2004). At Yellowstone, the combined conductive and convective heat flux is 1800 mW/m^2 (Morgan et al., 1977; Husen et al., 2004a); at Mary Bay, heat-flow values were measured at 15,600 mW/m^2 (Morgan et al., 1977). Hydrothermal features also are concentrated along the active Norris-Mammoth tectonic corridor (Sorey and Colvard, 1997) to the north of the caldera and the East Sheridan Fault Zone to the south of the caldera (Christiansen, 2001; Pierce, 1973; Meyer and Locke, 1986; Locke and Meyer, 1994) (Fig. 1).

Hydrothermal Explosions

Hydrothermal explosions are violent events resulting in the rapid ejection of boiling water, steam, mud, and rock fragments and the creation of craters that span areas from a few meters up to more than 2 km in diameter. These explosions occur in near-surface environments in which near-boiling water is present. If an environment of this sort experiences a sudden pressure reduction, the contained fluids may flash to steam (Fig. 3), resulting in a significant volume increase and fragmentation of the enclosing rocks (McKibbin, 1991; Smith and McKibbin, 2000; Browne and Lawless, 2001).

Hydrothermal explosions are a type of nonjuvenile eruption, or "boiling-point eruption" (Mastin, 1995), and are distinguished from phreatic or phreatomagmatic explosions by lack of an associated magmatic eruption (Mastin, 1991). We employ the term "explosion" for these hydrothermal events as opposed to "eruption" to avoid confusion and follow terminology presented in Muffler et al. (1971). These events expel fragments of only nonjuvenile material entrained in a mixture of gas, steam, mud, or liquid water at boiling temperatures and are strictly hydrothermal. Hydrothermal explosions are not volcanic and do not directly involve any magma (cf., Muffler et al., 1968, 1971; Mastin, 1995); however, others have used the term "hydrothermal eruption" rather than "hydrothermal explosion" to describe identical processes in other areas (cf. Nelson and Giles, 1985; Hedenquist and Henley, 1985; Browne and Lawless, 2001).

Hydrothermal explosion craters are common in many volcanic terrains or areas of high heat flow, such as in New Zealand, Indonesia, Japan, Greece, Central America, and the western United States (for example, Inyo Craters [California], Bodie and Steamboat Hot Springs [Nevada]) (White, 1968; Bryan, 2001) where abundant hydrothermal activity occurs (Browne and Lawless, 2001; White, 1967, 1968). In Yellowstone, formation of hydrothermal features is related to convective meteoric-hydrothermal fluid circulation, steam separation associated with the sudden reduction of pressure in the system, and CO_2 accumulation and release above an actively degassing magmatic system (Husen et al., 2004a; Werner and Brantley, 2003; Lowenstern and Hurwitz, 2008).

Yellowstone's hydrothermal explosion craters are roughly circular to oval in plan-view and have steep inner slopes surrounded by an apron of ejected breccia (Fig. 4A). Crater diameters range from <10 m to more than 2 km and depths vary from a few meters to several hundred meters (Fig. 5A), depending roughly on crater diameter and host rock composition (Muffler et al., 1971). Ejecta aprons surrounding large explosion craters are generally as much as tens of meters higher than surrounding topography; associated outer debris aprons generally slope less than 10° and may extend away from crater rims for several kilometers. Smaller craters are common within parent craters. Hydrothermally altered explosion breccia, comprised of silicified multigenerational breccias, and younger craters on main crater floors indicate that hydrothermal activity associated with a particular system can be sustained and episodic; however, the principal explosion events may occur in a matter of minutes to hours (Browne and Lawless, 2001).

Hydrothermal explosions involve significant amounts of water that cause explosion-associated breccia deposits to be rich in mud. Ejected hydrothermal explosion breccia typically is a poorly sorted, matrix-supported, sedimentary breccia composed of hydrothermally altered lithic clasts enclosed in a mud matrix; bedding in the deposit is generally indistinct or absent (Muffler et al., 1971; Mastin, 1995). Most clasts are subangular to subrounded (Fig. 4D) and decrease in size and concentration away from source. Many explosion breccia deposits have a range of clast types. Rock fragment compositions reflect the host rock

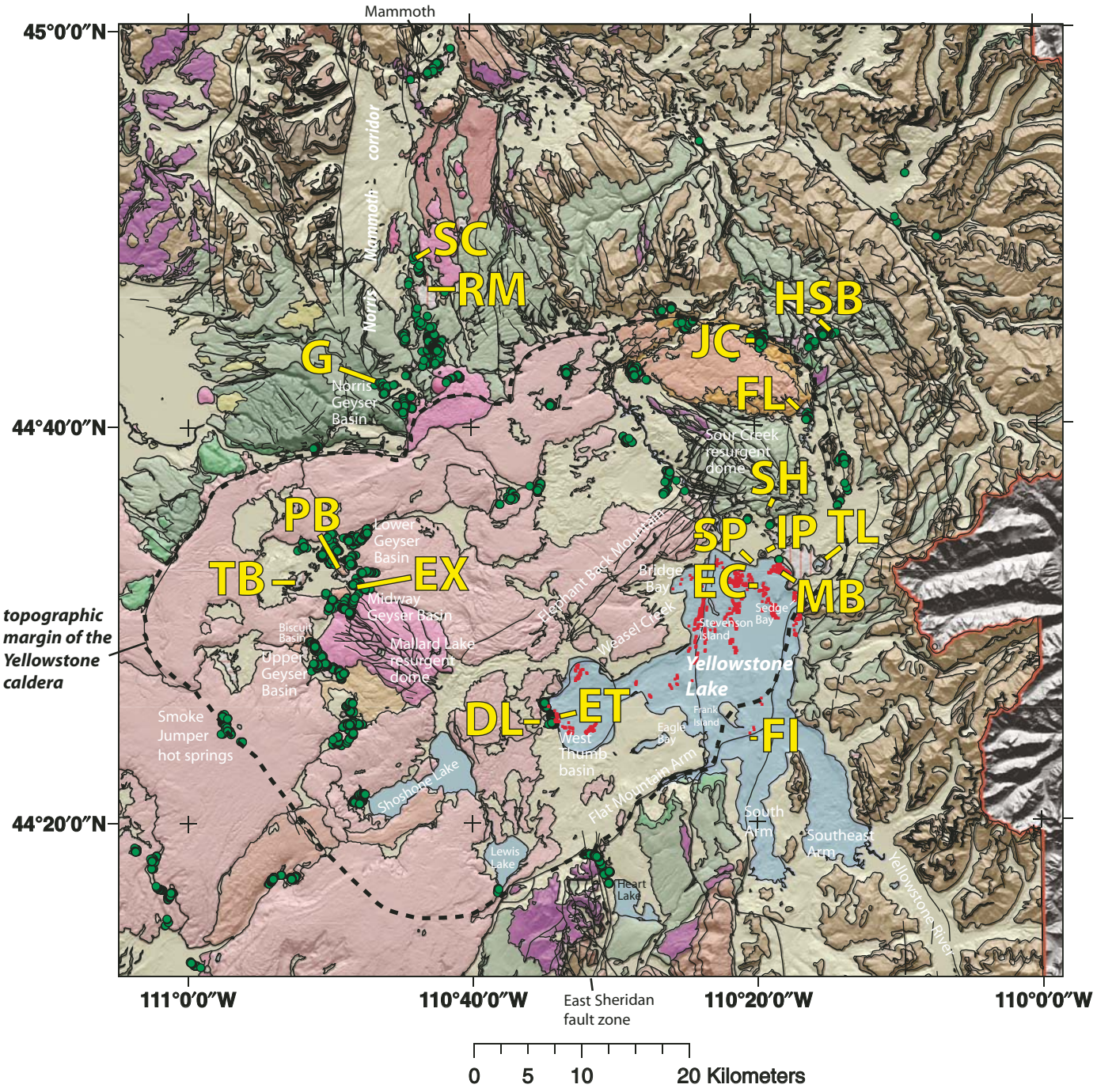

Figure 1. Index map showing location and distribution of large hydrothermal explosion craters in Yellowstone National Park. Also shown are the location of the Yellowstone caldera and other major structural features. Major geologic units are shown as: light tan—undifferentiated Quaternary sediments; light green—Lava Creek Tuff; pink—postcaldera rhyolitic lava flows; purple—Huckleberry Ridge Tuff; light brown—Tertiary volcanic units; medium brown—Paleozoic sedimentary units; brown—pre-Cambrian units; green dots—individually mapped hot springs; red dots—sublacustrine hydrothermal vents; bold black dotted line—topographic margin to the Yellowstone caldera. Abbreviations for hydrothermal explosion craters: MB—Mary Bay; TL—Turbid Lake; TB—Twin Buttes; PB—Pocket Basin; RM—Roaring Mountain; FI—Frank Island; FL—Fern Lake; EC—Elliott's crater; SP—Storm Point; DL—Duck Lake; ET—Evil Twin; IP—Indian Pond; HSB—Hot Spring Basin; JC—Joseph's Coat; SH—Sulfur Hills; G—the Gap; SC—Semicentennial. Modified from Christiansen (2001).

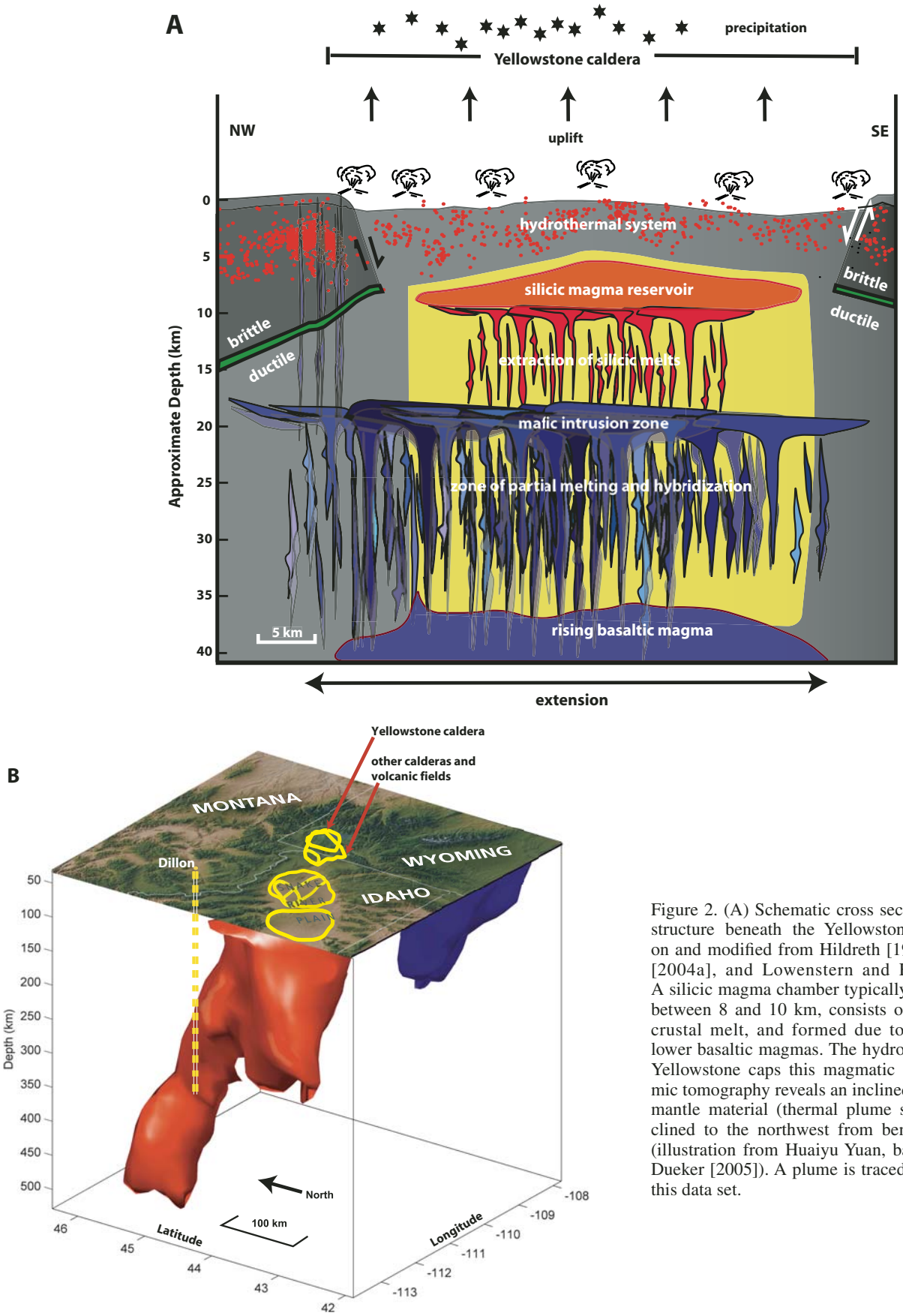

Figure 2. (A) Schematic cross section of the crustal structure beneath the Yellowstone caldera (based on and modified from Hildreth [1981], Husen et al. [2004a], and Lowenstern and Hurwitz [2008]). A silicic magma chamber typically resides at depths between 8 and 10 km, consists of partially molten crustal melt, and formed due to the intrusion of lower basaltic magmas. The hydrothermal system at Yellowstone caps this magmatic system. (B) Seismic tomography reveals an inclined conduit of warm mantle material (thermal plume shown in red) inclined to the northwest from beneath Yellowstone (illustration from Huaiyu Yuan, based on Yuan and Dueker [2005]). A plume is traced to ~500 km with this data set.

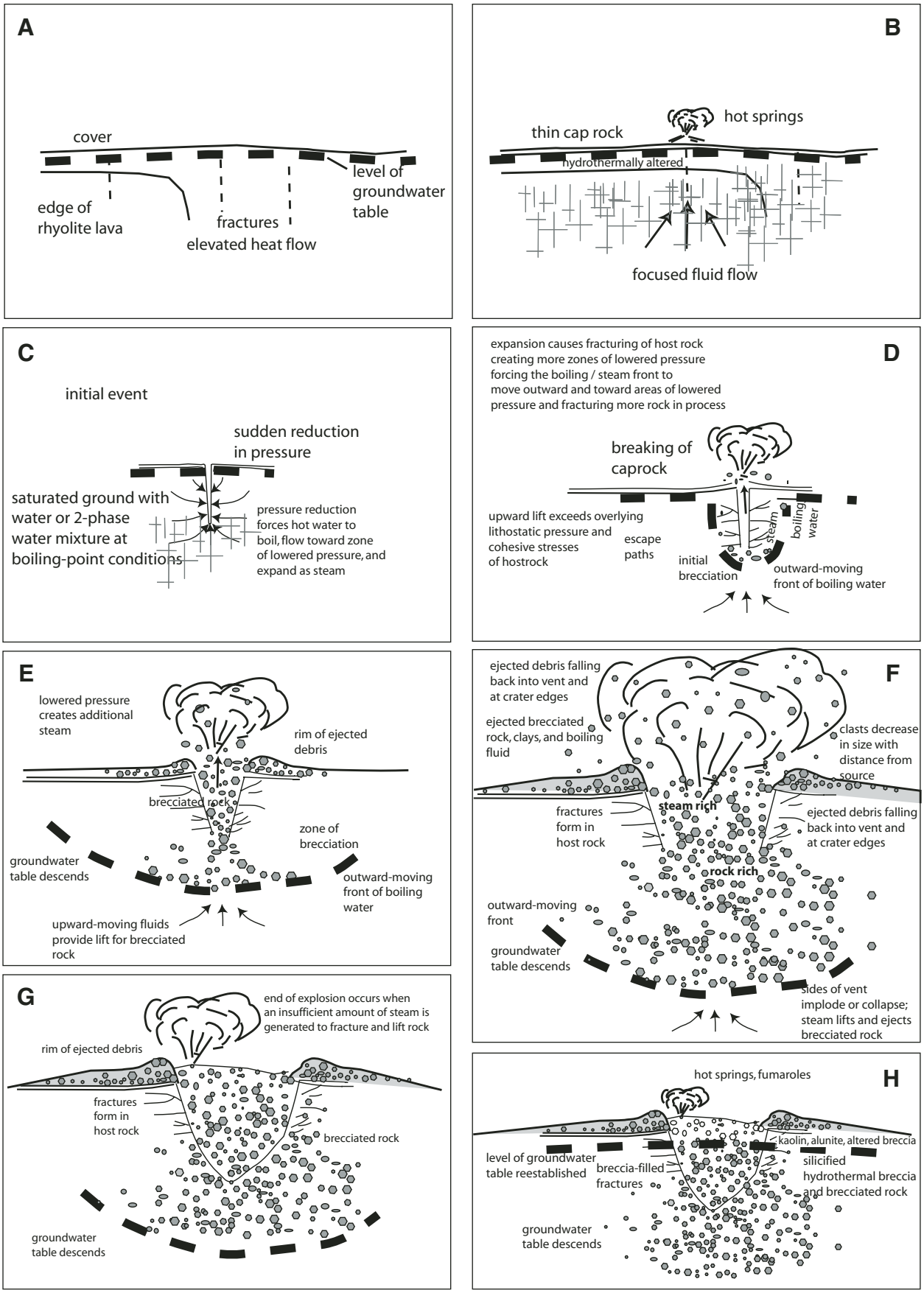
A
cover
level of groundwater table
edge of rhyolite lava
fractures
elevated heat flow
B
hot springs
thin cap rock
hydrothermally altered
focused fluid flow
C
initial event
sudden reduction in pressure
saturated ground with water or 2-phase water mixture at boiling-point conditions
pressure reduction forces hot water to boil, flow toward zone of lowered pressure, and expand as steam
D
expansion causes fracturing of host rock creating more zones of lowered pressure forcing the boiling / steam front to move outward and toward areas of lowered pressure and fracturing more rock in process
breaking of caprock
upward lift exceeds overlying lithostatic pressure and cohesive stresses of hostrock
escape paths
steam
boiling water
initial brecciation
outward-moving front of boiling water
E
lowered pressure creates additional steam
rim of ejected debris
brecciated rock
zone of brecciation
groundwater table descends
outward-moving front of boiling water
upward-moving fluids provide lift for brecciated rock
F
ejected debris falling back into vent and at crater edges
ejected brecciated rock, clays, and boiling fluid
clasts decrease in size with distance from source
fractures form in host rock
steam rich
ejected debris falling back into vent and at crater edges
rock rich
outward-moving front
groundwater table descends
sides of vent implode or collapse; steam lifts and ejects brecciated rock
G
end of explosion occurs when an insufficient amount of steam is generated to fracture and lift rock
rim of ejected debris
fractures form in host rock
brecciated rock
groundwater table descends
H
hot springs, fumaroles
kaolin, alunite, altered breccia
level of groundwater table reestablished
breccia-filled fractures
silicified hydrothermal breccia and brecciated rock
groundwater table descends

in which the explosion occurred and thus may be used to approximate the maximum depths affected by explosions. The matrices of most breccia deposits are composed of fine-grained, hydrothermally altered mud and sand, and may be present downwind from the explosion crater source (Meyer, 1993; Grant Meyer, 2005, written commun.).

Hydrothermal explosions reflect rapid changes in pressure that lead to flashing of water to steam and result in fragmentation of overlying and surrounding strata. Sealed near-surface discharge conduits resulting from hydrothermal mineral precipitation can create a confined or constricted system, with temperature–depth (pressure) characteristics between the hydrostatic and lithostatic curves, or in extreme cases on the lithostatic curve (Fig. 6). Explosions result when a hydrothermal system experiences an abrupt drop in the confining pressure. The pressure decrease causes spontaneous boiling and promotes an explosive event. For example, if a lithostatically confined fluid at a given depth has a temperature higher than required for hydrostatic boiling (Fig. 6) and a seismic or some other event fractures the confining rock, an immediate shift to a hydrostatic pressure regime will occur. This will cause the attendant confining pressure to drop and will promote sudden fluid boiling. Boiling causes rapid and violent steam generation, with a significant volume increase that is rapidly transmitted to adjacent hydraulically connected reservoirs; this leads to catastrophic failure and explosion of the entire system (Muffler et al., 1971; Fournier et al., 1991; Browne and Lawless, 2001).

Spontaneous changes in pressure may trigger hydrothermal explosions; such events may include earthquakes, landslides where overburden is suddenly removed, or lowering of the water table associated with drought (Browne and Lawless, 2001). For subaqueous systems, these mechanisms plus sudden changes in water level due to drainage of glacially dammed lakes (Muffler et al., 1971) or the drawdown phase of large waves produced by fault movement or large landslides (Morgan and Shanks, 2005) may trigger hydrothermal explosions. Elsewhere hydrothermal explosions are known to be secondary events associated with volcanic eruptions (Marini et al., 1993; Simmons et al., 1993; Nairn et al., 2005).

Figure 3. Diagram showing the evolution and processes associated with hydrothermal explosions. (A) Conditions contributing to the location and development of hydrothermal systems include elevated heat flow, water, and zones of weakness or focused flow such as fractures and edges of low-permeability rhyolite lava flows. (B) Focused flow of hydrothermal fluids creates thermal areas with hot springs, geysers, and mud pots at the surface. Over time, the subsurface becomes hydrothermally altered and a thin siliceous cap rock forms in places. (C) A hydrothermal explosion is initiated by a sudden reduction in pressure on the steam-saturated hydrothermal system resulting in steam generation and a sudden rush of hot water toward the new zone of low pressure. (D) Hydrothermal explosion occurs due to expansion as a boiling front moves outward from the initiation point, lifting caprock and fracturing host rock. (E) Explosion continues as the groundwater table descends. As the boiling fluid front advances, fluids flash to steam and lift brecciated rock, and a rim of fractured rock is deposited around the crater. (F) Fractured rock, mud, steam, and boiling water are ejected and deposited as fall material that partially fills the crater and creates a debris apron of flow material outside the crater. (G) Hydrothermal explosion stops when boiling fronts no longer advance and the system no longer has energy to eject material. (H) Hydrothermal activity in and around explosion crater continues for thousands of years. Diagrams slightly modified from Browne and Lawless (2001) and Smith and McKibbin (2000).

Large Hydrothermal Explosion Events in Yellowstone

In Yellowstone, large hydrothermal explosion craters (Fig. 1) are herein considered features that are >100 m in diameter and produce significant volumes (0.01 to >0.03 km^3) of ejecta. A bimodal distribution exists between explosion craters in Yellowstone with regard to size. Most of the historic small hydrothermal explosions create craters that have areas smaller than 0.001 km^2; with diameters <10 m. In contrast, the large hydrothermal explosion craters have areas more than two orders of magnitude greater and are between 0.1 and 5.0 km^2 (Fig. 5A) with diameters >100 m. Many explosion craters in Yellowstone were identified and described in the landmark paper by Muffler et al. (1971). Wold et al. (1977) mapped and described the large hydrothermal explosion crater on the floor of Yellowstone Lake in Mary Bay; several additional large explosion craters were discovered during more recent multibeam swath-sonar and seismic reflection surveys (Morgan et al., 2003; 2007a, 2007b).

At least 20 large postglacial hydrothermal explosion events have occurred over the last 14–16 ka in Yellowstone (Figs. 1 and 5) (Morgan et al., 2007a; Muffler et al., 1968, 1971, 1982a; White et al., 1988; Pierce et al., 2002a; 2007a; Richmond, 1973, 1974, 1976, 1977; Christiansen, 2001). Hydrothermal explosion deposits exhibit remarkable variability among type of rock ejected and depth of rock evacuated by the explosion, but they also share some common features, such as a roughly round or oval crater, evidence for multiple explosion events, and continuing hydrothermal activity.

Most explosion craters are found inboard or along the topographic margin of the 0.64-Ma Yellowstone caldera (Fig. 1) where heat-flow values are high and thermal basins are well-developed. Within Yellowstone Lake, heat-flow measurements from the west side of West Thumb Basin exceed 1500 mW/m^2; heat-flow values in the northern basin of Yellowstone Lake are tenfold that in West Thumb (Morgan et al., 1977) and these areas host large hydrothermal explosion craters and abundant sublacustrine hydrothermal vents (Morgan et al., 2007a). A few craters are present outside the caldera along the tectonically active, north-trending Norris-Mammoth corridor. Along the East Sheridan Fault Zone, a linear fault scarp has numerous thermal features at its base (Fig. 1, Table 1).

Importance of Hydrothermal Explosion Studies

Hydrothermal explosions are powerful local events which may occur with little or no warning, and thus are potential natural hazards. Compared to other hydrothermal features such as

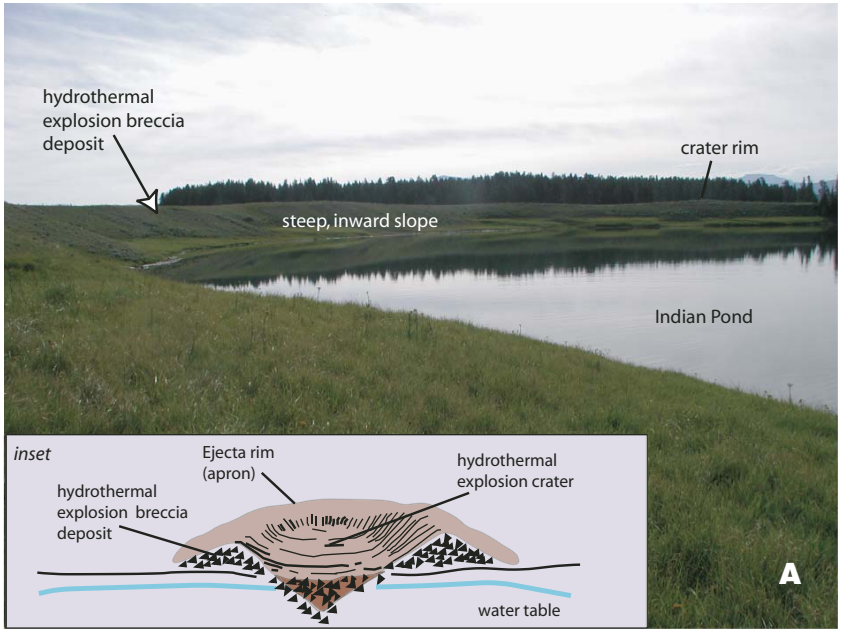

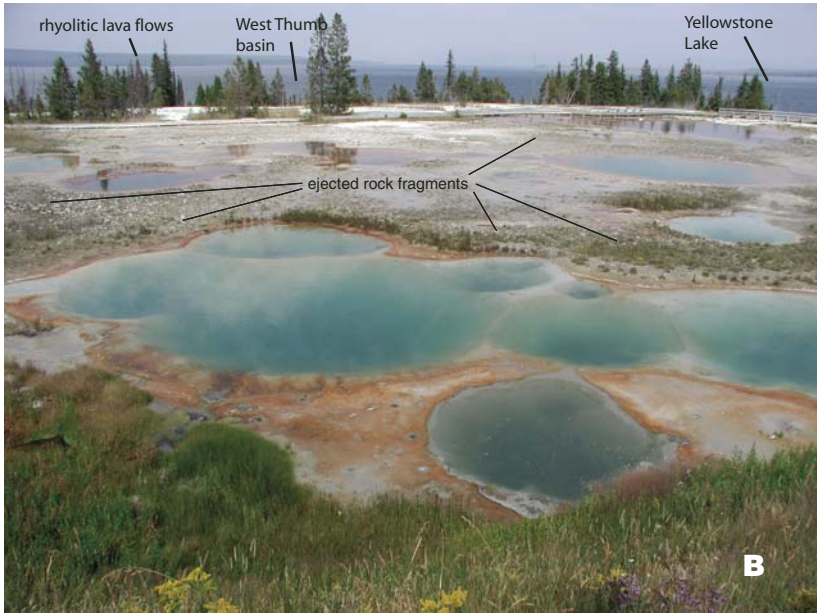

Figure 4. Examples of hydrothermal craters and products. (A) Photograph across the Indian Pond hydrothermal explosion crater looking to the northeast. Note the rim of ejected material surrounding the steep inward slope around the pond. Inset shows a diagram of general features of hydrothermal explosion craters and deposits. (B) Smaller (2–5 m diameter) craters at West Thumb Geyser Basin, looking to the east. In the background is Yellowstone Lake. (C) Photograph of Sapphire Pool at Biscuit Basin, which erupted violently following the 1959 Hebgen Lake earthquake, enlarging its pool and ejecting large blocks of sinter (photo, July 2004). (D) Photograph of an altered lithic clast from the breccia deposit that rims the Turbid Lake hydrothermal explosion crater. The clast is a silicified, heterolithic, matrix supported, hydrothermally altered breccia with a matrix of fine-grained altered mud.

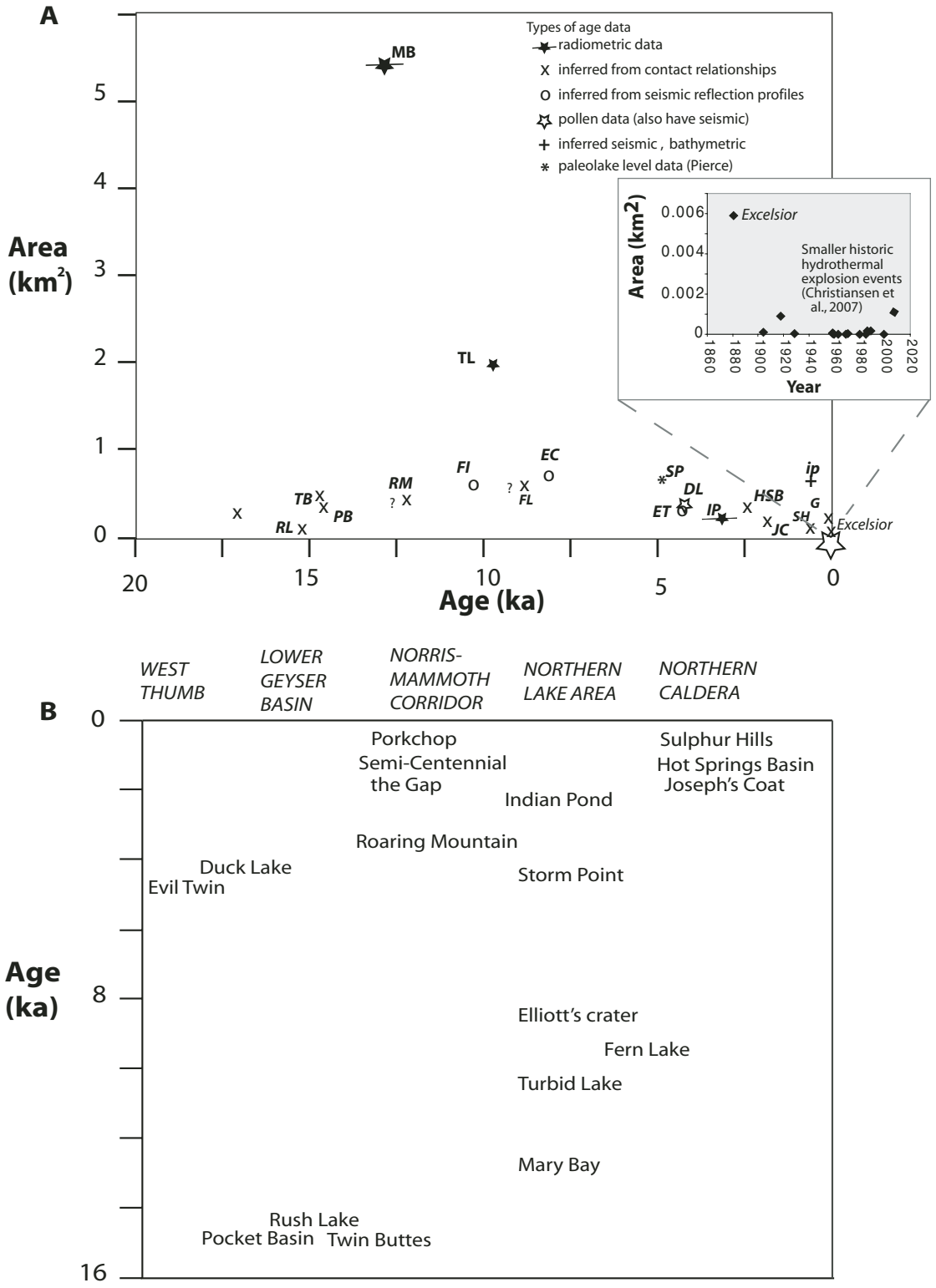

Figure 5. Age spectrum and area of large hydrothermal explosion craters in Yellowstone National Park. Most of the ages are estimated and not well-constrained. Many of the large explosions created craters with areas in excess of 500 m^2. The Turbid Lake and Mary Bay events are extreme compared to other events in Yellowstone and worldwide. Note that over the past 200 yr, more than 100 small hydrothermal explosion events occurred and 95% of these produced craters less than 10 m in diameter (Lowenstern et al., 2005). Abbreviations: MB—Mary Bay; TL—Turbid Lake; RL—Rush Lake; TB—Twin Buttes; PB—Pocket Basin; RM—Roaring Mountain; FI—Frank Island; FL—Fern Lake; EC—Elliott's crater; SP—Storm Point; DL—Duck Lake; ET—Evil Twin; IP—Indian Pond; HSB—Hot Springs Basin; JC—Joseph's Coat; SH—Sulfur Hills; G—the Gap; ip—inflated plain.

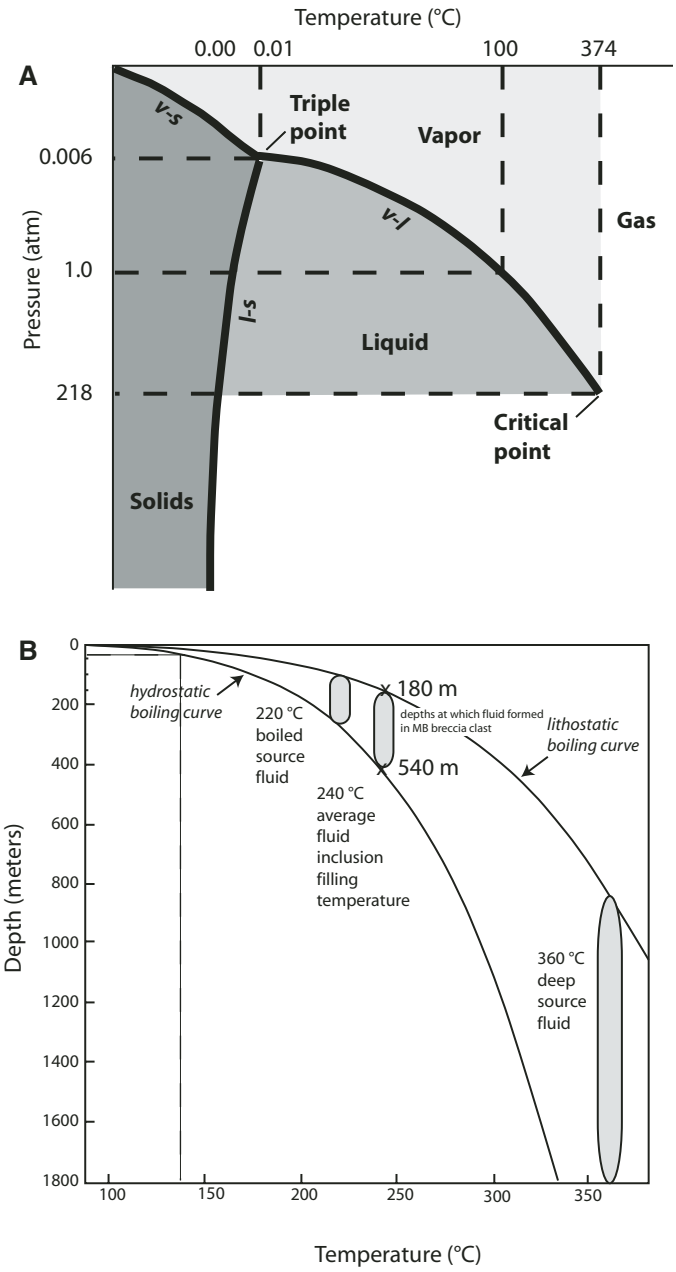

Figure 6. (A) Phase relations for pure water, showing the boiling curve extending to the critical point at 374 °C and 218 atm. (B) Hydrostatic and lithostatic boiling curves showing that waters on the lithostatic curve, or between lithostatic and hydrostatic conditions, will flash to steam if there is a sudden shift to hydrostatic conditions. Pressure-temperature (P-T) conditions are also plotted for several inferred source fluids. A deep neutral-chloride source fluid at ~360 °C is believed to underlie thermal systems throughout the park (Truesdell et al., 1977; Fournier, 1989). The 220 °C boiled source fluid is determined from geochemical studies of hydrothermal vents in Yellowstone Lake (Shanks et al., 2005; Balistrieri et al., 2007) and the 240 °C fluid is measured from fluid inclusions in a lithic clast of Mary Bay explosion breccia (Alexandra M. Skewes, 2000, written commun.).

geysers and hot springs in Yellowstone, large hydrothermal explosions are relatively uncommon events and appear to have occurred every 700–1000 yr over the past 14–16 ka (Fig. 5, Table 1). Small historic hydrothermal explosion events have been documented in Yellowstone (Fournier et al., 1991; Marler and White, 1975; Hutchinson, 1996; Heasler et al., 2008; Heasler and Jaworowski, 2008), but many known events are not described in sufficient detail to allow interpretation of the processes and triggering mechanisms. Large explosion events are very rarely observed and documented; thus much uncertainty remains about precursory signals and processes preceding an explosion. In the 1880s, however, Excelsior Geyser in Midway Geyser Basin is known to have exploded and erupted 63 times in 11 days, with each eruption averaging 6.5 min and the water column height reaching elevations of 50–300 ft, averaging 100 ft (Allen and Day, 1935). According to Philetus Norris, the superintendent of YNP who witnessed an explosion, the geyser pool was considerably enlarged, all movable rock around the geyser's borders was cleared, and a ridge of exploded rock from 1- to 2-m high surrounded the new enlarged pool at a distance of 6–15 m (Lowenstern et al., 2005). Currently the diameter of the pool for Excelsior Geyser measures ~107 m in maximum diameter (Christiansen et al., 2007).

Large hydrothermal explosions are certainly much less destructive than catastrophic events associated with caldera-forming volcanic eruptions and large magnitude earthquakes, but they are a potentially significant hazard. The relative frequency of large hydrothermal explosions suggests that potentially explosive systems warrant monitoring (Lowenstern et al., 2005). Ejection of large blocks of rock, boiling water, steam, and mud, and the associated fall and flow of muddy slurries several meters thick for distances of hundreds of meters from vent sources would affect many square kilometers. Understanding precursors and potential explosion triggers and the processes involved are required in order to plan monitoring strategies and anticipate hydrothermal explosions.

The purpose of this study is to determine the timing, distribution, and possible causes of large (>100 m diam) hydrothermal explosion events in Yellowstone (Fig. 1, Table 1). Previous studies suggested that many large hydrothermal explosion events in Yellowstone are associated with recession of the late Pleistocene glaciers, with sudden drainage of ice-dammed lakes a key triggering mechanism (Muffler et al., 1968, 1971). The broad spectrum of ages and geologic settings for large hydrothermal explosion craters documented in this study, however, require consideration of additional processes and alternative triggering mechanisms.

METHODOLOGY AND FIELDWORK

Field Methods

On Yellowstone Lake, we employ an 8-m-long aluminum vessel (the National Park Service RV Cuttroat). A small (~1.5 m × 1 m × 1 m), submersible remotely operated vehicle

TABLE 1. DESCRIPTIVE INFORMATION FOR LARGE HYDROTHERMAL EXPLOSION CRATERS IN YELLOWSTONE NATIONAL PARK

Feature	Crater			Deposit			Rim height (m)	Maximum water depth (m)	Total depth-rim to floor (m)	Elevation of perched water table above groundwater level (m)	Geologic setting	Age (est) (ka)
	Maximum length (m)	Maximum width* (m)	Diameter (average) (km)	Area (crater) (km^2)	Area covered by deposit (km^2)	Estimated volume (km^3)						
Norris-Mammoth corridor												
Roaring Mountain east crater complex	644	504	0.574	0.255			58	0	58		LCT, along N-M tectonic corridor	<16
Roaring Mountain north crater	314	289	0.302	0.071			33	0	33		LCT, along N-M tectonic corridor	<16
The Gap-Norris Geyser Basin	114	105	0.162	0.009			16	unknown	16		LCT, along N-M tectonic corridor	<16
Horseshoe Hill explosion crater											LCT, along N-M tectonic corridor	
Lower and Upper Geyser Basins												
Pocket Basin	758	418	0.588	0.249			41	0	41		Qal and Qg, in basin surrounded by rhyolitic lava flows	<16
Rush Lake	342	240	0.291	0.064			23	unknown	23		Qal and Qg, in basin surrounded by rhyolitic lava flows	<16
Twin Buttes	641	624	0.633	0.314			129	unknown	129		thermal kame in basin surrounded by rhyolitic lava flows	<16
West Thumb area												
Duck Lake	733	500	0.617	0.288			35	18	53		edge of Dry Creek flow	4–6 ka
Evil Twin	553	544	0.549	0.236			27	42	27		high heat flow, edge of Aster Creek flow	4–6 ka
Northern and Central Yellowstone Lake area												
Turbid Lake	1685	1502	1.594	1.988			85	42	127	30 m above level of Yellowstone Lake	Qal, along the topographic margin of Yellowstone caldera	9.4
Indian Pond	495	418	0.457	0.163			11	27	38	6 m above level of Yellowstone Lake	Qal, along the Weasel Creek-Storm Point linear trend	2.9
Mary Bay	2400	2824	2.612	5.323	~30 km^2	>0.03 km^3	60	53	113	in Yellowstone Lake	high heat flow, in rhyolite lava, area subject to active deformation	13.0
Elliott's crater	938	727	0.833	0.536			52	60	52	in Yellowstone Lake	high heat flow, inside edge of lava flow, area subject to active deformation	8.0
Frank Island crater	770	712	0.741	0.431			21	50	21	in Yellowstone Lake	along edge of Aster Creek flow and topographic margin of Yellowstone caldera	old

(*continued*)

TABLE 1. DESCRIPTIVE INFORMATION FOR LARGE HYDROTHERMAL EXPLOSION CRATERS IN YELLOWSTONE NATIONAL PARK (*continued*)

	Crater			Deposit								
Feature	Maximum length (m)	Maximum width* (m)	Diameter (average) (km)	Area (crater) (km^2)	Area covered by deposit (km^2)	Estimated volume (km^3)	Rim height (m)	Maximum water depth (m)	Total depth-rim to floor (m)	Elevation of perched water table above groundwater level (m)	Geologic setting	Age (est) (ka)
Storm Point	840	795	0.818	0.524			15				Qal, along the Weasel Creek-Storm Point linear trend	4–6
North Basin Hydrothermal Dome (inflated plain)	850	665	0.758	0.444			30			in Yellowstone Lake	Qal, along the Weasel Creek-Storm Point linear trend, along edge of lava flow	<2
Other structures												
Slide block-Elk Pt	1529	1079	1.304	1.296				102		in Yellowstone Lake		
Lake Hotel graben	2505	395	1.450	1.650				70		in Yellowstone Lake	along the northern trend of the Eagle Bay fault zone	
Upper Pelican river												
Sulphur Hills crater	354	248	0.301	0.069			50	0	50		LCT, along resurgent-related fault in the Sour Creek dome	very young
Fern Lake	1095	540	0.818	0.464			38	8	46	~6 m	edge of tuff of Sulphur Creek and Canyon lava flow near topographic margin of Yellowstone caldera	
Hot Spring Basin Group	289	268	0.279	0.243			39	0	39		LCT and thermal kame, along topographic margin of Yellowstone caldera	very young
Joseph's Coat	397	341	0.369	0.106			35	0	35		thermal kame, edge of Canyon Flow along topographic margin of Yellowstone caldera	

*Maximum width is measured perpendicular to maximum length.

(ROV) is attached to the vessel by a 200-m tether. The ROV, built and operated by Eastern Oceanics, provides live videographic and photographic coverage and remote control of cameras and sampling equipment. The ROV has a full-depth rating of 300 m, can measure temperature, conductivity, and depth of underwater hydrothermal vents, and can retrieve hydrothermal vent fluid and solid samples up to 40 cm long for examination and analysis. The submersible ROV has descended into vent craters to collect hydrothermal fluid and solid samples at depths up to 15 m below the level of the surrounding lake bottom.

On land, detailed measured sections, excavations and augering, and stratigraphic relations were used to document total explosion breccia deposit thickness and thickness variation. Some of the study locations are shown in Figure 7. One site (#499) included detailed descriptions and sampling of a mineralized hydrothermal breccia pipe, informally referred to as the Black Dog hydrothermal breccia pipe. Lidar (light detection and ranging) profiles of breccia-mantled shorelines were used to estimate the changes in thickness of the Mary Bay breccia and the doming of the Storm Point geothermal area (Pierce et al., 2002a, 2007a). Where exposed, lithic fragments from the various hydrothermal explosion deposits were identified, classified, and maximum diameters were measured. In some cases, detailed maps were prepared by tape and compass techniques and structural measurements of bedding, faults, fractures, and joints were made. In Yellowstone Lake, the orientation of fractures was determined by orienting the submersible remotely operated vehicle (ROV) along the trend of the fracture and taking the compass reading from the ROV.

Geochronology

Two different geochronologic methods were employed in this study. Samples of units containing charcoal and humic deposits bracketing the hydrothermal explosion breccia deposits were prepared at the U.S. Geological Survey (USGS) ^{14}C laboratory in Reston, Virginia. ^{14}C ages were determined at the Center for Accelerator Mass Spectrometry (CAMS) at the Lawrence Livermore National Laboratory in Livermore, California (Table 2). ^{14}C ages were used to calculate or bracket the ages of the hydrothermal explosion events.

$^{40}Ar/^{39}Ar$ dating methods were used to determine volcanic eruption ages for clasts of felsite porphyries incorporated into the Mary Bay hydrothermal explosion breccia deposit and to estimate their possible source. Sanidine crystals separated from three samples were dated by the single-crystal $^{40}Ar/^{39}Ar$ laser-fusion method. Separation, irradiation, and analytical procedures are described in McIntosh and Chamberlin (1994). Samples were analyzed by W.C. McIntosh at the New Mexico Bureau of Geology, Socorro, New Mexico.

Chemistry, Mineralogy, Oxygen Isotope, and Fluid Inclusion Analyses of Hydrothermal Explosion Deposits

Representative samples of lithic clasts were collected from hydrothermal explosion breccia deposits. Samples were crushed and ground to <200 mesh for chemical analyses. All analyses were done in the USGS analytical laboratories in Denver, Colorado. Major element analyses were carried out on fused pellets by wavelength dispersive X-ray fluorescence (Table 3) (Taggart, 2002). Trace and minor element analyses of 40 elements were done by inductively coupled plasma-mass spectrometry (ICP-MS) following sample dissolution in HCl-HNO_3-$HClO_3$-HF solution (Lamothe et al., 1999). Mercury was analyzed on separate acid dissolutions using flameless atomic absorption (AA) analysis (Kennedy and Crock, 1987).

Oxygen isotope analyses were conducted to determine the extent of hydrothermal alteration and constrain the temperatures of hydrothermal processes. Silicate samples were analyzed with BrF_5 in nickel reaction vessels (Clayton and Mayeda, 1963) to liberate O_2, which was converted to CO_2. Oxygen isotope values ($\delta^{18}O$) were analyzed on the purified CO_2 using a Finnigan 252 isotope ratio mass spectrometer and calibrated relative to the Vienna-Standard Mean Ocean Water (VSMOW) standard with reproducibility of approximately ±0.2 per mil. Carbon and oxygen isotope values in carbonate minerals were determined by reaction with phosphoric acid in an automated extraction system interfaced to a Micromass Optima isotope ratio mass spectrometer. Precision relative to VSMOW and Vienna-Pee-Dee Belemnite (VPDB) standard are estimated to be about ±0.05 per mil.

Representative minerals from the hydrothermal explosion deposits were analyzed in the X-ray diffraction laboratory at the USGS in Denver, Colorado. Bulk, unoriented powders were analyzed using Cu Kα radiation on an automated Phillips diffractometer and mineral abundances were determined as major, minor, or trace based on major characteristic mineral peaks (Table 4).

Scanning electron microscopic analyses were completed to determine microstructures and compositions of phases using a JEOL 5800-LV scanning electron microscope with an Oxford ISIS Energy Dispersive X-ray spectrometer at the USGS Microprobe Laboratory, Denver, Colorado.

Fluid inclusion measurements from the cemented matrix of the Mary Bay breccia deposit were analyzed by Alexandra Skewes at the University of Colorado, Boulder, Colorado. Several samples of breccia and veins were examined although only one breccia sample yielded fluid inclusions suitable for thermometric studies. Three doubly polished thin sections were made from different parts of the cemented matrix of this breccia. The fluid inclusions in hydrothermal wairakiite were analyzed using a modified U.S. Geological Survey Fluid Inclusion Stage (A. Skewes, 2000, written commun.; Werre et al., 1979). Inclusion-filling temperatures and salinities (expressed in terms of weight percent NaCl equivalent) were determined by measuring the freezing point depression of the solution as described by Potter et al. (1978).

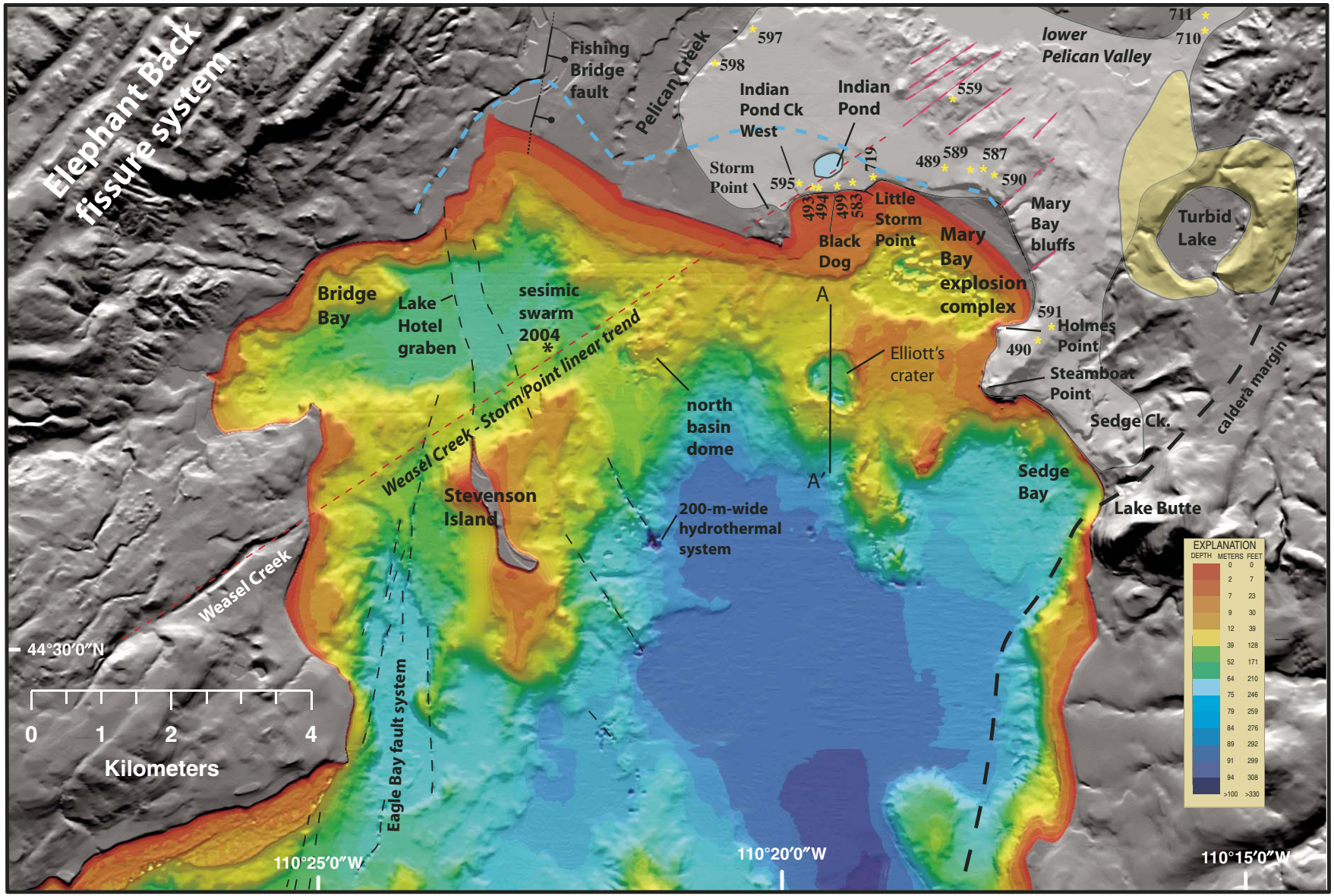

Figure 7. Index map of the northern Yellowstone Lake area using a rainbow-shaded bathymetric map of northern Yellowstone Lake (Morgan et al., 2003, 2007b) surrounded by gray-shaded topography showing sites and features discussed in the text. The line A-A′ represents a seismic reflection profile shown in Figure 12. Distribution of the Mary Bay hydrothermal explosion deposit is shown in light gray; distribution of the Turbid Lake hydrothermal explosion deposit is shown in light yellow; it is distributed discontinuously to the west exposed along the north shore of Yellowstone Lake. Red dashed line in lake represents the Weasel Creek–Storm Point linear trend. Bathymetric depths are represented by scale.

TABLE 2. RADIOCARBON AGES OF CHARCOAL AND WOOD SAMPLES FROM HYDROTHERMAL EXPLOSION BRECCIA DEPOSITS AND NEARBY SOILS AND SEDIMENTS (^{14}C RESULTS)

WW	Sample ID	Material	Region	δ^{13}C	^{14}C age	±	Dated on
WW5415	YNP-336.3	wood	Yellowstone NP, WY	–25	2785	35	09/28/05
WW5418	YNP-02-583.2	charcoal in carbonized soil at base of Indian Pond	Yellowstone NP, WY	–25	2895	35	09/28/05
WW5419	YNP-02-583.3	charcoal in lake sediments above Turbid Lake	Yellowstone NP, WY	–25	4325	35	09/28/05
WW5420	YNP-03-719.1	charcoal in soil directly below Indian Pond	Yellowstone NP, WY	–25	2875	35	09/28/05

Note: Samples were processed at the ^{14}C laboratory of the U. S. Geological Survey in Reston, Virginia. ^{14}C ages were determined at the Center for Accelerator Mass Spectrometry (CAMS), Lawrence Livermore National Laboratory, Livermore, California. The quoted age is in radiocarbon years (B.P.) using the Libby half life of 5568 yr. The WW number is the identification assigned to a sample by the USGS ^{14}C laboratory. Values reported for δ^{13}C are the assumed values according to Stuiver and Polach (Radiocarbon, v. 19, p. 355, 1977) when given without decimal places. Values measured for the material itself are given with a single decimal place.

Special Mapping Techniques

From 1999 to 2002, Yellowstone Lake was surveyed using state-of-the-art bathymetric, seismic, and submersible remotely operated vehicle (ROV) equipment, as summarized by Morgan et al. (2003, 2007a). The survey was navigated to an accuracy of ≤1 m using a differential global positioning system (GPS), and includes over 241,000,000 soundings that were used to produce high-resolution continuous overlapping coverage of the lake's bathymetry. During bathymetric mapping in 1999, 2000, and 2001, over 2500 linear kilometers of high-resolution seismic reflection profiling were used to characterize strata in the upper ~25 m of lake-bottom deposits. In 2003, seismic reflection surveys of the South, Southeast, and Flat Mountain Arms were completed.

These data complimented that of the newly acquired (1996) high-resolution aeromagnetic data of YNP. The aeromagnetic survey was flown along closely spaced (every 400 m), north-south–trending flight lines at low flight elevations (draped at <350 m above existing terrain) and allowed resolution of low-amplitude, short-wavelength magnetic anomalies. This grid is at a scale that can resolve features useful for mapping individual geologic units, faults, and areas of hydrothermal alteration (Finn and Morgan, 2002).

RESULTS

Large Hydrothermal Explosion Events in Yellowstone National Park

New mapping, sampling, and analysis in this study shows that large hydrothermal explosions have occurred repeatedly during the past 14 ka in Yellowstone and are primarily within the Yellowstone caldera (Fig. 1, Table 1). Many of the large hydrothermal explosion craters (Figs. 7 and 8) are within or near the edges of postcaldera rhyolite lava flows (Morgan and Shanks, 2005). Other craters, such as the Turbid Lake and Fern Lake craters (Fig. 1), and the Frank Island crater in Yellowstone Lake, occur along the topographic margin of the Yellowstone caldera. Still others occur outside the caldera along active N-S fault zones such as the Norris-Mammoth Corridor structural zone.

Most subaerial hydrothermal-explosion craters, including Twin Buttes crater in the Lower Geyser Basin (Muffler et al., 1971, 1982a), the 9.4-ka Turbid Lake crater (Love et al., 2007; Richmond, 1977; Muffler et al., 1971; Pierce et al., 2002a), and the 2.9-ka Indian Pond crater (Table 2) (Richmond, 1977; Pierce et al., 2002a, 2007a; Muffler et al., 1971), are now occupied by lakes (Christiansen, 1974; Richmond, 1973; U.S. Geological Survey, 1972). All of the craters have the topographic or bathymetric characteristics of nested craters within a larger parent crater; these composite features represent multiple cratering events that occurred over a period of time. Many smaller craters within parent craters may have formed from a variety of processes, including multiple steam explosions and collapse due to dissolution of underlying material beneath siliceous hydrothermal cap rock (Shanks et al., 2005). Some hydrothermal explosion craters now occupied by lakes, such as Indian Pond and Duck Lake, have water levels perched well above nearby Yellowstone Lake, indicating a crater floor composed of low permeability clays and silica (Table 1).

Several large (>500 m) explosion craters have been delineated beneath Yellowstone Lake; these include the (6 ka?) Evil Twin explosion crater in the western West Thumb Basin, the (>10 ka) Frank Island crater in the south central basin, the >8-ka Elliott's crater in the northern basin (Johnson et al., 2003; Morgan et al., 2003), and the 13-ka Mary Bay crater (Fig. 5; Pierce et al., 2002a; 2007a; Wold et al., 1977; Morgan et al., 2003).

Evil Twin, Elliott's, and Mary Bay explosion craters all contain smaller, nested craters indicative of multiple explosive cratering events that are younger than the main explosion event. In contrast to subaerial craters, which have radial aprons

TABLE 3. CHEMICAL COMPOSITION OF HYDROTHERMAL EXPLOSION BRECCIA AND BLACK DOG BRECCIA PIPE SAMPLES

Field number	YNP-98-299.1	YNP-98-299.3	YNP-98-299.5	YNP-98-299.9	YNP-98-299.14	YNP-98-376.2
Field description	Lithic clast from Mary Bay breccia deposit: silicified, dark gray, matrix-supported multigenerational breccia with cross-cutting mineralized veins; breccia clasts include several silicified lake bed fragments	Lithic clast from Mary Bay breccia: dark gray chalcedonic multigenerational breccia with open vugs lined with euhedral quartz and finely disseminated pyrite; sulfides lining fractures	Lithic clast from Mary Bay breccia: gray, poorly sorted (1 mm-2 cm), heterolithic breccia; clasts in breccia include chalcedony, quartz-phyric rhyolite, and multigenerational breccia	Lithic clast from Mary Bay breccia: dark gray chalcedony with sulfides, euhedral quartz vugs, and intergranular gray-grain wairakiite?	Lithic clast from Mary Bay breccia: light gray, fine-grained silicified lake sediments	Lithic clast from Mary Bay breccia: highly altered massive clast with euhedral quartz and sulfides; thermal cracks throughout clast
SiO_2	72.1	85.8	71.7	79.6	80	79.6
Al_2O_3	10.5	6.57	12.8	9.61	9.03	9.86
CaO	1.35	0.15	1.89	0.22	0.32	0.13
Fe_TO_3	4.43	1.33	2.83	0.92	0.96	0.57
K_2O	2.73	3.01	4.25	5.88	6.87	6.61
MgO	0.34	0.34	1.04	0.47	0.6	0.1
MnO	0.02	0.02	0.04	< 0.01	0.03	< 0.01
Na_2O	3.66	< 0.15	2.81	1.31	< 0.15	1.07
P_2O_5	0.15	0.11	0.16	0.07	0.09	0.07
S	2.25	0.19	0.14	0.35	b.d.	0.25
TiO_2	0.23	0.17	0.31	0.09	0.25	0.1
LOI (925 °C)	2.5	1.69	1.45	0.92	0.7	0.63
TOTAL	100.3	99.4	99.4	99.4	98.9	99
Ag	0.78	0.70	0.93	0.67	0.79	0.56
As	96	72	2	36	7.1	18
Ba	725	670	1000	130	820	180
Be	3.3	4.8	3.2	6.8	2.8	2.8
Cd	0.23	0.04	0.08	0.06	0.01	0.05
Co	6.2	3.0	5.3	0.20	1.8	0.25
Cr	49	40	50	< 10	48	< 10
Cs	2.0	16	1.6	2.8	6.0	2.5
Cu	16	8.2	8.3	3.6	5.0	3.7
Ga	10.5	29	20	13	12	11
Ge	0.39	0.61	1.2	0.60	0.43	0.39
Hg	0.08	0.08	<0.02	0.05	0.02	0.05
Li	45	170	31	80	130	56
Mo	7.9	1.4	1.2	3.4	0.43	6.2
Nb	31	31	46	36	41	28
Ni	27	9.8	15	< 1	11	< 1
Pb	33	18	23	24	22	20
Rb	115	260	110	300	510	320
Sb	2.0	16	0.87	2.1	1.1	2.2
Sc	4.4	4.0	5.5	1.2	5.0	0.7
Se	6.0	1.3	0.7	1.0	0.6	0.7
Sr	290	49	380	55	240	74
Ta	2.4	1.1	2.8	0.84	3.1	0.36
Th	10.3	14	19	23	20	17
Tl	0.85	1.1	0.66	1.3	2.3	1.6
U	2.0	3.2	3.6	4.3	3.9	4.6
V	8.8	26	36	1.6	20	1.4
W	2.2	4.7	1.4	5.3	2.4	2.7
Y	29	34	46	57	82	30
Zn	67	22	65	39	34	15

(*continued*)

TABLE 3. CHEMICAL COMPOSITION OF HYDROTHERMAL EXPLOSION BRECCIA AND BLACK DOG BRECCIA PIPE SAMPLES (*continued*)

Field number	YNP-98-376.6	YNP-98-376.8a	YNP-98-376.10	YNP-98-377.1	YNP-98-377.3	YNP-97-MBX-1
Field description	Lithic clast from Mary Bay breccia: massive mineralized clast impregnated with veins of calcite	Lithic clast of Mary Bay breccia: silicified laminated lake sediments with sulfide mineralization along fractures	Lithic clast from Mary Bay breccia: red oxidized, massive mineralized Lithic with vugs of clear euhedral quartz crystals	Lithic clast from Mary Bay breccia: large (0.5 m diam) red clast of mineralized multigenerational breccia, sulfides, pyrite, unidentified green mineral, quartz	Lithic clast from Mary Bay breccia: multigenerational breccia with chert, vugs of clear euhedral quartz, and cross-cutting quartz veins	Lithic clast from Mary Bay breccia: individual chalcedonic breccia fragment from YNP-97-MBX
SiO_2	77.8	65.4	73.0	76.9	75.6	65.95
Al_2O_3	8.47	14.3	13.0	10.4	12.3	22.7
CaO	1.31	2.78	0.64	0.35	0.26	2.66
Fe_TO_3	1.98	4.62	2.28	1.86	0.92	0.66
K_2O	5.21	1.95	5.52	4.37	6.57	5.18
MgO	0.69	2.97	0.22	0.81	0.13	0.63
MnO	0.02	0.05	0.04	0.01	< 0.01	<0.01
Na_2O	0.74	1.91	3.27	2.33	2.63	1.89
P_2O_5	0.16	0.26	0.09	0.14	0.07	0.05
S	0.78	0.23	0.12	0.48	0.26	0.2
TiO_2	0.22	0.55	0.23	0.21	0.12	0.12
LOI (925 °C)	1.39	4.44	0.54	1.6	0.54	n.d
TOTAL	98.8	99.5	99	99.5	99.4	n.d
Ag	1.1	0.47	1.3	0.57	0.71	0.45
As	49	12	3.1	150	41	6.2
Ba	840	1300	1100	770	220	220
Be	2.4	1.8	3.6	3.4	7.6	3.1
Cd	0.06	0.11	0.09	0.04	0.04	<0.1
Co	2.8	17	1.5	1.5	0.79	1.5
Cr	34	170	< 10	41	< 10	13
Cs	6.6	4.4	3.0	2.5	2.7	36
Cu	20	22	6.1	10	4.5	4
Ga	12	19	24	11	13	22
Ge	0.37	0.60	1.3	0.30	0.33	0.2
Hg	0.06	0.10	0.02	0.05	0.03	
Li	96	14	14	48	42	50
Mo	2.7	1.0	3.2	5.3	4.0	1.8
Nb	32	16	66	28	33	44
Ni	7.1	68	5.4	9.6	1.2	9.3
Pb	21	23	24	16	24	13
Rb	180	67	150	170	330	210
Sb	1.6	0.72	0.44	2.2	2.2	0.8
Sc	4.1	11	3.2	4.3	1.4	2
Se	2.5	0.2	1.2	1.9	2.6	<1
Sr	220	570	88	270	100	150
Ta	0.87	0.89	2.9	0.92	1.1	3.1
Th	12	8.5	26	11	23	15
Tl	1.0	0.50	0.80	0.89	2.0	1.0
U	2.3	2.2	2.9	2.0	4.7	2.2
V	6.0	100	13	20	6.6	11
W	2.7	3.5	3.6	2.0	1.8	3.6
Y	29	20	64	24	66	48
Zn	48	67	77	51	20	9

(*continued*)

TABLE 3. CHEMICAL COMPOSITION OF HYDROTHERMAL EXPLOSION BRECCIA AND BLACK DOG BRECCIA PIPE SAMPLES (*continued*)

Field number	YNP-97-MBX-2	YNP-97-MBX-3	YNP-97-MBX-4	YNP-97-MBX-5	YNP-97-MBX-6	YNP-98-299.12
Field description	Lithic clast from Mary Bay breccia: individual chalcedonic breccia fragment from YNP-97-MBX	Lithic clast from Mary Bay breccia: individual chalcedonic breccia fragment from YNP-97-MBX	Lithic clast from Mary Bay breccia: individual chalcedonic breccia fragment from YNP-97-MBX	Lithic clast from Mary Bay breccia: individual chalcedonic breccia fragment from YNP-97-MBX	Lithic clast from Mary Bay breccia: individual chalcedonic breccia fragment from YNP-97-MBX	Lithic clast from Mary Bay breccia: quartz-phyric rhyolite; hydrothermal quartz overgrowths on phenocrysts; small veins of finely disseminated pyrite and elongated black crystals
SiO_2	88.31	66.19	77.08	47.89	63.27	80.9
Al_2O_3	7.37	12.8	14.2	22.7	20.8	9.09
CaO	0.42	12.6	0.28	5.04	3.36	0.79
Fe_TO_3	1.27	1	0.89	14.3	2.14	0.71
K_2O	1.93	4.7	5.18	1.69	5.06	3.88
MgO	0.33	0.38	0.17	3.98	0.61	0.25
MnO	0.01	0.05	0.01	0.59	0.01	0.02
Na_2O	0.27	1.25	1.48	2.7	0.81	1.84
P_2O_5	<0.01	<0.01	<0.01	0.34	0.11	0.08
S	<0.3	0.9	0.7	0.3	3.5	0.43
TiO_2	0.08	0.08	0.05	0.5	0.33	0.09
LOI (925 °C)	n.d	n.d	n.d	n.d	n.d	1.21
TOTAL	n.d	n.d	n.d	n.d	n.d	99.3
Ag	0.29	0.36	0.16	0.2	0.32	0.81
As	30	46	11	18	68	100
Ba	230	130	1100	330	620	370
Be	3.6	1.3	3.6	3.7	3.0	2.6
Cd	0.6	0.2	0.3	0.4	<0.1	0.12
Co	2.8	1.8	24	4.6	3.2	6.8
Cr	69	54	140	150	22	< 10
Cs	2.1	2.6	5.0	12	54	2.6
Cu	33	8	20	10	10	5.6
Ga	15	13	25	21	22	17
Ge	0.4	0.2	0.6	0.4	0.2	0.47
Hg						0.08
Li	41	25	15	230	66	30
Mo	130	29	47	12	23	2.0
Nb	12	33	11	6.0	27	44
Ni	710	730	100	1600	8.2	23
Pb	30	21	20	5.5	14	33
Rb	190	240	43	120	200	170
Sb	2.8	3.4	1.6	18	1.9	5.1
Sc	1	0.7	11	2	5.0	1.4
Se	1	<1	<1	<3	1	1.2
Sr	310	89	700	95	120	230
Ta	0.4	2.1	0.8	0.3	1.5	0.69
Th	12	14	6.7	2.0	7.6	49
Tl	1.2	1.5	0.3	0.4	1.1	1.7
U	2.1	2.5	2.4	0.8	1.7	6.9
V	11	3	91	20	8	1.9
W	3.6	8.6	2.2	2	4.8	4.0
Y	37	28	22	7.7	26	57
Zn	98	33	82	40	30	36

(*continued*)

TABLE 3. CHEMICAL COMPOSITION OF HYDROTHERMAL EXPLOSION BRECCIA AND BLACK DOG BRECCIA PIPE SAMPLES (*continued*)

Field number	YNP-00-497.2	YNP-00-489.5	YNP-00-530.10	YNP-00-497.4	YNP-01-559.1	YNP-01-572.1
Field description	Lithic clast from Mary Bay breccia: hydrothermally altered quartz-phyric rhyolite	Lithic clast from Mary Bay breccia: hydrothermally altered quartz-phyric rhyolite	Lithic clast from Mary Bay breccia: hydrothermally altered quartz-phyric rhyolite	Lithic clast from Mary Bay breccia: hydrothermally altered quartz-phyric rhyolite	Lithic clast from Mary Bay breccia: hydrothermally altered quartz-phyric rhyolite	Lithic clast from Mary Bay breccia: hydrothermally altered quartz-phyric rhyolite
SiO_2	83.63	89.64	89.88	87.44	88.49	84.25
Al_2O_3	10.01	6.8	7.18	8.5	7.94	10.58
CaO	0.81	<0.1	<0.1	<0.1	0.14	<0.1
Fe_TO_3	<0.1	<0.1	<0.1	<0.1	<0.1	<0.1
K_2O	5.06	3.37	2.77	3.85	3.13	4.82
MgO	0.4	0.13	0.12	0.15	0.25	0.28
MnO	0.006	0.003	0.001	0.003	0.004	0.005
Na_2O	<1	<1	<1	<1	<1	<1
P_2O_5	<0.01	<0.01	<0.01	<0.01	<0.01	<0.01
S	<0.05	<0.05	<0.05	<0.05	<0.05	<0.05
TiO_2	0.08	0.05	0.05	0.05	0.05	0.07
LOI (925 °C)	n.d.	n.d.	n.d.	n.d.	n.d.	n.d.
TOTAL	n.d.	n.d.	n.d.	n.d.	n.d.	n.d.
Ag	0.76	0.40	0.56	0.80	0.58	1.0
As	31	26	12	20	24	46
Ba	110	82	64	81	140	170
Be	1.7	2	3.6	3.4	1.8	6.2
Cd	< 7	< 7	< 7	< 7	< 7	< 7
Co	< 0.5	< 0.5	< 0.5	< 0.5	< 0.5	< 0.5
Cr	< 20	< 20	< 20	< 20	< 20	< 20
Cs	14	1	1	1	1	2
Cu	< 40	< 40	< 40	< 40	< 40	< 40
Ga	7.2	6.7	9.2	9.8	7.5	9.6
Ge	0.1	0.3	0.4	0.3	0.2	0.6
Hg						
Li	100	170	180	150	84	41
Mo	5.3	3.2	1.2	0.8	2.4	1.6
Nb	46	34	34	49	40	54
Ni	< 50	< 50	170	50	< 50	54
Pb	22	10	10	27	24	23
Rb	230	150	130	180	110	180
Sb	2.4	2.4	2.1	2.5	2.1	2.3
Sc	9	8	10	9	8	9
Se						
Sr	92	69	20	30	66	110
Ta	3.6	2.2	2.2	2.9	2.8	3.6
Th	10	10	10	10	10	20
Tl	< 2	< 2	< 2	< 2	< 2	< 2
U	3.7	3	3.2	3.8	3.7	5.4
V	< 5	< 5	< 5	34	< 5	< 5
W	1.2	1.6	2.6	1.7	0.8	1.9
Y	24	23	33	38	32	50
Zn	< 400	< 400	< 400	< 400	< 400	< 400

(*continued*)

TABLE 3. CHEMICAL COMPOSITION OF HYDROTHERMAL EXPLOSION BRECCIA AND BLACK DOG BRECCIA PIPE SAMPLES (*continued*)

Field number	YNP-00-491.1	YNP-02-595.1	YNP-04-739.1	YNP-02-589.1	YNP-98-338.1	YNP-98-334.1
Field description	Lithic clast from Mary Bay breccia: hydrothermally altered quartz-phyric rhyolite with calcite veins	Lithic clast from Mary Bay breccia: hydrothermally altered quartz-phyric rhyolite	Lithic clast from Mary Bay breccia: hydrothermally altered quartz-phyric rhyolite	Lithic clast from Mary Bay breccia: hydrothermally altered quartz-phyric rhyolite	Lithic clast from Indian Pond explosion breccia	Lithic clast from Turbid Lake explosion breccia
SiO_2	86.6	81.1	84.8	81.1	65.5	74.6
Al_2O_3	7.25	9.73	8.06	10.2	14.1	10.6
CaO	0.19	0.16	0.09	0.22	3.55	0.63
Fe_TO_3	0.22	0.67	0.23	0.73	3.47	2.16
K_2O	3.87	6.1	5.06	3.68	2.53	5.91
MgO	0.18	0.16	0.46	0.21	1.81	0.82
MnO	<0.01	<0.01	<0.01	<0.01	0.04	0.02
Na_2O	1.5	1.53	1.17	3.45	2.48	0.81
P_2O_5	<0.01	<0.01	<0.01	0.01	0.23	0.24
S	<0.05	<0.05	<0.05	<0.05	b.d.	0.16
TiO_2	0.05	0.08	0.06	0.08	0.45	0.32
LOI (925 °C)	0.4	0.6	0.55	0.45	4.6	2.62
TOTAL	100.26	100.13	100.48	100.13	98.8	98.9
Ag	<1	<1	<1	1	0.44	0.55
As	<30	40	<30	<30	9.7	5.7
Ba	82.4	115	167	108	1300	1700
Be	<5	<5	<5	5	3.1	1.2
Cd	<0.2	<0.2	<0.2	<0.2	0.16	0.04
Co	<0.5	<0.5	<0.5	0.8	8.6	0.98
Cr	10	30	<10	40	96	75
Cs	2.5	2.8	2.5	1.8	6.0	3.5
Cu	<5	<5	<5	<5	17	5.6
Ga	8	12	9	13	21	12
Ge	<1	<1	<1	<1	0.63	0.56
Hg	n.d.	n.d.	n.d.	n.d.	0.15	0.02
Li	130	30	50	20	16	100
Mo	7	4	<2	5	1.1	1.4
Nb	33	44	34	50	19	28
Ni	<5	9	<5	13	42	7.0
Pb	32	24	21	25	29	17
Rb	166	265	220	167	66	270
Sb	n.d.	n.d.	n.d.	n.d.	0.30	0.88
Sc	<5	<5	<5	<5	8.5	5.3
Se	n.d	n.d	n.d	n.d	0.3	0.6
Sr	50.9	56.4	66.7	102	760	330
Ta	3.3	3.5	2.6	6.4	1.4	1.4
Th	11.9	15.7	18.2	18.7	16	9.7
Tl	0.6	1.1	1	<0.5	0.60	4.1
U	3.3	4.62	3.86	4.77	4.2	1.8
V	<5	<5	<5	<5	65	40
W	2	2	1	1	2.1	3.7
Y	51.9	54.4	54.9	53.8	35	16
Zn	11	5	16	12	65	18

(*continued*)

TABLE 3. CHEMICAL COMPOSITION OF HYDROTHERMAL EXPLOSION BRECCIA AND BLACK DOG BRECCIA PIPE SAMPLES (*continued*)

Field number	YNP-98-335.1	YNP-98-349.2	YNP-98-349.3	YNP-98-330.3	YNP-98-330.6	YNP-05-740.3c
Field description	Lithic clast from Turbid Lake explosion breccia	Sulphur Hills breccia—yellow background denotes sinter is especially siliceous	Sulphur Hills—conglomerate with alunite???	Lithic clast from Fern Lake explosion breccia: silicified poorly sorted sandstone	Lithic clast from Fern Lake explosion breccia: silicified multigenerational breccia with green mineralized clast	Lithic clast from Duck Lake explosion breccia clast: hydrothermally altered, light gray sinter—yellow background denotes sinter is especially siliceous
SiO_2	71.5	92.6	76	78.6	83.2	97.9
Al_2O_3	13.8	1.27	7.13	10.9	8.09	0.96
CaO	0.56	0.04	0.07	0.12	0.09	0.07
Fe_TO_3	2.37	0.1	1.72	0.2	0.99	0.14
K_2O	4.79	0.2	1.88	6.42	4.38	0.08
MgO	0.44	< 0.10	< 0.10	< 0.10	< 0.10	0.17
MnO	< 0.01	< 0.01	< 0.01	< 0.01	0.01	<0.01
Na_2O	2.29	< 0.15	< 0.15	1.14	0.46	0.08
P_2O_5	0.19	0.08	0.18	0.08	0.09	<0.01
S	0.11	0.24	1.8	0.07	0.1	<0.05
TiO_2	0.4	0.29	0.31	0.19	0.12	0.28
LOI (925 °C)	2.3	3.79	10.9	0.85	1.41	0.7
TOTAL	98.8	98.6	100	98.6	98.9	100.38
Ag	0.97	0.74	0.68	0.88	0.54	1
As	45	9.8	23	8.9	20	<30
Ba	1700	890	860	720	920	265
Be	2.8	0.60	0.58	3.6	3.3	<5
Cd	0.06	0.03	0.01	0.03	0.03	<0.2
Co	3.5	0.13	0.40	0.19	0.17	<0.5
Cr	88	13	66	12	< 10	<10
Cs	6.6	2.2	1.4	3.9	5.0	4.3
Cu	16	5.4	10	3.9	2.7	<5
Ga	20	3.2	25	18	11	21
Ge	0.57	0.30	0.31	0.78	0.83	1
Hg	0.05	4.20	0.35	0.25	0.02	n.d.
Li	33	15	6.1	52	43	40
Mo	7.0	6.4	7.6	1.8	1.3	5
Nb	48	36	36	47	29	47
Ni	10	< 1	1.4	< 1	< 1	<5
Pb	24	12	30	18	16	35
Rb	160	5.4	16	310	150	191
Sb	1.4	4.2	2.5	1.4	6.5	n.d.
Sc	8.3	1.6	3.6	2.2	2.2	<5
Se	3.7	0.7	1.8	0.3	0.6	n.d
Sr	420	34	260	61	40	14.8
Ta	3.8	0.76	2.2	3.3	1.6	3.6
Th	18	14	13	27	17	26.2
Tl	1.3	0.1	0.2	1.7	1.2	0.9
U	2.8	4.2	3.1	4.5	3.6	6.96
V	51	6.1	23	5.1	11	<5
W	4.1	8.9	6.1	3.1	2.9	2
Y	26	16	11	20	31	64.2
Zn	30	< 5	6.6	11	7.2	52

(*continued*)

TABLE 3. CHEMICAL COMPOSITION OF HYDROTHERMAL EXPLOSION BRECCIA AND BLACK DOG BRECCIA PIPE SAMPLES (*continued*)

Field number	YNP-05-744.3	YNP-05-740.4	YNP-05-740.3d	YNP-05-740.1	YNP-05-742.1a	YNP-98-359
Field description	Lithic clast from Duck Lake explosion breccia: sinter with reed imprints—yellow background denotes sinter is especially siliceous	Lithic clast from Duck Lake explosion breccia: hydrothermally altered, light gray ignimbrite with light gray pumice and black glassy to perlitic obsidian (tuff of Bluff Pt?)	Lithic clast from Duck Lake explosion breccia: hydrothermally altered, light gray ignimbrite with light gray pumice and black glassy to perlitic obsidian (tuff of Bluff Pt?)	Lithic clast from Duck Lake explosion breccia: hydrothermally altered, light gray ignimbrite with light gray pumice and black glassy to perlitic obsidian (tuff of Bluff Pt?)	Lithic clast from Twin Buttes explosion breccia: altered, vesicular, flow-banded, purple, vapor-phased, porphyritic (small crystals) rhyolite	Pocket Basin breccia
SiO_2	91.4	79.2	74.7	77.8	74.7	85.8
Al_2O_3	2.8	9.84	11.7	12.5	11.4	6.65
CaO	0.24	0.18	0.42	0.14	0.4	0.14
Fe_TO_3	0.61	1.41	1.5	0.75	1.48	0.71
K_2O	0.72	5.93	5.18	4.31	5.16	4.17
MgO	0.27	0.24	0.15	0.12	0.15	<0.10
MnO	<0.01	0.02	0.02	<0.01	0.02	0.01
Na_2O	0.45	1.62	2.96	1.43	3.03	<0.15
P_2O_5	<0.01	0.01	<0.01	0.01	<0.01	0.12
S	<0.05	<0.05	<0.05	0.08	<0.05	
TiO_2	0.1	0.13	0.16	0.16	0.16	0.17
LOI (925 °C)	2.75	0.8	3.35	2.75	3.05	1.35
TOTAL	99.34	99.38	100.14	100.05	99.55	99.1
Ag	<1	1	1	<1	<1	< 0.1
As	<30	<30	<30	<30	<30	42
Ba	128	551	353	777	281	260
Be	<5	<5	<5	<5	7	5.1
Cd	<0.2	<0.2	<0.2	<0.2	<0.2	<0.1
Co	0.7	<0.5	<0.5	0.5	0.7	0.2
Cr	10	<10	<10	<10	20	13
Cs	3.6	2.2	4.9	30.5	81.7	5.8
Cu	<5	<5	<5	<5	<5	3
Ga	5	20	20	18	23	8.4
Ge	4	1	2	2	<1	2.1
Hg	n.d.	n.d.	n.d.	n.d.	n.d.	
Li	<10	<10	40	30	210	120
Mo	<2	<2	5	<2	2	6
Nb	7	43	45	40	34	27
Ni	<5	<5	<5	<5	<5	1
Pb	6	33	31	27	35	<20
Rb	32.1	150	197	331	314	140
Sb	n.d.	n.d.	n.d.	n.d.	n.d.	4.1
Sc	<5	<5	<5	<5	<5	13
Se	n.d	n.d	n.d	n.d	n.d	
Sr	36.2	24.1	18.1	284	21.1	20
Ta	1.7	4.6	9.8	3.5	4.7	1.4
Th	3.5	18.1	23.9	19	19	11
Tl	<0.5	<0.5	1	0.8	1.3	0.8
U	6.75	5.32	6.61	4.89	6.03	3.1
V	6	<5	<5	<5	<5	14
W	2	2	2	2	2	3.6
Y	7.4	33.1	60.6	35.8	39.3	31
Zn	8	13	53	43	43	11

(*continued*)

TABLE 3. CHEMICAL COMPOSITION OF HYDROTHERMAL EXPLOSION BRECCIA AND BLACK DOG BRECCIA PIPE SAMPLES (*continued*)

Field number	YNP-05-743.1b	YNP-98-378.1	YNP-98-378.2	YNP-98-378.4	YNP-98-378.5	YNP-98-378.11
Field description	Lithic clast from Pocket Basin explosion breccia: white, fine-grained sinter with orange oxidation stains	Black Dog Vent—brecciated zone, light gray lake sediments to replace silicious and pyrite rich clasts	Black Dog Vent—clay-rich lake muds, pyrite rich	Black Dog Vent—boxwork, fine sands	Black Dog Vent—breccia from center of pipe	Black Dog Vent—breccia, pyrite, quartz, chalcopyrite
SiO_2	72	78.3	76.8	71.6	77	71.7
Al_2O_3	10	8.9	7.17	10.4	8.78	8.89
CaO	2.38	0.47	1.42	3.33	1.75	2.05
Fe_TO_3	1.36	2.49	3.31	2.63	2.8	5.49
K_2O	4.13	3.77	1.4	1.96	2.1	2.46
MgO	0.27	0.39	0.82	1.89	0.97	2.16
MnO	0.01	0.01	0.02	0.04	0.02	0.05
Na_2O	0.59	1.5	1.38	2.42	1.31	1.98
P_2O_5	<0.01	0.13	0.2	0.17	0.16	0.17
S	<0.05	1.2	1	0.41	0.68	1.7
TiO_2	0.14	0.27	0.29	0.35	0.3	0.36
LOI (925 °C)	6.55	2.67	5.66	3.93	3.54	3.15
TOTAL	97.43	100.1	99.5	99.1	99.4	100.2
Ag	1	0.71	0.35	0.33	0.47	0.58
As	<30	100	830	80	160	250
Ba	71.9	950	760	910	800	910
Be	<5	1.8	1.6	1.4	1.9	1.7
Cd	<0.2	0.06	0.08	0.08	0.11	0.13
Co	<0.5	6.1	12	10	8.0	15
Cr	20	50	55	120	78	200
Cs	3.8	3.4	5.8	4.5	5.5	3.1
Cu	<5	16	25	13	15	16
Ga	4	13	11	13	16	13
Ge	1	0.56	0.98	0.70	0.60	0.64
Hg	n.d.	0.2	3.8	2.0	1.1	1.0
Li	170	75	130	300	150	480
Mo	13	5.0	1.4	2.2	7.8	9.1
Nb	56	29	14	16	18	25
Ni	<5	19	55	40	30	61
Pb	14	n.d	n.d	n.d	n.d	n.d
Rb	6.7	160	60	55	88	86
Sb	n.d.	3.4	0.36	0.29	3.7	1.9
Sc	<5	4.4	6.1	7.6	5.8	11
Se	n.d	1.8	0.2	0.2	1.2	1.3
Sr	19	200	320	600	390	340
Ta	8.5	1.7	0.99	0.69	1.4	2.0
Th	16.9	8.1	6.7	6.5	6.9	8.4
Tl	<0.5	0.95	0.4	0.3	0.53	1.2
U	4.74	1.4	1.5	1.7	1.7	1.5
V	<5	32	49	56	45	62
W	55	9.1	8.5	5.5	4.8	3.8
Y	15.5	24	18	19	20	24
Zn	<5	23	50	44	41	88

Note: Major element oxide concentrations are in wt% and minor element are in ppm.

TABLE 4. X-RAY DIFFRACTION DATA FROM HYDROTHERMALLY ALTERED AREAS IN YELLOWSTONE NATIONAL PARK

Sample #	Locality	Major	Minor	Trace	Comments
YNP-98-338.1	Indian Pond expl. breccia	cristobalite, anorthite, albite	qtz, heulandite, clinopt, montmor		minor amorphous material, feldspar is albite or anorthi, zeolite is heulandite and/or clinopt
YNP-99-11a	altered Aster Ck	qtz, clinop?, heulandite	cristobal, montmor		zeolite is heulandite and/or clinop; possesses very small amount of poorly xlized clay
YNP-99-415.5	Elephant Back lava			qtz, anorth, cristo, talc 2M	major amorphous material
YNP-99-423	Solfatara Flow-gas vents--Qhi	qtz, cristobalite	trid		minor amorphous material
YNP-99-423.17	Solfatara Flow-gas vents--Qhi	sulfur			
YNP-99-423.18	Solfatara Flow-gas vents--Qhi	qtz, cristobal	trid, hm,	kaolinite	
YNP-99-425.1	Lava Creek Tuff near Norris	qtz, anorth, cristob	orthoc, trid		
YNP-99-431	Lava Creek Tuff near Norris	qtz	albite, orthoc		
YNP-99-432	Lava Creek Tuff near Norris	cristob, albite	qtz, orthoc		
YNP-99-439.1	Hot Spring Basin explosion crater	Sulfur, cristobal?			possible trace cristobal
YNP-99-443.15	Lava Creek Tuff near Norris	cristobal, albite	qtz, orthocl	trid	possible trace tridymite
YNP-99-453.3	Mt Sheridan--Factory Hill		qtz	cristob, kaolinite	mostly amorphous material
YNP-99-461.5	Factory Hill-explosion breccia	qtz	albite, orthocl		
YNP-99-463.1	Heart Lake G.B.-siliceous sinter	qtz	cristob, kaolin,	trid	mostly amorphous material, possible trace tridymite
YNP-99-463.4	Heart Lake G.B.- orange ppt on gray muds	qtz, cristob	kaolinite, trid?		mostly amorphous material, possible trace tridymite
YNP-99-462.1	Rustic Geyser--orange slime			qtz	mostly amorphous material
YNP-99-462.2a	Rustic Geyser-algae above sinter	qtz	crisob	augite, kaolinite	minor amorphous material
YNP-99-462-2b fibers	Rustic Geyser-algae above sinter				all amorphous material, no xline phases
YNP-99-462.3 fibers	Rustic Geyser-algae above sinter				all amorphous material, no xline phases
YNP-99-462.4	Heart Lake G.B.- sinter		qtz	anorthite	major amourphous material
YNP-99-462.11	Heart Lake G.B.- sinter				mostly amorphous material, very small amount of an unidentified phase
YNP-99-463.3a grey	Heart Lake thermal nodules			qtz	mostly amorphous material
YNP-99-463-3b red	Heart Lake thermal --dk red hm nodules		qtz, cristob	augite, hm	mostly amorphous material
YNP-99-465.4	Yellowstone Lake spire--sinter	qtz		anorthite	mostly amorphous material
YNP-99-465.5	Yellowstone Lake spire--sinter			qtz, montmor, crist, anorth	mostly amorphous material, clay is poorly crystalline
YNP-99-465.6	Yellowstone Lake spire--sinter				all amorphous material, no xline phases
YNP-99-465.7	Yellowstone Lake spire--sinter		qtz	cristob, anorth	major amorphous material
YNP-99-465.8	Yellowstone Lake spire--sinter			qtz, cristob, anorth	mostly amorphous material
YNP-99-465.9	Yellowstone Lake spire--MnFe ext coating		qtz, cristob	anorthit	mostly amorphous material

(*continued*)

TABLE 4. X-RAY DIFFRACTION DATA FROM HYDROTHERMALLY ALTERED AREAS IN YELLOWSTONE NATIONAL PARK (*continued*)

Sample #	Locality	Major	Minor	Trace	Comments
YNP-99-472.1	Osprey Basalt		qtz	cristob, anorth, trid, alunite	major amorphous material
YNP-99-478.1	Imperial Geyser-stick covered with Si gel		calcite, qtz	anorthite	major amorphous material
YNP-99-478.4	Imperial Geyser-bluish green mineral		qtz, anorthite, cristob, sanidine	trid	
YNP-99-478.6	Imperial Geyser--orange and green bacteria		qtz, crist, anorth, sanidine	heulandite	
YNP-99-481.1	Yellowstone Lake spire--white chalky sinter			qtz	mostly amorphous material
YNP-99-481.2	Yellowstone Lake spire--white chalky sinter			qtz	mostly amorphous material
YNP-99-481.3	Yellowstone Lake spire--white chalky sinter			qtz	mostly amorphous material
YNP-99-482.1	Yellowstone Lake spire--in mud		qtz, trid	anorthite	mostly amorphous material
YNP-99-482.2	Yellowstone Lake spire			qtz, trid	mostly amorphous material, possible tr trid
YNP-99-483.1	pipe from West Thumb			qtz	mostly amorphous material
YNP-99-483.2	pipe from West Thumb			qtz, trid	mostly amorphous material, possible tr trid
YNP-99-483.3	pipe from West Thumb		qtz	trid, anorthite	mostly amorphous material
YNP-99-483.4	pipe from West Thumb		qtz, trid	anorthite	mostly amorphous material, possible tr trid
YNP-99-484.1	Storm Point--ss	anorthite	trid, qtz, augite		minor amorphous material, poss tr trid
YNP-99-484.2	Storm Point--ss	clinoptilolite, anorth	trid, qtz		minor amorphous material
YNP-99-484.3	Storm Point--oxdiz cong		anorth, trid, qtz	augite	minor amorphous material
YNP-99-484.4	Storm Point--	alunite	cristob, qtz		minor amorphous material
YNP-99-484.5	Storm Point	alunite	qtz, cristobalite		minor amorphous material
YNP-99-484.6	Storm Point--ox ss cong	anorthite, trid	qtz	augite	minor amorphous material, poss px
YNP-99-484.7	Storm Point--ox ss	anorthite	trid, clinop, qtz	augite	minor amorphous material; possible px
YNP-99-484.8	Storm Point--mudstorone--sl ox	qtz	anorthite, trid	clinoptilolite	minor amorphous material

Note: atz—quartz; trid—triymite; cristob—cristobalite; clinop—clinoptilolite; anorth—anorhtite; orthoc—orthoclase; montmor—montmorillonite; px—pyroxene; xline—crystalline.

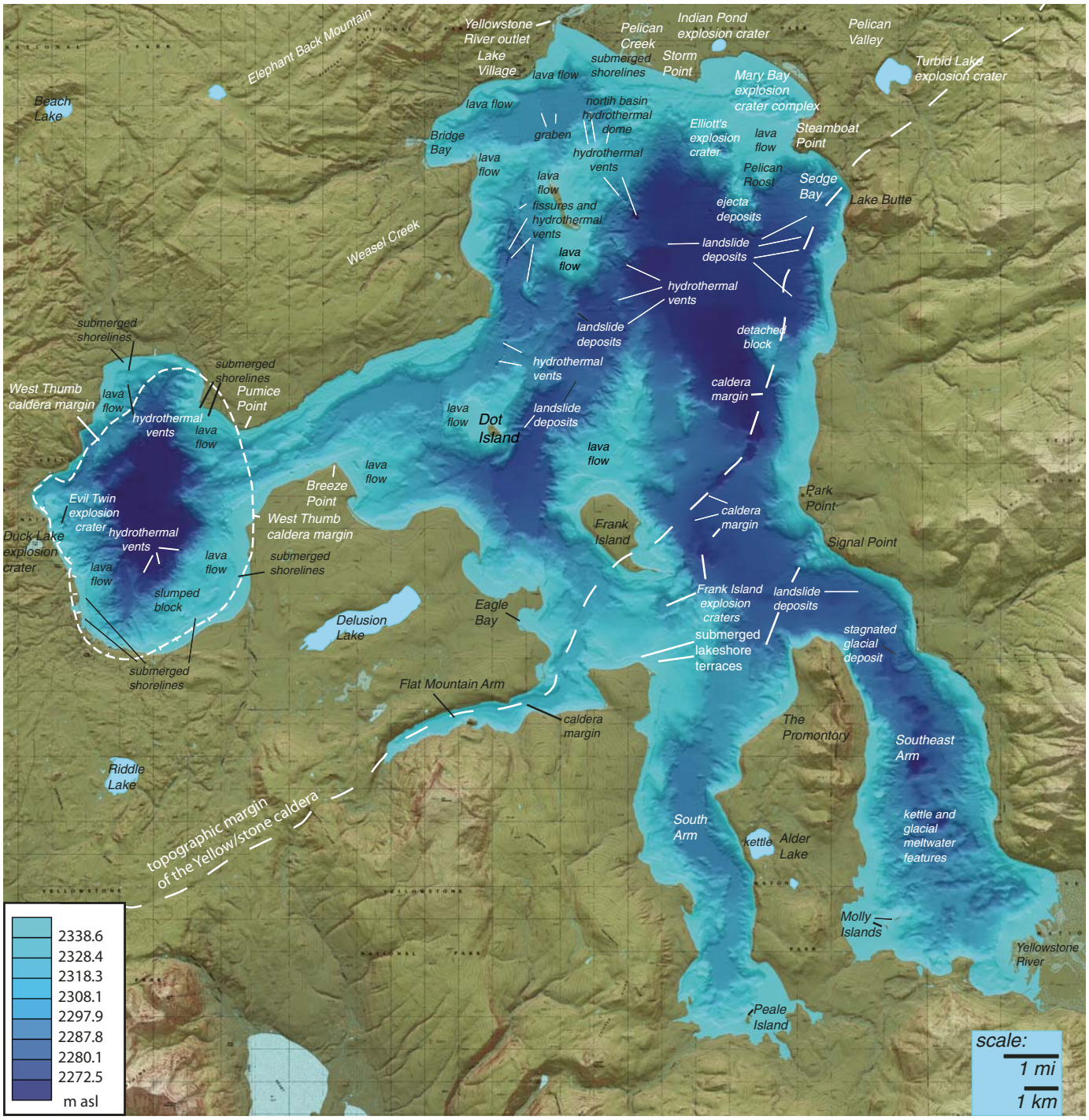

Figure 8 (*on this and following two pages*). (A) High-resolution multibeam swath sonar bathymetric map of Yellowstone Lake; depths shown in shades of blue, with dark blue representing greater depths and light blue representing shallower depths. See text for discussion of labeled structural, hydrothermal, and physiographic features (Morgan et al., 2007b).

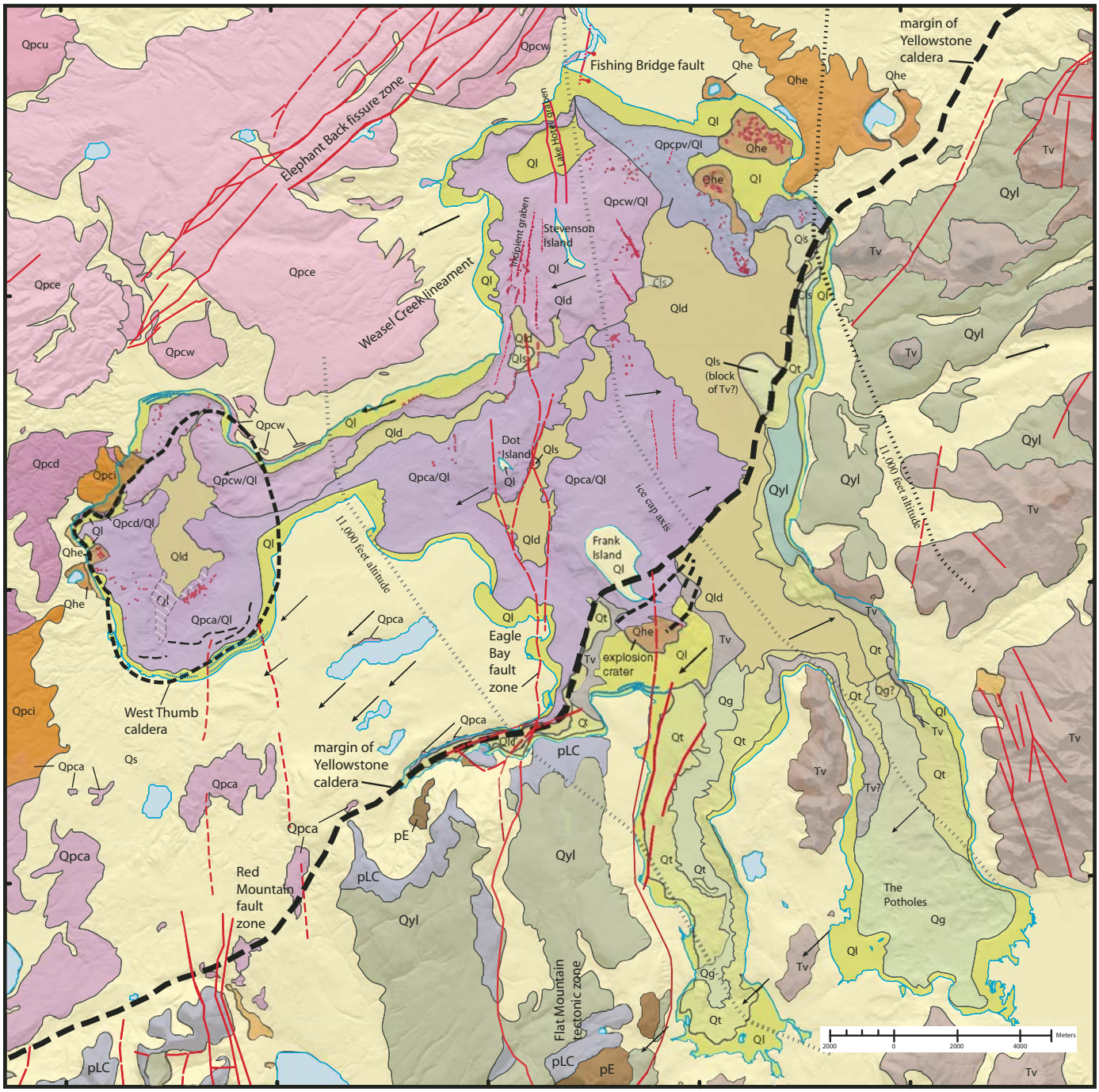

Figure 8 (*continued; legend on following page*). (B) Geologic map of Yellowstone Lake and surrounding area showing structural features and rhyolite lava flows that exert control on the location of hydrothermal vents (Morgan et al., 2007b). Mapping and the description of map units outside of Yellowstone Lake are from Christiansen (2001).

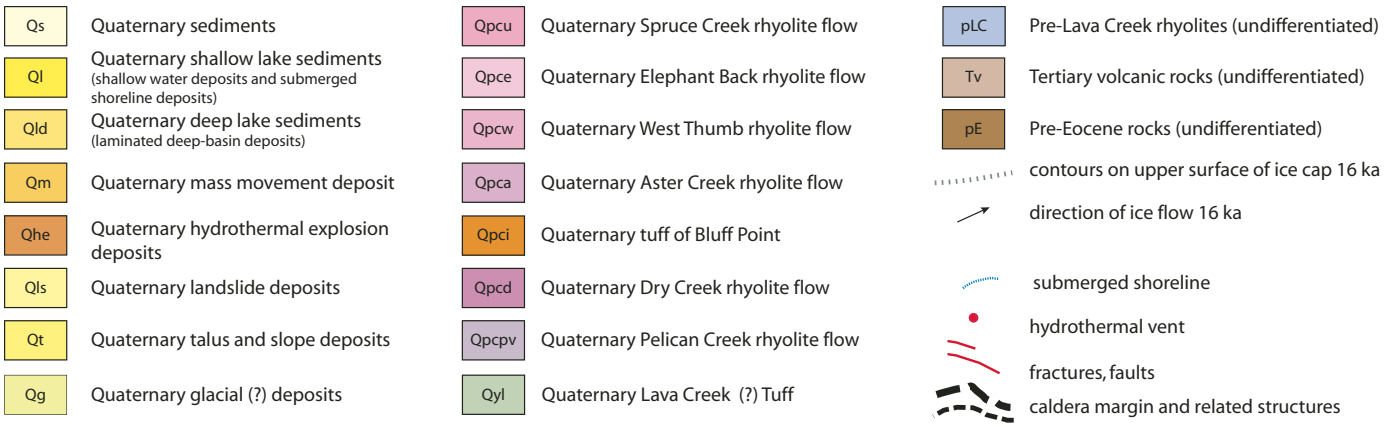

Figure 8 (*legend*).

of explosion breccia deposits that rim craters (Hamilton, 1987; Muffler et al., 1971), many of the sublacustrine circular depressions lack obvious raised rims. This probably indicates more widespread dispersal of ejection deposits into lake water. Except for deposits derived from the Mary Bay hydrothermal explosion events, material from the sublacustrine explosion events has not been identified subaerially.

All of the identified large explosion craters in Yellowstone Lake (Fig. 8), except for the older, sediment-filled Frank Island crater, host active, relatively high-temperature (72° to ≥95 °C) hydrothermal systems (Balistrieri et al., 2007; Morgan et al., 2003; Shanks et al., 2007; Gemery-Hill et al., 2007). Large, subaerial explosion craters at Joseph's Coats, Hot Spring Basin Group, Fern Lake, Turbid Lake, Sulfur Hills, Twin Buttes, Pocket Basin, and the Gap at Norris Geyser Basin also host ongoing hydrothermal activity within and surrounding the craters. Continued hydrothermal activity near many large explosion craters suggests the possibility of recurrent explosions and may allow direct study and sampling of the hydrothermal system responsible for the explosions. Hydrothermal systems associated with each crater were probably significantly changed, physically and chemically, by the explosive events, but ongoing evolution of thermal water offers additional opportunities for understanding and monitoring these systems.

Northern Basin of Yellowstone Lake and Vicinity

Large-scale hydrothermal activity in Yellowstone Lake is associated with (1) some of the highest heat flow in Yellowstone (Morgan et al., 1977), (2) seismically active areas (Fig. 9) with extension and migration of hydrothermal fluids (Waite and Smith, 2002; Smith, 1991), and (3) high chloride flux from numerous hydrothermal vents in Yellowstone Lake (Shanks et al., 2005). Heat-flow studies show that the northern basin of Yellowstone Lake has extremely high heat flux (15,600 mW/m^3 in Mary Bay) compared to most other areas in the lake (Morgan et al., 1977). Some seismic events (Figs. 9E and 9F) have focused along extensional structures in Yellowstone Lake including the Eagle Bay fault and its northern continuation (the Lake Hotel graben), the fissures west of Stevenson Island, and northwest-trending structures east of Stevenson Island and south of Elliott's crater (Fig. 9).

Seismic reflection profiles across large explosion craters in Yellowstone Lake (Johnson et al., 2003; Morgan et al., 2003) depict circular, large, flat-bottomed or V-shaped sediment-filled craters containing numerous smaller craters of variable diameter and depth as well as many active hydrothermal vents and

Figure 9. Maps showing earthquake events in Yellowstone National Park at various time intervals over the past 25 yr (Yellowstone Volcano Observatory data, http://volcanoes.usgs.gov/yvo). (A) In the 5 yr interval between 1981 and 2006, 26,588 earthquakes generally cover the entire Yellowstone area. Earthquakes occurred within the Yellowstone caldera and along active faults to the west and south outside the caldera. Earthquake depths are greater outside the active Yellowstone caldera. (B) Earthquakes parkwide during the 10 yr interval between 1996 and 2006. Within the Yellowstone caldera, clusters of earthquakes' epicenters extend from the Norris-Mammoth corridor south into the Lower Geyser Basin and are concentrated in Yellowstone Lake and West Thumb, and in both the resurgent domes. (C) Earthquakes parkwide during the 5 yr interval between 2001 and 2006, showing basically the same pattern as in B. (D) Earthquakes parkwide during the 1 yr interval between 2005 and 2006, showing (within the caldera) concentrations in northern Yellowstone Lake, in the Sour Creek resurgent dome, in the Southeast Arm, and in the Mary Mountain area. (E) Earthquakes in the area around Yellowstone Lake over the 10 yr interval from 1996 to 2006 showing abundant earthquakes in Sour Creek dome, in the northern lake around Stevenson Island, in the central lake around Frank Island and the caldera margin, along the Eagle Bay fault zone, and along the western edge of West Thumb. (F) Earthquakes in the area of Yellowstone Lake over a 5 yr interval from 2001 to 2006. Earthquakes are focused in the northern basin along vent-lined fractures east of Stevenson Island, vents southeast of Storm Point, and vents southwest of Storm Point. Earthquake clusters also are at the entrance to the Southeast Arm, east of Dot Island, south of Rock Point, west and south of West Thumb, and at the Sour Creek resurgent dome.

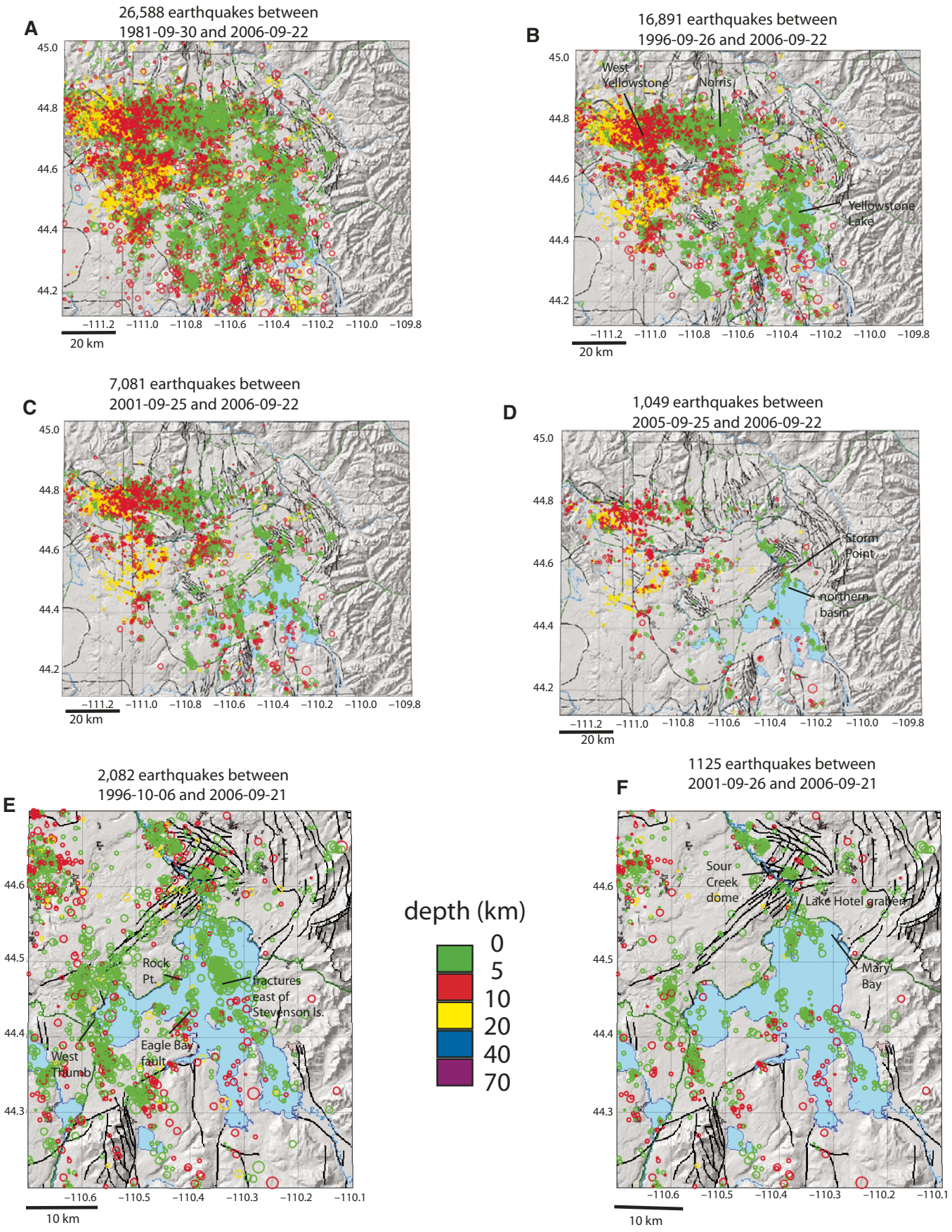
A
26,588 earthquakes between
1981-09-30 and 2006-09-22
B
16,891 earthquakes between
1996-09-26 and 2006-09-22
West Yellowstone
Norris
Yellowstone Lake
C
7,081 earthquakes between
2001-09-25 and 2006-09-22
D
1,049 earthquakes between
2005-09-25 and 2006-09-22
Storm Point
northern basin
E
2,082 earthquakes between
1996-10-06 and 2006-09-21
Rock Pt.
fractures east of Stevenson Is.
Eagle Bay fault
West Thumb
F
1125 earthquakes between
2001-09-26 and 2006-09-21
Sour Creek dome
Lake Hotel graben
Mary Bay
depth (km)
0
5
10
20
40
70
20 km
10 km

domal structures, also of various dimensions. The nested craters, products of either late-phase explosions associated with the initial event or on-going hydrothermal venting, either have flat bottoms that have been filled with later lacustrine sediments or are V-shaped.

Much of the material below the floor of the larger composite craters is characterized by chaotic reflections or is nonreflective due to significant amounts of contained gas (as steam or CO_2) and/or hydrothermally altered rock (Johnson et al., 2003; Morgan et al., 2003). Based on observations from subaerial hydrothermal explosion craters, material filling the large craters is most likely explosion breccia and later lacustrine sediments. Where unaltered, postexplosion lacustrine deposits exhibit moderate- to high-amplitude, continuous, parallel reflections indicative of a period of continuous, uninterrupted deposition. Flanks of the large hydrothermal explosion craters show no constructive rim of ejected material, unlike their subaerial equivalents, which probably results from explosion into a different medium. Flanks of the large craters are outward sloping and are mantled with younger lacustrine sediment.

Hydrothermal breccia deposits exposed in wave-cut bluffs along the northern shore of Yellowstone Lake between Storm Point and Mary Bay provide evidence concerning the recent hydrothermal history of the northern lake area. Several sets of hydrothermal explosion deposits, representing the Indian Pond, Turbid Lake, and Mary Bay explosions, are intercalated with lake sediments and can be linked with explosive activity in this area over the past 14 ka (Fig. 10).

Indian Pond Hydrothermal Explosion Crater

Indian Pond is an oval, ~500-m-wide, lake-filled crater <1 km north of Yellowstone Lake (Figs. 4, 7, and 11). The crater is rimmed by an apron of explosion breccia that rises on the north and east sides ~11 m above the present-day water level of Indian Pond, and extends more than 600 m to the east-northeast (Fig. 11A). Low-resolution bathymetric surveys of Indian Pond (Yellowstone National Park, 1966) indicate the pond has steep inward-dipping slopes around its perimeter and has at least three elongate, east–west-trending basins or smaller craters on the crater floor (Fig. 11B). The average depth of the crater floor is ~13 m below current pond level; depths of smaller craters within the larger crater are 6–10 m. Lake level in Indian Pond is ~6 m above that of Yellowstone Lake.

Exposures of hydrothermal explosion deposits from the Indian Pond and Mary Bay craters overlie older lake sediment along Indian Pond creek and another incised drainage ~200 m to the west, referred to informally as Indian Pond Creek West. The Indian Pond explosion breccia is a poorly sorted, matrix-supported breccia deposit; the matrix is light-medium brown clay that has a pervasive greenish stain. Hydrothermal alteration minerals include cristobalite, albite, quartz, heulandite, clinoptilolite, and montmorillonite (Table 4). Lithic clasts in the breccia are generally angular to subangular and are composed primarily of cemented sand and gravel and include subordinate angular clasts of silicified lake sediment and well-sorted, fine-grained indurated goldish-tan siltstone (Figs. 11E and 11F). The maximum dimension of lithic fragments of cemented beach gravels and sands are up to 2 m at the crater rim. In the wave-cut benches along the north shoreline of Yellowstone Lake, Indian Pond lithic fragments are up to 30 cm long and average 3–7 cm.

The thickness of the Indian Pond breccia in the wave cut bench is less than 1 m. Northeast of the crater, thicknesses are estimated to be more than 4 m. Indian Pond deposits are not present in exposures 100–200 m southwest and west of the crater. This distribution suggests a nonsymmetrical explosion directed to the northeast, with minimal deposition to the west and southwest. A radiocarbon age on charcoal from the soil immediately below Indian Pond is 2895 yr (Table 2, Fig. 10), which probably closely dates the explosion.

Elliott's Crater

Elliott's crater is a large (>900 m diam) composite crater in northern Yellowstone Lake (Figs. 7 and 8), as well-illustrated in a north-south seismic reflection profile (Fig. 12A). Laminated lacustrine sediments accumulated on the floor of the crater and on its southern flank following the major explosive event that formed Elliott's crater more than 8 ka (Johnson et al., 2003). On the seismic profile, opaque zones within the stratified sedimentary crater fill probably indicate the presence of hydrothermal fluids and (or) gases (Johnson et al., 2003). Zones of seismic nonreflectivity on the floor and flanks of the large crater are interpreted as hydrothermally altered explosion-breccia deposits.

Outside the crater, seismic-reflection profiles indicate a hummocky ridge that extends for ~3 km south-southeast of Elliott's crater (Fig. 7) that is characterized by chaotic, nonreflective materials interpreted as an outflow breccia deposit derived from Elliott's crater (Johnson et al., 2003). If this interpretation is correct, these deposits indicate a directed blast of breccia to the south-southeast of the crater. The deposits overlie a buried rhyolite lava flow, which may account for some of the distinctive bathymetry of this deposit (Morgan et al., 2003, 2007a; Morgan and Shanks, 2005).

The northern rim of Elliot's Crater rises ~40 m above the flat-bottomed main crater floor whereas the southern crater rim is ~30 m above the crater floor. The elevation of the northern crater rim relative to the southern rim (Fig. 12A) may reflect (1) location of the crater on the edge of a rhyolitic lava flow (Morgan and Shanks, 2005), (2) sediment accumulation due to near-shore depositional processes, and/or (3) doming associated with hydrothermal inflation, as documented by Johnson et al. (2003) for other domes on the lake floor. Many smaller hydrothermal vents identified on the flanks of the explosion crater (Fig. 12A) provide evidence of ongoing hydrothermal activity over an area larger than the crater itself.

Younger explosion craters (100 to >300 m diam, 5–9 m deep) occur within the main crater floor near the southwest rim, indicating that younger explosion events followed the main explosive event. In the younger craters, hydrothermal vents actively

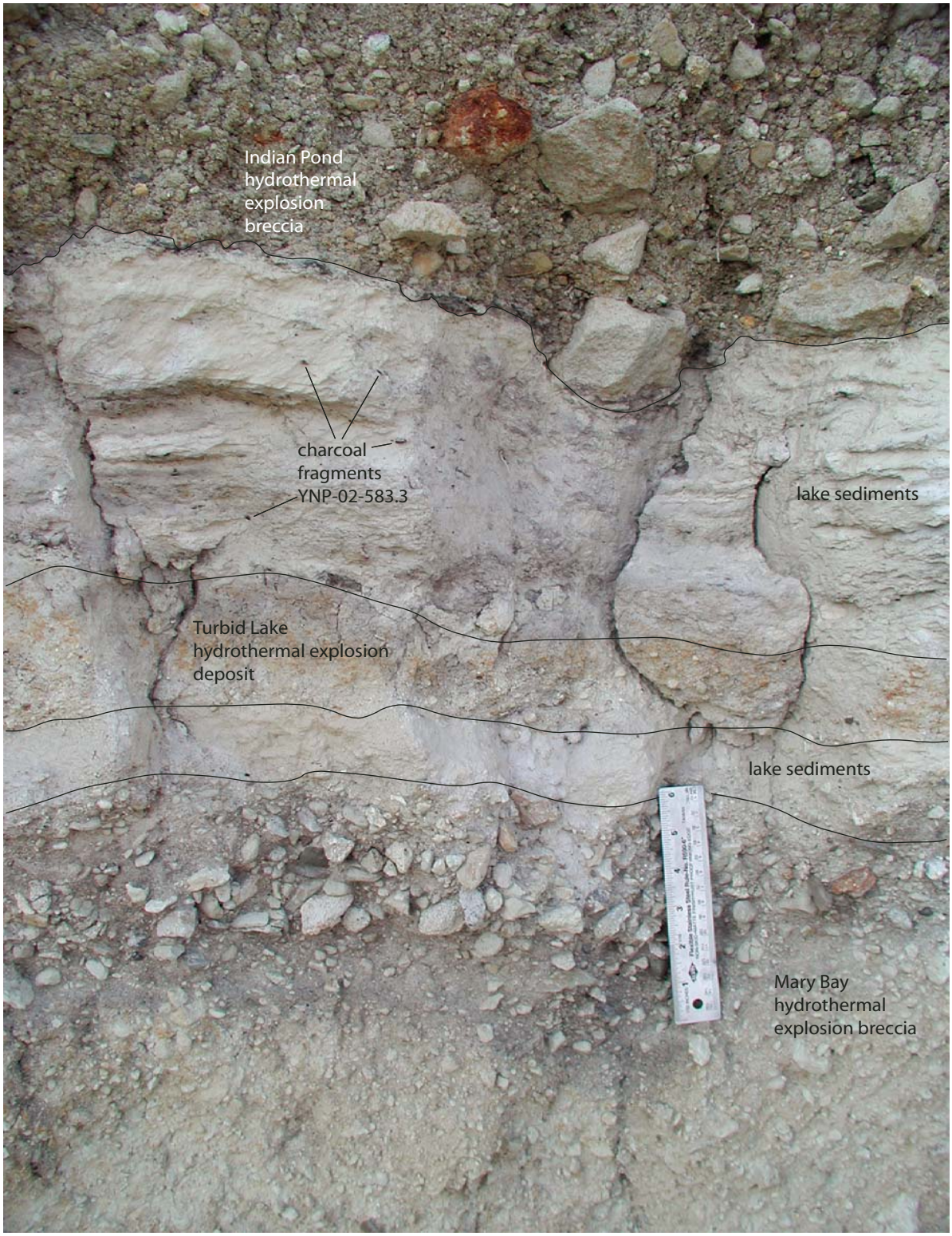

Figure 10. Explosion breccia stratigraphy in wave-cut terraces west of Mary Bay showing the Indian Pond, Turbid Lake, and Mary Bay explosion breccias intercalated with soils and lake sediments. Following the Mary Bay explosion event, deposition of lacustrine sediments continued until 9.4 ka when a distal facies of the Turbid Lake explosion breccia was deposited along the shores of northern Yellowstone Lake 4.5–5 km from the center of the Turbid Lake crater. This deposit is separated from the overlying Indian Pond explosion breccia by 25 cm of lacustrine sediments. Above this is a soil containing charcoal fragments with an age of ~3.1 ka, which is immediately overlain by 40 cm of greenish stained Indian Pond explosion deposit. The sequence is capped by 1.5–2 m of eolian sand. The Indian Pond deposit is the last major hydrothermal explosion deposit known in this area.

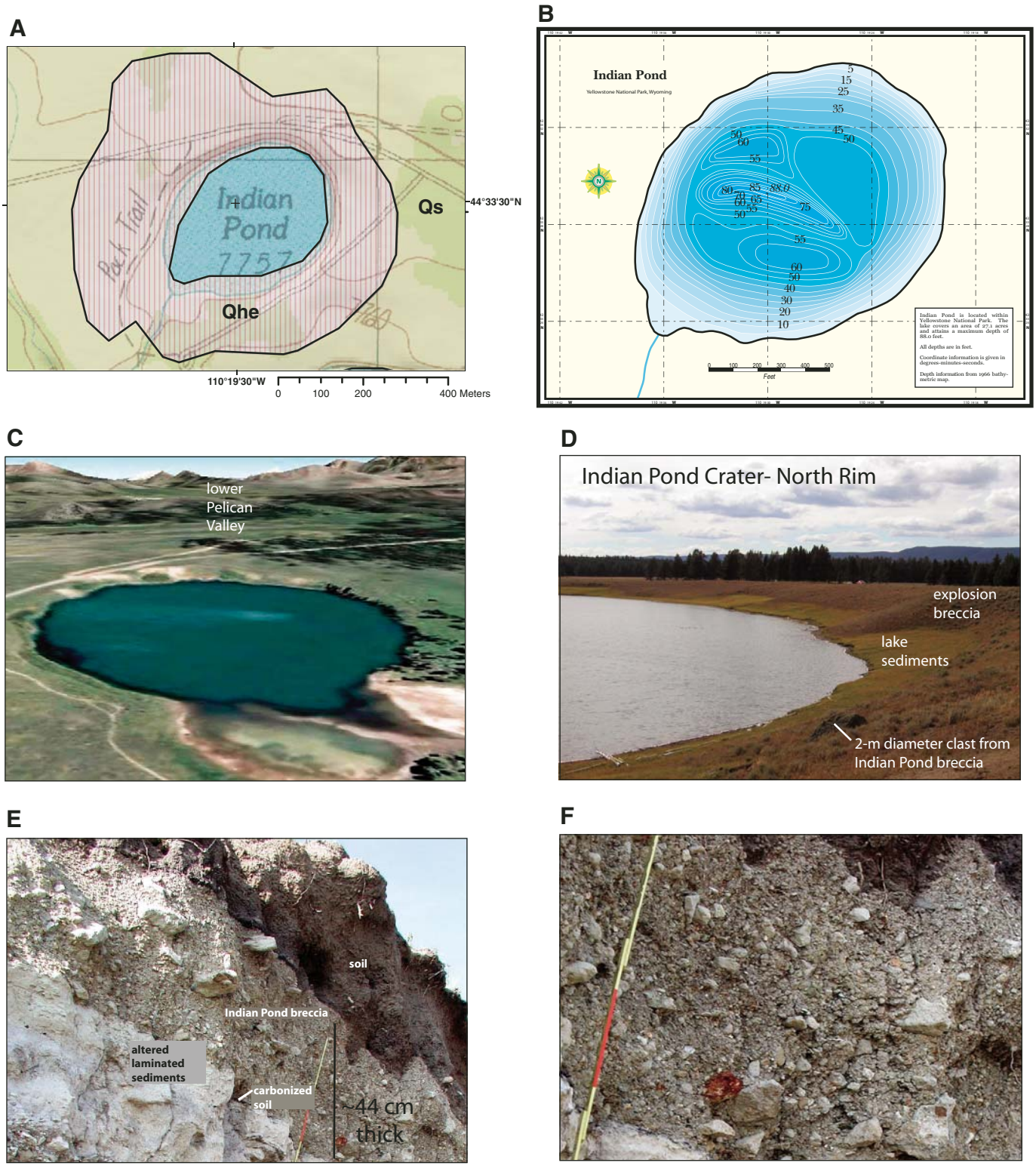

Figure 11. Indian Pond hydrothermal explosion crater. (A) Geological map after Christiansen (2001). Abbreviations for units are as follows: Qs—Quaternary sediments; Qhe—Quaternary hydrothermal explosion deposits. (B) Map prepared by Eric Wienckowski (2009). Bathymetric contours shown are in feet (modified from Fish and Wildlife Service, R. A. Hutchinson). (C) Google Earth perspective view of explosion crater looking north. Note prominent ejecta apron and steep inward dipping crater slopes. (D) Indian Pond crater north rim, looking west. (E) Indian Pond breccia deposit ~1 m thick in wave-cut bluff along north shore of Yellowstone Lake. (F) Close view of Indian Pond breccia deposit. Clasts are dominated by silicified beach sands.

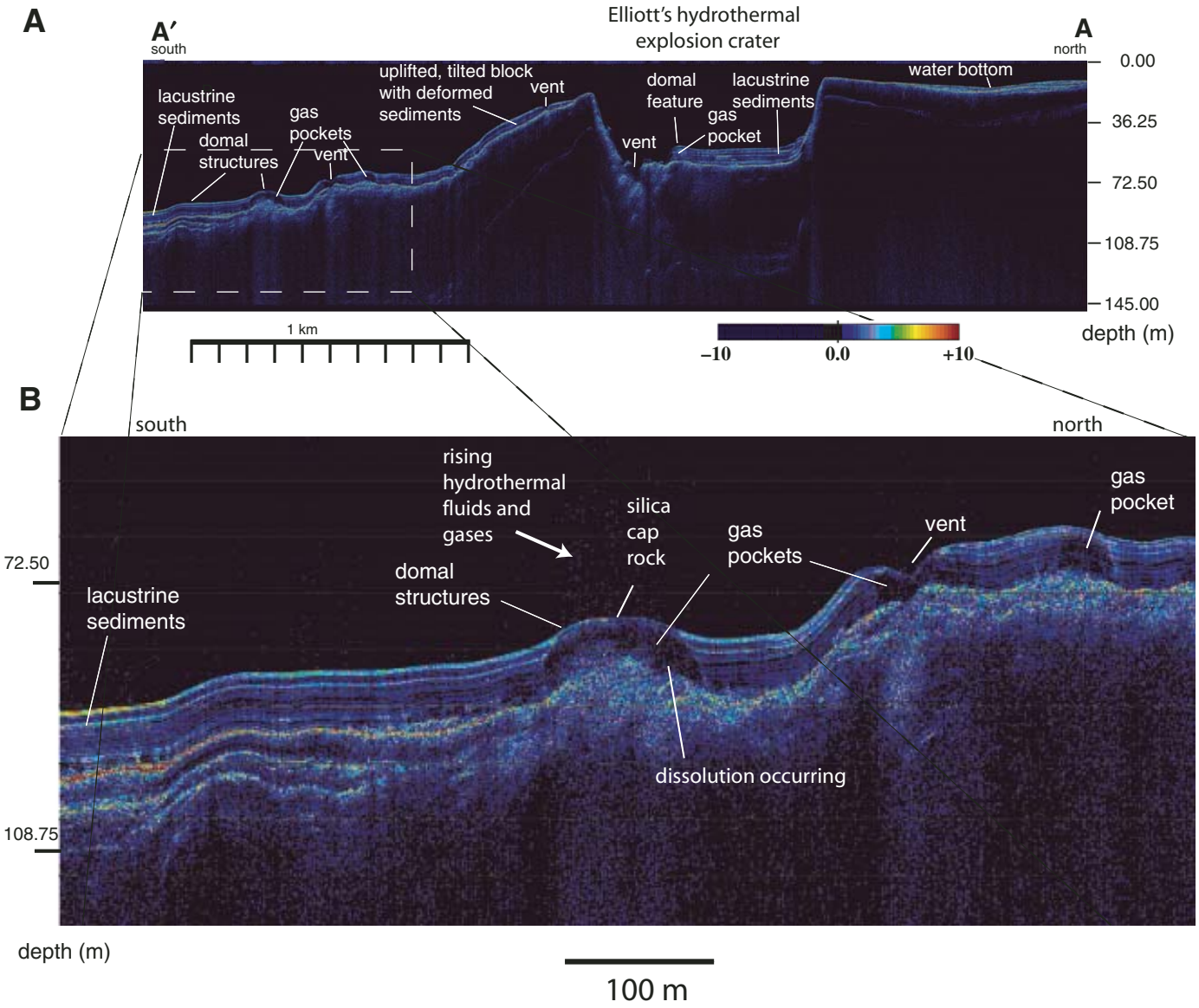

Figure 12. (A) North-south–trending seismic reflection profile through Elliott's crater, as depicted in Figure 8 as A-A′, shows precrater doming, steep crater walls, younger crater inside main crater, layered lake-sediment fill in crater, and minor vent craters and domes out of the main crater (Morgan et al., 2003). (B) Close-up image of Figure 12A highlighting the various domes on the lake floor in this area.

expel fluid with temperatures ranging from 51 to 91 °C, indicating continued thermal activity.

Along the southeast and eastern crater rim, outside the main crater, and more than 3 km from shore, a field of cobble- to boulder-sized, subrounded to angular rocks of varying lithologic compositions overlie lake sediment. This possible ejecta field was imaged by high-resolution seismic reflection profiles and directly observed and sampled using the ROV. These deposits are not mantled by younger lake sediment, and are therefore likely the product of very recent hydrothermal explosion events. Water depth near the southeast crater rim is ~20 m. Consequently, these deposits are at a depth too great to have been affected by surface wave action; thus the unsedimented rocks on the floor did not result from winnowing of fine lacustrine material by wave action.

Turbid Lake

Turbid Lake represents the second largest hydrothermal explosion crater in Yellowstone, its maximum diameter is greater than 1685 m and the crater covers an area close to 2.0 km^2 (Figs. 5 and 7, Table 1). Turbid Lake occurs along the eastern edge of the topographic margin of the Yellowstone caldera (Figs. 1 and 7) and is a compound hydrothermal explosion crater (Richmond, 1976; Muffler et al., 1971) composed of two primary craters

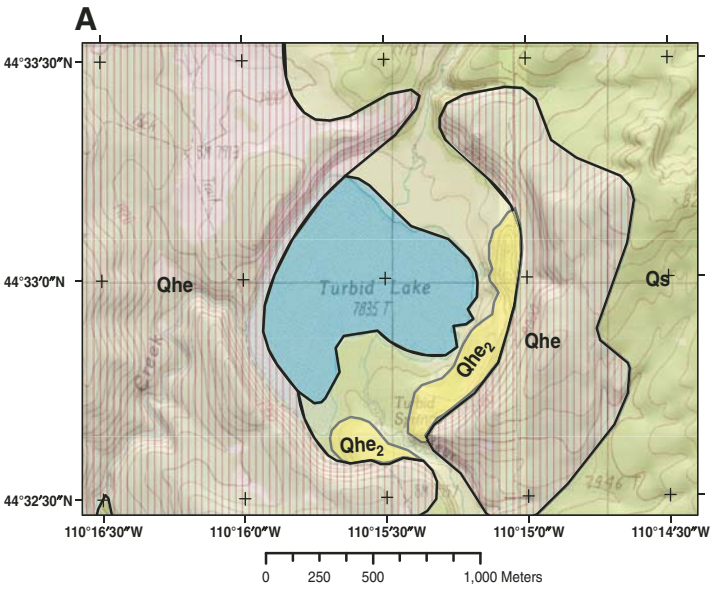
A
44°33′30″N
44°33′0″N
44°32′30″N
110°16′30″W
110°16′0″W
110°15′30″W
110°15′0″W
110°14′30″W
Qhe
Turbid Lake
7835 ft
Qhe2
Qhe
Qs
Qhe2
0
250
500
1,000 Meters


B
1675 m

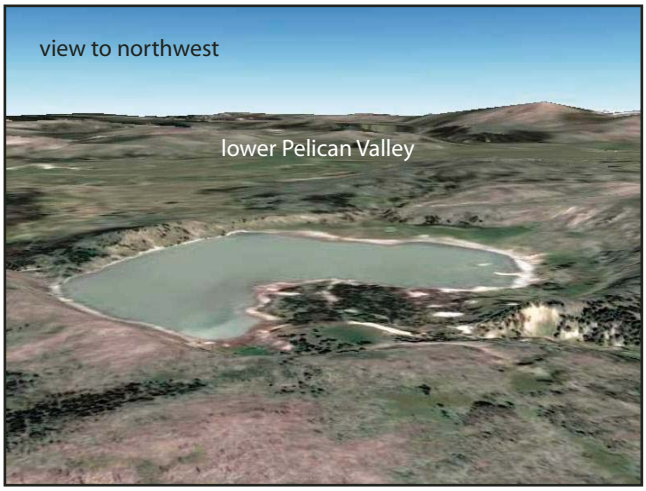
C
view to northwest
lower Pelican Valley


D

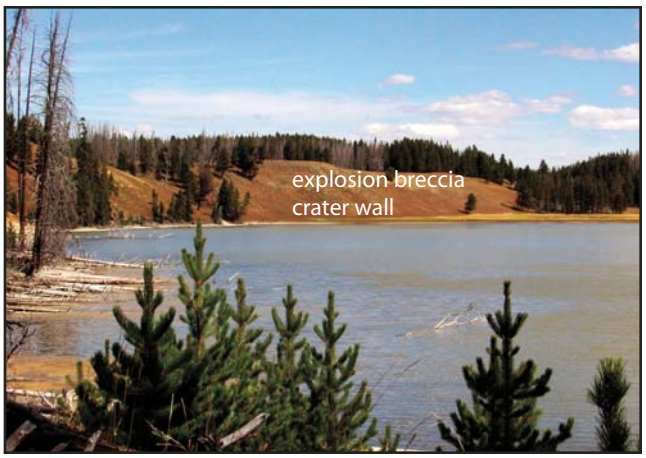
E
explosion breccia
crater wall


F
Turbid Lake explosion breccia

Figure 13. Turbid Lake hydrothermal explosion crater. (A) Geological map after Christiansen (2001). Abbreviations for units are as follows: Qs—Quaternary sediments; Qhe—Quaternary hydrothermal explosion deposits; Qhe_2—younger explosion breccia unit. (B) Google Earth vertical image of Turbid Lake with bathymetric contours (in feet) showing smaller craters on lake floor (bathymetric contours from Eric Wienckowski, 2009). (C) Google Earth perspective view of explosion crater looking north-northeast. Note prominent ejecta apron and steep inward dipping crater slopes. (D) Representative examples of breccia clasts from the Turbid Lake explosion breccia containing fragments of silicified Lava Creek Tuff collected along crater rim. (E) View north across Turbid Lake to crater rim composed of explosion breccia deposits. (F) Thinned Turbid lake explosion breccia deposits along wave-cut bluff, northern shore of Yellowstone Lake. Fragments are altered Lava Creek Tuff.

(Fig. 13). The larger primary crater is located in the main central part of the lake and is rimmed by an apron of explosion breccia that rises ~33 m above present lake level on its northern, western, and southern shores. Along its eastern edge, evidence for a younger second crater is preserved where a north-south–trending ridge of explosion breccia was deposited inside the main crater wall (Fig. 13B). The eastern main crater wall rises ~85 m above the present-day lake level. The main crater rim is breached on the north by the Sedge Creek inlet and on the south by the Bear Creek inlet. The west rim of the main crater is cut by Sedge Creek, which flows out of Turbid Lake and into northern Yellowstone Lake.

A reinterpolated map (Fig. 13B, Eric Wienckowski, 2009) of Turbid Lake floor based on a low-resolution bathymetric survey (Yellowstone National Park, 1975) indicates the lake has steep inward-dipping slopes around its central deep crater and contains multiple smaller craters at the periphery of the deep crater. Maximum water depth of the central crater is 42 m; water depths of smaller craters range from 5 to 17 m for craters along the northern and western edges of the main crater to as deep as 27 m in craters along its eastern edge (Table 1).

Hydrothermal explosion breccia is exposed along the banks of Sedge Creek and varies in thickness from 2 to 10 m. The matrix-supported breccia contains lithic clasts of subangular fragments of hydrothermally altered Lava Creek Tuff, gravels and sands cemented by hydrothermal silica, moderately to poorly sorted sulfidic sandstones, cemented pebble conglomerate, and chalcedonic breccia (Fig. 13D). The explosion breccia matrix is whitish, fine-grained clay. Charcoal fragments from immediately beneath the hydrothermal explosion deposit north of Bear Creek high on the southern crater rim have a corrected radiocarbon age of 9.4 to 9.5 ka (Pierce et al., 2002a, 2007a).

Acidic hot springs vent along the eastern and southeastern crater rim; mud pots along the southeastern lake shore have pH values of 1.1–1.5 and temperatures of 49–57 °C. Lake water as a whole has a pH value of 2.5–3.4 and temperatures of 21–24 °C, as sampled in 2002 and 1998, respectively (Gemery-Hill et al., 2007). The water level in Turbid Lake is ~31 m above that of Yellowstone Lake.

As noted by Muffler et al. (1971), a broad constructional outer ramp of hummocky explosion debris deposit slopes away from Turbid Lake toward the northwest and may indicate the primary flow direction of mud-rich slurry breccia. The explosion breccia may extend northwest and west as much as 4.5 km from its source. An exposure in the wave-cut terraces along Mary Bay includes a thin (27 cm), fine-grained, white clay that contains small angular clasts of Lava Creek Tuff (Fig. 13F). This deposit is overlain by lake sediments and Indian Pond explosion breccia and overlies lacustrine sediments and the Mary Bay explosion breccia (Fig. 10). The white clay deposit contains small fragments of charcoal, which have been mineralized and are therefore not suitable for dating. Analyses of charcoal samples from lacustrine sediments immediately above this exposure yield an age of 4325 ^{14}C yr B.P. (Table 2). Because this unit is bracketed between the Indian Pond and Mary Bay explosion breccia deposits, is below lake sediments that are 4300 yr old, and contains Lava Creek Tuff as its dominant clast type, we conclude that this is a distal facies of the Turbid Lake explosion breccia deposit. This deposit occurs about 4.6 km from the Turbid Lake crater rim.

Mary Bay Hydrothermal Explosion Crater

The Mary Bay hydrothermal explosion crater has formed a large embayment in the northern basin of Yellowstone Lake (Fig. 8A). The crater has a maximum diameter of 2.8 km (Table 1) making it the largest documented feature of this type in the world (Browne and Lawless, 2001). The central part of the crater shows clearly in the bathymetric image of the lake floor in Mary Bay (Fig. 7). The Mary Bay hydrothermal explosion crater extends subaerially northeast from the northern basin of Yellowstone Lake, where steep (~30° slope), 30–40-m-high cliffs expose explosion breccia in the upper part of the crater wall northeast of Yellowstone Lake (Fig. 7). The crater rim is ~50 m above lake level. On the floor of Yellowstone Lake, a well-defined crater rim incises the 6–8-m-deep platform shelf by ~10–15 m along the southern rim (Fig. 7), producing a relatively flat-bottomed crater at ~20 m water depth in the southern and western portions of the crater. Smaller, individual vent craters within the main, flat-bottomed crater are as deep as 35 m; consequently the total water depth to the bottom of individual craters is ~55 m, and the total relief from the rim to the bottom of the deepest crater is ~105 m.

The Mary Bay explosion crater is a complex of dozens of coalesced smaller craters within the larger main crater. Solids and hydrothermal vent fluids from many of these craters have been sampled at depths up to 53 m below lake level. Vent fluid temperatures generally range from 35 to 95 °C and pH values range from 4.9 to 6.6 (Shanks et al., 2005; Balistrieri et al., 2007; Shanks et al., 2007; Gemery-Hill et al., 2007). The predicted hydrostatic boiling temperature in the deep part of the Mary Bay crater is ~160 °C (Fig. 6B, Shanks et al., 2005; Balistrieri et al., 2007). ROV measurements indicate that fluids from one deep hydrothermal vent in Mary Bay have temperatures near the 120 °C limit of the temperature probes used. This is consistent

with previously determined values of extremely high heat flow in this area (Morgan et al., 1977).

Mary Bay hydrothermal explosion breccia. Exposures of the Mary Bay breccia deposit dominate the 4- to 5-m-high bluffs along the north shore of Yellowstone Lake, west of Mary Bay. The breccia deposit consists of a fine-grained, poorly indurated matrix that supports subangular clasts of hydrothermally altered rock fragments of various compositions that range from a few cm to >2 m in maximum diameter. Wave erosion of the cliff due to northeast-prevailing winds has produced a beach littered with lithic clasts derived from the Mary Bay deposit.

Size and lithology of Mary Bay breccia clasts were documented systematically in well-defined areas along the beach platform at three different sites (Fig. 7): (1) east of a fossil sublake-bottom hydrothermal vent system informally called Black Dog, (2) west of Black Dog, and (3) at a promontory informally called Little Storm Point. At each site, all clasts larger than 10 cm were described, counted, and measured in the area from the base of the bluff to the water line for a distance of ~75 m (Fig. 14). The most abundant clast types are quartz-phyric rhyolite, cemented well-sorted sand, cemented pebble conglomerate, cemented gravel conglomerate, chalcedonic silica, and chalcedonic silica breccia. Included in the chalcedonic silica breccia are silicified lake sediments and silicified lake sediment breccias. Many fragments are up to 1 m in maximum dimension and some are >2 m. The average maximum dimension of lithic fragments is slightly greater east of Little Storm Point (Fig. 7). Large boulders, greater than 2 m in maximum dimension, of cemented fluvial gravels, quartz-phyric rhyolite, and Tertiary trachyandesite are present along the shore east of Little Storm Point. Clasts have maximum diameters of 2.5 m on the exposed cliffs of the crater rim to the east.

All clasts, regardless of lithology, are cemented by silica and some are intensely silicified. Some also contain sulfide minerals. Less commonly identified lithic fragments include (Fig. 14) banded hydrothermal vein fragments of chalcedony, quartz, and calcite as well as brecciated felsite containing vugs filled with euhedral quartz and pyrite (Table 4). Many lithic clasts, at all locations along Mary Bay and in the Mary Bay bluffs, contain radial, prismatic thermal cracks, which indicate that the fragments were very hot and rapidly cooled upon being ejected (Figs. 15A, 15I–15N). Based on ages of charcoal and Glacier Peak ash in conformable lake sediments beneath the Mary Bay explosion deposit and the relationship of the Mary Bay eruption to the Yellowstone Lake shoreline sequence, the Mary Bay explosion occurred about 13 ka (Pierce et al., 2002a, 2007a).

Detailed stratigraphic observations of the Mary Bay breccia deposit indicate: (1) A large volume (>0.03 km^3) of mud, clay, and lithic fragments were ejected from the explosion crater complex and that some of this ejecta extends as muddy breccia-bearing flow deposits at least 3 to 4 km from its source crater complex (Fig. 8B). (2) Ejecta from the explosion fell and flowed from the explosive column, some falling back into the main crater. In some cases, this "fall back" onto the crater rim created channels in which ejecta deposits now fill. (3) Fragmental

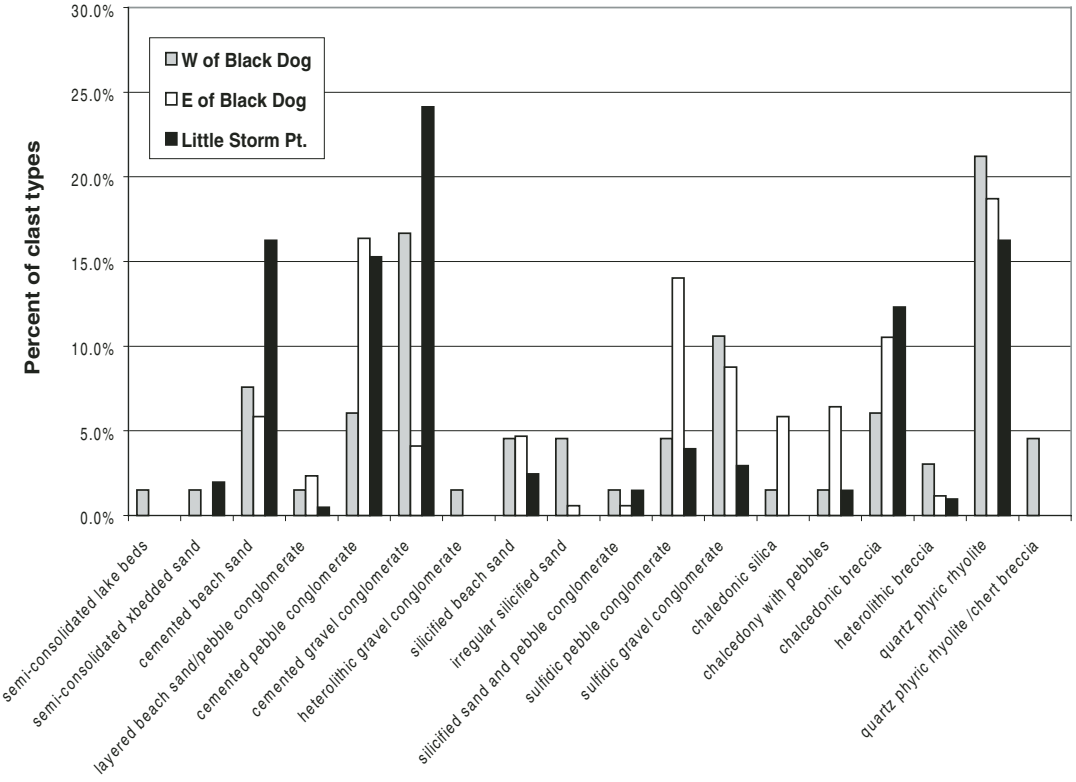

Figure 14. Types of lithic clasts from the Mary Bay hydrothermal explosion breccia based on systematic clast counts at three exposures along the northern shore of Yellowstone Lake. Lithic clast classification and lithic count sites were west of the Black Dog breccia pipe (gray), east of Black Dog (white), and farther east at Little Storm Point. Dominant lithic clasts in the Mary Bay breccia include a unique quartz-phyric rhyolite, cemented sands and gravel conglomerates, and chalcedony (chalcedonic silica) clasts and breccias. Clasts of Tertiary volcanic rocks also are present, but in minor amounts.

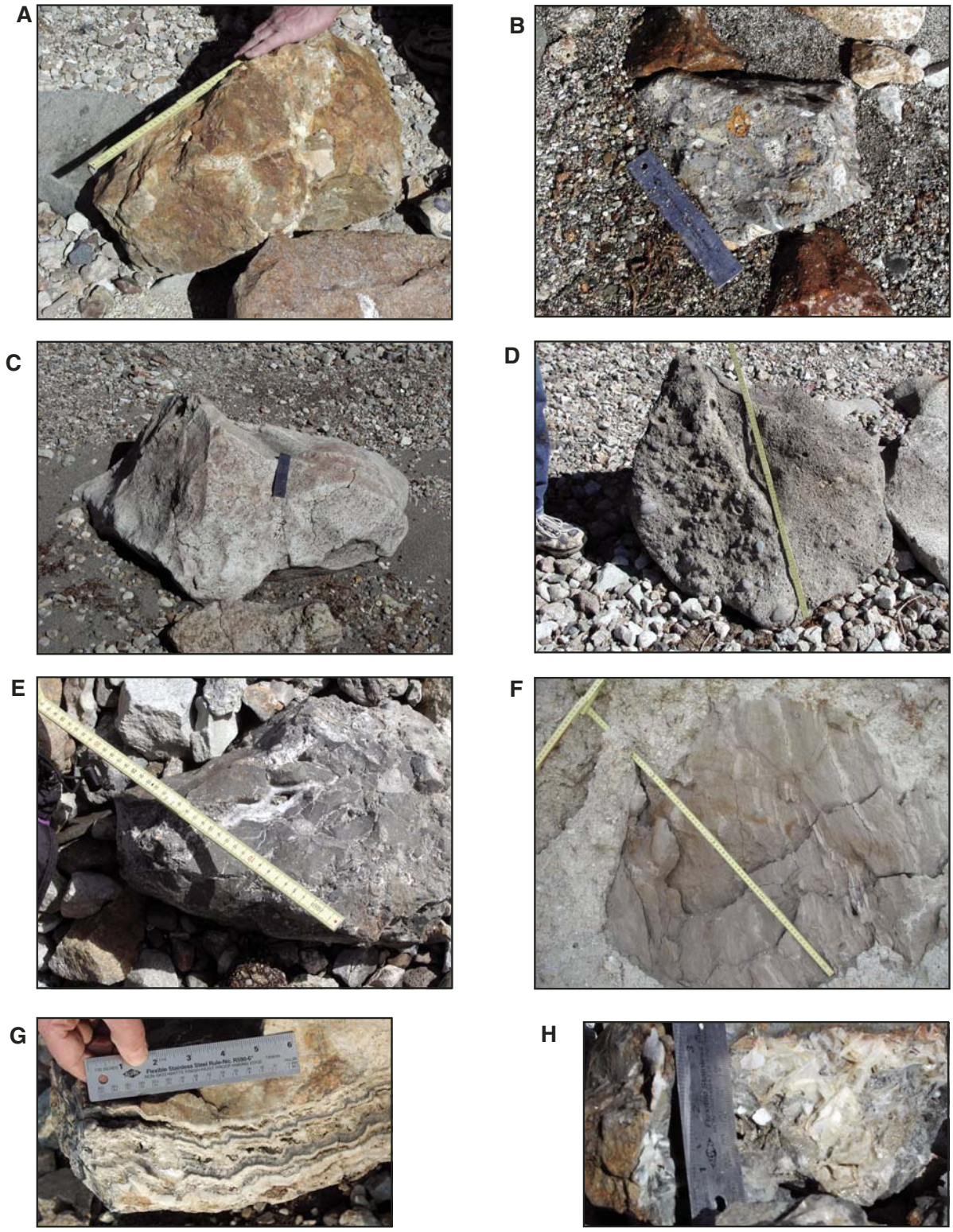

Figure 15 (*on this and following page*). Photos of lithic clasts from the Mary Bay hydrothermal explosion deposit. (A) Heterolithic clast with sulfide oxidation and multigenerational breccia. (B) Heterolithic clast containing matrix-supported fragments of silicified lake sediments, chalcedony, rhyolite, gravel, and sulfidic rhyolite in a silicified and pyritized matrix. (C) Clast of rhyolite with thermal cracks and dissolved quart phenocrysts. (D) Clast of silicified beach gravels and sands. (E) Clast of black chalcedony with cross-cutting veins of quartz. (F) Meter-sized clast of soft-bedded dark sand containing microfaults in Mary Bay breccia deposit. (G) Banded chalcedony vein filling matrix of rhyolite breccia. (H) Calcite crystals in cavity of multigenerational breccia.

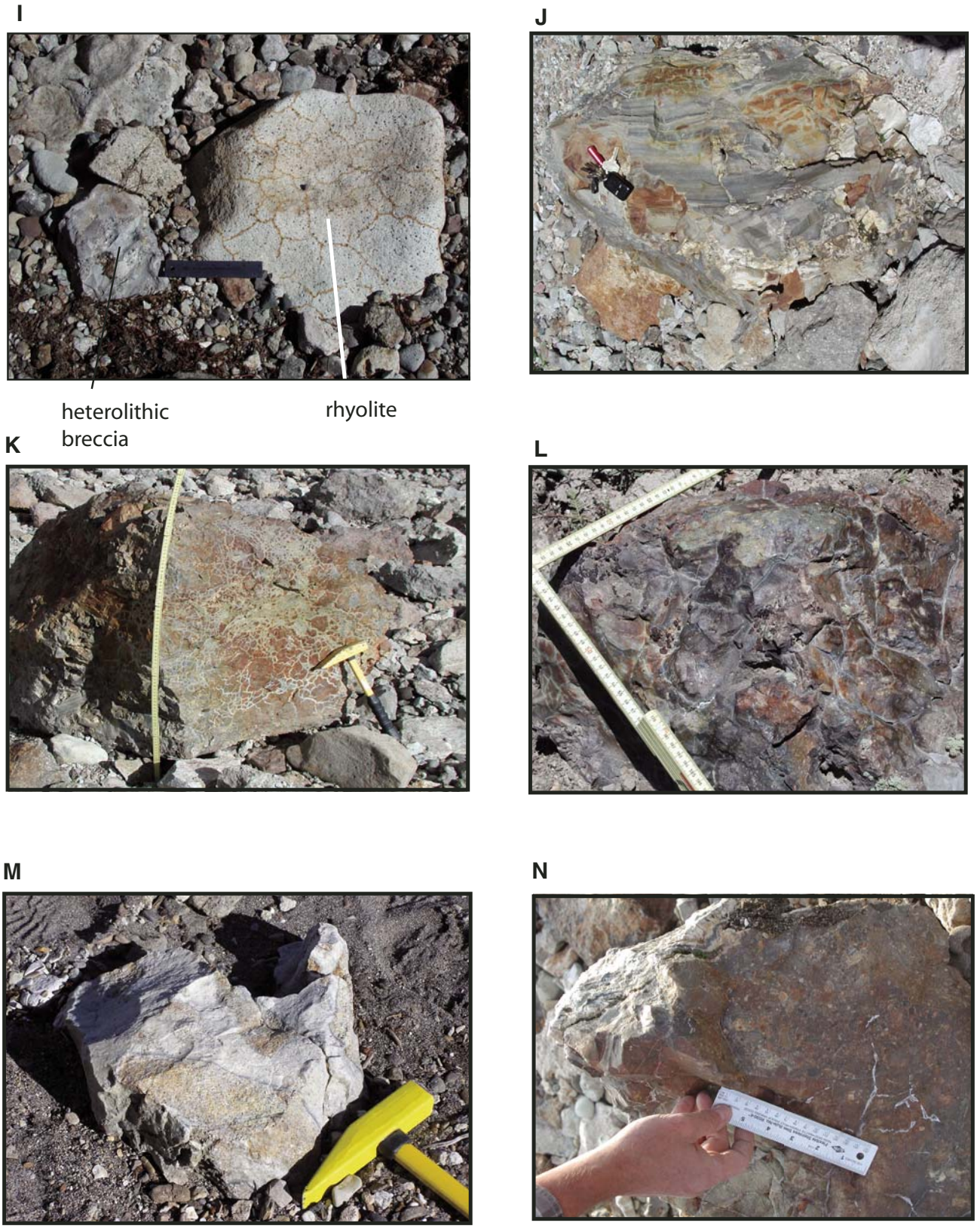

Figure 15 (*continued*). (I) Clasts of heterolithic breccia and rhyolite; note the thermal cracks in the rhyolite clast. (J) Clast of silicified and sulfidic lake sediments with thermal cracks and cross-cutting quartz veins. (K) Clast of silicified lake sediments with thermal cracks. (L) Thermal cracks in a clast of chalcedony. (M) Multigenerational rhyolitic breccia clast. (N) Silicified, multigenerational breccia clast.

material cross-cut underlying lake sediments and created dike-like ramps and sill-like injections on the margins of the ramps (Fig. 3H, breccia-filled fractures). (4) Previously unrecognized, hydrothermally altered rhyolitic lava flow(s) are present as lithic ejecta fragments (Morgan and Shanks, 2005). (5) A nearly continuous sheet of mixed-to-sorted sand and gravel occurs at the base of the Mary Bay explosion breccia deposit and is ascribed to large seismic-event waves that immediately preceded the hydrothermal explosion (Fig. 16). A thinner, sedimentary unit similar in character to this variable-appearing sand and gravel is present within the explosion breccia deposit and may suggest the generation of another large seismic-event wave immediately preceding a slightly later hydrothermal explosion (Fig. 17). Lacustrine and near-shore sediments are intercalated in the Mary Bay breccia deposit and may represent a few decades of time between successive explosion events, based on the thickness and character of the interbedded laminated sediment. (6) Some lithic fragments are multigenerational breccia clasts and represent repeated fragmentation within an active hydrothermal system and thus we infer that the Mary Bay hydrothermal system was active for quite some time prior to its explosion.

The Mary Bay explosion deposit (Figs. 7 and 8B) is distributed from its crater rim ~3.5–4 km to the northwest and ~2.5–3 km to the northeast; in the subaerial environment it covers ~30 km^2. Measured sections (Fig. 18) indicate how the Mary Bay deposit changes in thickness and clast size and distribution radially away from its crater source. Near source, at the crater rim, the deposit is at least 15 m thick and contains lithic clasts of

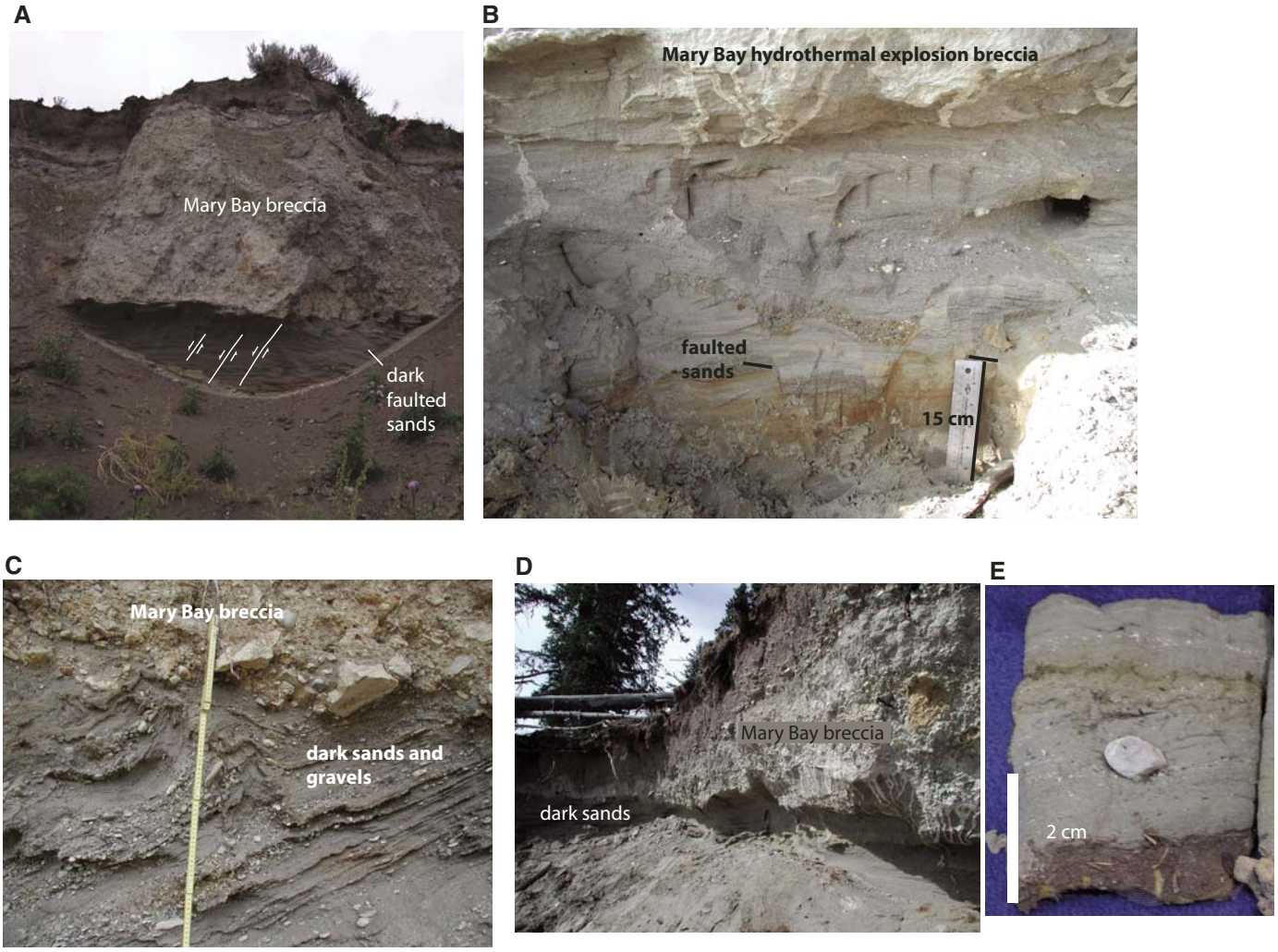

Figure 16. Photographs of dark sand that may represent a large wave deposit related to and immediately under the Mary Bay explosion deposit. (A) Exposure west of Mary Bay of the 5-m-thick Mary Bay breccia deposit overlying 80 cm of dark faulted sands. Lensoidal pattern is due to exposure; the unit is roughly tabular here. (B) Close-up image of faulted sands and pebbles underlying the Mary Bay breccia shows the variability within a single exposure as well as the fining and thinning of individual beds within the exposure. (C) Exposure of dark bedded sand and pebbles under the Mary Bay breccia deposit along Little Indian Pond Creek West. (D) Exposure of dark faulted sands beneath the Mary Bay breccia due east of Black Dog breccia pipe. (E) Photograph of tsunami peal from the December 26, 2004 tsunami event in Indonesia.

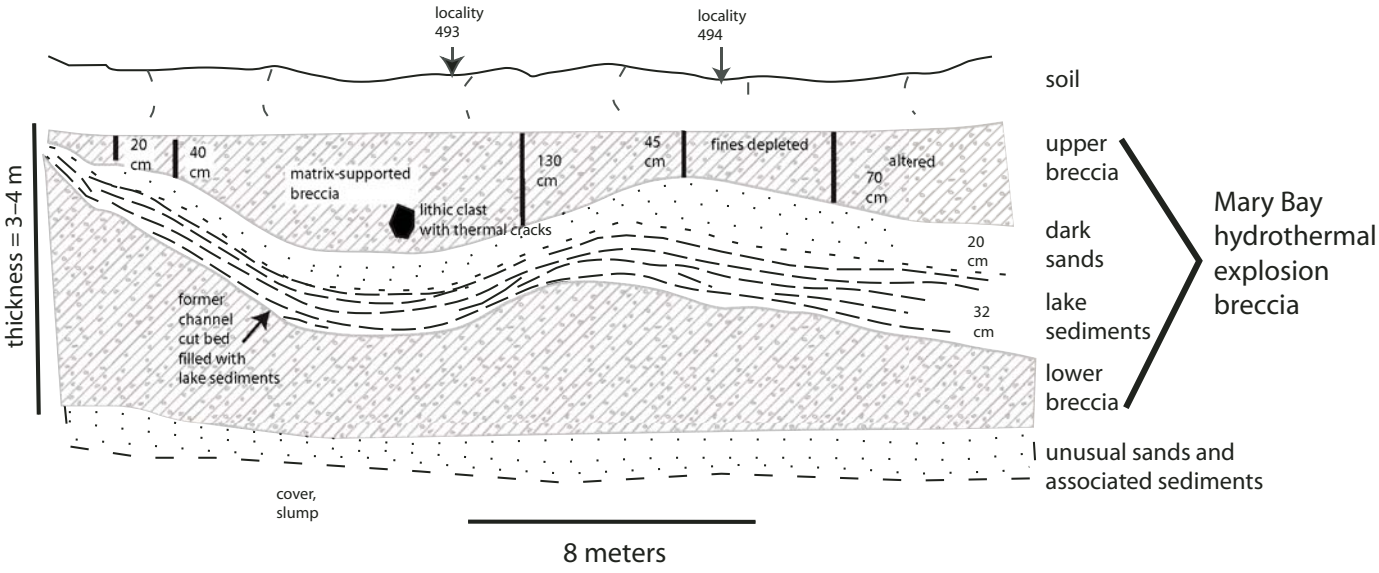

Figure 17. Schematic cross section of localities 493 and 494 showing an exposure along the northern shore of Yellowstone Lake where the two main phases of the Mary Bay hydrothermal explosion event are separated. The lower breccia is underlain by a fine- to coarse-grained sand to pebble deposit interpreted to be associated with triggering of the initial explosion event. Development of the Mary Bay hydrothermal explosion crater occurred over perhaps as long as several years to a few decades (based on the thickness of the intercalated lake sediments) and had several breccia-forming explosions indicated by the separation of upper and lower breccia with an intervening erosional surface overlain by ~50 cm of lake sediments. The unusual sand at the base of this section and the fine-bedded sand below the upper breccia may represent large wave deposits associated with the explosion event.

varying compositions and clasts as large as 2.5 m in maximum dimension. A block of hydrothermally altered basaltic andesite, similar to that found in the nearby Tertiary Absaroka Range, is ~12-m long × 1.5-m wide and may be related. A 4-m-long × 3-m-wide block of heterolithic breccia is contained nearby in the same exposure of the explosion breccia. Both of these clasts are much larger than other coarse (1 to 2 m maximum dimension) clasts in the exposure and may not be a part of the deposit but are mentioned here to note their presence.

At its distal exposures, along the bluffs of Pelican Creek (Fig. 18, site 1), the Mary Bay breccia includes two distinct units which together have a thickness of 57 cm. A thin (15 cm), upper horizon is a clast-supported, fines-depleted, box-work breccia in which clasts comprise ~30%–40% of the total rock volume; clasts are subrounded and most are less than 2 cm in maximum dimension. The lower horizon is a thicker (~35 cm), matrix-supported, mud-rich, and poorly sorted breccia deposit. It contains ~5%–10% lithic clasts that are subrounded and generally 1 to 2 cm in maximum dimension. Many of the clasts are the distinctive altered quartz-phyric rhyolite, providing a positive identification of this unit as the Mary Bay explosion deposit. The matrix of this lower unit is composed of vesicle-bearing mud with subordinate obsidian sand. A gradational contact separates the units. Deposits included in this exposure may have been emplaced as a single hydrothermal explosion flow unit that physically segregated during emplacement. At this location, the breccia deposit overlies massive, fine-grained, well-sorted, dark obsidian-rich sand that is 5–8 cm thick. The dark sand overlies a thick sequence of lacustrine sediment. We interpret the dark sand as being equivalent to the variable sand and gravel exposed beneath the Mary Bay deposits exposed in the wave-cut cliffs along the northern shore of Yellowstone Lake.

Multiple events associated with the Mary Bay hydrothermal explosion. At localities 493 and 494 along the northern shore of Yellowstone Lake (Figs. 7, 17, and 18), stratigraphic variations in the Mary Bay explosion breccia indicate a temporal hiatus between the initial Mary Bay explosion event and a later event. The Mary Bay breccia contains intercalated sedimentary units, including a 32-cm-thick sequence of lacustrine sediment overlain by 20 cm of fine-grained, dark obsidian sand (Fig. 17). Based on the thickness of these old deposits and sedimentation rates in Yellowstone Lake (Johnson et al., 2003; Otis, 1975; Otis et al., 1977), we estimate that several years to a few decades may have passed between the first explosion event, which deposited vast quantities of explosion breccia, and a second, somewhat smaller explosion event. A channel cut into the lower breccia and filled with lake sediments provides strong evidence for two events (Fig. 17). Evidence of multiple explosion events in the explosion breccia deposits is consistent with the composite nature of the Mary Bay hydrothermal explosion crater complex (Morgan et al., 2003, 2007a, 2007b). Alternatively, this lacustrine layer is inclined and is finer than the sandy sediment above and below the explosion deposit and may represent a slab of lake sediment from deeper in the section and ripped up by the explosion.

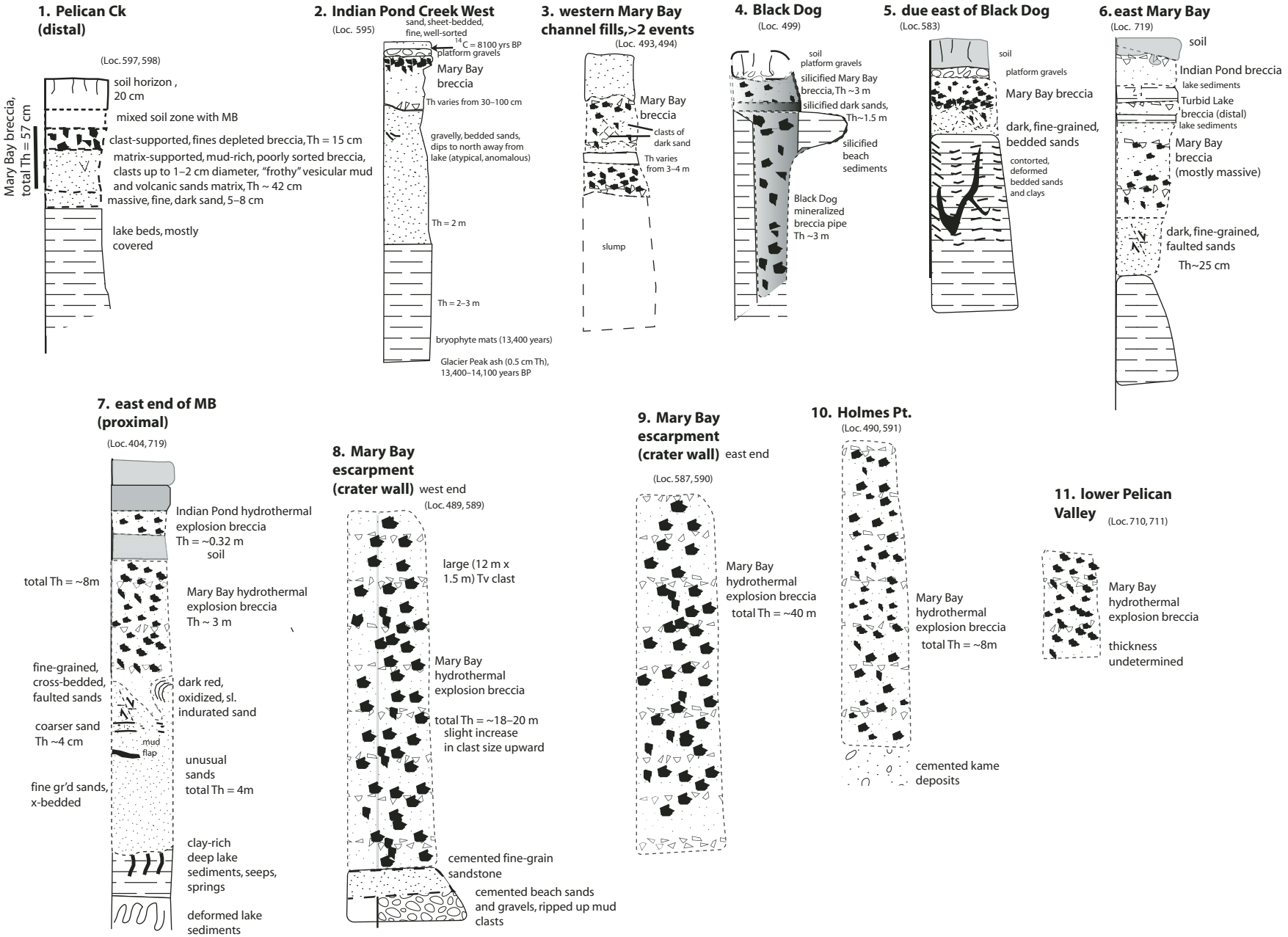

Figure 18. Composite sections of 11 exposures of the Mary Bay explosion breccia along the northern shore of Yellowstone Lake, Pelican Valley, and vicinity showing the variability in the appearance of the Mary Bay breccia. Figure 7 gives individual site localities of the sections. The Mary Bay hydrothermal explosion breccia deposit is bracketed primarily by lake sediments and soils, depending on the locality, and breccia thickness and lithic clast size decreases with distance from the crater. Th—thickness.

Breccia-filled fractures along the original Mary Bay crater wall. Wave-cut terrace exposures on the northern shore of Yellowstone Lake change dramatically on an annual basis due to variations in the intensity of storm wave activity. Early in this study (1996), several exposures along the northern shore between Storm Point and Mary Bay revealed thick Mary Bay breccia deposit exposures that appear to be bounded by near-vertical contacts (Fig. 19) (Morgan et al., 1998). The geometry of deposits exposed in these bluffs may represent a combination of two separate processes: (1) ejected material falling from the explosive column back into the explosion crater whose rim included excavated channels (Fig. 19A), and (2) breccia being injected into fractures formed along these channels by explosion events (Figs. 19B, C, D, and F).

Preexisting hydrothermal system(s) prior to large explosion event at Mary Bay. The precrater host rocks beneath Mary Bay were repeatedly brecciated and hosted an active, well-developed hydrothermal system prior to the Mary Bay explosion. Evidence

Figure 19. Exposures of the Mary Bay breccia deposit along the wave-cut terraces west of Mary Bay in 1997. (A)–(D) show unusually thick exposure of Mary Bay breccia consisting of a ramplike feature with sharp contacts with lake sediment (1.6 m person for scale). (C), (E), and (F) show details of contact zones showing interfingered Mary Bay breccia and lake sediments, and breccia filling fractures.

from the lithic clasts in the breccia deposits (Fig. 15) includes: extensive mineralization and alteration, multigenerational breccias and veins, fluid inclusion data indicating a hydrothermal system with temperatures as high as 294 °C, and "thermal cooling contraction cracks" in many clasts (Morgan et al., 2006). Lithic clasts of Mary Bay breccia (Figs. 14 and 15) contain a wide range of rock types including beach and alluvial sand, platform or alluvial gravel, deep lacustrine sediment, monolithic breccia, heterolithic breccia, chalcedony, and quartz-phyric rhyolites; all are intensely silicified. Many breccia clasts show evidence of repeated fragmentation (Fig. 15N). The assemblage of lithic clasts in the explosion breccia reflects the stratigraphic section that hosts the Mary Bay explosion crater. All these rock types have been hydrothermally altered with cryptocrystalline silica (chalcedony and/or cristobalite), sulfide minerals, chlorite, abundant vein calcite, and euhedral quartz- and pyrite-filled vugs and boxwork breccias. Some samples contain kutnahorite, $MnCa(CO_3)_2$ (Morgan et al., 1998) along with other contained carbonate minerals; this suggests that CO_2 was an important constituent of the mineralizing fluids.

Hydrothermally altered breccias ejected from deep within a hydrothermal system constrain preexplosion subsurface conditions. One heterolithic breccia that was analyzed for fluid inclusions contains clasts of igneous rocks with abundant quartz phenocrysts and fragments of preexisting breccia cemented by a matrix of wairakite and calcite (Skewes, 2000, written commun.). Wairakite crystals, restricted to the breccia matrix, contain up to 40 mol% analcime, which reflects high silica and high sodium contents in the protolith (Bird et al., 1984). Calcite precipitated after wairakite suggests that Ca and/or CO_2 content in the hydrothermal fluids increased with time (Skewes, 2000, written commun.). Primary fluid inclusions in wairakite (Fig. 20)

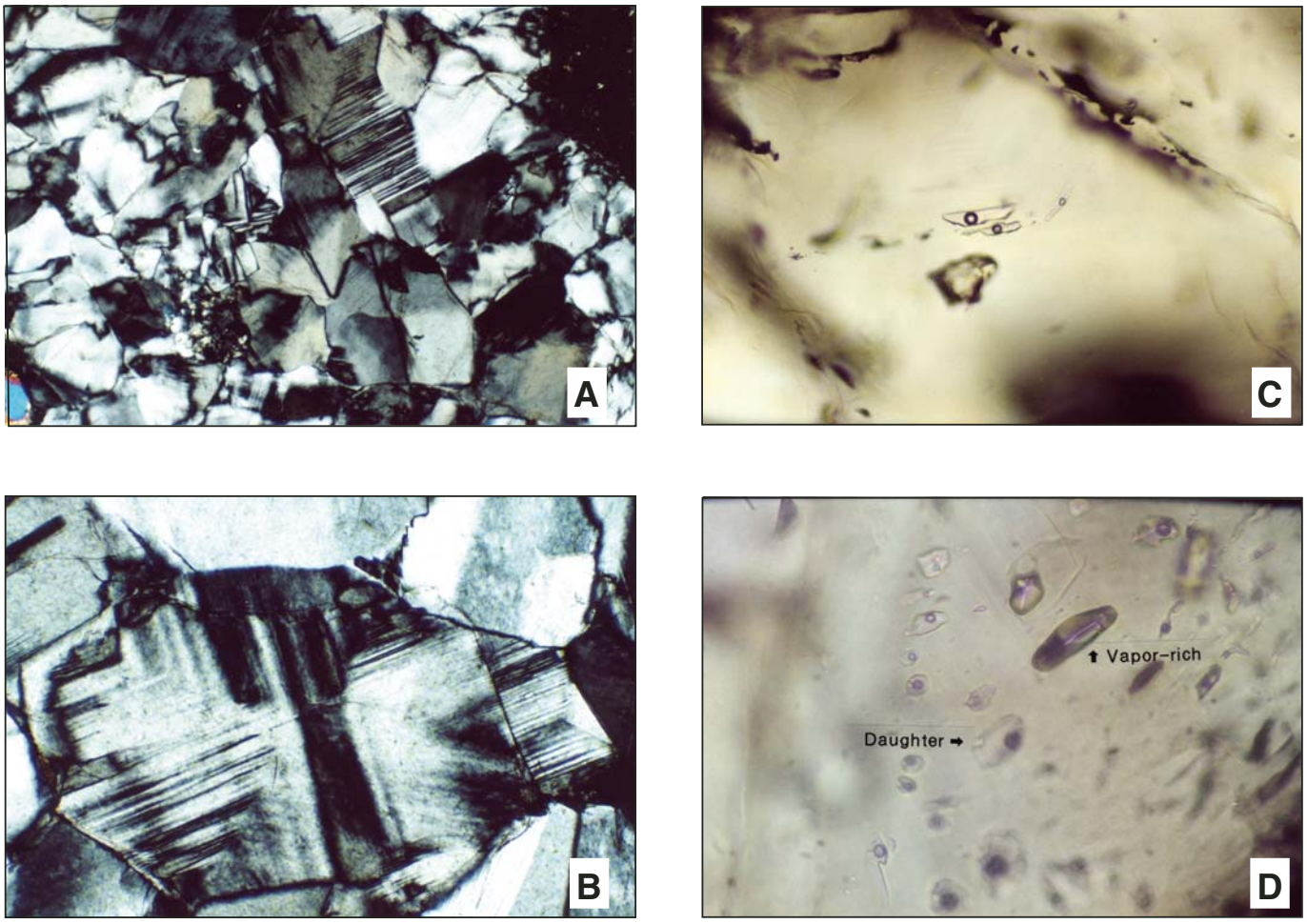

Figure 20. (A) Photomicrograph of the matrix of breccia sample YNP-98–299.2 formed by wairakite crystals with their distinctive lamellar twinning. Field of view = 5.5 mm × 3.7 mm. (B) Close-up of lamellar twinning in A. Field of view = 1.32 mm × 0.89 mm. (C) Photomicrograph of fluid inclusions in wairakite crystals from the matrix of the breccia sample in Figures 19A and 19B. The most common type of liquid-rich inclusion is shown. Field of view = 0.4 mm × 0.27 mm. (D) Vapor-rich inclusions coexist with liquid-rich inclusions in wairakite crystal, suggesting that this set of inclusions was trapped from boiling fluids. The liquid-rich inclusions also have an unidentified birefringent daughter mineral. Field of view = 0.28 mm × 0.19 mm. (From Alexandra M. Skewes, written commun., 2009.)

indicate temperatures between 228 °C and 294 °C, <3 wt% NaCl, and low CO_2 content. These temperatures imply entrapment at depths between 180 m (lithostatic pressure) and 540 m (hydrostatic pressure) (Fig. 6B). Fluid inclusions have liquid-vapor ratios consistent with entrapment as a single-phase fluid, indicating that the hydrothermal fluids were not boiling.

Mapping of paleoshorelines indicates that the lake level was ~17 m above the present lake level at the time of the Mary Bay explosion at ~13 ka (Pierce et al., 2002a, 2007a). We estimate that the volume of water in Yellowstone Lake was roughly 33% greater than today based on the calculations by Kaplinski (1991) for present-day volume.

High-resolution bathymetric and aeromagnetic data indicate that an unnamed rhyolite unit in the lower Pelican Valley (Morgan et al., 2003; Finn and Morgan, 2002; Morgan and Shanks, 2005) extends into the northern basin of Yellowstone Lake, including Mary Bay. Sanidine crystals from clasts of hydrothermally altered, quartz-bearing rhyolite yield a $^{40}Ar/^{39}Ar$ age of 600 ± 20 ka (W.C. McIntosh, 2002, written commun.). Another rhyolitic multigenerational breccia clast contains two distinct populations of sanidine crystals which may each have been derived from a distinct source in the lower Pelican Valley area; $^{40}Ar/^{39}Ar$ data for these two sanidine groups indicate: (1) an older 500 ka rhyolite and (2) a younger 200-ka rhyolite (W.C. McIntosh, 2002, written commun; Morgan and Shanks, 2005). The younger of these may be equivalent to the ~180-ka rhyolite of West Thumb, exposed nearby to the west along the Yellowstone River (Fig. 8). Rhyolite clasts in the Mary Bay breccia appear to be derived from a buried unit (the unnamed rhyolite in lower Pelican Valley, ~500–600 ka) that underlies the lower Pelican Valley and extends into the northern lake basin, and at least one additional rhyolite lava flow (~200 ka) buried by glacial, alluvial, and explosion deposits in the same vicinity.

Major and minor element abundances and stable isotope composition of quartz-phyric rhyolite clasts from the Mary Bay explosion breccia (Table 3) indicate that these rhyolites are similar to other rhyolites of the Yellowstone Plateau as well as the Lava Creek Tuff. Their rare-earth element patterns (Fig. 21) are similar to those of the Lava Creek Tuff and the rhyolitic lava flows of the Plateau Rhyolite.

Sand beds underlying the Mary Bay explosion breccia. A sedimentary sequence exposed in wave-cut cliffs north of Yellowstone Lake provides additional insight into the Mary Bay hydrothermal explosion event. A sequence of lake sediments overlain by the Mary Bay hydrothermal explosion deposit is separated locally by an unusual dark, well-sorted, sheet-bedded (low-angle) to cross-bedded, fine-grained sand to coarser pebble deposit. The physical characteristics and thickness of the unit below the Mary Bay explosion breccia are quite variable between exposures and the degree of sorting, bedding, and grain size are distinct relative to those of other beach-related sands exposed along the lakeshore. Cross-beds in the deposit are at a very low angle to the sheet-like bedding and may indicate sheet flow of sand in traction.

The sand deposit shows considerable variability, especially with respect to grain size, at different locations and in relation to the overlying Mary Bay explosion deposit (Figs. 16 and 19). The sand varies from a fine-grained (<2 mm) obsidian-rich, predominantly black to medium gray near locality 583 (Figs. 7 and 16B) to a coarser (clasts as large as 2–3 cm), less sorted, and somewhat thicker deposit at locality 595 (Fig. 7). At some exposures along Indian Pond Creek West and near its outlet along the northern shore of Yellowstone Lake, the degree of sorting decreases and the deposit contains 2–4 cm rounded pebbles of rhyolite (Fig. 16C). Here, the unit is bedded and includes alternating fine and coarse units; some horizons contain locally derived platform gravels. At this location, the unit is strongly cross-bedded, with dips as much as 25°–30° northward, away from Yellowstone Lake. Its contact with the overlying Mary Bay explosion deposit is undulatory. At other localities along the northern shore of Yellowstone Lake, exposures contain numerous small normal faults with offsets of several centimeters (Figs. 16A and 16B). At the most distal exposure along the upper banks of Pelican Creek (Fig. 18, site 1), the underlying sand is massive, very fine grained, well-sorted, and thin (5–8 cm).

Near-source facies of the Mary Bay breccia deposit contain large (up to 2.0 m in diameter), rounded clasts of nonindurated, fine-grained, bedded sand, some containing small faults (Fig. 15F). The sands clasts appear to be derived from the dark, bedded, and faulted sand that is exposed immediately below the lower Mary Bay breccia (Figs. 16 and 17). The cohesiveness of these clasts, given their softness relative to the hardness of other lithic clasts in the breccia, is remarkable and suggests: (1) limited interaction between clasts during emplacement and (2) proximity to source. At a few sites, the sand clasts show evidence of fragmentation upon emplacement (Fig. 15F). The nonindurated sand clasts are the only nonmineralized clast type contained in the breccia.

The sand units are coextensive with and below most of the Mary Bay explosion deposit and are present in nearly all exposures north and west of Mary Bay crater including along the north shore of Yellowstone Lake, Little Indian Pond Creek west drainage, and Pelican Creek. It is not recognized along the bluffs that form the crater wall northeast of Mary Bay or to the east but this may be due to preexisting topographic highs.

Based on the sedimentary structures and bedforms present in addition to the distribution and changes in thickness, the underlying sand deposits were likely deposited by an atypical large wave or series of waves, possibly due to a surge produced by an earthquake-generated wave on Yellowstone Lake or the hydrothermal explosion. Seismic activity, in tandem with the passing of a large wave may have been important in triggering the explosion of a sealed hydrothermal system located in what is now the Mary Bay crater complex. Small-scale faults that cut the sand indicate that seismic deformation continued after deposition of the sand (Figs. 16A and 16B).

The sand deposits that underlie the Mary Bay explosion deposit have many characteristics similar to those of known tsunami deposits (Fig. 16E) (Atwater et al., 1995; Chague-Goff

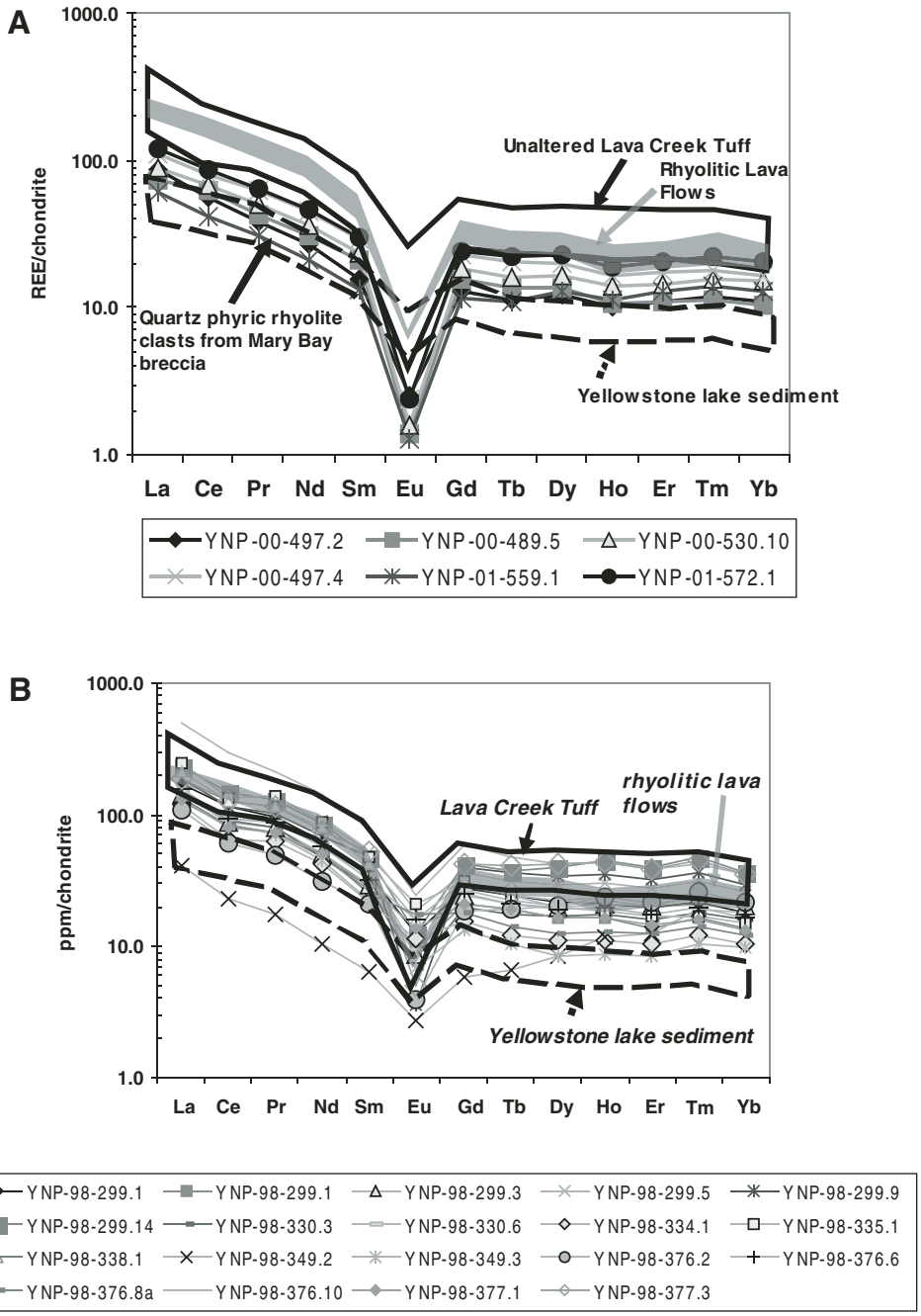

Figure 21. (A) Rare-earth element (REE) patterns for quartz-phyric rhyolite clasts from the Mary Bay explosion breccia deposit, showing they have the same pattern as unaltered rhyolites, but shifted to lower REE contents due to silicification and alteration. Ranges of values for Lava Creek Tuff, postcaldera rhyolitic lava flows, and deep-water sediments from Yellowstone Lake are given for comparison. (B) Rare-earth element patterns for other lithic clasts from Mary Bay and other hydrothermal explosion breccias. Ranges of values for Lava Creek Tuff, postcaldera rhyolitic lava flows, and deep-water sediments from Yellowstone Lake are given for comparison. Some chalcedonic silica clasts and breccias plot in the unaltered rhyolite field, suggesting they may be pervasively silicified rhyolites.

et al., 2002; Hawkes et al., 2007; Shiki et al., 2008). The characteristics include sharp lower contacts, fining and thinning upward, low-angle cross bedding (sheet bedding), and inclusion of coarser, locally derived clasts (Figs. 16B and 16E). In addition, multiple sets of units show evidence of reversals of current directions (Fujiwara, 2008). In coastal marine environments, the presence of marine faunal assemblages (foraminifera, clam shells) in layers within brackish or freshwater sediments is a key indicator of tsunami-generated deposits. Around Yellowstone Lake, we lack such indicators. Nonetheless, the geologic and sedimentological characteristics of the underlying sand, summarized above, suggest that these deposits may be from large waves related to the seismic activity that may have contributed to triggering the hydrothermal explosion.

Other Hydrothermal Explosion Craters North of Yellowstone Lake

Sulfur Hills hydrothermal explosion crater. An area of extensive hydrothermal alteration, known as Sulfur Hills for its abundant and active hot springs, fumaroles, and related sulfur

precipitates, is located north of Yellowstone Lake, atop the Sour Creek resurgent dome (Fig. 1). White, ice-contact hydrothermal deposits (Christiansen, 1975), sinter, and the products of acid hydrothermal alteration cover an area of ~2 km^2 capping the south-central portion of Sour Creek dome (Fig. 22). Reconnaissance mapping indicates that this area includes two large (~250–300 m diam) hydrothermal explosion craters, each rimmed by an apron of explosion breccia. The craters have steep, inward sloping, unvegetated crater walls. The explosion breccia deposit contains clasts of rounded stream gravel composed of rhyolite, sand grains of obsidian, and angular clasts of porcellanite in a silica-cemented matrix. Our observations and those of Christiansen (2001) suggest that the obsidian is most likely fragments of the Lava Creek Tuff, which underlies this site. Much of the explosion breccia debris surrounding the two craters is littered with lithic fragments ejected from the craters or smaller springs. In the western crater, north- to north-northeast–trending fissures or fractures host concentrations of fumaroles that are up to 50–75 m long. The morphology of these features suggests that they are very young, possibly postdating the Indian Pond explosion event.

Neither of these explosion craters contains water, most likely due to having an elevation >160 m above the nearby terrain and having a porous crater floor. Perhaps the craters are so young that the sinter has not altered to clay that would contribute to an impermeable layer on the crater floor. Active sulfur-depositing fumarolic activity associated with these craters is abundant. Fumarolic sulfur may derive from boiling thermal waters at depth, with oxidation of H_2S at the surface by atmospheric O_2 leading to native sulfur precipitation. Where steam is abundant, H_2O and H_2S react to create sulfuric acid. Vermillion Spring, at the base of Sulfur Hills to the south, was sampled in July 1998 and had a temperature of 53 °C and a pH of 2.3 due to acid sulfate processes.

Pervasive acid sulfate alteration assemblages are observed at Sulfur Hills. Outcrops of Lava Creek Tuff exposed immediately below the explosion craters have been variably altered by acidic hydrothermal processes; hard silicified rocks are common at the tops of the systems and kaolinite-rich alteration assemblages occur lower in the section.

Fern Lake hydrothermal explosion crater. The Fern Lake hydrothermal explosion crater is 10 km north-northeast of the Sour Creek resurgent dome at the edge of the Canyon flow, an older (483 ka) post-Yellowstone caldera rhyolitic lava flow (Muffler et al., 1971; Christiansen, 2001) (Fig. 1). The Fern Lake crater is oval-shaped and is ~500 m × 900 m; low-resolution bathymetric surveys indicate that the lake is ~8 m deep (Yellowstone National Park, 1975) (Fig. 23). The crater is rimmed by heavily vegetated, explosion breccia debris. Breccia fragments from the hydrothermal explosion deposit are silicified and contain subangular fragments of rhyolite, porcellanite, fine-grained sediment, and mineralized rock. The deposits are dominantly composed of quartz, orthoclase, clay minerals, and an unidentified green mineral (Figs. 4D and 24A, 24B). Chemical analyses of these fragments during scanning electron microscopy (SEM) examination indicate that they contain minor abundances of Pb, Sn, Cl, ±S and associated $CuCO_3$ phases (Table 3). Breccia fragments also contain pyrite, talc, and colliform silica (opal, cristobalite). The lead-, tin-, and copper-bearing minerals suggest that the explosion event incorporated fragments from deeper parts of an associated hydrothermal system (Morgan et al., 1998). Silicified wood fragments, pine needles, charcoal, and twig molds within the Fern Lake explosion breccia deposit indicate the area was at least partly forested at the time of the hydrothermal explosion. Radiocarbon dating of the charcoal has not been successful due to the silicification of the charcoal. Given the shallow depth of the lake, its smooth bottom, and heavy vegetative cover of the crater rim, the Fern Lake hydrothermal explosion crater is most likely relatively old (>10 ka?) but postglacial (<16 ka). No ice-contact hydrothermal deposits are known in the area. Thermal seeps were identified along the southeastern edge of the lake (Figs. 7 and 23A, 23B) and a spring sampled in July 2001 had a temperature of 44 °C and a pH of 5.5.

Hot Spring Geyser Basin. The Hot Spring Geyser Basin, along the northeastern edge of the Yellowstone caldera (Fig. 1), contains a large hydrothermal explosion crater (Prostka et al., 1975; Werner et al., 2000; Christiansen, 2001; Werner and Brantley, 2003). The crater is ~300 m × 250 m in diameter and is rimmed by explosion breccia deposits (Fig. 25). The crater is not water filled and current activity indicates its recent formation. The breccia deposit contains subangular to angular clasts of hydrothermally altered Lava Creek Tuff, Tertiary volcanic rock, fluvial sandstone, and sinter, porcellanite, and mineralized rock fragments. Numerous, large (>3 m) irregularly shaped ejecta blocks litter the crater rim; many of these blocks themselves contain large (up to 0.5 m) angular clasts (Figs. 25E and 25F). The crater is partly surrounded by active fumaroles and hot springs. Water in a thermal pool that occupies a small explosion crater a few hundred meters east of the main explosion crater had temperatures up to 86 °C, pH of 1.5, and sulfate concentration of 1000 mg/L when collected in July 1999. Acid sulfate altered rock is prevalent throughout the Hot Springs Geyser Basin area. Intense subsurface dissolution has created sinter capping hollow ground.

West Thumb Geyser Basin

Duck Lake Hydrothermal Explosion Crater

Duck Lake has long been recognized as a postglacial hydrothermal explosion crater (Muffler et al., 1971; Richmond, 1973; Christiansen, 2001) (Figs. 1, 8A, and 26). Its dimensions are ~700 m × 500 m (Table 1); the crater is ~20 m deep and is rimmed by an apron of hydrothermal explosion breccia that stands ~30 m above lake level. Duck Lake is ~0.6 km northwest of West Thumb Geyser Basin at the edge of the Dry Creek rhyolite lava flow. Water in Duck Lake is perched ~15 m above Yellowstone Lake level (Fig. 26A).

Water from the south-central edge of the crater has a pH value of 5.0, when sampled on July 20, 1998. Bubbles rising to

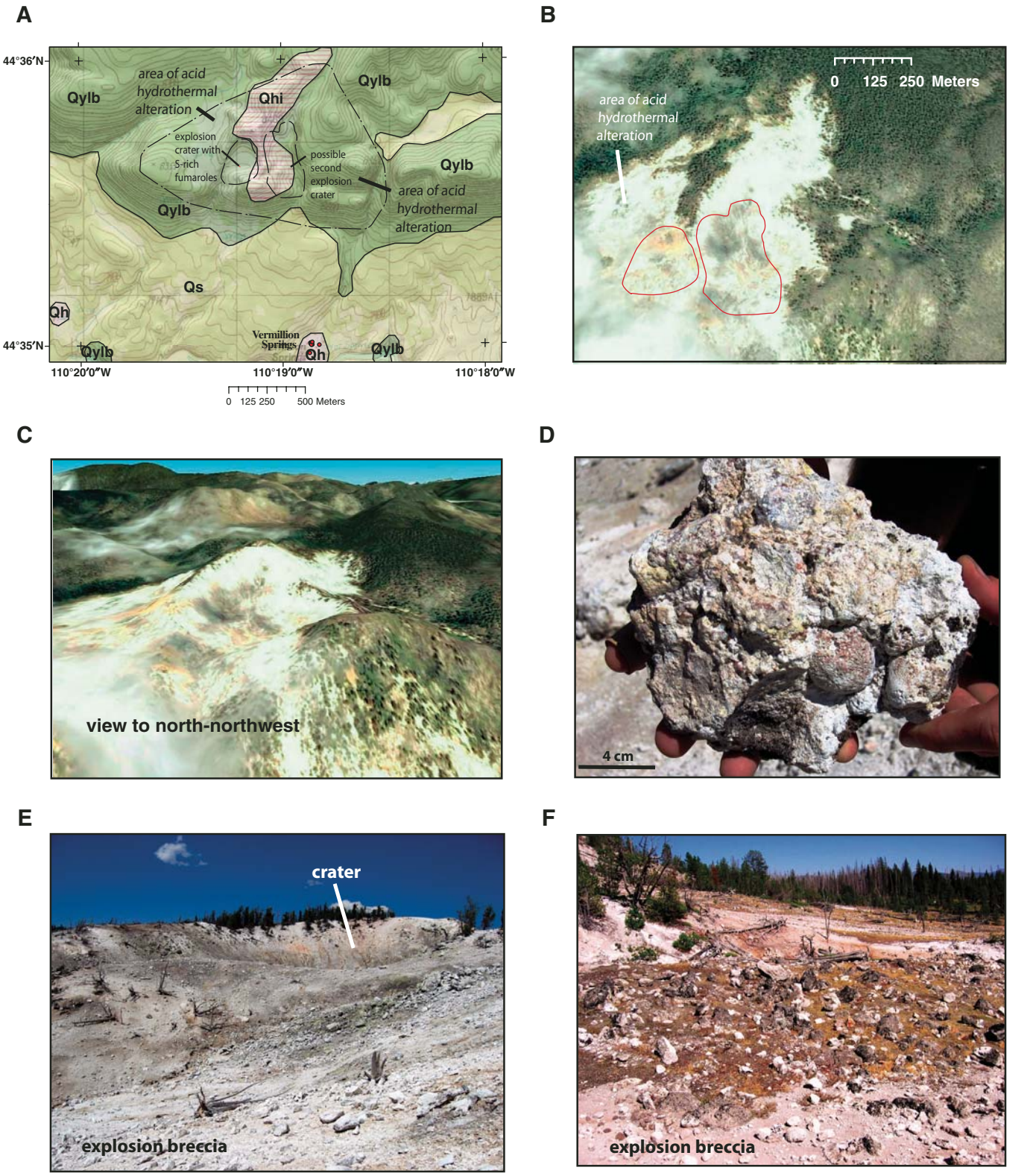

Figure 22. Sulfur Hills hydrothermal system and explosion craters on north flank of Sour Creek dome. (A) Geological map after Christiansen (2001). Abbreviations for units are as follows: Qs—Quaternary sediments; Qhi—Quaternary ice contact hydrothermal deposits; Qh—Quaternary hydrothermal deposits; Qylb—Lava Creek Tuff, member B. (B) Google Earth vertical image of Sulfur Hills. (C) Google Earth perspective view of explosion crater looking north-northwest. (D) Hydrothermally cemented ice-contact gravel. (E) View north into western hydrothermal explosion crater. Note prominent ejecta apron and steep inward dipping crater slopes. (F) Area of breccia fragments along crater rim.

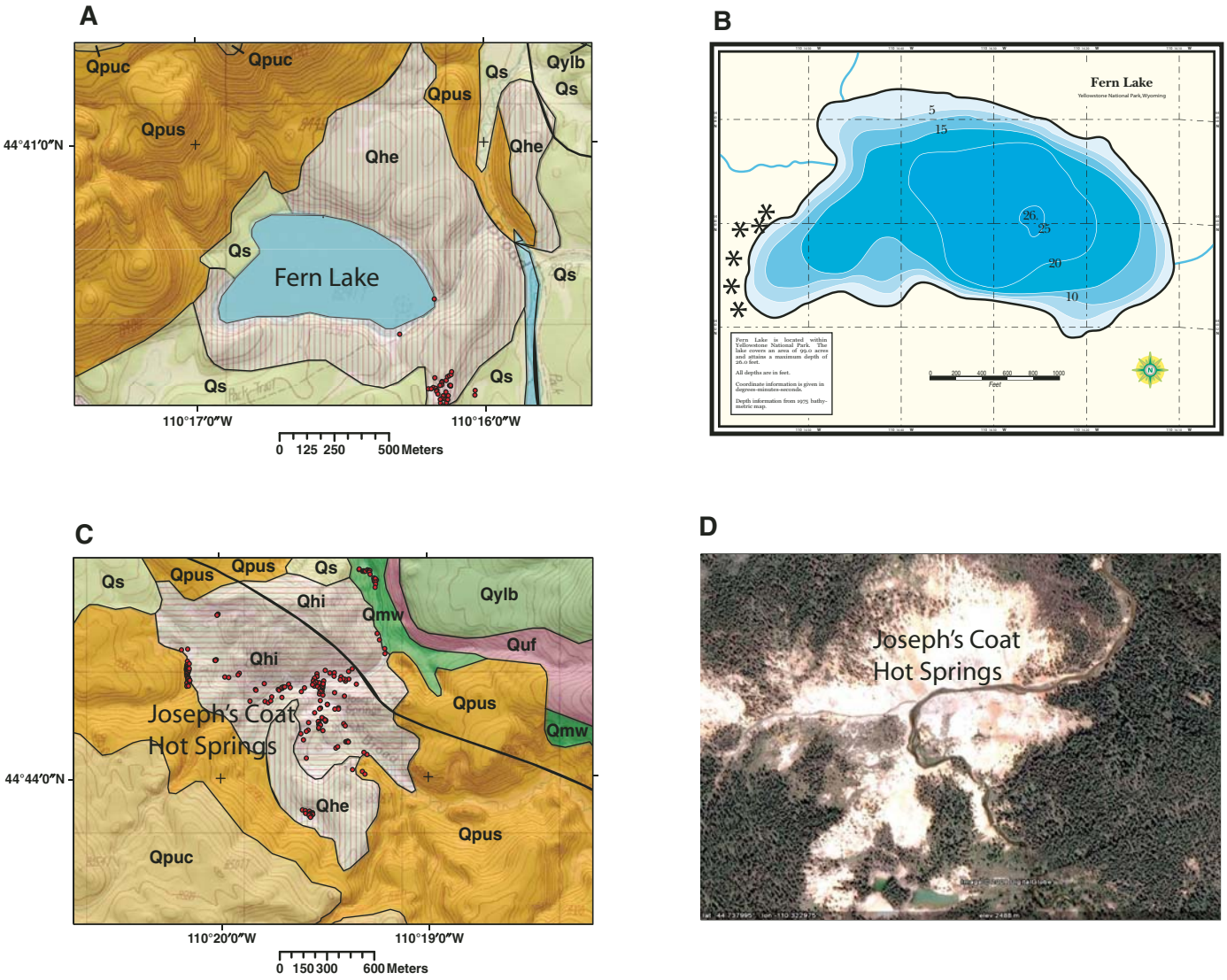

Figure 23. Fern Lake hydrothermal explosion crater. (A) Geological map after Christiansen (2001). Abbreviations for units are as follows: Qs—Quaternary sediments; Qhe—Quaternary hydrothermal explosion deposits; Qpus—Upper Basin Member–Tuff of Sulfur Creek; Qpuc—Upper Basin Member–Canyon flow; Qylb—Lava Creek Tuff, member B. Red dots indicate hydrothermal springs from the Park Service Inventory (Ann Rodman, 2005, written commun.). (B) Bathymetric map of Fern Lake, marked in feet (from Yellowstone National Park, 1966–1975). Map prepared by Eric Wienckowski (2009). Asterisks—hot springs on southwest edge of lake. (C) Geological map of Joseph's Coat Hot Springs area, after Christiansen (2001). Abbreviations for units are as follows: Qs—Quaternary sediments; Qhi—Quaternary ice contact hydrothermal deposits; Qhe—Quaternary hydrothermal explosion deposits; Qpus—Upper Basin Member–Tuff of Sulfur Creek; Qpuc—Upper Basin Member–Canyon flow; Qmw—Wapiti Lake flow; Quf—Undine Falls Basalt; Qylb—Lava Creek Tuff, member B. Red dots indicate hydrothermal springs from the Park Service Inventory (Ann Rodman, 2005, written commun.). (D) Google Earth vertical image of Joseph's Coat Hot Springs area.

the lake surface suggest the possibility of active hydrothermal vents in the lake. Duck Lake waters have low Cl content of 0.7 mg/L and oxygen and hydrogen isotope values that indicate low-temperature evaporation. All other trace elements have low concentrations. These data, taken together, suggest that Duck Lake is spring fed by meteoric waters and that hydrothermal input at present is small.

The explosion breccia deposit associated with the Duck Lake crater contains subangular, silicified clasts of cemented beach sand, sinter, lake sediment, obsidian fragments, and hydrothermally altered pumice. Many of the clasts are lithologically similar to nearby exposures of the tuff of Bluff Point.

Evil Twin Hydrothermal Explosion Crater

New bathymetric and seismic data (Morgan et al., 2007a, 2007b) indicate a 500-m-diam sublacustrine explosion crater, informally referred to as the Evil Twin explosion crater. The crater is in the western part of West Thumb Basin, near the currently

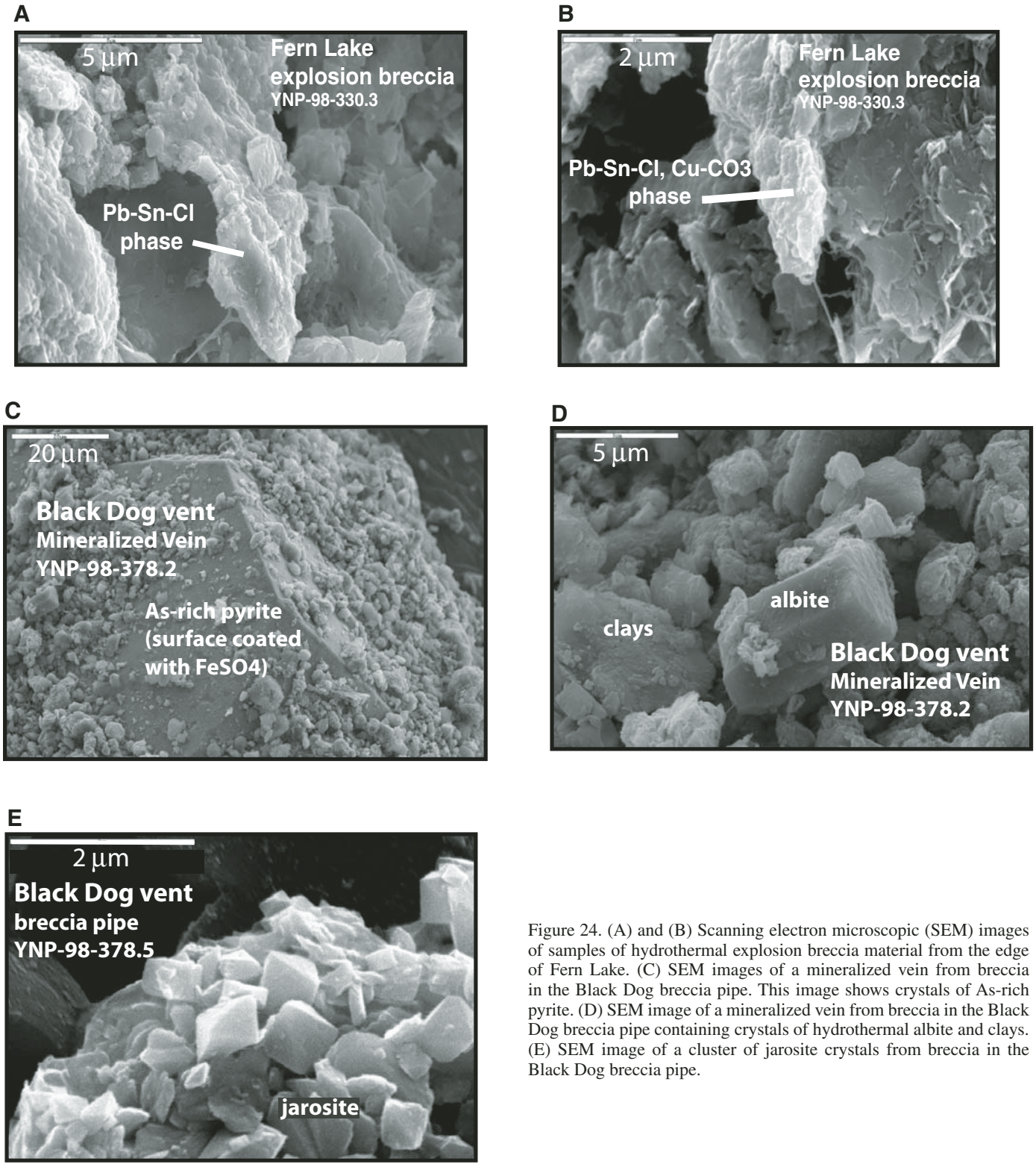

Figure 24. (A) and (B) Scanning electron microscopic (SEM) images of samples of hydrothermal explosion breccia material from the edge of Fern Lake. (C) SEM images of a mineralized vein from breccia in the Black Dog breccia pipe. This image shows crystals of As-rich pyrite. (D) SEM image of a mineralized vein from breccia in the Black Dog breccia pipe containing crystals of hydrothermal albite and clays. (E) SEM image of a cluster of jarosite crystals from breccia in the Black Dog breccia pipe.

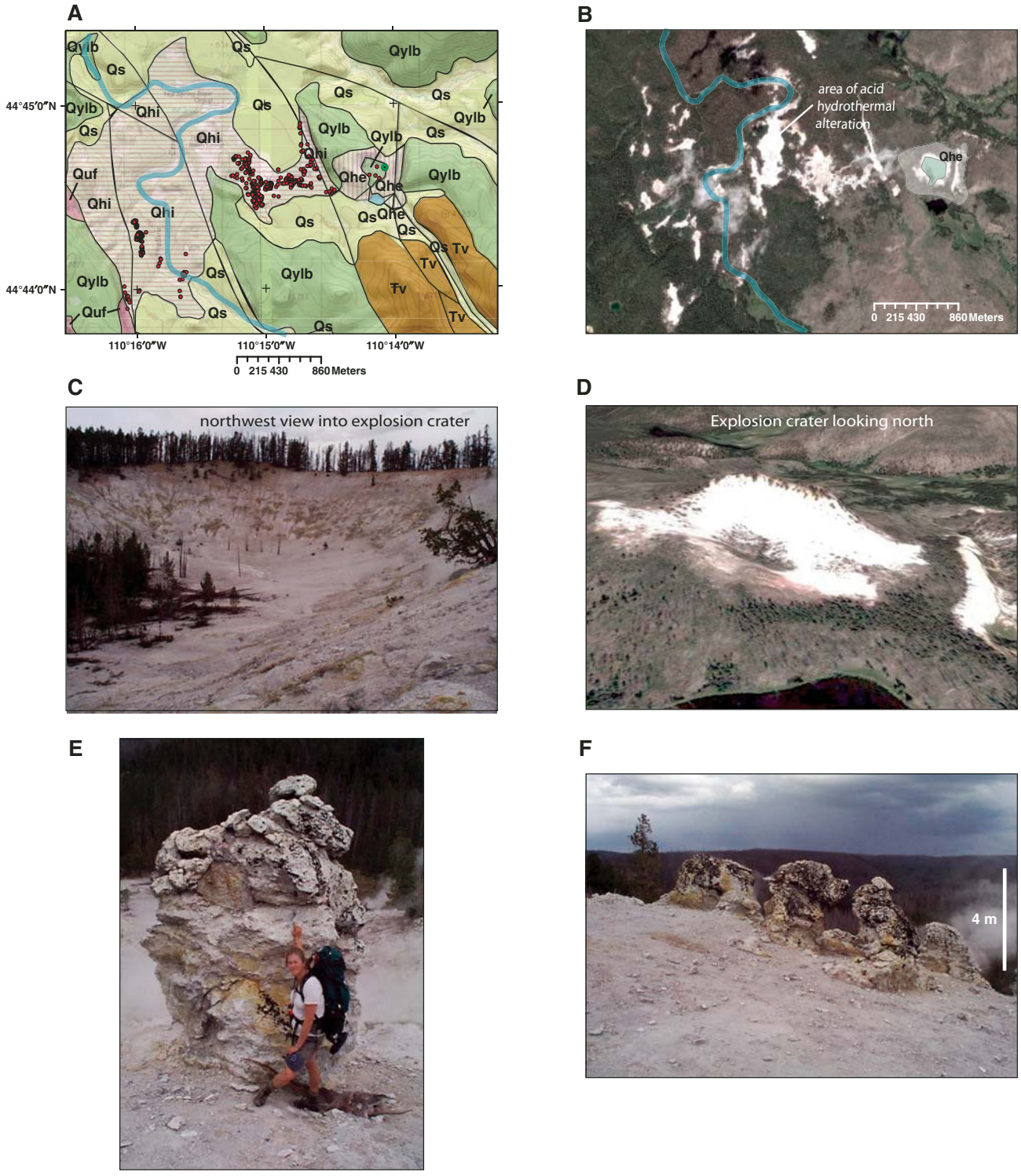

Figure 25. Hot Spring Basin Group. (A) Geological map after Christiansen (2001). Abbreviations for units are as follows: Qs—Quaternary sediments; Qh—Quaternary hot spring deposits; Qhi—Quaternary ice contact hydrothermal deposits; Qhe—Quaternary hydrothermal explosion deposits; Qyl a and b—Lava Creek Tuff; Quf—Quaternary Undine Falls Basalt; Tv—Tertiary Volcanic rocks. Red dots indicate hydrothermal springs from the Park Service Inventory (Ann Rodman, 2005, written commun.). Note active hot springs within the hydrothermal explosion crater. (B) Google Earth vertical image of Hot Springs Basin Group area. White areas are hydrothermal sinter deposits; hydrothermal explosion breccia deposit (Qhe) and the large explosion crater are highlighted. (C) Photograph into hydrothermal explosion crater looking northwest shows steep inward dipping crater walls littered with breccia. (D) Google Earth perspective view of explosion crater looking N. (E) Large (3.5 m) explosion breccia fragment of silicified sinter. (F) Several large (1 to 2 m) explosion breccia fragments of silicified sinter on crater rim.

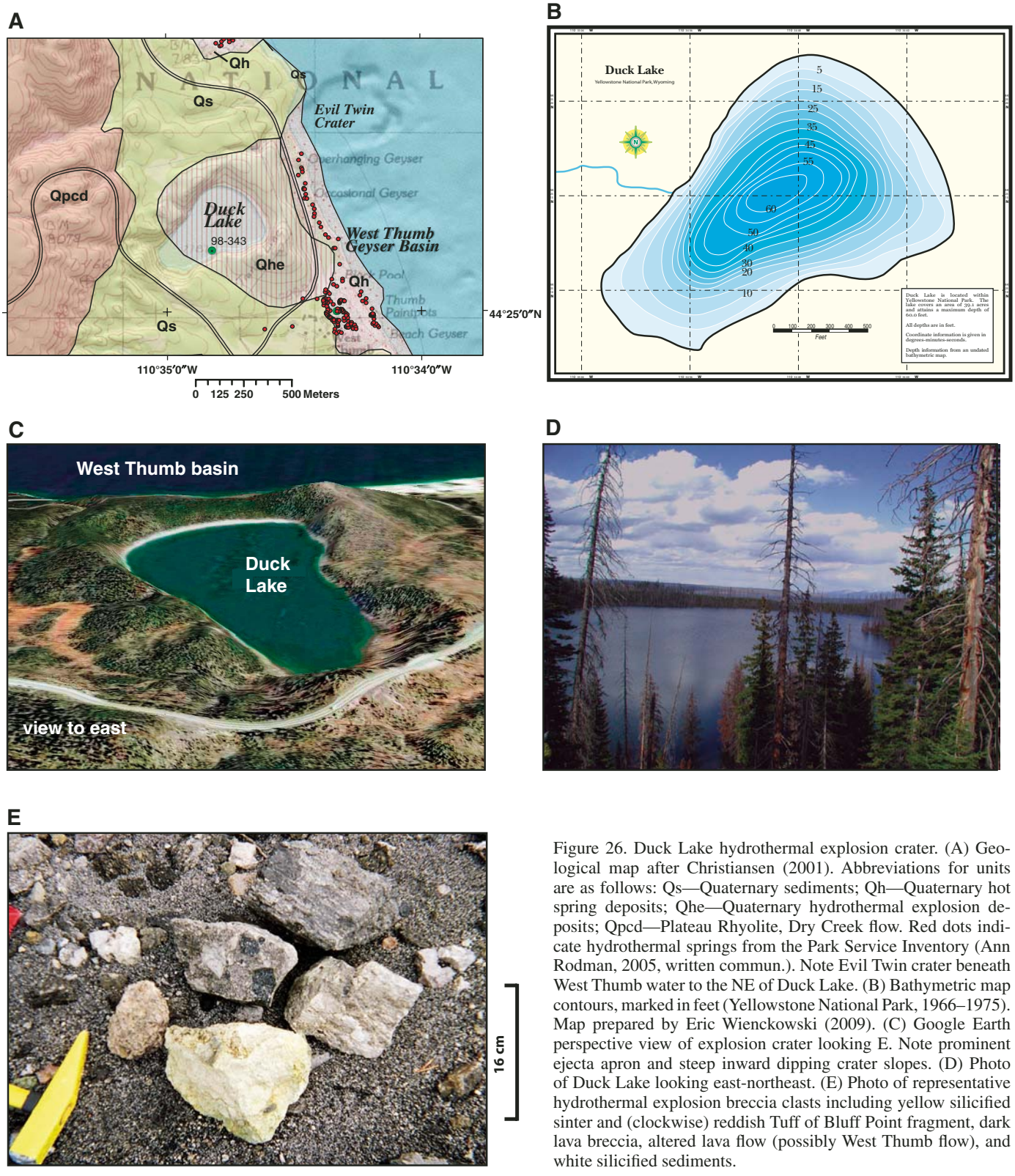

Figure 26. Duck Lake hydrothermal explosion crater. (A) Geological map after Christiansen (2001). Abbreviations for units are as follows: Qs—Quaternary sediments; Qh—Quaternary hot spring deposits; Qhe—Quaternary hydrothermal explosion deposits; Qpcd—Plateau Rhyolite, Dry Creek flow. Red dots indicate hydrothermal springs from the Park Service Inventory (Ann Rodman, 2005, written commun.). Note Evil Twin crater beneath West Thumb water to the NE of Duck Lake. (B) Bathymetric map contours, marked in feet (Yellowstone National Park, 1966–1975). Map prepared by Eric Wienckowski (2009). (C) Google Earth perspective view of explosion crater looking E. Note prominent ejecta apron and steep inward dipping crater slopes. (D) Photo of Duck Lake looking east-northeast. (E) Photo of representative hydrothermal explosion breccia clasts including yellow silicified sinter and (clockwise) reddish Tuff of Bluff Point fragment, dark lava breccia, altered lava flow (possibly West Thumb flow), and white silicified sediments.

active West Thumb Geyser Basin, and is only 300 m northeast of Duck Lake (Figs. 1, 8, 26A). In the west part of West Thumb Basin, high heat-flow values (1500 mW/m^2; Morgan et al., 1977) contributed to the formation of the Evil Twin explosion crater. The explosion crater has 12- to 20-m-high, nearly vertical walls and contains several smaller nested craters near its eastern edge. These nested craters are as deep as 42 m (water depth) and their morphologic expression indicates that their formation postdates that of the main crater. Data obtained using the submersible ROV indicate that hydrothermal fluids emanating from the smaller northeast-nested crater have a temperature of 72 °C. Water samples collected by the ROV at 35–42 m water depth in the southeastern nested crater in July 2000 had pH values as low as 6.6, temperature of 35 °C, chloride concentration of 24 mg/L, and As concentration of 170 µg/L, which indicates continued active hydrothermal venting.

Central Basin of Yellowstone Lake

Frank Island Hydrothermal Explosion Crater

New bathymetric and seismic data (Morgan et al., 2007a, 2007b) helped identify another large, subaqueous hydrothermal-explosion crater south of Frank Island. The crater is >700-m-wide, oval-shaped, steep-walled, and flat-bottomed (Fig. 8A). Previous interpretations of the lower-resolution seismic reflection profiles suggested that this structure was the topographic margin of the Yellowstone caldera (Otis, 1975). The new higher-resolution swath sonar and shallower seismic reflection profiles indicate that this structure, while on the slumped margin of the Yellowstone caldera, has characteristics very similar to those of other younger hydrothermal explosion craters in Yellowstone Lake (Morgan et al., 2003). Subdued topography suggests that this explosion crater is one of the oldest recognizable craters within Yellowstone Lake. Currently, this crater is in an area where heat-flow values are relatively low (~200 mW/m^2; Morgan et al., 1977) and direct observations with the ROV in 2002 do not indicate current hydrothermal activity within this crater.

Possible Explosion Craters East of Frank Island

New bathymetric and seismic data (Morgan et al., 2007a, 2007b) also indicate several craterlike structures along the topographic margin of the Yellowstone caldera in the central basin of Yellowstone Lake east of Frank Island (Fig. 8A). As many as nine of these features, ranging from 100 to >500 m in diameter have been identified. These craters may have formed by hydrothermal explosions but have not been investigated in enough detail for definite conclusions.

Lower Geyser Basin

Large hydrothermal explosion craters in Lower Geyser Basin include the Twin Buttes and Pocket Basin craters, both studied extensively by Muffler et al. (1968, 1971).

Figure 27. Twin Buttes ice-contact deposits and explosion craters. (A) Geological map after Christiansen (2001). Abbreviations for units are as follows: Qs—Quaternary sediments; Qh—Quaternary hot spring deposits, Qhi—Quaternary ice contact hydrothermal deposits; Qhe—Quaternary hydrothermal explosion deposits. (B) Google Earth vertical image of Twin Buttes. (C) Google Earth perspective view of explosion craters and buttes of thermal kame deposits looking north. Note prominent ejecta aprons and steep inward dipping crater slopes. (D) Photograph of crater rim with large (1.5 m) ejecta fragments. (E) Explosion crater near western butte, looking west. (F) View of eastern explosion crater, looking north. (G) Closer view of 1.5-m-diam ejecta clast of hydrothermally cemented glacial material. (H) Close-up of 15-cm-diameter ejecta fragment.

Twin Buttes

Twin Buttes is a complex of cemented hydrothermal ice-contact deposits (Figs. 1 and 27). Hydrothermal-explosion breccia deposits surround several large craters in this area (Fig. 27A). Based on similarity in comparisons with the nearby Pocket Basin explosion crater, Muffler et al. (1968, 1971) suggested that the Twin Buttes explosion may have occurred immediately after Pinedale glaciation (~13–15 ka) due to rapid draining of a glacially dammed lake. Muffler et al. (1971) cite evidence of interbedded lake sediments and gravels in cores from the Lower Geyser Basin area, which they attribute to repeated filling-draining cycles of an ice dammed lake.

The Twin Buttes ice-contact deposits stand high along the northwest margin of the rim of the explosion crater complex and additional hydrothermal ice-contact deposits crop out on the south edge of Twin Buttes and in the area south of Imperial and Spray Geysers (Fig. 27A) (Muffler et al., 1971). The central part of Twin Buttes contains several nested explosion craters in a depression ~500 m × 600 m (Figs. 27B and 27C). Three of these craters are filled by lakes that are perched ~80 m above the elevation of the nearby Firehole River floodplain. Hydrothermal explosion breccia has been mapped (Christiansen, 2001; Christiansen and Blank, 1974) along the south and east rims of the explosion crater area and extends ~1 km to the northeast as a breccia lobe that may represent a directed blast.

Hydrothermal explosion breccia from the Twin Buttes crater includes a variety of silicified sandstone and conglomerate (Muffler et al., 1971); many of these blocks are cemented by opal and zeolite minerals and presumably were derived from the hydrothermally cemented ice-contact deposits that underlie the buttes. Rhyolite fragments identified as clasts in the breccia deposit may have been derived from rhyolitic lava flows inferred in the shallow subsurface (Fig. 1).

Pocket Basin

Pocket Basin, also in Lower Geyser Basin (Muffler et al., 1971, 1982a), is in the broad, flat alluvial valley of the Firehole River ~4 km northeast of Twin Buttes (Figs. 1 and 28). It forms an elongate, northeast-trending, flat-bottomed crater associated with a well-defined breccia deposit at its rim, which has been

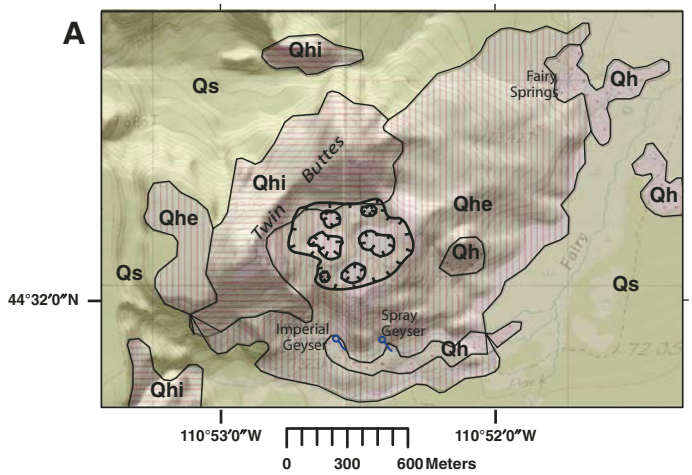
A
Qhi
Qs
Fairy Springs
Qh
Qhi
Twin Buttes
Qhe
Qhe
Qh
Qs
Qh
Qs
44°32′0″N
Imperial Geyser
Spray Geyser
Qh
Qhi
110°53′0″W
110°52′0″W
0 300 600 Meters

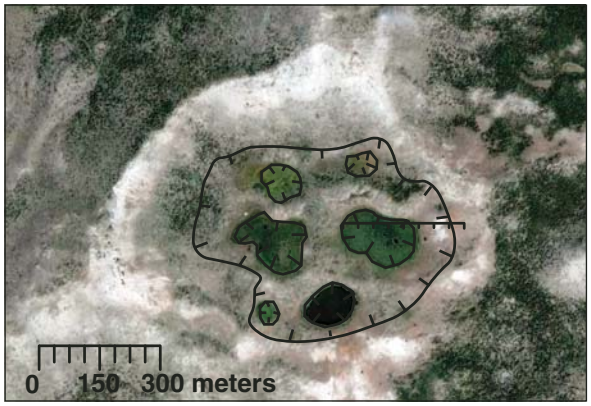
B
0 150 300 meters

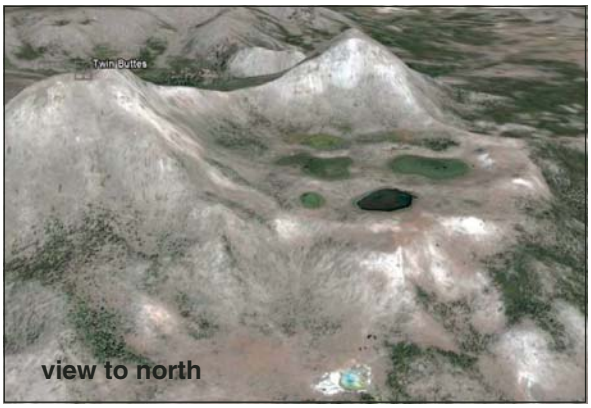
C
Twin Buttes
view to north


D


E


F


G
36 cm

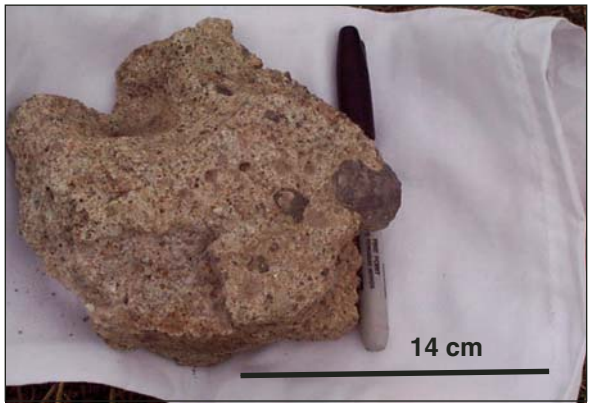
H
14 cm

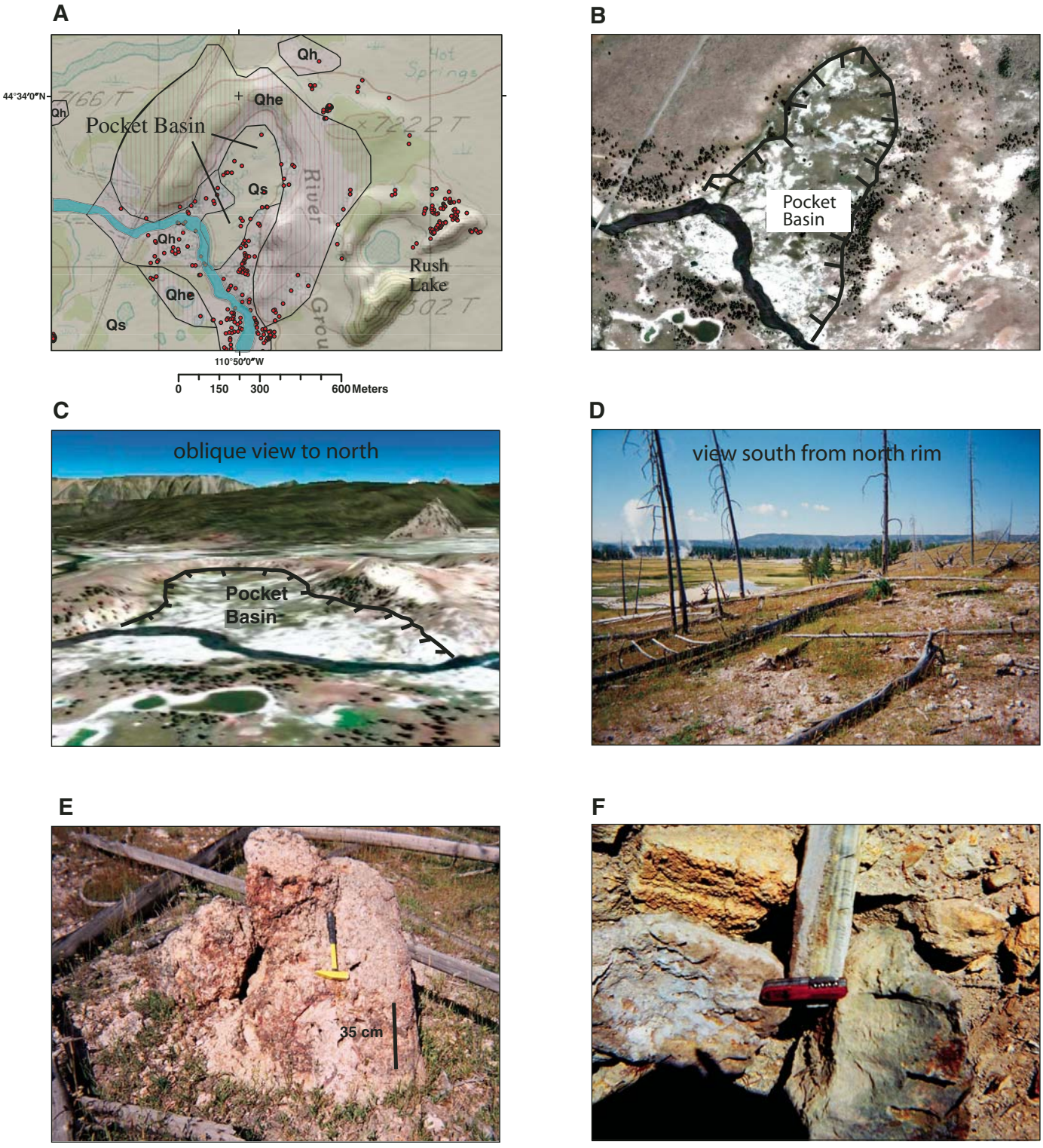

Figure 28. Pocket Basin hydrothermal explosion crater. (A) Geological map after Christiansen (2001). Abbreviations for units are as follows: Qs—Quaternary sediments; Qh—Quaternary hot spring deposits; Qhe—Quaternary hydrothermal explosion deposits. Red dots indicate hydrothermal springs from the Park Service Inventory (Ann Rodman, 2005, written commun.). (B) Google Earth vertical image of Pocket Basin. (C) Google Earth perspective view of explosion crater looking north. Note prominent ejecta apron and steep inward dipping crater slopes. (D) View south into Pocket Basin crater from north rim. Note breccia clasts on rim and hydrothermal activity in distance. (E) Large (1.5 m) ejecta clast of oxidized and silicified glacial deposits. (F) Representative hydrothermal breccia clasts including white siliceous sinter and silicified bedded deposits. Angular vugs are casts of pyrite crystals that commonly contain powdery iron sulfates.

breached on its southwest margin by the Firehole River (Muffler et al., 1971). The crater is ~300 m × 500 m and the ejecta rim rises in most places ~10 m above the floor of Pocket Basin; a maximum relief crater wall is ~20 m on the east side. The floor of the crater is at about the same elevation as that of the surrounding floodplain and contains abundant hot springs, diatomaceous sediment, and modern sinter deposits, especially in its southeast part.

Clasts of Pocket Basin explosion breccia, collected from deposits on the crater rim around the basin include chalcedony, chalcedonic breccia, and silicified fine-grained laminated mudstone and siltstone (lake deposits?) (Figs. 28D, 28E, and 28F). Muffler et al. (1982a) report cores from the Fountain Flats Bridge area that contain fragments of Pinedale lake sediment and possibly older, silicified lake sediment at greater depth; these observations suggest a sizeable lake in the area at the end of Pinedale glaciation (Pierce, 1979). Other explosion breccia clasts include quartz-cemented sandstone and occasional fragments of well-crystallized quartz veins up to 4 cm thick with euhedral crystals growing inward toward vein clusters. Many fragments are stained orange, and some contain angular, orange stained cavities, some of which contain powdery material; all of these features probably represent oxidation of sulfide minerals. Volcanic rock clasts have not been found in the explosion breccia; however, Muffler et al. (1971) report occasional rounded rhyolitic fragments that were probably derived from underlying alluvial or glacial deposits.

Muffler et al. (1971) argued that Pocket Basin formed during the waning stages of Pinedale glaciation. The inferred timing of explosion supports the theory (Muffler et al., 1971) that a pressure decrease accompanied rapid drainage of an ice-dammed lake and may have triggered the hydrothermal explosion. Late glacial damming of late glacial lakes and their sudden release is indicated by alternations of lake sediment and gravel cored in bridge abutments in the Lower Geyser Basin (Pierce et al., 2003). Age constraints established from Muffler et al. (1971) suggest that clasts from its hydrothermal explosion breccia are probably derived from early Pinedale hydrothermally cemented kame gravels that, in places, the breccia overlies. The course of the Firehole River was constrained by the distribution of glacial ice to the east and west of the explosion crater, which further aids in establishing the timing of the explosion.

Norris-Mammoth Corridor

Roaring Mountain

A number of hydrothermal explosion features occur atop Roaring Mountain and along its east flank (Figs. 1 and 29A–29C). Most are small, 100- to 200-m-diam features, but in the area ~1.6 km east of Lemonade Lake, smaller irregular craters coalesce in a 350-m × 500-m area. All of these craters are overgrown with vegetation, making geologic observations and detailed interpretation difficult. Breccia identified in or near the crater support the interpretation that these features may be explosion craters.

Two of the craters are clearly explosion craters. The northernmost one is 270 m in diameter and 40–60 m deep, has steeply dipping inner walls, and is associated with hydrothermal explosion breccia that consists of angular fragments of altered Lava Creek Tuff (Muffler et al., 1971). The explosion deposit, which lies above an altered section of the Lava Creek Tuff, contains angular fragments of the ignimbrite, 2–15 cm in diameter, in a fine-grained clay-rich matrix. The deposit is distributed in a radial manner ~1.5–3 km across on the uplands of Roaring Mountain. The deposit thickens from <1 m at its distal exposure to 5 m near its center, where nearby explosion craters are 15–50 m deep (Pierce, 1973). Both matrix and contained fragments were hydrothermally altered before the deposit was emplaced.

Semi-Centennial Hydrothermal Explosion Crater

The Semi-Centennial hydrothermal explosion crater is 500 m north of Lemonade Lake at Roaring Mountain in Obsidian Creek and formed in 1922 (Allen and Day, 1935; Whittlesey, 1988; Christiansen et al., 2007). Water in hot springs that flow into and line the floor of the crater is ~40 °C. The crater is ~25 m in diameter and is <3 m deep. Red microbial mats and tiny (<1 cm) red worms were identified at the edge of the crater pool. Steam issues from fumaroles at the edge of the crater, where elemental sulfur has precipitated from H_2S gas. The pH of water in the crater pool is 3–3.5. Morphologic characteristics suggest that no major explosions have been recorded since the initial crater-forming event.

Chemistry and Oxygen Isotopes of Hydrothermal Explosion Deposits

Breccia Geochemistry

Composition characteristics of lithic breccia clasts from the Mary Bay, Indian Pond, Turbid Lake, Sulfur Hills, Fern Lake, Twin Butte, and Pocket Basin hydrothermal explosion deposits and from a hydrothermal breccia pipe, informally referred to as the Black Dog hydrothermal breccia pipe, were determined by geochemical analyses (Table 3). Macroscopic observations indicate that lithic clasts in the breccia deposits from different explosion craters vary due to entrainment of distinct subsurface lithologies in the explosion ejecta. Clast types include silicified and mineralized fragments of sinter, varieties of chalcedony and chalcedony breccia, silicified lake beds, sands, platform gravels, rhyolitic lava flows, and the Lava Creek Tuff. Mineralogy of silicic lithic clasts from breccia deposits is dominated by quartz, chalcedony, and amorphous silica, based on scanning electron microscopy (SEM) and X-ray diffraction (XRD) studies (Table 4). Some lithic clasts from the Mary Bay explosion breccia, especially quartz phyric rhyolites, have abundant calcite and euhedral quartz crystals in veins. Pyrite is a common minor phase in almost all breccia lithic clasts (Fig. 24C). A few samples from the Mary Bay breccia deposit contain a brown carbonate mineral identified as kutnahorite, $MnCa(CO_3)_2$. Samples from Turbid Lake and Fern Lake have persistent but

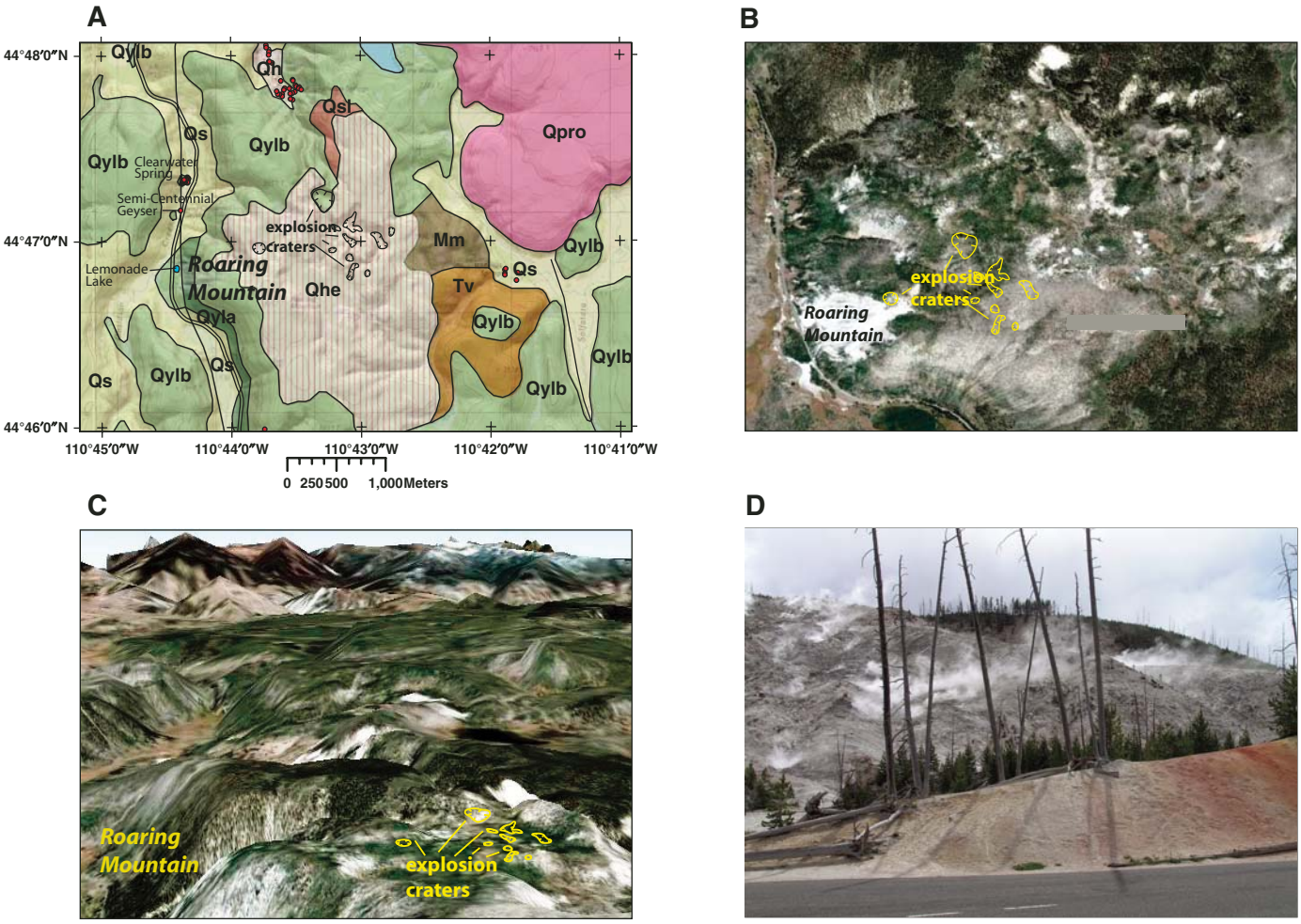

Figure 29. Roaring Mountain explosion craters. (A) Geological map after Christiansen (2001). Abbreviations for units are as follows: Qs—Quaternary sediments; Qh—Quaternary hot spring deposits; Qhe—Quaternary hydrothermal explosion deposits; Qpro—Obsidian Cliff flow; Tv—Tertiary Volcanic rocks; Qyla and Qylb—Lava Creek Tuff, Members A and B; Mm—Mesozoic Madison Limestone. Red dots indicate hydrothermal springs from the Park Service Inventory (Ann Rodman, 2005, written commun.). (B) Google Earth vertical image of Roaring Mountain area. (C) Google Earth perspective view of explosion craters above Roaring Mountain, looking north. Note chaotic terrain due to numerous small craters. (D) Photograph of steam vents on the western slope of Roaring Mountain.

very minor amounts of unidentified Cu-Sn-CO_3-Cl bearing phases, based on SEM studies (Figs. 24A and B).

Major element data indicate that breccia clasts span a broad composition range, with SiO_2 ranging from 47.9 to 97.9 wt.%, as would be expected given the diversity of lithologies represented (Table 3). Several quartz-phyric rhyolite clasts from the Mary Bay explosion deposit, considered samples of altered rhyolitic lava flow or a shallow intrusive (Morgan and Shanks, 2005), contain highly elevated SiO_2 abundances (Table 3) due to intense and pervasive silicification. Sulfur abundances of the breccia samples (<0.05 to 3.5; ave. 0.7 wt.% S) are generally higher than is common for high-silica rhyolites (typically <0.01 wt%), which indicates that significant pyrite and other hydrothermal sulfide minerals have been added during pre-explosion hydrothermal alteration.

Comparative Geochemistry

The geochemical composition of a number of rock types, including sublacustrine and subaerial sinter, altered and unaltered lake sediments, and the Lava Creek Tuff and rhyolitic lava flows throughout YNP were analyzed in order to allow comparison with lithic clasts from hydrothermal explosion breccia. Many lithic fragments from the hydrothermal breccia deposits have abundant SiO_2 (Tables 3 and 5), which indicates intense hydrothermal silicification. Sublacustrine hydrothermal sinter deposits contain significant contents of Al_2O_3, CaO, Fe_TO_3, K_2O, MgO, and Na_2O, similar to those of lake sediments (Table 5). SEM images of sublacustrine hydrothermal deposits show that most contain abundant diatoms, the principal component of Yellowstone Lake sediments. Field evidence (Fig. 30) indicates that sublacustrine hydrothermal silicification occurs due to fluids flowing

TABLE 5. COMPARATIVE GEOCHEMISTRY BASED ON AVERAGE COMPOSITIONS OF HYDROTHERMAL EXPLOSION BRECCIA SAMPLES AND OTHER HYDROTHERMAL DEPOSITS AND HOST LITHOLOGIES

	Mary Bay chalcedonic and sedimentary lithics	Mary Bay-Quartz phyric rhyolite lithics	Indian Pond lithics	Turbid Lake lithics	Sulphur Hills lithics	Fern Lake lithics	Duck Lake lithics	Pocket Basin lithics	Black Dog breccia-pipe lithics	Sublacustrine hydrothermal siliceous deposits	Bridge Bay spires	West Thumb subaerial sinters	Sublacustrine hydrothermal vent muds	Yellowstone Lake deep water sediments	Postcaldera rhyolites	Lava Creek Tuff
	Average (n = 16)	Average (n = 9)	Average (n = 1)	Average (n = 2)	Average (n = 2)	Average (n = 2)	Average (n = 4)	Average (n = 2)	Average (n = 4)	Average (n = 34)	Average (n = 4)	Average (n = 6)	Average (n = 13)	Average (n = 20)	Average (n = 17)	Average (n = 45)
SiO_2	73.73	85.69	65.50	73.05	84.30	80.90	76.60	78.90	75.08	79.44	83.63	92.38	69.71	85.18	74.89	75.49
Al_2O_3	12.58	8.63	14.10	12.20	4.20	9.50	11.36	8.33	8.83	5.76	4.64	0.54	13.89	3.72	13.29	12.39
CaO	1.92	0.27	3.55	0.60	0.06	0.11	0.29	1.26	1.80	1.19	0.64	0.10	1.52	0.62	0.42	0.44
Fe_TO_3	2.43	0.46	3.47	2.27	0.91	0.60	1.29	1.04	3.34	3.16	3.00	0.11	4.71	1.87	1.69	1.80
K_2O	4.48	4.17	2.53	5.35	1.04	5.40	5.15	4.15	2.34	0.86	0.40	0.09	1.45	0.52	5.68	5.06
MgO	0.78	0.23	1.81	0.63	–	–	0.17	0.27	1.25	0.52	0.41	–	1.24	0.65	0.05	0.16
MnO	0.07	0.00	0.04	0.02	–	0.01	0.02	0.01	0.03	0.14	0.04	0.01	0.12	0.10	0.04	0.03
Na_2O	1.87	1.91	2.48	1.55	–	0.80	2.26	0.59	1.72	1.06	0.44	0.32	1.19	0.40	3.63	3.23
P_2O_5	0.13	0.01	0.23	0.22	0.13	0.09	0.01	0.12	0.17	0.27	0.48	0.07	–	0.54	0.04	0.07
S	0.69	–	–	0.14	1.02	0.09	0.08	–	1.00	2.47	0.20	–	0.04	0.17		
TiO_2	0.21	0.06	0.45	0.36	0.30	0.16	0.15	0.16	0.31	0.25	0.12	0.03	–	0.13	0.20	0.17
Ag	0.62	0.73	0.44	0.76	0.71	0.71	1.00	1.00	0.49	0.23	0.17	0.06	0.15	0.30	0.31	0.23
As	42.52	28.43	9.70	25.35	16.40	14.45	–	42.00	284	585.31	562.75	7.13	219.64	360.00	6.30	4.27
Ba	598	112	1300	1700	875	820	491	166	866	503.69	1779.75	43.17	695.64	280.95	286.2	410.0
Be	3.52	3.39	3.10	2.00	0.59	3.45	7.00	5.10	1.68	1.29	17.75	29.88	2.16	3.71	5.26	4.98
Cd	0.15	–	0.16	0.05	0.02	0.03	–	–	0.09	0.26	0.55	0.02	0.17	0.29	0.08	0.12
Co	4.72	0.80	8.60	2.24	0.27	0.18	0.60	0.20	10.22	7.69	13.30	0.24	17.86	6.73	0.45	0.48
Cr	67.69	26.67	96.00	81.50	39.50	12.00	20.00	16.50	100.6	35.22	–	29.00	118.14	–	1.23	2.37
Cs	9.13	2.96	6.00	5.05	1.80	4.45	29.83	4.80	4.46	32.75	4.83	82.17	–	13.48	3.91	2.48
Cu	11.00	–	17.00	10.80	7.70	3.30	–	3.00	17.00	15.31	14.00	7.90	32.86	17.29	2.29	4.25
Ga	17.19	9.20	21.00	16.00	14.10	14.50	20.25	6.20	13.20	10.78	8.73	117.33	26.21	–	22.5	22.77
Ge	0.50	0.32	0.63	0.57	0.31	0.81	1.67	1.55	0.70	2.50	2.70	1.88	3.26	15.48	1.31	1.48
Hg	0.06	–	0.15	0.04	2.28	0.14	–	–	1.62	5.59	–	–	16.00	1.92		
Li	65.69	95.50	16.00	66.50	10.55	47.50	93.33	145.00	227	9.51	21.68	6.32	39.07	13.57	27.8	25.40
Mo	15.64	3.39	1.10	4.20	7.00	1.55	3.50	9.50	5.10	8.02	15.55	0.41	11.75	13.86	3.93	2.98
Nb	31.39	41.80	19.00	38.00	36.00	38.00	40.50	41.50	20.40	8.91	8.75	1.43	–	5.21	51.2	66.88
Ni	208.4	59.20	42.00	8.50	1.40	–	–	1.00	41.00	28.21	143.25	4.80	59.29	33.00	0.57	2.95
Pb	21.36	21.80	29.00	20.50	21.00	17.00	31.50	14.00	–	15.44	5.63	1.40	28.07	6.94	31.7	32.50
Rb	204.7	179.8	66.00	215.0	10.7	230.0	248.0	73.35	89.80	32.23	12.85	13.70	48.26	20.00	194.0	172.3
Sb	3.61	2.30	0.30	1.14	3.35	3.95	–	4.10	1.93	7.14	11.35	39.50	12.73	37.19	0.47	0.23
Sc	3.77	8.83	8.50	6.80	2.60	2.20	–	13.00	6.98	14.34	2.00	–	–	3.44	2.32	13.32
Se	1.56	–	0.30	2.15	1.25	0.45	–	–	0.94	0.97	–	–	0.60	1.00	0.90	
Sr	223.9	66.3	760.0	375.0	147.0	50.5	86.8	19.5	370.0	220.03	118.50	5.63	276.43	88.24	13.8	19.13
Ta	1.45	3.31	1.40	2.60	1.48	2.45	5.65	4.95	1.36	0.76	0.10	0.20	–	0.30	3.25	3.25
Th	16.11	13.45	16.00	13.85	13.50	22.00	20.00	13.95	7.32	4.22	2.03	0.46	10.78	3.49	27.3	27.30
Tl	1.12	0.90	0.60	2.70	0.15	1.45	1.03	0.80	0.68	1.09	9.10	0.12	0.91	0.31	1.02	0.85
U	3.02	3.94	4.20	2.30	3.65	4.05	5.71	3.92	1.56	1.36	2.13	0.22	3.44	1.78	6.54	4.23
V	21.40	34.00	65.00	45.50	14.55	8.05	–	14.00	48.80	37.60	66.25	1.40	107.50	48.29	0.88	5.27
W	3.39	1.58	2.10	3.90	7.50	3.00	2.00	29.30	6.34	65.74	136.70	3.58	77.57	40.38	3.20	2.41
Y	39.26	41.50	35.00	21.00	13.50	25.50	42.20	23.25	21.00	10.96	9.05	1.18	–	12.86	53.8	45.00
Zn	46.28	11.00	65.00	24.00	6.60	9.10	38.00	11.00	49.20	23.55	24.00	14.00	67.93	35.62	64.2	87.77

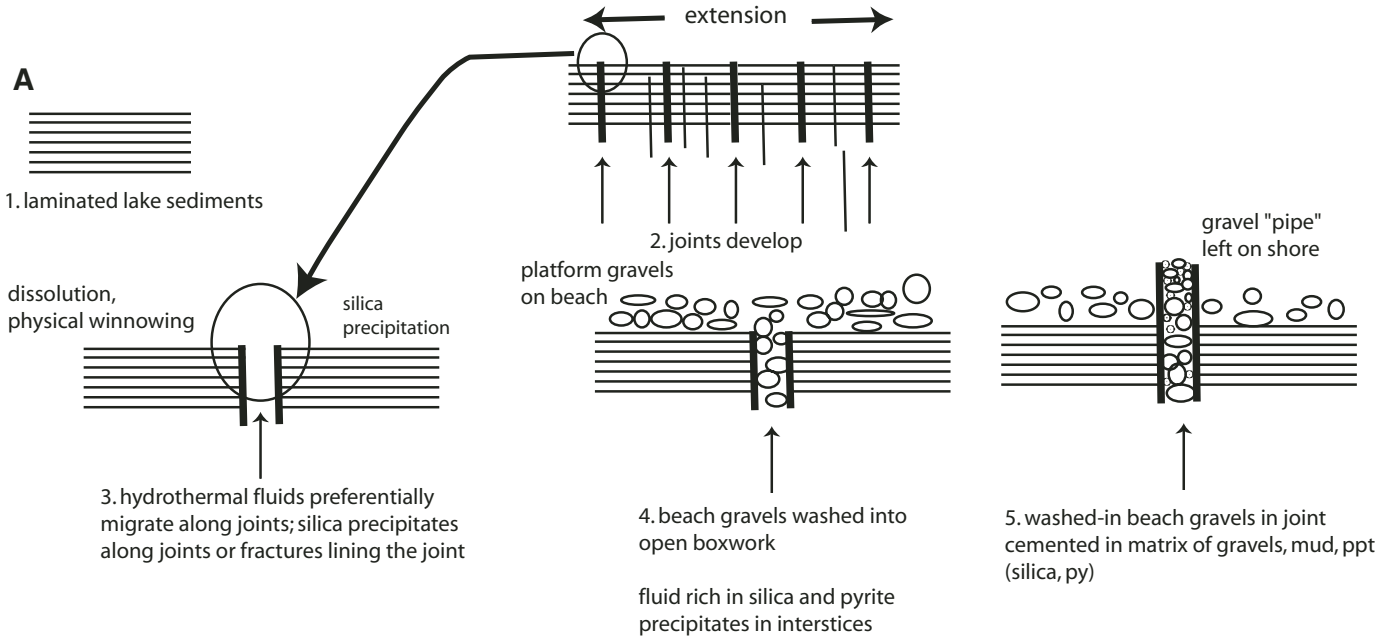

Figure 30 (*on this and following two pages*). (A) Schematic diagram showing the development of joint structures at Bridge Bay. 1. Laminated lake sediments along the beach at Bridge Bay are immediately to the southeast of the northeast-trending Elephant Back Fissure Zone and are affected by the regional stresses associated with the active deformation of the Yellowstone caldera. 2. Sets of northeast- and northwest-trending joints develop in laminated lake muds allowing the flow of ascending hydrothermal fluids. 3. An area between joints is altered, dissolved, and physically winnowed away, leaving a large sheeted void. Silica is precipitated along walls of joints. 4. Rounded beach gravels are washed into the joint and are cemented in place by fluids rich in silica and pyrite. 5. The silicified gravel joint or dike is more resistant than its host rock and forms sheets of gravel pipes or dikes on the beach.

along porous zones or structural channelways resulting in mineralization along fractures or joints and in pore space within lake sediment (Shanks et al., 2007). Hydrothermally altered muds collected from active sublacustrine hydrothermal vent sites contain significantly higher Al_2O_3 and Fe_TO_3 but have lower SiO_2 than sublacustrine sinter due to alteration processes that remove SiO_2 (Shanks et al., 2005, 2007). In particular, Shanks et al. (2005, 2007) provide strong geochemical evidence that vent fluids, under certain conditions of cooling and mixing with bottom water, can become undersaturated with chalcedonic silica leading to massive dissolution of diatomaceous lake sediment and collapse to form the hydrothermal craters imaged by multibeam bathymetry and seismic reflection.

In contrast, silicic lithic clasts from the Mary Bay breccia and those in the Black Dog breccia pipe contain higher Al_2O_3, Fe_TO_3, and S contents than modern sublacustrine sinter deposits. Mary Bay explosion breccia clasts composed of quartz-phyric rhyolite are chemically similar to Lava Creek Tuff and caldera-filling rhyolitic lava flows but have significantly more SiO_2 than unaltered rhyolites due to intense alteration and silicification (Table 5).

Minor and trace elements. Balistrieri et al. (2007) have shown that sublacustrine Yellowstone Lake hydrothermal vent water contributes substantial concentrations of As, B, Cl, Cs, Ge, Hg, Li, Mo, Sb, Tl, and W into the lake. Comparison of the concentration of these elements in lake water with the flow-weighted flux of elements from significant streams that drain into the lake indicates that these elements are enriched in lake waters by at least an order of magnitude due to influx of hydrothermal vent fluids. These elements also are enriched in sublacustrine vent fluid samples and are diagnostic of hydrothermal fluids throughout Yellowstone (Ball et al., 1998; Gemery-Hill et al., 2007; Nordstrom et al., 2005; Thompson and DeMonge, 1996). Cl is a conservative element that is highly concentrated in hydrothermal fluids and is enriched by about a factor of 10 in lake water relative to stream influx. By comparison with other areas of the park (Fournier et al., 1976; Friedman and Norton, 2007), Cl in lake water indicates that ~10% of the total hydrothermal water flux in YNP occurs on the floor of Yellowstone Lake (Fig. 31; Balistrieri et al., 2007).

Hydrothermal explosion breccia clasts provide a window into subsurface hydrothermal systems that existed before and at the time of explosion. Minor element contents of clasts may help identify the host rocks that explosion craters excavated as well as compositional changes that accompanied the hydrothermal alteration process (Tables 3 and 5, Fig. 32).

Data presented here suggest that the geothermal elements As, Cs, Li, Mo, Sb, and W can be used as a suite of elements to distinguish various hydrothermal products which formed in different environments and were subjected to various hydro-

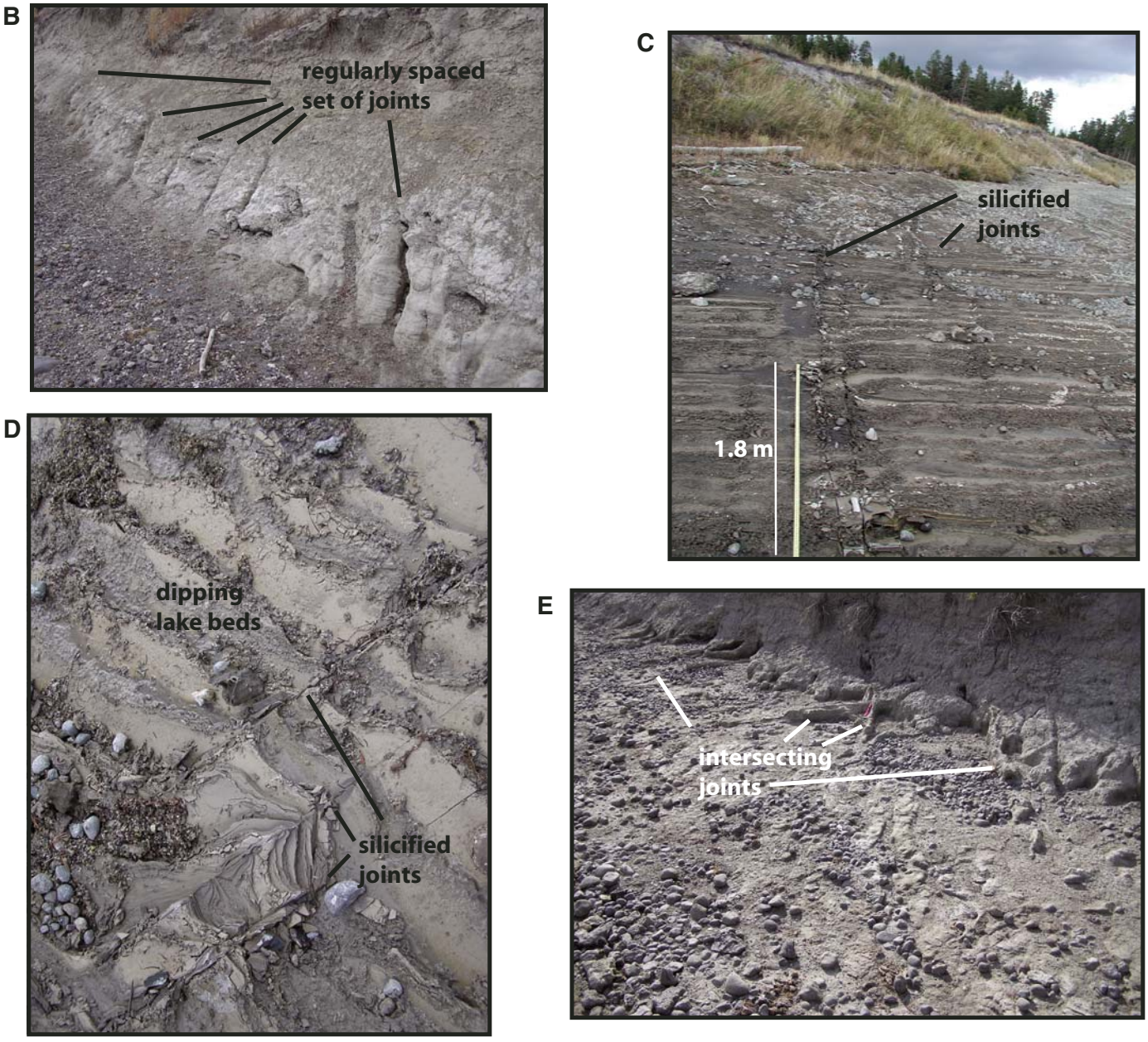

Figure 30 (*continued*). (B) Set of northeast-trending joints exposed in lake sediments along the bluffs at Bridge Bay. (C) View of beach at Bridge Bay and northwest-trending set of joints in lake sediments exposed along the bluffs. Individual joints are 6–12 cm wide and semiregularly spaced about every 2 m. (D) Altered, dipping lake sediments cut by northwest-trending joints lined with silica and raised slightly above the surrounding host rock. Individual joints are <0.5 cm thick and trend along the same joint for tens of meters on beach. (E) Sets of intersecting northeast- and northwest-trending joints filled with beach detritus and silicified. Individual joints are ~10–20 cm thick. Joints are spaced every 20–50 cm. Some of the silicified joints stand in relief ~15 cm.

thermal processes. Similarly, Sturchio et al. (1986), in a study of near-surface hydrothermal alteration and silicification of the Biscuit Basin rhyolitic lava flow in cores Y7 and Y8 (White et al., 1975), showed alteration products are rich in Cs, Li, and Sb. They concluded that these elements are added during intense alteration and silicification. Unfortunately, they did not analyze As, Mo, or W.

Comparison of geochemical data for hydrothermal explosion breccia clasts with other Yellowstone hydrothermal deposits and with rhyolites and lake sediments (Tables 3 and 5, Fig. 32) indicates generally similar hydrothermal processes in the modern systems as operated in the older systems that developed into hydrothermal explosions. Explosion breccia clasts represent a broad variety of lithologies with a broad spectrum

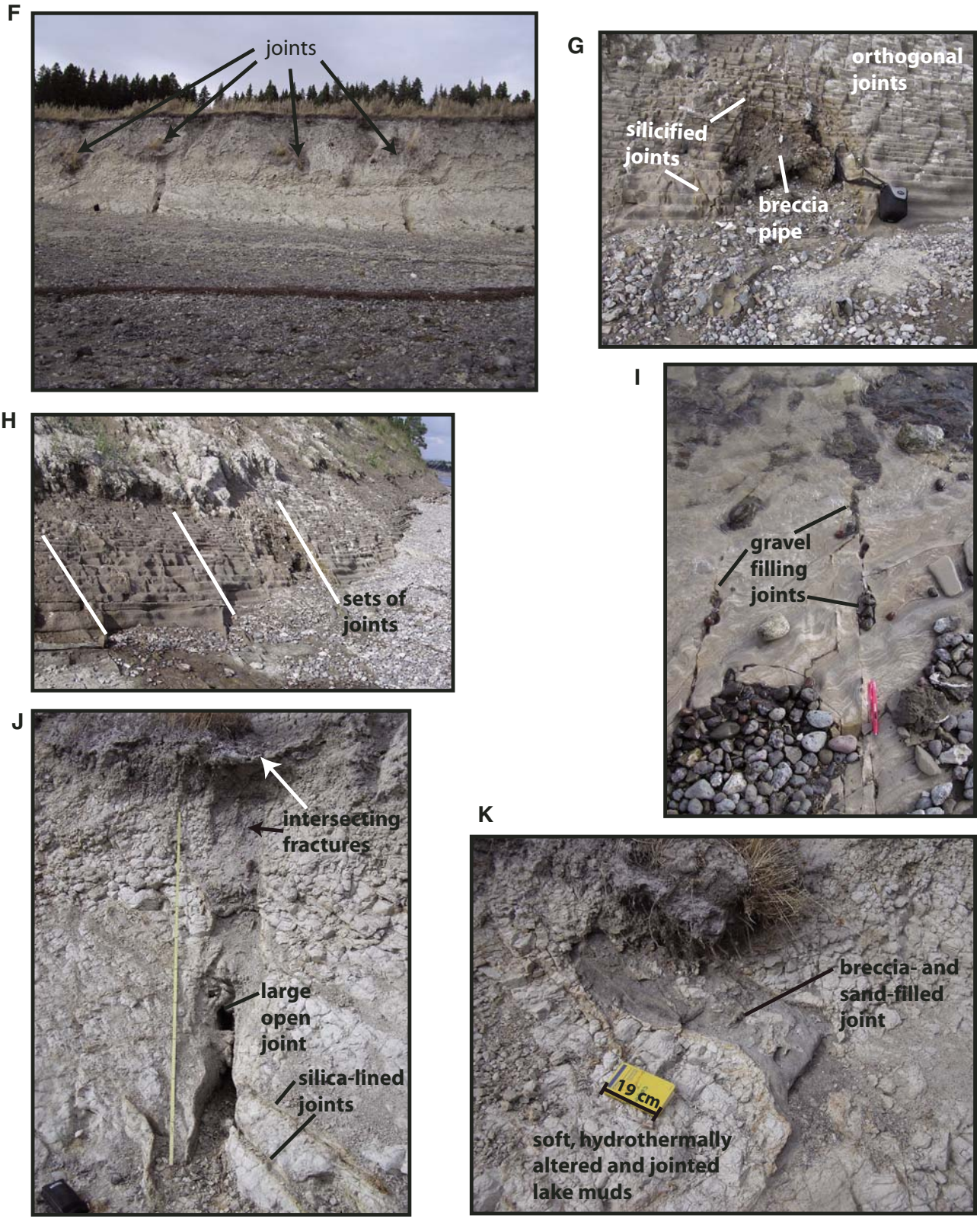

Figure 30 (*continued*). (F) Open joints exposed in bluffs along beach. (G) A 60-cm-wide breccia pipe in a set of intersecting orthogonal joints in altered lake muds. (H) Set of orthogonal joints exposed in bluffs. (I) Gravels filling northwest-trending silicified joints on beach. (J) Large open northeast-trending joint. Joint is ~20–35 cm wide. (K) Breccia- and sand-filled large (40 cm wide) joint in hydrothermally altered orthogonally jointed soft lake muds.

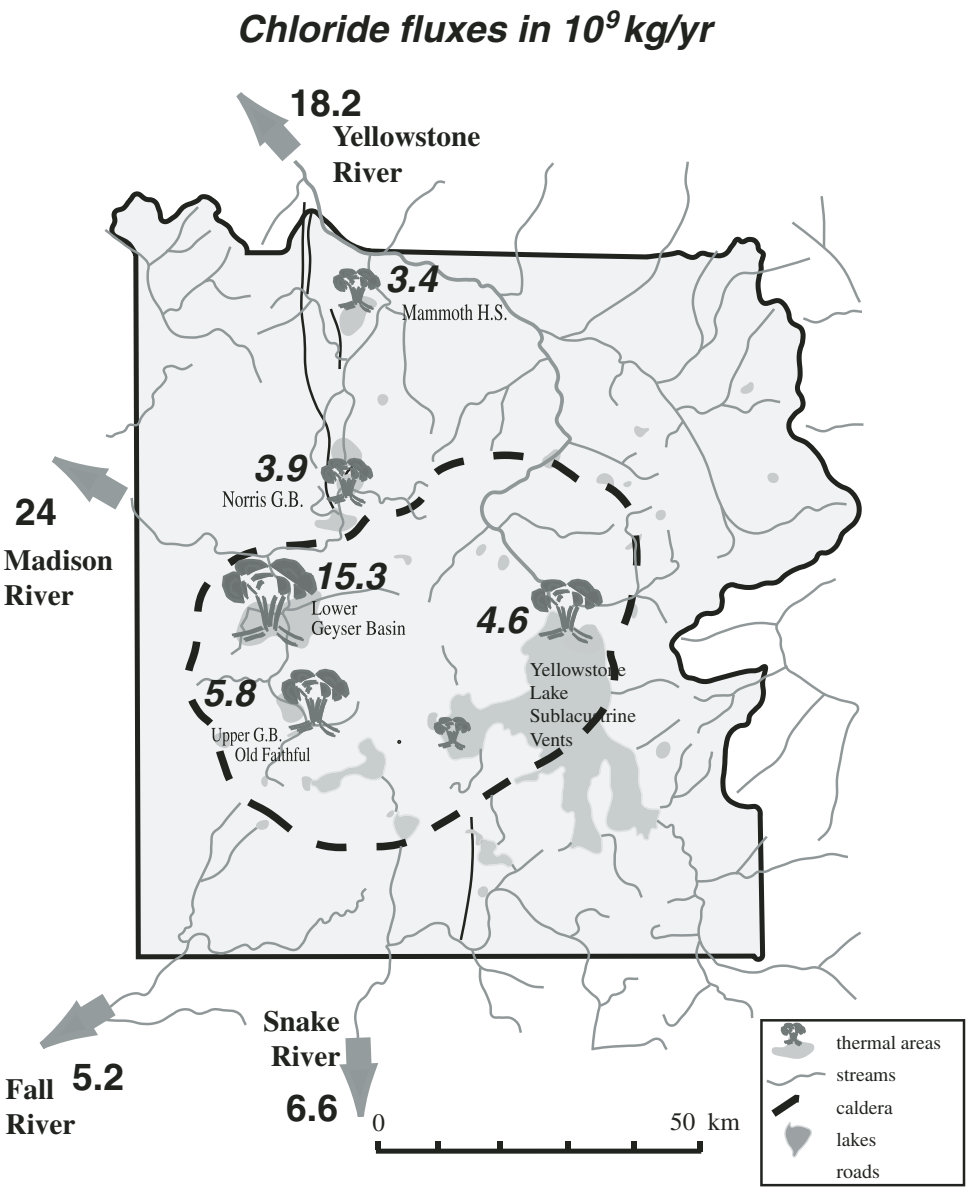

Figure 31. Chloride fluxes from major thermal areas in Yellowstone National Park. Cl flux is directly related to hydrothermal water flux and is determined by outflow in rivers and streams. These values indicate that fluxes in Yellowstone Lake are similar to Norris, Mammoth, and Upper Geyser Basins.

of alteration intensity (Table 3); many show significant concentrations of Cs, Li, Mo, Sb, and W, but not As. The five enriched elements are generally higher than in Yellowstone rhyolites (Table 5). Variations of these elements do not clearly fingerprint a specific type of hydrothermal environment, but are perhaps most similar to the Black Dog breccia (Fig. 32). This is reasonable considering that Black Dog represents a subbottom hydrothermal feeder conduit, and the explosion breccia clasts were probably mostly altered in a similar subsurface hydrothermal system.

Stable Isotopes. Stable isotope analyses of carbonate minerals from veins in lithic breccia clasts contained in explosion breccia deposits (Table 6) suggest that these minerals equilibrated with Yellowstone thermal waters at hydrothermal temperatures. The oxygen isotope composition of present-day Yellowstone Lake water is –16.5 per mil, whereas the composition of meteoric water from streams draining into the Lake ranges from –20 to –17.5 per mil (Shanks et al., 2005; Balistrieri et al., 2007). Temperature calculations based on calcite-water oxygen isotopic fractionation (O'Neil et al., 1969) with Yellowstone Lake water (with $\delta^{18}O$ = -16.5 per mil) for carbonate minerals in the breccia samples (Table 6) give temperatures ranging from 165 to 390 °C. Most values are in the range from 175 to 304 °C, which corresponds well with fluid inclusion filling temperatures of 228–294 °C determined for wairakite ($CaAl_2Si_4O_{10}[OH]_4$) from a breccia clast in the Mary Bay deposit (Fig. 20). Carbon isotope values ($\delta^{13}C_{PDB}$) of calcite from veins in Mary Bay explosion breccia clasts range from –6.9 to –3.5 per mil, which is consistent with derivation from magmatic CO_2 released by magma degassing beneath the Yellowstone caldera.

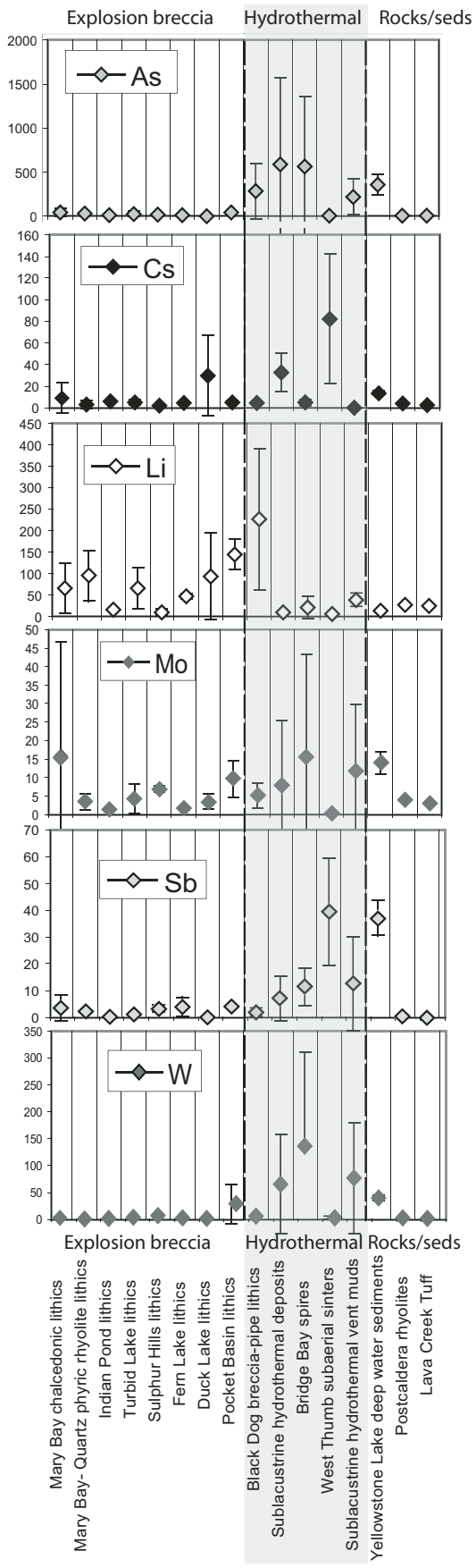

Figure 32. Trace-element distribution for selected geothermal indicator elements in hydrothermal explosion breccia, hydrothermal mineralization, and unaltered rhyolites and lake sediments. These patterns show that the breccias are hydrothermally altered and strongly enriched in As, Li, Mo, Sb, and sometimes Cs and W, like sublacustrine hydrothermal mineralization.

Oxygen isotope values for vein quartz separates from breccia clasts have a range from –10.4 to 4.6 per mil (Table 6), which correspond to temperatures of 102 to 344 °C using the Clayton et al. (1972) quartz-water fractionation data and assuming equilibration with Yellowstone Lake water having $\delta^{18}O$ of –16.5. Similarly, $\delta^{18}O$ values of silica separates from sample YNP-97-MBX range from –7.7 to 7.1 per mil (Table 6), which correspond to temperatures in the range between 84 and 264 °C. Most of the quartz samples give temperatures similar to oxygen isotope temperatures calculated from calcite data.

Variations in oxygen isotope temperatures may represent actual temperature variations in depositional hydrothermal systems as seen in modern sublacustrine hydrothermal systems (Shanks et al., 2007). Alternatively, the isotopic value of the hydrothermal fluids could have varied due to water-rock interaction. Sturchio et al. (1990) determined similar isotopic ranges in samples from the research drill cores from Lower Geyser Basin and suggested that isotopically heavy silica deposits can form at high temperature from water that is $\delta^{18}O$-enriched due to decompressional boiling or water-rock reaction. They suggest that rapid reaction with freshly exposed rhyolite leads to short-term ^{18}O enrichment of hydrothermal waters. Similarly, hydrothermal fluids from the deep hydrothermal system at Mary Bay may have had values significantly higher than –16.5 due to water-rock reactions in the subsurface, which would increase $\delta^{18}O$ values of the water. If isotopic composition of the hydrothermal water was as high as –10 per mil in some cases, then low calculated temperatures, such as those for YNP-97-MBX-5, would be more in accord with other temperature indicators.

In summary, oxygen isotope data for calcite indicate a subsurface hydrothermal temperature range of 175–304 °C, which corresponds well with fluid inclusion filling temperatures of 228–294 °C. Oxygen isotope temperatures for vein quartz separates from breccia clasts indicate a range of 102–344 °C, and some chalcedonic silica fragments suggest temperatures as low as 84 °C. Low temperatures calculated from oxygen isotope data for silica may indicate that hydrothermal fluids had elevated $\delta^{18}O$ at times due to rapid reaction with fresh rhyolite, perhaps during fracturing and/or hydrothermal explosion events. Alternatively, siliceous materials with lower calculated temperatures (higher $\delta^{18}O$ values) may represent lake-bottom material that experienced hydrothermal mineralization and was subsequently incorporated into explosion breccia deposits. Shanks et al. (2005) have shown that silicified sublacustrine hydrothermal vent deposits form near the sediment-water interface in the temperature range from 78 to 164 °C.

TABLE 6. OXYGEN ISOTOPE TEMPERATURES OF CALCITE AND QUARTZ VEINS FROM MARY BAY HYDROTHERMAL EXPLOSION BRECCIA*

	$\delta^{13}C_{calcite}$PDB	$\delta^{18}O_{calcite}$	$\Delta^{18}O_{calcite\text{-}YMW}$	T(°C)	$\delta^{18}O_{quartz}$	$\Delta^{18}O_{quartz\text{-}YMW}$	T(°C)
YNP-97-MBX-1					–7.7	8.81	264
YNP-97-MBX-2					–0.7	15.80	152
YNP-97-MBX-3					–6.7	9.85	242
YNP-97-MBX-4					–5.2	11.27	216
YNP-97-MBX-5					7.1	23.62	84
YNP-97-MBX-6					–6.3	10.17	236
YNP-98-299.1	–5.03	–8.62	7.88	235	–5.80	10.70	226
YNP 98-299.1A	–6.88	–13.06	3.44	390			
YNP 98-299.1B	–5.10	–4.92	11.58	165			
YNP-98-299.9					4.00	20.50	107
YNP-98-330.3					4.60	21.10	102
YNP-98-376.6	–5.45	–9.53	6.97	258			
YNP-98-376.7	–4.79	–10.63	5.87	290			
YNP-00-487.1					–4.10	12.40	197
YNP-00-487.1A	–4.24	–9.65	6.85	261			
YNP-00-487.2					–6.20	10.30	233
YNP-00-491.1	–3.53	–9.32	7.18	252			
YNP-00-492.6					–10.40	6.10	340
YNP-00-495.7A	–5.29	–9.01	7.49	245			
YNP-00-495.7B	–5.05	–11.03	5.47	304			
YNP-00-497.1	–4.21	–8.02	8.48	222			
YNP-00-497.5					–10.50	6.00	344
YNP-00-497.5A	–4.93	–5.53	10.97	175			
YNP-00-497.5B	–4.53	–6.46	10.04	191			
YNP-00-497.7A	–3.99	–6.20	10.30	186			
YNP-00-497.7B	–4.33	–9.41	7.09	255			
YNP-00-497.8					–6.30	10.20	235
YNP-00-497.8A	–4.22	–6.79	9.71	197			
YNP-00-497.8B	–4.82	–7.57	8.93	212			

*Assumes isotopic equilibration with Yellowstone meteoric water (YMW) with $\delta^{18}O$ = –16.5.

Related Hydrothermal Features

Other large, related hydrothermal features in Yellowstone, such as hydrothermal domes, smaller explosion craters, and selected fractures with warm/hot spring seeps, have been studied to understand the timing, stratigraphy, and variations of hydrothermal activity in Yellowstone. Field observations and measurements allow insight into processes operating at various scales over short periods.

Large Hydrothermal Domes

Hydrothermal domes are rounded to oval, hemispherical-shaped features with domal roofs whose once near-horizontal bedding has been pushed upward (Fig. 12B); these features can range in size from less than a few meters to more than 1 km in diameter; the vertical dimension can range from <1 m to a few tens of meters (Johnson et al., 2003; Morgan et al., 2007a). The domes are pockmarked with later and smaller hydrothermal vents or collapse craters. Peripheral to some hydrothermal domes are active hydrothermal vents (Morgan et al., 2007a). Close association with hydrothermal processes and development of a siliceous, nearly impermeable cap rock helps support the hypothesis that hydrothermal fluids/gases are involved in the uplift and deformation.

Storm Point hydrothermal dome. Located along the northern shore of Yellowstone Lake (Fig. 7), Storm Point is significantly elevated above the surrounding terrain and stands about 15 to 20 m above lake level (Fig. 33). Storm Point is a dome where the exposed strata are dipping away in all directions from the central high area. This convex-upward structure is related to a large hydrothermal center as evidenced by elevated ground temperatures, hydrothermally altered rock, and numerous active and inactive hydrothermal vents and structures exposed along the perimeter of Storm Point. Doming is evident in high-resolution LIDAR data (Pierce et al., 2002a, 2007a) and in the diversion of stream channels away from these uplifted areas. The dome measures ~840 m × 795 m and has multiple craters exposed on its top (Fig. 33). Bedded, cemented beach sands and gravels and altered laminated lake sediments on the eastern, southern, and western edges of the dome dip from 8° to 15° East, 15°–22° South, and 5°–8° West, respectively. West of Storm Point, the 8-ka S2 shoreline and younger shorelines tilt away from Storm Point by ~6 m over a distance of 1 km. Doming of the Storm Point area is estimated to have occurred 4–6 ka (Pierce et al., 2007a).

At least 15 craters have been identified on the top of the Storm Point dome; diameters of individual craters range from ~5 m to as large as 80 m (Fig. 33A). Many of these features are compound and involve small craters nested within larger parent craters. The surface of the eastern half of the Storm Point dome is mostly bare and unvegetated, except for some grasses and *Dichanthelium lanuginosum* (Stout and Al-Niemi, 2002),

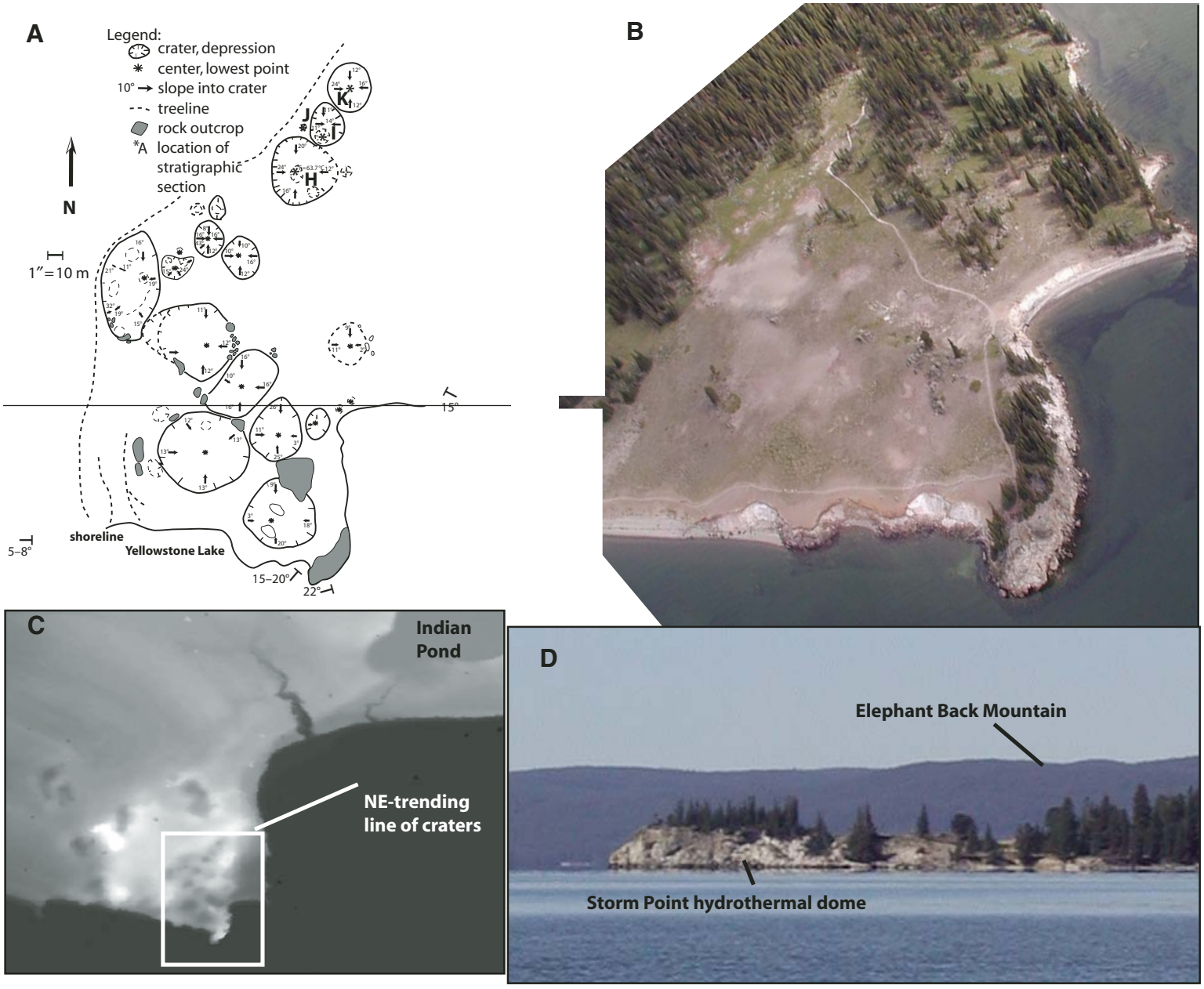

Figure 33. Hydrothermal features of Storm Point dome. (A) Detailed line map of craters and features on the top of the Storm Point hydrothermal dome. (B) Aerial photograph of the Storm Point hydrothermal dome. North is top of photo. Photograph is oriented the same and covers the same area as line map in A. Photograph courtesy of Paul Doss, University of Southern Indiana. (C) LIDAR DEM (digital elevation model) image of Storm Point hydrothermal dome. Box covers same area as line map in A. Image courtesy of Ray Watts, U.S. Geological Survey. (D) View of the Storm Point hydrothermal dome from the east. Elephant Back Mountain is in background.

which is common in many thermal areas in Yellowstone (http://plantsciences.montana.edu/stout/hotplants/research.htm).

Most craters at Storm Point cannot be unambiguously interpreted as subaerial hydrothermal explosion craters because very little hydrothermal explosion breccia has been identified and most craters do not have a rim of ejecta around their edges. It is possible that if the ejected material was composed of sinter, as is typical around smaller craters, it may have disintegrated rapidly and been removed by erosion. Marler and White (1975) documented the disintegration of large sinter blocks ejected from Link Geyser in Upper Geyser Basin in as little as a decade. Most of the substrata at Storm Point, however, are underlain by resistant, silicified gravel and lake sediment derived from rhyolite. Consequently, most of the craters may have formed by solution collapse. Some craters are rimmed by isolated blocks of slightly tilted hydrothermally cemented beach sand and sediment but contain no breccia fragments. Major amounts of alunite in Storm Point samples (Table 4) support the presence of acid sulfate hydrothermal systems, which commonly lead to collapse features. Fine, well-sorted eolian sands cover the floors of most craters; prevailing wind direction is to the northeast.

Thermal activity at Storm Point is ongoing. Active hydrothermal vents occur beneath Yellowstone Lake where it impinges on the edge of the Storm Point dome. The floors of many subaerial craters on Storm Point are above ambient temperatures and retain little snow in winter. Temperatures as high as 68 °C have been measured in near-surface sandy, eolian crater fill; in the upper 10 cm, temperatures range more typically between 18 and 56 °C (collected July 2003).

Domes on the floor of Yellowstone Lake. High-resolution bathymetric mapping has revealed the presence of many domes ranging from meters to several hundred meters in diameter on the floor of Yellowstone Lake; seismic survey data indicate that some of these domes preserve hydrothermal features (e.g., Fig. 12B) (Morgan et al., 2003; Johnson et al., 2003; Morgan and Shanks, 2005). Seismic images of hydrothermal-vent features typically show V-shaped structures associated with reflective layers that are deformed or have sediments draped across their edges. Areas of high opacity (those lacking discernable seismic reflections) extend laterally from directly beneath and outward from vent craters into surrounding sedimentary deposits. These opaque zones delineate subsurface pockets that contain steam and (or) CO_2 gas-charged fluids, or hydrothermally altered rock (Johnson et al., 2003). In Yellowstone Lake, areas of opacity in the seismic data spatially correspond to zones of low magnetic intensity in the aeromagnetic data (Finn and Morgan, 2002; Morgan et al., 2003) and represent areas of subsurface hydrothermal alteration that are larger than indicated by the surficial distribution of individual hydrothermal vents. Field evidence for lateral migration of hydrothermal fluids in the subsurface is exposed along the shoreline of Yellowstone Lake.

Many active sublacustrine hydrothermal vents are in thermal areas associated with small (1–10 m high) topographic domes (see Fig. 12B). We infer that silica-enriched hydrothermal fluids permeate, silicify, and seal porous near-surface sediment resulting in a low permeability cap. Here sealed, laminated, diatomaceous, lacustrine sediment is inferred to have been arched upward (Johnson et al., 2003) by buoyantly ascending steam and CO_2-rich hydrothermal fluids. Silicified cap sediments probably compact less than laterally equivalent nonsilicified mud surrounding the silicified cap; this difference in degree of silification of sediment may contribute somewhat to dome formation. Seismic reflection data (Otis et al., 1977; Morgan et al., 2003; Johnson et al., 2003), however, indicate a thickness of only 10–20 m of Holocene diatomaceous lake sediment. These postglacial lake sediments are underlain by noncompactable coarser-grained glaciolacustrine sediment or rhyolitic lava and thus limit the absolute magnitude of expected compaction. Studies of marine sediment indicate that the upper 10 m of similar sediment will compact by 10%–20% or 1 to 2 m (Breitzke, 2000). Consequently differential compaction may contribute to dome development of some small domes but compaction is unlikely to be a major contributor to dome height.

Several large (10–40 m high; 500–1000 m diameter) hydrothermal domes have been recognized in the northern central basins of Yellowstone Lake and are interpreted as once horizontally laminated sediment that was silicified and uplifted into convex upward domes (Johnson et al., 2003). Large sublacustrine domes include the north basin hydrothermal dome, a large dome south of Stevenson Island off Sand Point, and Elliott's Crater (Fig. 7). A line of sublacustrine domes extends northeast from the north basin hydrothermal dome toward Storm Point (Fig. 34A). The domes are similar to subaerial domes such as the large ~4–6-ka dome at Storm Point.

Smaller domes emerge from shallow parts of Yellowstone Lake in the late summer and fall when lake levels are low. Another example is a 10-m-diameter dome in Sedge Bay (Figs. 7 and 8), where Sedge Creek enters the northeast part of the lake. It is composed of beach sand and gravel that have been arched upward, silicified, and fractured. Active sublacustrine hydrothermal systems vent along joints and at the perimeter of the dome and provide habitat for otters in the winter. Another small dome (<10 m in diameter), in the lake east of Storm Point, also is composed of silicified beach sediment.

North Basin hydrothermal dome ("inflated plain"). The most pronounced dome in the northern basin of Yellowstone Lake, informally referred to as the northern basin hydrothermal dome (north basin dome) (Figs. 7 and 34), was originally identified during the 1999 bathymetric survey (Morgan et al., 1999) and was resurveyed in 2002 to determine whether this feature is actively deforming (Morgan and Shanks, 2005). Within survey error (60 cm), differential analysis of the two bathymetric data sets indicates no measurable changes associated with the structure. While dozens of vent systems are quite active on and surrounding the north basin dome (Figs. 34A and 34B), the morphology of the feature remained unchanged during the three-year survey recurrence interval.

The north basin dome covers an ~0.7-km-diam oval area, has a relatively flat top covered with small hydrothermal vent craters, and stands ~30 m above the surrounding lake floor (Fig. 34A).

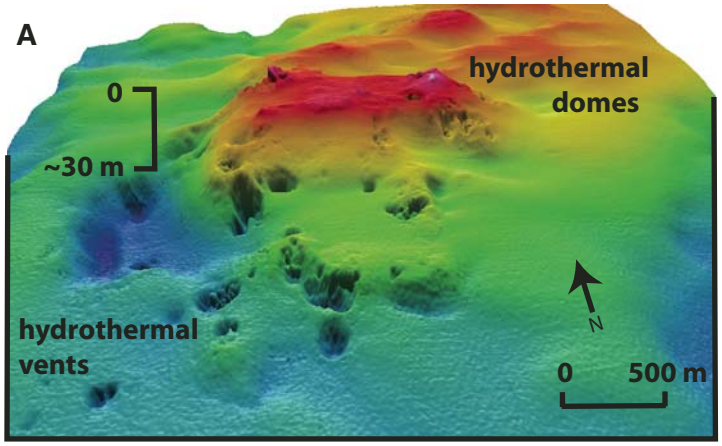
A
0
~30 m
hydrothermal domes
hydrothermal vents
N
0 500 m

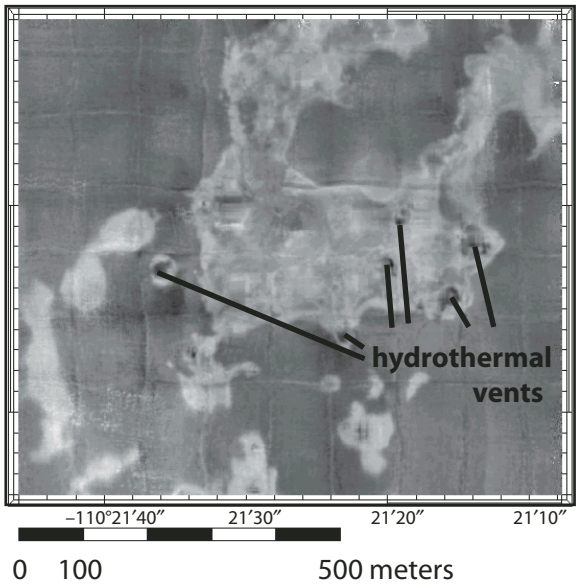
B
hydrothermal vents
–110°21′40″
21′30″
21′20″
21′10″
0 100 500 meters

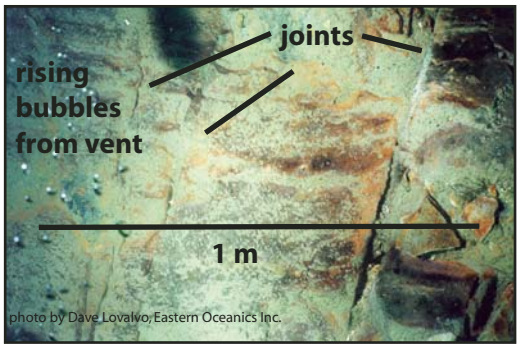
C
joints
rising bubbles from vent
1 m
photo by Dave Lovalvo, Eastern Oceanics Inc.

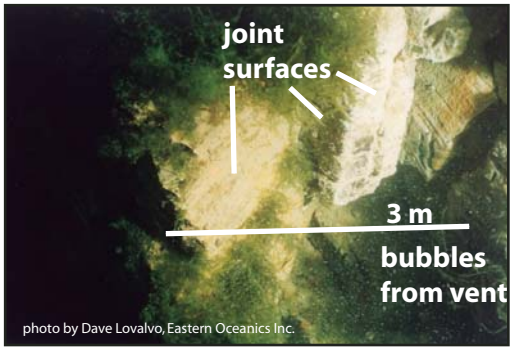
D
joint surfaces
3 m
bubbles from vent
photo by Dave Lovalvo, Eastern Oceanics Inc.


E
2 m
joint block
photo by Dave Lovalvo, Eastern Oceanics Inc.

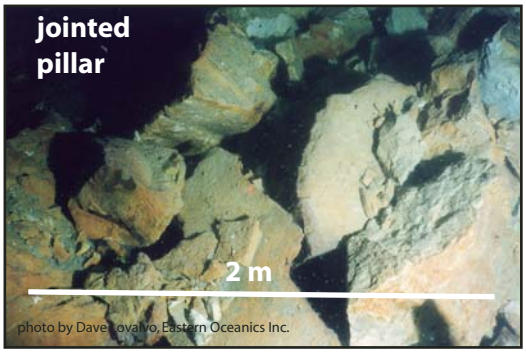
F
jointed pillar
2 m
photo by Dave Lovalvo, Eastern Oceanics Inc.

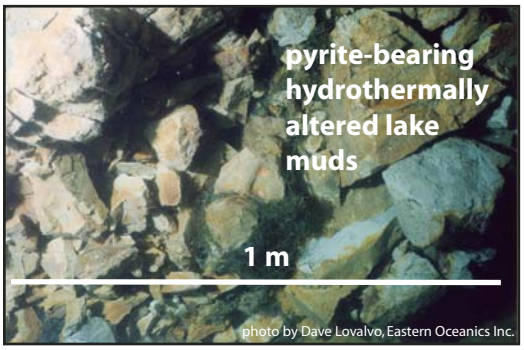
G
pyrite-bearing hydrothermally altered lake muds
1 m
photo by Dave Lovalvo, Eastern Oceanics Inc.

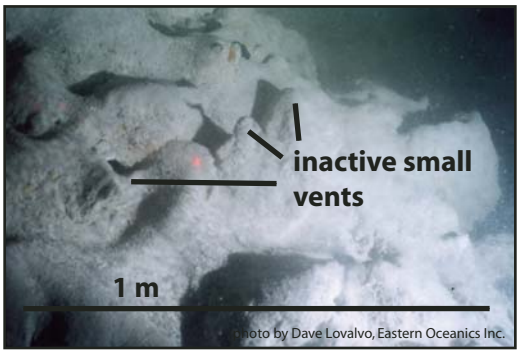
H
inactive small vents
1 m
photo by Dave Lovalvo, Eastern Oceanics Inc.

Figure 34. (A) Three-dimensional color-shaded-relief image of the north basin dome. Area shown is same as area in B but the image is rotated so that north is at 340° and is tilted 20°. Total depth ranges from 5.56 to 49.76 m. (B) Grayscale backscatter-amplitude map of the same area shown in A. Bright areas are reflective due to their relative hardness and degree of silicification. Dark areas are sites of active hydrothermal vents. The range of reflectivity is from 26 to –20 dB. (C) Set of northeast-trending joints on manganese-oxide-stained vertical joint plane. Rising on left, bubbles from a hydrothermal vent. (D) Blocks of orthogonally jointed mineralized lake sediments. (E) Pillars of orthogonally jointed mineralized lake sediments. (F) Fallen pillar. (G) Pyrite-bearing hydrothermally altered lake sediments; fresh surface has blue tint. (H) Small inactive hydrothermal vents in hydrothermally altered lake muds. All photographs taken with camera mounted on the submersible ROV by Dave Lovalvo, Eastern Oceanics.

Part of the relief associated with this feature may be due to its location within and along the edge of a rhyolite lava flow (Fig. 7) (Morgan and Shanks, 2005; Morgan et al., 2007a). Observations made with the submersible ROV, however, indicate that parts of the feature have steep to near vertical dipping beds comprised of silicified and strongly jointed lake sediment (Figs. 34C–34E). Seismic reflection data show 1- to 2-cm-thick alternating laminated beds characteristically associated with lake sediment on the flanks of the larger main dome also are dipping outward, typical of a dome and similar to structures observed at Storm Point.

ROV observations and high-resolution bathymetric data of the north basin dome (Fig. 34A) indicate that it is pockmarked by numerous hydrothermal vents and craters. A sonar backscatter amplitude map presents clear evidence of hydrothermal alteration (Fig. 34B). Some sediment-covered areas on the dome are highly reflective, which indicates that these areas are harder and may represent parts of a silicified cap rock. In contrast, less reflective material at other parts of the dome may represent less silicified rock. Presently active vent sites are not reflective, are not silicified, and, in fact, are experiencing dissolution by venting fluids to form vent craters (Shanks et al., 2005, 2007).

Smaller domes (150 to >260 m in diam) immediately northeast of the north basin dome are aligned with a linear trend that includes Storm Point and Indian Pond to the northeast and a trough to the southwest. This structure is similar and subparallel to fissures on Elephant Back Mountain (Morgan and Shanks, 2005), is referred to as the Weasel Creek-Storm Point linear trend (Figs. 7 and 8), and is host to numerous thermal features. Similarly, Muffler et al. (1971) noted concentrations of thermal features along major northwest- and southwest-trending lineaments on Lower Geyser Basin.

ROV observations indicate that the top of the north basin dome has dozens of small, very active hydrothermal vents. The surface of the dome is 15–25 m below lake level whereas the periphery of the north basin dome has vents at depths as great as 45–60 m (Fig. 34). Laminated lake sediments that are silicified and strongly vertically jointed make up most observable parts of the dome (Figs. 34C–34F). Shanks et al. (2005, 2007) have calculated that although silica can be deposited where hydrothermal vent fluids mix with lake-bottom water under certain circumstances, silica deposition is promoted where hydrothermal fluids are conductively cooled. Conductive cooling is most effective where hydrothermal fluids permeate into layered lake sediment away from vent conduits; sediment and associated pore space is silicified resulting in a cap of low permeability.

Hydrothermal fluids venting from the north basin dome ascend along well-developed joints or fractures, most of which are aligned in the present-day regional stress field. Most joints trend N35°–45°E or N305°–315°W. Individual vent crater diameters range from a few centimeters to >10 m; individual crater depths are as great as 10 m. Unusual topographic features abound on the north basin dome. These include ridges, small domes, and open fractures tens of meters deep (Fig. 34). Typically, laminated sediment is inclined on many of the small domes; the tops of many small domes are breached and emanate shimmering hydrothermal fluids. Larger crater complexes up to 75 m in diameter also are present (Fig. 34).

On the north basin dome, euhedral quartz and pyrite crystals are concentrated along well-developed joints coated with Mn- and Fe-oxide in pyritized and silicified lake sediment. Many lake sediment samples from this area are rich in dark, gray-colored, iron-sulfide-bearing clay and smell strongly of H_2S. Often smaller silicified pipelike structures extend off main joints (Figs. 34C, D, and E). A large linear vent depression occurs at the southwest edge of the north basin dome at a depth of ~58 m; here sonar amplitude data indicate the area atop the dome to be very hard and probably strongly silicified.

Temperatures of the hydrothermal fluids sampled from 1999 through 2004 from the north basin dome range from 39 up to 99 °C (Gemery-Hill et al., 2007) and probes inserted deep into vents indicate temperatures from 88 to 100 °C (W. Seyfried and K. Ding, 2003, personal commun.). Most of the fluids from these vents are near neutral pH but range from 4.9 to 7.3, averaging 6.3 (Gemery-Hill et al., 2007). Temperatures and gases from the many active vents on top of the north basin dome are quite variable and suggest that fracture systems beneath the north basin dome vents consist of many independent systems, only partly interconnected.

White microbial mats, amphipods, fresh water sponges, and fish occupy and thrive along crater walls and active vents. Many species of Nanoarchea have colonized these areas (John Varley and Eric Mather, 2005, personal commun.; Clingenpeel et al., 2008). On parts of the north basin dome, hydrothermal activity flourished in the past but has subsequently waned (Fig. 33H). At these sites, unconsolidated sediment has accumulated and the lake floor is unvegetated but is covered with abundant soft clay, fine sediment, and layers of diatomaceous ooze.

As hydrothermal systems such as those on the north basin dome evolve, small and large domes may be preserved, hydrothermal explosions may cause crater formation, collapse features may develop due to hydrothermal dissolution, and the dome surfaces may develop a pockmarked surface that represents small distinct vent craters (Shanks et al., 2005).

Joints

In and around Yellowstone Lake (Fig. 7), evidence of active deformation in the area underlain by the 0.64-Ma Yellowstone caldera is preserved by former lake shorelines. The elevations of lake shorelines display regular, slow cycles of inflation interspersed with periods of more rapid deflation (Hamilton, 1987; Meyer and Locke, 1986; Locke and Meyer, 1994; Pierce et al., 2007a). Inflation-deflation cycles proceed on a millennium time frame (Pierce et al., 2007a). Additional evidence for active deformation can be seen in the strongly developed joints exposed along the Mary Bay shore near the Black Dog hydrothermal breccia pipe and along the western shore of Bridge Bay. The diversity of hydrothermally altered sublacustrine sediment and hydrothermal activity around and within the caldera in Yellowstone Lake, coupled with active deformation of the Yellowstone caldera, provide a unique opportunity to examine how shallow hydrothermal systems form and develop.

The northern two-thirds of Yellowstone Lake are within and along the southeast margin of the Yellowstone caldera (Fig. 8). Detailed observation of active systems at Bridge Bay, Storm Point, Mary Bay, West Thumb, Sulfur Hills, and on the floor of Yellowstone Lake (Figs. 1, 7, and 8), combined with chemical data and physical models, have contributed to understanding the structural framework of the complex hydrothermal systems in Yellowstone. Joints, fractures, breccia-filled voids, and vent craters associated with prominent fissure systems are part of shallow hydrothermal systems, driven by ascending thermal fluids.

Field evidence from the shore and bottom of Yellowstone Lake indicates that some hydrothermal fluids ascend along vertical fractures or sets of parallel joints aligned with the regional stress field. Detailed field observations indicate that: (1) hydrothermal fluid flow is localized along vertical fractures and permeable zones; and (2) fluid flow is affected by regional structures that have a strong influence on the fluid flow path. The permeability of joints is variable and controlled by in situ stress conditions and pressure of the flowing fluid (Germanovich and Astakhov, 2004).

Bridge Bay: Shallow deformation processes associated with hydrothermal fluids. Bridge Bay, located along the northwest shore of the northern basin of Yellowstone Lake (Fig. 7), is a relatively shallow embayment surrounded by 3- to 4-m-high wave-cut terraces. Hydrothermally cemented beach gravel and sand form resistant ledges on these terraces. Lower in the sequence are laminated, fine-grained lake sediments that are variably altered, locally deformed, and strongly jointed (Fig. 30). Several cold spring seeps are localized midway down the steep bluffs at the contact between fine-grained permeable sediment above and clay-rich, bedded, and locally deformed mud below.

Joints in the lacustrine laminated sediment are well-developed; prominent sets of N35°E and N45°W-trending joints are exposed for over 1 km along bluffs bordering the lake (Figs. 30B–K). Joint sets are strongly dominated by prevailing regional stresses reflected in the consistent joint trends that are subparallel to structures at nearby Elephant Back Mountain (Fig. 8) and Sour Creek dome (Christiansen, 2001, Plate 1) (Fig. 1). Less developed joint sets are oriented due north and 105°. Most joints along Bridge Bay serve or have served as conduits for hydrothermal fluids, as indicated by warm flowing water and (or) mineralized rock preserved below lakeshore bluffs. Silicified fragments or ledges (Fig. 30) persist due to intense silicification where ascending hydrothermal solutions have impregnated laminated lacustrine sediment immediately adjacent to joint planes. Many of the joints are filled with quartz precipitate, which form sheetlike, planar structures that stand in relief as less resistant deposits erode along the shoreline (Figs. 30C, D, and E). Along some mineralized joints, focused fluid flow promoted formation of individual vent structures. These structures are preserved and surrounded by silicified lake sediment that preserves evidence of plastic deformation. The deposits most likely were deformed prior to silicification, possibly due to slumping into older vent craters or associated with fissure dilation.

Hydrothermal fluids ascending along joint conduits cause alteration, dissolution, and physical winnowing of finer materials, which results in void formation (Fig. 30A). Along the modern northern Yellowstone Lake shoreline, coarse, rounded platform gravels as well as other clastic material rest unconformably on strongly jointed, laminated, variably dipping, bedded, clay-rich lake beds. In places along the shoreline, where platform gravels are abundant, waves wash the gravels into joints, resulting in structures that resemble "gravel pipes" (Fig. 30A). Ascending hydrothermal fluids precipitate silica and pyrite along the joint walls and interstitial to clastic materials that fill voids along the joints. The result of this process is a structurally controlled fissure that has incorporated rounded and angular platform gravels cemented by precipitates from hydrothermal fluids (Fig. 30).

Locally, where orthogonal joint sets intersect fluids migrating along horizontal bedding planes, highly angular clasts are formed. These clasts fall onto the shoreline or into silicified, open joints. Breccia-filled voids or pipes form at joint intersections. A schematic sketch (Fig. 30A) illustrates the joint formation process; the range of joint types exposed on the shoreline and in wave-cut bluffs indicates various stages of joint development at Bridge Bay.

Storm Point joints. At the west and northeast edges of Storm Point, orthogonal sets of joints are similar but generally less well-developed and less abundant than at Bridge Bay. Southeast of Storm Point, predominant joint sets trend N75°W and N30°E (Fig. 33A). One hydrothermally cemented, gravel-filled joint strikes N60°E and is 0.5–1 m wide and 6–8 m long. This exposure is an excellent example of a large joint fissure filled by gravel, fine-grained sand, and mud that washed into a large planar void and later was cemented by ascending hydrothermal fluids; these fluids deposited silica, chalcedony, quartz, and pyrite that cemented the deposit. Along the shore to the west of Storm Point, excellent exposures of orthogonal and parallel joint sets are preserved in wave-cut bluffs. These joint sets may localize a line of hydrothermal craters that trend N10°E. Additionally, at both the west and northeast sites, excellent examples of lateral

fluid migration are preserved in zones that contain large, horizontally oriented vugs in well-sorted, fine-grained, obsidian-rich, now silicified sand.

Black Dog hydrothermal breccia pipe. Along the north shore of Yellowstone Lake in Mary Bay, ~1 km northeast of Storm Point and south of Indian Pond, orthogonal joint sets are exposed along a 150-m stretch of shoreline. At the approximate center of this area, a mineralized breccia pipe informally referred to as the Black Dog hydrothermal breccia pipe is exposed in the bluffs (Fig. 35A); its dark color reflects the finely disseminated pyrite present in the siliceous breccia matrix. To the west, joints in clay-rich, laminated lake sediment trend N45°E and N35°W. To the east, orthogonal joints trend N30–45°E and N40–45°W; a less well-developed joint set trends N10°E. Joints at the Black Dog structure trend N40°W and intersect an E-W–trending set.

The Black Dog breccia body is roughly cylindrical, ~5 m high, and averages ~2 m in diameter (Fig. 35B). The breccia body is clast supported and contains randomly oriented angular to rounded lithic clasts; most are silicified, laminated lake sediments with a few cemented beach gravels. Clasts are 1–60 cm in diameter and are altered from light gray argillite to thoroughly silicified black fragments with abundant finely disseminated pyrite (Fig. 35C). Several clasts are composed of multigeneration breccia and some have thermal cracks.

Excellent exposures of the breccia body show characteristics similar to those observed in joint fissures at Bridge Bay, except that Black Dog is a larger body that contains intensely mineralized breccia clasts in a mineralized matrix. Fractures within the breccia body are lined with drusy quartz as well as euhedral clear quartz, pyrite, and a green unidentified mineral. Much of the sandy matrix is now black and contains abundant finely disseminated pyrite. Angular, silicified clasts of laminated lake sediment are common in the breccia body and appear to be locally derived; these clasts appear to have been incorporated into an evolving, sublacustrine, near-shore hydrothermal vent.

The base of the breccia body extends downward as joints along which hydrothermal fluids ascend. Temperatures of fluids seeping out along these joints in recent years were ~18 °C in September 2000; an orange bacterial mat was associated with these seeps. Small, active hydrothermal springs were exposed on the shoreline ~60 m to the east of the mineralized breccia body. A vigorous 15-cm-diam spring had a temperature of ~42.1 °C and pH of 6.4 when sampled on September 2, 2000 (Gemery-Hill et al., 2007). An adjacent spring had a temperature of ~32.8 °C and was covered with orange and green bacterial mats. This latter spring is on trend with a large fracture filled by Mary Bay explosion breccia deposits.

The Black Dog breccia body has been slowly eroding due to strong wave action. Present exposures suggest that the breccia body was an open and vigorous hydrothermal system prior to emplacement of the Mary Bay explosion deposit. The breccia body is directly in contact with overlying Mary Bay explosion breccia (Figs. 35B and 35D). Silicified, laminated lake sediment grading upward into silicified laminated beach sand is exposed on the perimeter of breccia. At this location, the Mary Bay breccia deposits and dark sand that directly overlies the mineralized breccia pipe deposit are completely silicified and form a local resistant knob; this suggests that hydrothermal activity continued for some time after emplacement of the explosion breccia.

Collapse Craters and Dissolution

Craters also can form by collapse associated with dissolution of silica. Examples of subaerial collapse craters can be seen at West Thumb and other geyser basins throughout the park. At sublacustrine vents, samples of altered vent sediment indicate SiO_2 depletion and Al_2O_3 and CaO enrichment relative to unaltered Yellowstone Lake sediment (Shanks et al., 2005, 2007). Silica leaching can lead to formation of large voids beneath or at vents. Eventually, layered sediments founder into the subjected silica dissolution zone producing a hydrothermal vent crater (Shanks et al., 2005, 2007). In contrast with subaerial explosion craters that produce an apron of explosion breccia deposits distributed around the crater rim, collapse craters exhibit once-horizontal-but-now-inward-tilted and silicified rock fragments that are distributed near their original formation site around the collapsed crater. Unlike the broad range of rock types found as clasts in most hydrothermal explosion breccia deposits, fragments associated with collapsed craters are surficially derived; the lithology reflects the cap rock of uniform lithology.

Collapse craters in the geyser basins of Yellowstone are especially associated with acidic water that forms when H_2S in steam condensate is oxidized to H_2SO_4. We infer most of the craters atop the Storm Point hydrothermal dome to be collapse in origin. Similarly, most of the craters identified on the north basin dome in the northern basin of Yellowstone Lake appear to have formed as well through dissolution and collapse (Figs. 34A and 34B).

DISCUSSION

The Yellowstone caldera is underlain by a large (~25,000 km^3), partially crystallized and periodically replenished magma chamber (Fig. 2A) (Eaton et al., 1975; Fournier, 1989, 1999; Fournier et al., 1976; Lehman et al., 1982; Stanley et al., 1991; Wicks et al., 1998; Christiansen, 2001; Miller and Smith, 1999) that is above a 100-km-wide thermal plume that has been imaged to at least 500-km depth (Fig. 2B) and has a temperature estimated to be ~180 °C above ambient (Yuan and Dueker, 2005; Waite and Smith, 2004). A mantle plume under the southwest-moving North American plate is the inferred cause of the 16-Ma, 700-km-long Yellowstone hot spot track (Pierce and Morgan, 1990, 1992; Pierce et al., 2002b; Smith and Braile, 1994; Camp, 1995; Camp and Ross, 2004; Shervais and Hanan, 2008; Allen et al., 2008; Lay et al., 2009). Isostatic compensation associated with hot mantle material directly beneath the Yellowstone Plateau contributes significantly to its elevation and that of the surrounding mountains. The Yellowstone Plateau, a broad high terrain, receives as much as 180 cm of precipitation per year from moist, northeast-moving weather systems. The abrupt increase in

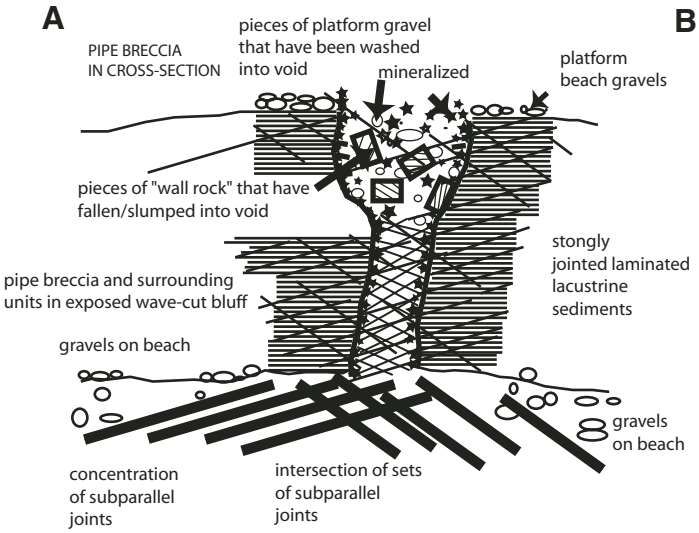
A
PIPE BRECCIA
IN CROSS-SECTION
pieces of platform gravel
that have been washed
into void
mineralized
platform
beach gravels
pieces of "wall rock" that have
fallen/slumped into void
stongly
jointed laminated
lacustrine
sediments
pipe breccia and surrounding
units in exposed wave-cut bluff
gravels on beach
gravels
on beach
concentration
of subparallel
joints
intersection of sets
of subparallel
joints

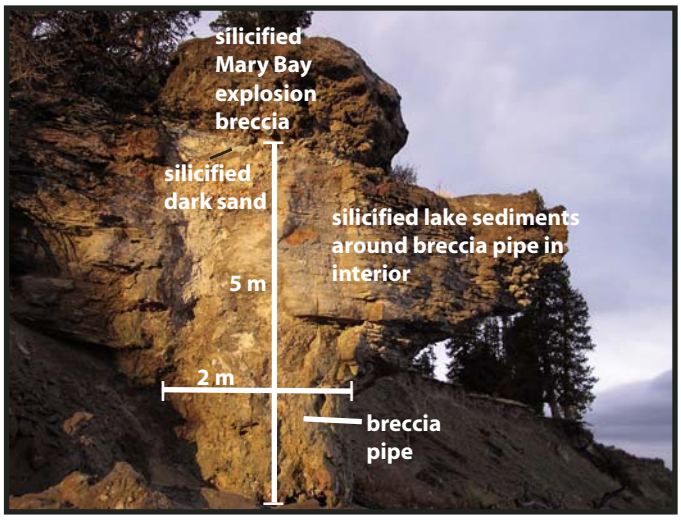
B
silicified
Mary Bay
explosion
breccia
silicified
dark sand
silicified lake sediments
around breccia pipe in
interior
5 m
2 m
breccia
pipe

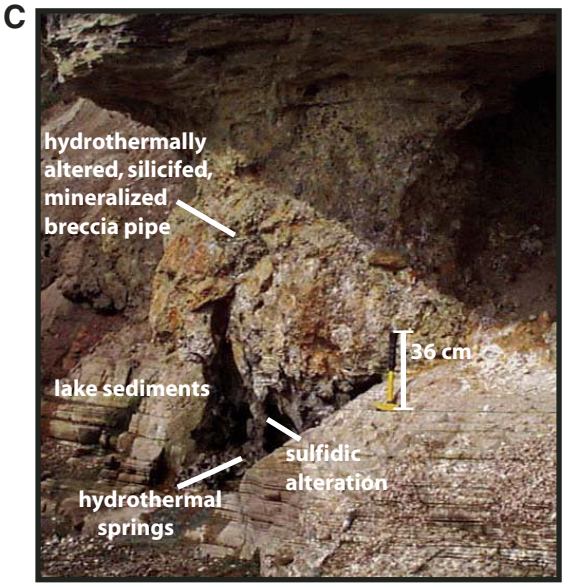
C
hydrothermally
altered, silicifed,
mineralized
breccia pipe
36 cm
lake sediments
sulfidic
alteration
hydrothermal
springs


D
Mary
Bay
cliffs


E
northeast-trending
fractures

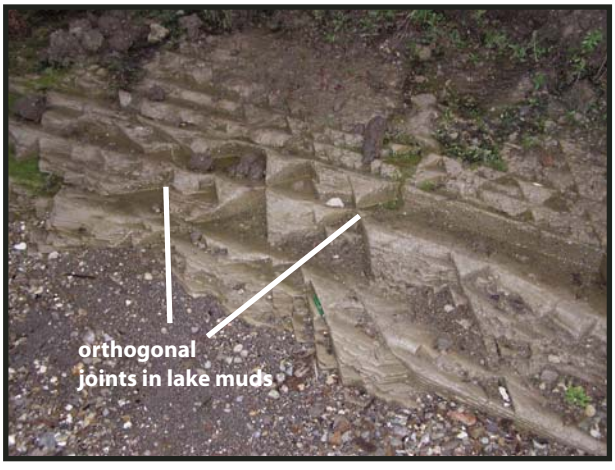
F
orthogonal
joints in lake muds

Figure 35. (A) Schematic cross section of the Black Dog breccia pipe exposed in bluffs west of Mary Bay along the northern shore of Yellowstone Lake. (B) 2004 photo from the west of Black Dog breccia pipe and surrounding silicified lake sediment beds overlain by a knob of silicified Mary Bay hydrothermal explosion breccia deposit. A fine-grained bedded dark sand is immediately below the Mary Bay breccia. The dark sand, Mary Bay breccia, lacustrine sediments, and breccia material in the pipe are silicified, forming a resistant minor promontory along the bluffs west of Mary Bay. This is the only location where the Mary Bay breccia deposit is silicified, suggesting that Black Dog was hydrothermally active when Mary Bay erupted and that activity continued for some period of time after eruption. (C) Close-up image of Black Dog breccia pipe surrounded by bedded lake sediments. The breccia in the pipe is clast-supported and thoroughly mineralized with quartz, amorphous silica, pyrite, and other sulfides. In contrast, the breccia in the Mary Bay explosion deposit is matrix supported. (D) View from west, similar to that in B, of the Black Dog breccia pipe taken by J. David Love in 1955. (E) View from the west at sunset of the Mary Bay cliffs, part of the crater wall of the Mary Bay hydrothermal explosion crater. (F) Set of orthogonal joints in bedded lake muds immediately east of the Black Dog breccia pipe. Individual joints are spaced every 2–5 cm.

elevation of ~1 km from the eastern Snake River Plain northeast to the Yellowstone Plateau is responsible for the rapid and heavy precipitation on the plateau (Pierce et al., 2007b). The combination of mantle heat and percolating meteoric water associated with abundant precipitation combine to yield the well-developed hydrothermal system present at Yellowstone today.

Hydrothermal activity in Yellowstone is dominated by meteoric water; hydrogen isotope data indicate that >70%–85% of water involved in the hydrothermal systems is derived from snowpack (Truesdell et al., 1977; Rye and Truesdell, 1993). A broad array of hydrothermal processes operate at various scales within Yellowstone and allow insights into variables that control localization, timing, duration, fluctuations, interconnections, and causes of hydrothermal activity and hydrothermal explosions. The following basic conditions are requisite for large (>100 m) hydrothermal explosion events: (1) a fractured and interconnected system of fluid channelways; (2) a water-dominated system at near-boiling conditions; (3) a through-flowing geothermal system such that water-rock reactions can affect system permeability and porosity over time (Andre et al., 2006); (4) sustained high heat flow; (5) active deformation including that associated with the inflation and deflation of the Yellowstone caldera to maintain and restore fracture permeability; and (6) an environment subject to sudden pressure changes such as those associated with seismic events, drought and climate variation, fracturing, landslides, and confining conditions.

Controls on Distribution and Development of Hydrothermal Systems in Yellowstone National Park

The combination of high heat flow, abundant meteoric water, and regional tectonic structures contribute significantly to the general location of hydrothermal features (Christiansen, 2001). Preexisting north-trending basin and range structures extend beneath caldera-related rocks of the Yellowstone Plateau and continue to influence fracture-controlled fluid flow and distribution of hydrothermal features (Christiansen, 2001). On a subregional scale, hydrothermal systems are concentrated in several structural and lithologic settings: (1) along tectonic zones outside the Yellowstone caldera, (2) near the topographic margin of the Yellowstone caldera, (3) within the Yellowstone caldera along the edges of rhyolite lava flows, and (4) along extensional faults associated with active deformation of the Yellowstone caldera (Fig. 1) (Pelton and Smith, 1982; Dzurisin et al., 1994; Pierce et al., 2002a, 2007a; U.S. Geological Survey, 1972; Christiansen, 2001; Morgan and Shanks, 2005; Jaworowski et al., 2006).

Influence of Lava Flows on Fluid Flow

Previous studies suggest that hydrothermal features within the Yellowstone caldera are concentrated along an inferred ring-fracture zone and by pre-existing basin-and-range faults that extend beneath the caldera (Christiansen, 2001; Ruppel, 1972). As hydrothermal fluids ascend along subsurface regional structures and approach the surface, their flow paths are strongly influenced by thick (150–300 m) rhyolite lava flows filling the Yellowstone caldera. There have been >40 postcaldera eruptions, including the 21 rhyolite units in the Central Plateau Rhyolite Formation, principally consisting of lava flows that fill the topographic depression created by caldera collapse. Mapping of more than 10,000 thermal features by the Yellowstone Center for Resources using differential GPS (A. Rodman, 2005, written commun.) shows thermal areas concentrated along the edge of lava flows, in basins between adjacent lava flows, or at the volcanic vent for the lava flow (Morgan and Shanks, 2005). This suggests that ascending hydrothermal fluids are horizontally diverted around low permeability lava flow interiors through permeable basal breccias and underlying sediments to vent at lava flow edges (Fig. 36).

Morgan et al. (2003) carried out two-dimensional fluid flow modeling (Fig. 37) to better understand the influence of rhyolite lava flows on subsurface hydrology. Convection in a high heat-flow regime causes water to flow upward. Flow is substantial through lava flows if they are uniformly fractured. Field observations (Morgan and Shanks, 2005; Bonnichsen and Kauffman, 1987), however, indicate that many rhyolitic lava flows have permeable basal flow breccias that may direct fluid flow laterally away from thicker, less-permeable interiors of rhyolite flows, especially if those flows are largely unfractured. Hydrothermal fluids then emerge at flow margins, which is consistent with many of the mapped locations of hydrothermal activity in Yellowstone (Fig. 36).

Pools of standing mosquito-infested waters suggest that the poor drainage of snow-melt runoff from high plateau surfaces of individual rhyolite lava flows reflects low porosity in the interior of massive rhyolitic lava flows. Dobson et al. (2003) have determined that a Central Plateau rhyolite lava flow has low measured permeabilities that average <0.1 millidarcy. Where fractured, the rhyolite has higher local permeability zones (up to

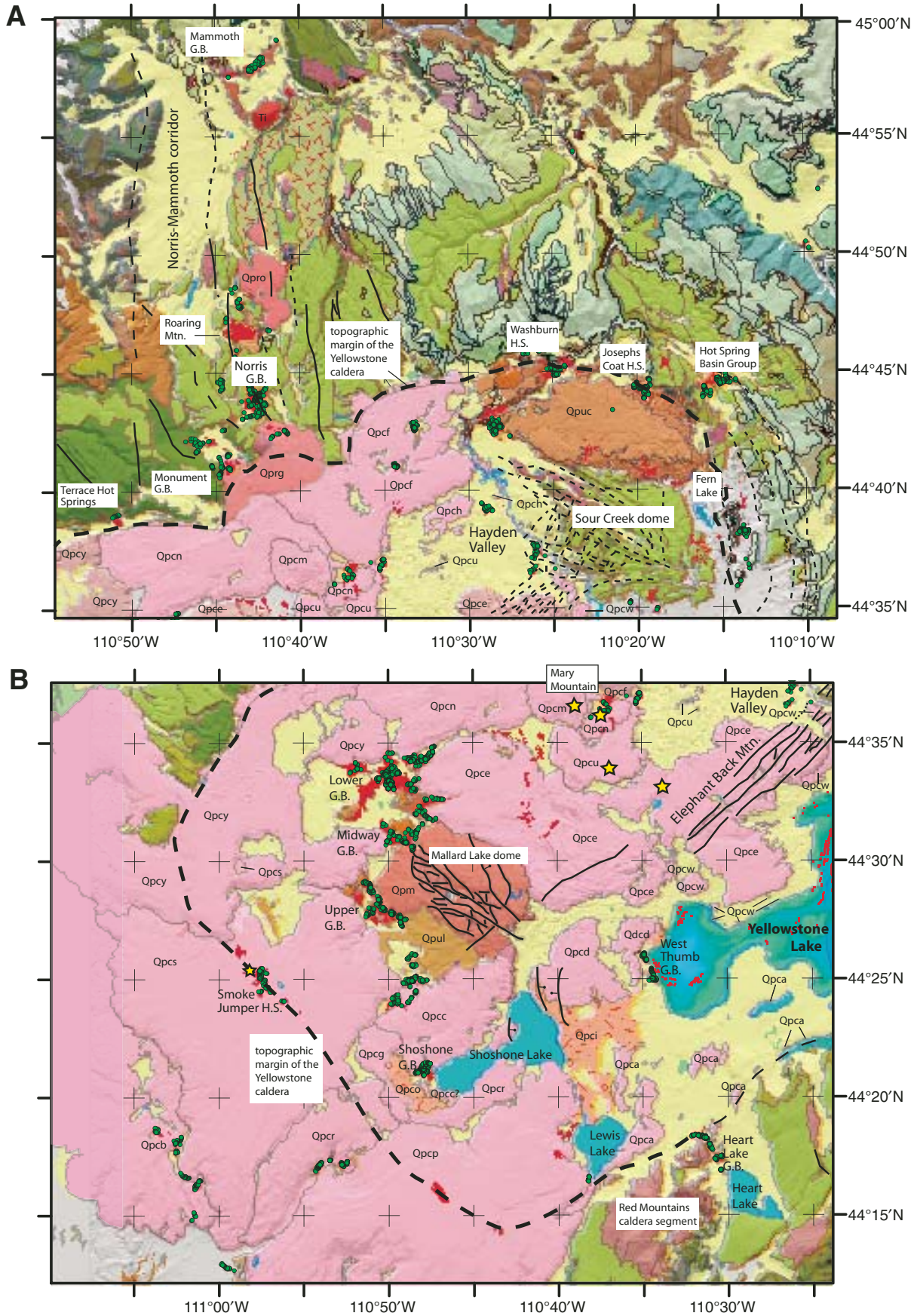
A
Mammoth G.B.
Ti
Norris-Mammoth corridor
Qpro
Roaring Mtn.
Norris G.B.
topographic margin of the Yellowstone caldera
Washburn H.S.
Josephs Coat H.S.
Hot Spring Basin Group
Qpuc
Qpcf
Qprg
Monument G.B.
Terrace Hot Springs
Fern Lake
Qpch
Sour Creek dome
Hayden Valley
Qpcy
Qpcn
Qpcm
Qpcu
Qpce
Qpcw
45°00′N
44°55′N
44°50′N
44°45′N
44°40′N
44°35′N
110°50′W
110°40′W
110°30′W
110°20′W
110°10′W
B
Mary Mountain
Hayden Valley
Elephant Back Mtn.
Lower G.B.
Midway G.B.
Mallard Lake dome
Upper G.B.
Qpcs
Qpm
Qpul
Qdcd
West Thumb G.B.
Yellowstone Lake
Qpcd
Qpca
Smoke Jumper H.S.
Qpcc
Qpci
topographic margin of the Yellowstone caldera
Qpcg
Shoshone G.B.
Shoshone Lake
Qpco
Qpcc?
Qpcr
Qpcb
Qpcp
Lewis Lake
Heart Lake G.B.
Heart Lake
Red Mountains caldera segment
44°35′N
44°30′N
44°25′N
44°20′N
44°15′N
111°00′W
110°50′W
110°40′W
110°30′W

Figure 36. Geologic maps highlighting the locations of hydrothermal areas in relation to various structures and deposits in YNP (modified after Christiansen, 2001). Features are represented as: the Yellowstone caldera (thick dashed black line); Norris-Mammoth tectonic corridor (thinner dashed black lines); general locations for faults or fissures at Sour Creek dome, Mallard Lake dome, and Elephant Back Mountain (thin black lines); thermal areas (areas in red). The locations of individual hydrothermal vents determined by differential global positioning system (GPS) (Ann Rodman, Yellowstone Center for Resources, 2005, written commun.) are plotted in green and represent data collected up to the summer of 2005; this is a work in progress. Yellow stars are shown to represent individual lava flow eruptive vents at the Elephant Back, Mary Lake, Spruce Creek, and Nez Perce flows (Fig. 9A) and Summit Lake flow (Fig. 9B). Units in pink, outlined in gray, represent Quaternary Central Plateau postcaldera rhyolitic lava flows and include Qpcy—West Yellowstone flow; Qpcn—Nez Perce flow; Qpcm—Mary Lake flow; Qpcf—Solfatara Plateau flow; Qpch—Hayden Valley flow; Qpcu—Spruce Creek flow; Qpce—Elephant Back flow; Qpcw—West Thumb flow; Qpcs—Summit Lake flow; Qpcr—Bechler River flow; Qpcb—Buffalo Lake flow; Qpca—Aster Creek flow; Qpcc—Spring Creek flow; Qpcd—Dry Creek flow; Qpci—Tuff of Bluff Point; Qpco—Tuff of Cold Mountain Creek. Units in tan are rhyolites Quaternary Upper Basin postcaldera rhyolitic lava flows and include Qpuc—Canyon flow and Qpul—Scaup Lake flow. Unit in medium pink in Figure 9B is the rhyolite of the Mallard Lake Member, Qpm—Mallard Lake flow. Units in dark pink in Figure 9A on the edge and north of the Yellowstone caldera are postcaldera rhyolitic lavas and include Qprg—Gibbon River flow and Qpro—Obsidian Creek flow. Other geologic units on map but not individually labeled include the Quaternary Lava Creek Tuff (light green); Quaternary basalt lava flows (purple); Quaternary sediments (yellow); Huckleberry Ridge Tuff (dark purple); Tertiary volcanic rocks (light brown); Precambrian rocks (brown); Tertiary–Mesozoic–Paleozoic rocks (dark olive and brown). (A) Geologic map showing hydrothermal vent and thermal area distribution in the northern Park along the northern margin of the Yellowstone caldera and the Norris-Mammoth tectonic corridor. (B) Geologic map showing hydrothermal vent and thermal area distribution in the western Park along the southwestern margin of the Yellowstone caldera and includes thermal areas at the Lower, Midway, Upper, Shoshone, and West Thumb Geyser Basins (G.B.). Yellowstone Lake is shown on the right; red areas in lake represent thermal areas.

346 millidarcy) that can transmit hydrothermal fluids. Such local zones of enhanced fracture permeability may account for hydrothermal areas like Smoke Jumper hot springs (Fig. 36B), which occurs in the interior of the Summit Lake flow at the fractured intersection of the volcanic vent area and the topographic margin of the caldera (Christiansen, 2001).

Local Structural Control

Joints associated with venting hydrothermal fluids and/or hydrothermal alteration at Bridge Bay, Storm Point, Mary Bay, and the north basin dome have consistent orientations that reflect a regional extensional stress field associated with continued active deformation of the 0.64-Ma Yellowstone caldera (Fig. 7). Joints have two dominant orientations, N35–45°E and N40–45°W, and a less prevalent joint set at N0–10°E; the northeast set is subparallel to northeast-trending fissures on the Elephant Back rhyolite flow (Christiansen, 2001). The northwest set is subparallel to vent-hosting fissures east of Stevenson Island and south of Elliott's crater in Yellowstone Lake (Fig. 7).

Elephant Back Mountain, located between the two resurgent domes of the Yellowstone caldera (Fig. 1), is in an area where recent inflation and deflation of the caldera has been measured. From 1923 to 1985, the amount of inflation measured at Elephant Back Mountain was ~760 mm (Pelton and Smith, 1979, 1982; Dzurisin et al., 1994). Subsequently, between 1985 and 1995, a period of subsidence ensued that was followed by inflation (Wicks et al., 1998; Lowenstern et al., 2006). The fissures on Elephant Back Mountain most likely have accommodated this inflation-deflation cycle and have been reactivated on multiple occasions. High-resolution aeromagnetic data (Finn and Morgan, 2002) indicates that the fissures are coincident with low values of magnetic intensity; these zones probably result from magnetite in the rhyolite lava having been hydrothermally altered to nonmagnetic hematite. The fissures are zones of weakness that most likely served as conduits for hydrothermal fluids.

High-resolution bathymetric data for Yellowstone Lake just southeast of Elephant Back Mountain reveal another strongly pronounced northeast-trending topographic fissure, referred to as the Weasel Creek-Storm Point linear trend (Fig. 7). This 14-km-long feature extends from Weasel Creek, a linear stream valley west of the lake, continues beneath the lake as a trough-like feature, northeastward through several active hydrothermal features (including the north basin dome) and emerges from the lake near Storm Point. The 2.9-ka Indian Pond hydrothermal explosion crater is to the northeast along this trend. Following this trend, northeast-oriented fractures are apparent in the ridge covered with Mary Bay hydrothermal explosion deposit (Fig. 7). The Indian Pond explosion crater and the Storm Point and north basin hydrothermal domes are spaced roughly 1.2–2.4 km apart and may reflect zones where hydrothermal circulation cells are spaced approximately every 2 km.

Another northeast-trending structure, along which the Elliott's and Mary Bay explosion craters occur, is ~2 km southeast of and parallel to the Weasel Creek-Storm Point trend. Elliott's crater and the Mary Bay complex are ~1.8 km apart. Northeast of the Mary Bay crater wall and due south of the Sour Creek resurgent dome are strong northeast-trending trenches (Fig. 7), These structures may be related to the magmatic-hydrothermal inflation-deflation process operating beneath Elephant Back Mountain and the Sour Creek resurgent dome (Fig 1). The Weasel Creek-Storm Point trend is also reflected in aeromagnetic data as a series of magnetic low anomalies (Finn and Morgan, 2002) and is spatially coincident on the 450-mm-uplift contour interval of >700-mm maximum inflation for Elephant Back from 1923 to 1985 (Pelton and Smith, 1979, 1982; Dzurisin et al., 1994).

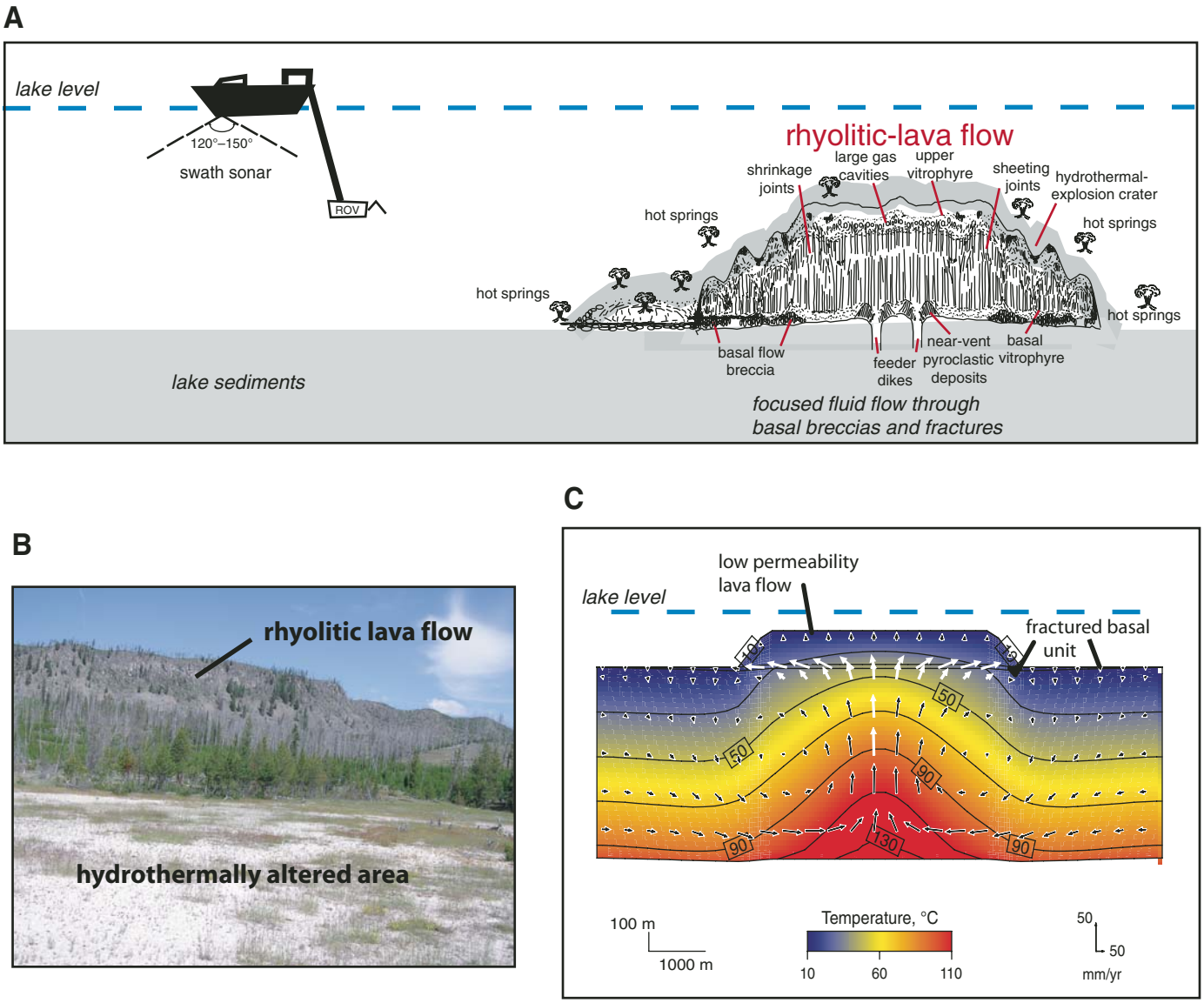

Figure 37. (A) Schematic diagram showing physical features of a rhyolitic lava flow (modified from Bonnichsen and Kauffman, 1987). (B) Photograph of the edge of a rhyolitic lava flow at Biscuit Basin. Note the abundance of thermal features at the base and edge of the flow. (C) Two-dimensional fluid-flow model with a simple glaciolacustrine-sedimentary aquifer that includes a basal breccia zone beneath a low-permeability lava flow. The lower sedimentary unit is overlain by a thin, fractured, lava-flow unit (20 m thick) that extends the entire width of the sedimentary prism. Above the more permeable basal unit is a 170-m-thick low-permeability unfractured lava flow. Flow vectors indicate strong upflow under the lava flow with maximum subsurface temperatures of ~150 °C and flow rates up to 160 mm/yr. Upflow is deflected laterally within the 20-m-thick "basal" fractured zone toward the flow edges resulting in hydrothermal venting on the lake floor near the margins of lava flows.

Hydrothermal Processes Related to Alteration, Self-Sealing, and Dissolution

Chemical evolution of fluid in hydrothermal systems involves convective flow, water-rock interaction, boiling and mixing of fluids as they migrate laterally and ascend buoyantly, and dissolution and precipitation of minerals in the near-surface and surface environment (Fournier, 1999; Shanks et al., 2005; Nordstrom et al., 2005). Chemical and physical processes involve development of fluid-flow paths through interconnected pore spaces or, more likely, along fractures or channelways and through larger void spaces (Fig. 3A). Deep circulation of fluids along the flow paths is favored by density differences related to thermal expansion, viscosity of fluid with increase in temperature, and the increase in solubility of silica with increase in temperature (White, 1967; Fournier and Rowe, 1966). Once hydrothermal flow paths are established, these systems evolve as minerals or amorphous materials are dissolved and (or) precipitated and as water cir-

culating in the reservoir responds to these changes. Over time, surface manifestations of these transformations might include cessation of flow, onset of geysering, small explosive events, development of mudpots, and changes in pH or amount of water or steam available in the reservoir. Seismic and tectonic forces related to active deformation of the Yellowstone caldera also are important in creating new fluid conduits and maintaining open, mineralized, and established flow systems.

Self-sealing processes in hydrothermal systems contribute significantly to fractures and pores in reservoir rocks being filled and substantially reducing system permeability (Facca and Tonani, 1967). In a circulation cell, high temperatures near the base of the cell contribute to increased solubility of silica and creation of void spaces. In contrast, silica and other minerals such as K-feldspar, chalcedony, and zeolites, precipitate at lower temperatures in the upper parts of the convecting cell and contribute to decreasing porosity and permeability to the cap rock (White, 1967). Self-sealing processes play an important role in the development of cap rocks in hydrothermal fields (Xu and Pruess, 2001), collapse craters, hydrothermal domes, and perhaps caldera inflation and deflation (Pierce et al., 2007a). Evidence of operational self-sealing processes includes the inferred partial cap at the north basin dome in the northern basin of Yellowstone Lake (Fig. 34B) and other sublacustrine sites (Johnson et al., 2003), at subaerial sites like Storm Point, and other thermal areas in Yellowstone. Direct evidence for cap rock fragmentation by hydrothermal explosions is provided by silicified surficial (lake, glacial, and beach) sediment in lithic clasts in deposits such as Mary Bay, Turbid Lake, and Indian Pond explosion breccias.

Mastin (1995, 2001) calculated that hydrothermal explosions release ~250 kJ/kg, which is about one-tenth the energy of an equivalent mass of gunpowder. These relatively low energies suggest that the types of hydrothermal explosions that excavate large craters in Yellowstone most likely occur in areas where the enclosed rocks have been weakened by fracturing and hydrothermal alteration; these are more vulnerable to explosions than rocks not fractured or altered.

Alteration, Dissolution, and Self-Sealing in Subaerial Environments

Yellowstone thermal basins commonly contain the following: (1) sinter or travertine terraces or broad cones formed by surficial sheet flow of thermal waters away from pools or geysers; (2) deep, steep-sided thermal pools, (3) hollow ground beneath thin crust, (4) collapse structures, (5) a variety of nearly sealed geysers and spouters, and (6) constructional deposits around vents. Large surface water pools typically do not have prominent raised ejecta rims and so are not hydrothermal explosion features; rather, these form by dissolution or collapse. Depending on the style of fluid flow and venting, and temperature gradients within a reservoir, compositionally similar hydrothermal fluids can evolve to create constructional forms associated with precipitation or consume earth materials via dissolution.

The nature of hydrothermal alteration in the near-surface part of geyser basins is well-understood as a result of the 1960s USGS research drilling program, which cored hydrothermally altered rocks and sampled subsurface hydrothermal fluids in thermal areas throughout YNP (White et al., 1975; Bargar and Beeson, 1980, 1981, 1984, 1985; Bargar and Muffler, 1975, 1982; Keith and Bargar, 1993; Keith et al., 1978; Sturchio et al., 1986, 1988). Most subaerial thermal systems within or marginal to the Yellowstone caldera are hosted by high-silica rhyolite ignimbrites (Lava Creek Tuff) or lava flows, or in detrital deposits derived from rhyolite. Alteration studies of USGS drill cores (Bargar and Beeson, 1980) and explosion breccia samples analyzed by XRD in this study (Table 4) indicate that various silica phases, clay minerals, and zeolites form during alteration. In addition, many major oxide components of host rhyolites, including Na, K, Ca, and Mg, are commonly removed during hydrothermal alteration (Bargar and Beeson, 1980; Sturchio et al., 1986). Sturchio et al. (1986) conclude that ~10^3–10^4 kg of water has reacted with every kg of rock in the hydrothermal upflow zones studied in the Y-7 and Y-8 drill holes.

Dobson et al. (2003, 2004) used a combined fluid flow and geochemical reaction model to conclude that hydrothermal processes involve a large amount of rhyolitic glass dissolution and precipitate illite, celadonite, iron oxides, and some zeolite minerals. Starting conditions for the flow-reaction model used fresh rhyolitic rock (~82% glass) and the measured permeabilities of cores from the Y-8 drill hole in the Biscuit Basin area (Dobson et al., 2003). Results indicate that 95% of the contained glass was dissolved after 50,000 d (~137 yr) of reaction. Thus subsurface development of void space along flow paths occurs within a relatively short period. In addition, reacted fluids actively deposit celadonite and oxides, but also have the potential to precipitate other minerals, especially silica phases, during ascent and cooling.

High-resolution aeromagnetic data (Finn and Morgan, 2002) indicate that subsurface alteration around hot spring areas involves a much larger area than surface features might indicate. The data suggest that subsurface lateral migration of hydrothermal fluids effectively removes or destroys primary magnetic minerals. Throughout the Yellowstone caldera and the Norris-Mammoth tectonic corridor, zones with regularly spaced fissures or faults have regularly spaced magnetic lows, which may depict hydrothermal convection cells spaced every couple kilometers (Finn and Morgan, 2002), as also hypothesized in the northern basin of Yellowstone Lake. Consequently, interconnected, subsurface hydrothermal flow systems may cover fairly substantial areas.

Alteration, Dissolution, and Self-Sealing in Sublacustrine Environments

High-resolution bathymetric mapping and seismic reflection studies in Yellowstone Lake, coupled with direct lake-floor observations and sampling by submersible ROV, provide evidence of both extensive hydrothermal dissolution of lake sediments and localized precipitation of silica (Morgan et al., 2003; Shanks et al., 2005). These studies indicate that most sublacustrine

hydrothermal vents are characterized by V-shaped vent craters or conical local cavities at vent sites. Over 650 vent structures are identified (Fig. 8B) on the bathymetric map of Yellowstone Lake (Morgan and Shanks, 2005).

Shanks et al. (2005, 2007) studied geochemical variations in hydrothermally altered mud collected from vent craters and concluded that ~63 wt% of the SiO_2 has been leached from original lake sediment. Consequently, development of void space with sediment on the lake floor and in the shallow subsurface, especially along interconnected flow paths, is a consistent ramification of sublacustrine venting at or near the lake bottom. Hydrothermal fluids, however, also can and do deposit siliceous materials as they cool following venting at the lake bottom. Siliceous deposits of opal, chalcedony, and, in some cases, quartz (Table 4) form a broad variety of conduits, pipes, and tabular deposits (flanges) along joints and permeable horizontal layers in lake-bottom sediment. Similar deposits are observed in Lake Taupo, New Zealand, which also lies above a crystallizing magma chamger in a significant caldera (Jones et al., 2007).

Geochemical reaction modeling (Shanks et al., 2005, 2007) suggests that the fluids that initially dissolve diatomaceous lake sediment (or rhyolitic glass) can subsequently redeposit silica as amorphous silica (the most soluble form of silica) at the lake bottom when hydrothermal fluids either mix with cold lake water or conductively cool within conduits or permeable sediment horizons. Cooling without mixing is most effective in terms of the quantity of silica deposited per kg of vented hydrothermal fluid because dilution during mixing with essentially silica-free lake water lowers SiO_2 concentration in the mixed fluid and supersaturation is eliminated more quickly (Shanks et al., 2007).

Seismic reflection studies near sublacustrine vent areas display horizontal zones in sediments with no reflections, which are interpreted as zones of lateral hydrothermal fluid flow accompanied with or without gas (steam, CO_2) that persist for significant distances away from vent craters (Johnson et al., 2003). Lateral hydrothermal fluid flow in sediment represents an excellent mechanism for conductive cooling and silicification and alteration of lake sediments. Acoustic backscatter data for surficial sediments on the north basin dome in north-central Yellowstone Lake (Figs. 7 and 34B) indicates sediment that has been altered and silicified. In areas like the north basin dome, where large hydrothermal systems probably have persisted for thousands of years and where venting and alteration have been extensive, it is likely that the systems are at least partly sealed by a low permeability cap; further, these systems probably are underlain by a well-developed network of interconnected fluid channelways and voids.

Different stages of deformation and doming by hydrothermal fluids/gases are imaged in seismic reflection profiles over vent areas beneath Yellowstone Lake (Johnson et al., 2003) (Fig. 12). Low-relief domes of various sizes are well-documented on the lake floor (Johnson et al., 2003). Seismic data characterized by chaotic reflections suggest that small domes on the flanks of Elliott's crater (Fig. 12A) contain pockets of hydrothermal fluids and (or) gases. These zones of chaotic reflections are beneath areas where horizontally bedded lake sediments have been arched upward to form mound-shaped features (Fig. 12B). Hydrothermal fluids appear to have been injected into porous sediment along edges or fractured areas within rhyolite lava flows or into fractures produced by periodic inflation and deflation of the Yellowstone caldera associated with migrating hydrothermal fluids or magmatic gases (Waite and Smith, 2002). Once introduced, circulation of hydrothermal fluids causes dissolution of material in the deeper parts of circulation cells and precipitation of silica in the upper parts of these systems to form an impermeable cap. Partially or fully self-sealed systems develop when porosity in surficial sediment and in fractures along the flow path is reduced. Thermal fluids continue to be injected into these systems; accumulation of hot, buoyant fluid beneath the silicified cap may contribute to flexing the sedimentary strata upward into a domal structure. Barriga and Fyfe (1988) proposed a mechanism to address the space issue in developing volumes for subseafloor precipitation of massive sulfide deposits. In that proposal, they suggest an impermeable "rubber-like" seal of gelatinous silica under which a buoyant mass of hydrothermal fluids are trapped below and inflate the cap rock (Barriga and Fyfe, 1988). Some extremely large domes, including Storm Point and the north basin dome may include multiple smaller domes that contribute to the evolution of the larger system; in systems such as these, the hydrothermal system may be partially capped. Domal features may be precursors to development of hydrothermal explosion craters; however, some domes, particularly those that are only partly sealed, may never experience explosion crater development (Morgan et al., 1998).

Large Hydrothermal Explosions

One of the distinctive characteristics of large hydrothermal explosion craters in Yellowstone is the very large crater size and volume of ejected material relative to the majority of hydrothermal explosion features noted elsewhere in the world (Table 1). The characteristics of worldwide hydrothermal explosion craters, not including examples from YNP, have been compiled by Browne and Lawless (2001). They identify 31 historical and 47 prehistoric events. Of the historic events, only nine have diameters greater than 100 m, five are larger than 200 m, and no historical events produced a crater greater than 500 m. Of the prehistoric events outside of Yellowstone, 44 had craters greater than 100 m in diameter, 37 are larger than 200 m, and a single crater larger than 500 m is identified (Browne and Lawless, 2001).

Most historic hydrothermal explosions in Yellowstone have produced relatively small crater diameters (<10 m). In contrast, more than 20 prehistoric hydrothermal explosion events occurring within the past ~16 ka (during and after the most recent Pinedale deglaciation), however, created ten craters with diameters >500 m and three with diameters >1000 m. These latter 13 craters are at the extreme high end of the size spectrum for known hydrothermal explosion craters (Table 1; Fig. 38). Compared with small hydrothermal explosion events known to occur in active thermal

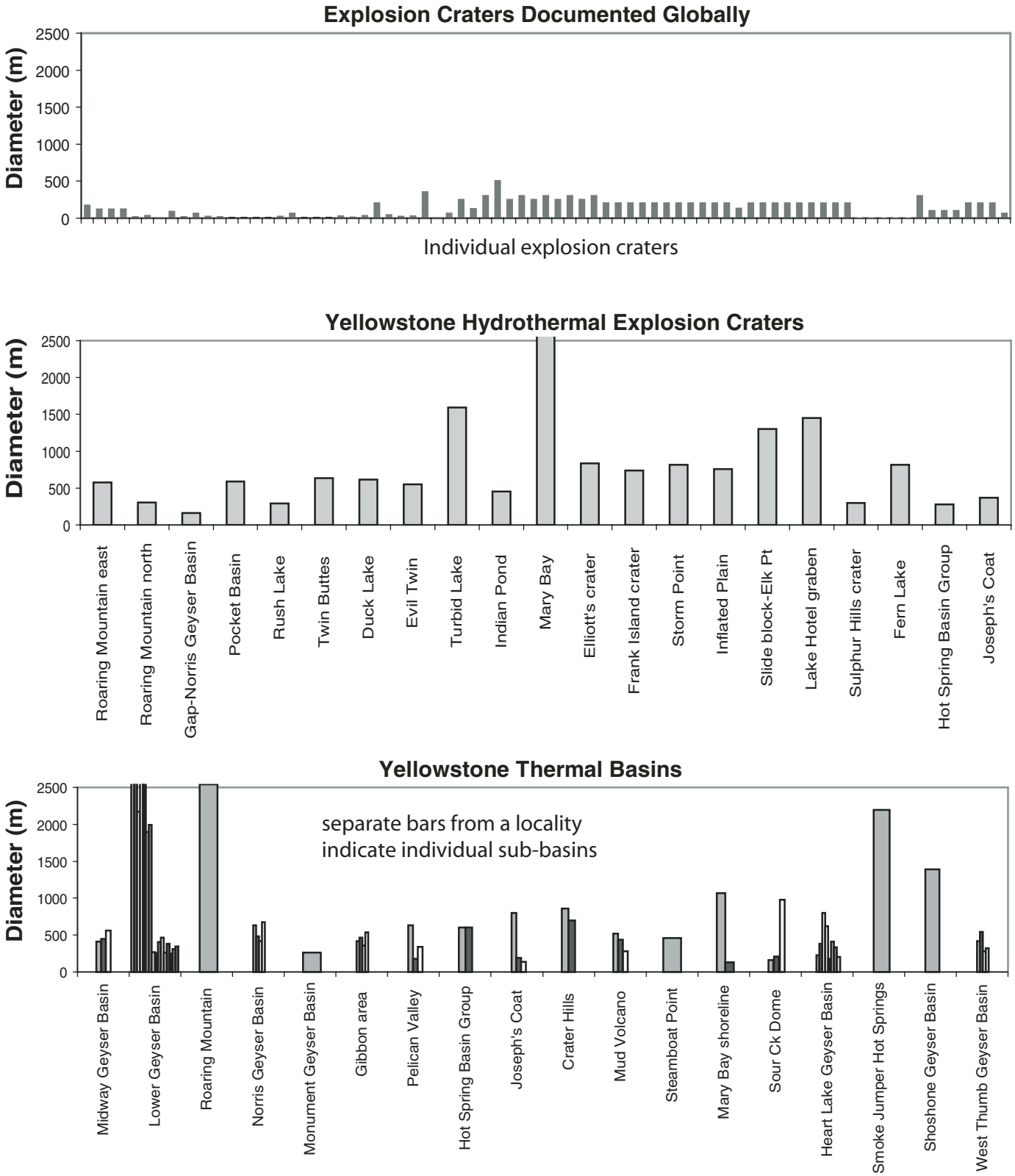

Figure 38. (A) Maximum diameter of hydrothermal explosion craters in New Zealand and elsewhere (Browne and Lawless, 2001). The diameters of the majority of the hydrothermal explosion craters are less than 200–300-m. (B) Long diameter of large hydrothermal explosion craters in Yellowstone National Park. The diameters of the majority of the hydrothermal explosion craters are >500 m. (C) Long diameter of selected thermal areas and geyser basins in Yellowstone National Park. The diameters of the majority of these sites are greater than 500 m.

areas about once every two years, large hydrothermal explosions are relatively rare (Lowenstern et al., 2005). The dimensions of large prehistoric, postglacial hydrothermal explosion craters in Yellowstone are comparable in scale with those of many thermal areas well-developed in Yellowstone (Fig. 39), which may suggest a possible relationship. Large hydrothermal explosion craters may be the end products of a chain of rare events that lead to a series of nearly simultaneous explosions that ultimately engulf large parts or all of a thermal basin. Such events may occur in established thermal areas when the thermal flux increases and/or the confining pressure decreases to a threshold value, perhaps in response to seismic activity, drought and water table decline, or change in hydrostatic pressure. Seismic events and deformation can reopen interconnected hydrothermal fluid flow paths or cause sudden shifts in confining pressure. Clear evidence exists in Yellowstone, which suggests that seismicity and sudden changes in water level over active hydrothermal fields acted as significant triggers that resulted in large explosions. Pocket Basin, Twin Buttes, Mary Bay, and Indian Pond may represent examples of these mechanisms.

Large hydrothermal explosion events in Yellowstone have the following characteristics: (1) the lithic clasts and matrix of explosion deposits are hydrothermally altered, which indicates hydrothermal activity was ongoing at the time of the explosion; (2) hydrothermal explosion breccia deposits are volumetrically significant (Table 1), thus preexplosion hydrothermal activity was extensive and affected large areas that were incorporated into the explosion deposit; (3) many lithic clasts contained in explosion breccia deposits preserve evidence of multiple fracturing, alteration, and recementation events that occurred in a pre-existing hydrothermal system; and (4) the dimensions of documented, large hydrothermal explosion craters in Yellowstone are similar to those of many of the currently active geyser basins or thermal areas (Fig. 39). Many thermal basins in Yellowstone are characterized by (1) high-temperature convective hot-water systems and extremely high heat flow; (2) extensive systems of hot springs, fumaroles, geysers, sinter terraces, mud pots, and, in places, small hydrothermal explosion craters; (3) widespread alteration; (4) large areal dimensions (greater than several hundred meters); and (5) intermittent but long-lived systems (White et al., 1988) known to have persisted for 15,000 yr to as much as 375,000 yr, as indicated by U-series chronology (Sturchio et al., 1994).

Triggering Mechanisms of Large Hydrothermal Explosions

Development of a large hydrothermal explosive event requires a sudden near-surface pressure decrease associated with a hydrothermal system in which liquid water or a two-phase gas-water mixture is at or near boiling point conditions (McKibbin, 1991; Smith and McKibbin, 2000). If a partially sealed hydrothermal system experiences an abrupt pressure reduction, liquids in the reservoir can boil and flash to steam (Fig. 3). The volume expansion accompanying this phase change can further fracture the surrounding rock, resulting in outward ejection of material thereby creating a substantial crater. Sustaining the explosion requires that fluids continue to boil explosively, flashing to steam, which requires depressurizing additional fluids contained in interconnected joints or channelways. The advancing flashing front continues to fracture host rocks as it propagates laterally and downward from the near-surface point of pressure release. As fluids explosively expand toward areas of lower pressure, this upward movement fractures and removes remaining overlying rock (Fig. 3) excavating broken rock from and dramatically enlarging the crater. A considerable volume of the ejecta falls back into the explosion crater.

Fluids continue to boil as they ascend, resulting in an explosion column that contains more steam at its top than base (Smith and McKibbin, 2000). The explosion terminates once the descending boiling front enters (1) a zone of negligible porosity or permeability, (2) fluids at or near boiling temperatures become unavailable (Smith and McKibbin, 2000), and/or (3) the amount of steam generated is insufficient to eject the fractured rocks (Browne and Lawless, 2001). Hydrothermal explosions produce a breccia zone at a depth that may host precious metal mineralization (Weed and Pirsson, 1891; Henley et al., 1984; Hedenquist and Henley, 1985; White et al., 1991; Fournier et al., 1994b). Mineral deposits containing gold, uranium, mercury, lithium, and other strategic minerals are known to be associated with hydrothermal explosion deposits (Sillitoe et al., 1984; Sillitoe, 1985; Silberman and Berger, 1985; Nelson and Giles, 1985; Vikre, 1985). Some of the hydrothermal explosion deposits in Yellowstone have elevated concentrations of some of these elements (Table 3).

Formation of large hydrothermal explosion craters of the scale described here has not been witnessed, so triggering mechanisms must be inferred from geologic evidence. Muffler et al. (1971) and Pierce et al. (2003) present evidence that the Pocket Basin explosion event occurred in the waning stages of the Early Pinedale Glaciation when an ice-dammed lake overlying an active hydrothermal system suddenly drained, resulting in a sudden confining pressure decrease, which triggered the explosion. While correctly noting that most other hydrothermal explosion craters in Yellowstone also are postglacial, they suggest that many other explosion events may have been triggered similarly. This process may be applicable to the formation of some craters in Yellowstone; however, radiocarbon ages and other evidence (Pierce et al., 2007a) indicate that many of these large hydrothermal explosions are younger than Pinedale deglaciation and therefore, other hydrothermal explosion triggering mechanisms than those related to recession of glacial ice must be considered.

Many areas now occupied by large explosion craters probably were previously occupied by thermal basins or extensive, well-established thermal areas that catastrophically failed during an event triggering hydrothermal explosion to producing large craters and voluminous hydrothermal explosion deposits. Events that trigger the explosions must be capable of affecting the majority of or an entire thermal basin over a relatively short time period. The best indication of triggering mechanisms comes from geologic observation of the largest and best-preserved deposits

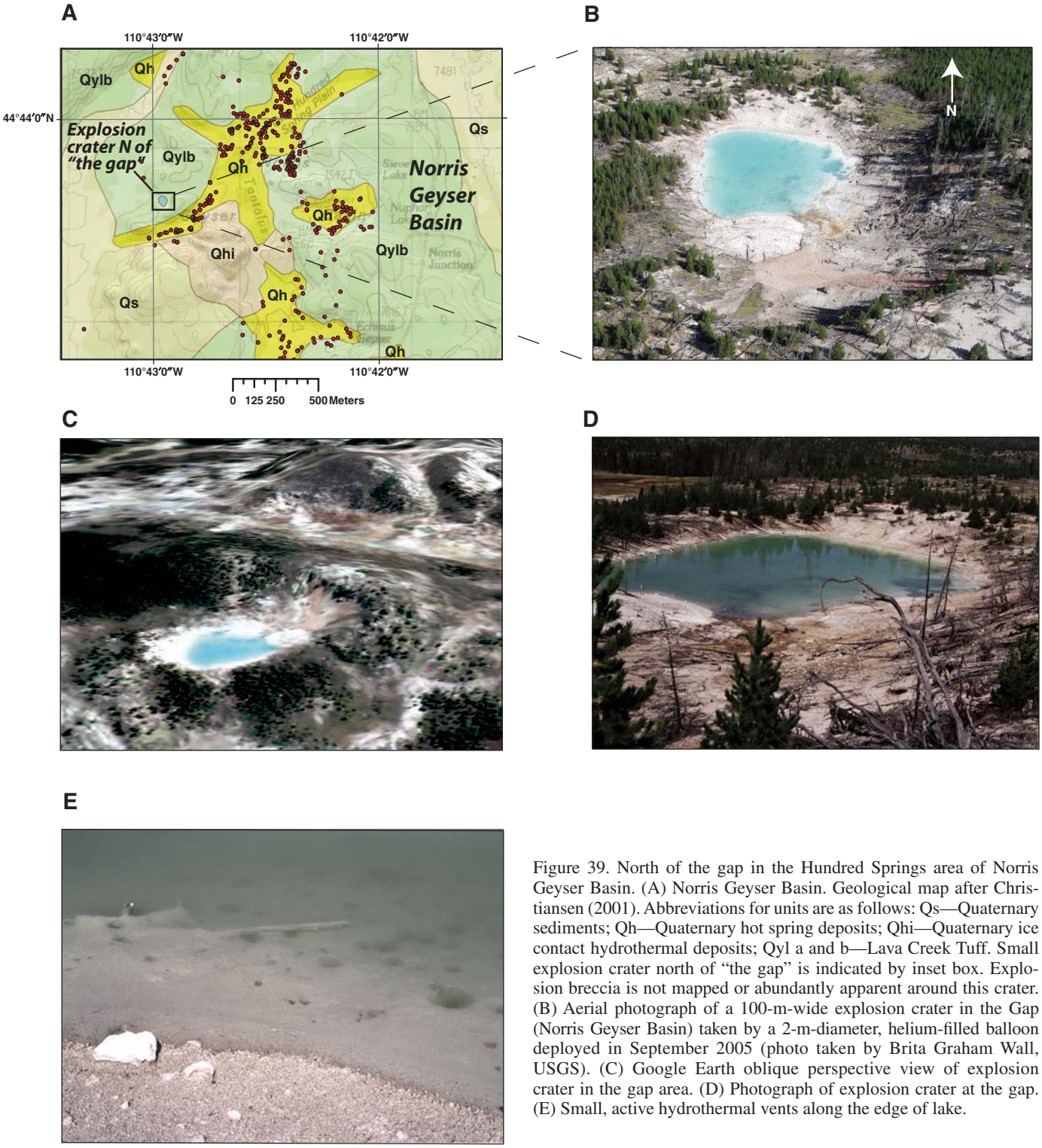

Figure 39. North of the gap in the Hundred Springs area of Norris Geyser Basin. (A) Norris Geyser Basin. Geological map after Christiansen (2001). Abbreviations for units are as follows: Qs—Quaternary sediments; Qh—Quaternary hot spring deposits; Qhi—Quaternary ice contact hydrothermal deposits; Qyl a and b—Lava Creek Tuff. Small explosion crater north of "the gap" is indicated by inset box. Explosion breccia is not mapped or abundantly apparent around this crater. (B) Aerial photograph of a 100-m-wide explosion crater in the Gap (Norris Geyser Basin) taken by a 2-m-diameter, helium-filled balloon deployed in September 2005 (photo taken by Brita Graham Wall, USGS). (C) Google Earth oblique perspective view of explosion crater in the gap area. (D) Photograph of explosion crater at the gap. (E) Small, active hydrothermal vents along the edge of lake.

and from smaller historic events that were witnessed and, in some cases, studied before and after explosion.

The Mary Bay hydrothermal explosion: An extreme event. The Mary Bay event, which produced the largest known hydrothermal explosion crater in the world (Browne and Lawless, 2001), occurred at ~13 ka, shortly after the last glacial ice receded from the central basin of Yellowstone Lake at 16 ka (Pierce, 2004). The diameter and ejecta volume of the Mary Bay crater are approximately an order of magnitude greater than documented for other similar events (Table 1). Paleoshorelines indicate that lake level at the time of the Mary Bay event was ~17 m above the present lake level (Pierce et al., 2002a, 2007a). Consequently, the top of the hydrothermal system responsible for crater formation of the crater must have been submerged beneath at least 30 m of water.

Several factors may have combined to contribute to and eventually trigger the cataclysmic Mary Bay explosion. Prior to the cataclysmic explosion, the setting at Mary Bay area was (1) dominated by extremely high heat flow, (2) had been repeatedly subjected to inflation and deflation of the Yellowstone caldera, and (3) had an active well-developed sublacustrine hydrothermal system with significant alteration and vein formation. Superimposed on this active system, a significant seismic event related to formation of the sublacustrine Lake Hotel graben less than 6 km to the west may have helped trigger the explosion. The seismic event also may have generated a large wave due to lake-bottom displacement.

Recent deformation associated with ongoing geologic evolution of the Yellowstone caldera has been significant as indicated by deformed terraces around Yellowstone Lake (Locke and Meyer, 1994; Meyer and Locke, 1986; Pierce et al., 2002a), changes in gradient along the Yellowstone River, and uplift (Fig. 1) of Elephant Back Mountain (Dzurisin and others; 1994; Wicks et al., 1998). North-trending extensional structures also are numerous in the northern basin of Yellowstone Lake as indicated by joints documented in Mary Bay, north-northeast–trending vent-dominated fissure west of Stevenson Island, northwest-trending vent-dominated fissures east of Stevenson island, the young, north-trending Fishing Bridge fault (Pierce et al., 2007a) (Fig. 8B), and the active north-trending Lake Hotel graben (Fig. 7) (Morgan et al., 2003). Structures west of Stevenson Island, described as fissures by Johnson et al. (2003), are linear, open fractures or dilational faults (Ferrill et al., 2004) that cut sediments on the lake floor; the walls of these structures are coated by ferromanganese stains suggestive of active fluid circulation. The Lake Hotel graben, fractures west of Stevenson Island, and north-trending faults south of Rock Point are all active structural components of the Eagle Bay fault zone. Recent activity along these structures is indicated by displacement of surficial lake-bottom sediment.

Seismic reflection data and stratigraphic interpretation indicate that the Lake Hotel graben is young and still active; three major seismic events have contributed to its formation (Johnson et al., 2003). The initial event at ~12–15 ka resulted in a total displacement of ~95 cm. Based on this estimated displacement age and proximity of the associated graben to Mary Bay (~6 km), we infer that seismic activity associated with initiation of the Lake Hotel graben may have been at ~13 ka, roughly coincident with the Mary Bay hydrothermal explosion. The seismic energy and water displacement related to the fault movement may have worked separately or in tandem to trigger the Mary Bay hydrothermal explosion.

Given the 5-km-thick seismogenic crust estimated by Smith and Braile (1994) within the Yellowstone caldera and the suggested maximum length of the Eagle Bay-Lake Hotel fault zone, Johnson et al. (2003) suggested that the rupture area for a potential earthquake could be as large as 125 km^2; a rupture area that could generate an earthquake as large as M 6.5. Johnson et al. (2003) estimated that rupture of just the Lake Hotel segment of the fault zone would yield an earthquake of M 5.3.

The Lake Hotel graben forms a north-trending structure ~3.5 km in length, and ~1 km wide; the volume of the down-dropped block and spontaneously displaced water is ~2,200,000 m^3. Waves generated by the sudden lowering of the lake floor may have generated a sequence of events which led to a large hydrothermal explosion. Within 2 km, the near-shore Lake Hotel graben changes in present-day lake depth from ~60 m to <10 m at the southern edge of a rhyolite lava flow (Fig. 8B). The height of waves moving outward from the area near the Lake Hotel graben would probably have increased due to this sudden lake-floor shoaling. Formation of the graben probably produced a tsunami-like wave at 13 ka that would have washed back and forth across shallow lake bottom up to 2 km inland from the present shoreline, swished sand in traction, and eventually deposited sand with sheet-like bedding. As observed in tsunamis elsewhere, water withdrawal on the trough side of the wave would contribute to suddenly reducing the hydrostatic pressure on the thermal area at Mary Bay. If the thermal system was at the pressure boiling point, the thermal fluids would flash to steam, resulting in a hydrothermal explosion at Mary Bay. The margin of error on the estimated time line for the seismic event is much larger than that for the radiocarbon date.

Graben formation followed by a slight decrease in lake level probably caused a sudden pressure reduction above the hot and venting hydrothermal system in Mary Bay. This slight but critical reduction may have initiated a catastrophic hydrothermal explosion. It should be noted that whereas the amount of displaced water amounts to only about a 7 cm decrease in lake level if distributed over the entire lake surface, the sudden wave produced by the displacement is what might be significant rather than the amount of lake level drop. Waves have been noted in lakes in New Zealand with sublacustrine hydrothermal systems; it is suspected that some waves are hydrothermal explosions occurring on the lake floor while others may be caused by a fissure opening and closing in the lake bed due to earth movements (Ron Kearn, written commun., 2005).

Detailed stratigraphic studies of the Mary Bay explosion breccia deposit indicate that a wave deposited a sand unit tens

of cm thick immediately below the Mary Bay explosion breccia deposit. The conformable contact has no soils, ashes, other deposits, or evidence of any erosion. A second similar event is indicated by a thinner sand deposit beneath an upper second explosion breccia deposit. A 20–32-cm-thick discontinuous sequence of gray laminated lake sediments separates the two deposits; based on the lamina, the time represented may be decades to a few centuries. In this case, the occurrence of multiple sand units could be related to multiple explosion events.

Ground shaking associated with the first explosive event is indicated by multiple normal faults with displacements less than 5–10 cm, which cut the lower wave-generated sand deposit (Morgan et al., 2002). Hydrothermal explosion models proposed by Smith and McKibbin (2000) and Browne and Lawless (2001) (Fig. 3) and witnessed explosion events suggest that hydrothermal crater formation may involve more than one explosion and that explosions may continue for minutes, hours, or days following the initial event. Faults preserved in wave-generated sand, breccia-filled fractures exposed along wave-cut benches and the inferred Mary Bay crater wall (Figs. 16 and 19), and multiple emplacement units of the Mary Bay breccia deposit suggest continued ground shaking and explosive activity associated with the Mary Bay event. A volume of >0.03 km^3 of material is estimated as having been ejected during the Mary Bay event after the initial explosion (Fig. 7). Proximal to its source, the Mary Bay deposit is a very poorly sorted, matrix-supported breccia. Its distal exposures, however, include an exposure along the bluffs at Pelican Creek where the flow deposit is separated into discrete internal units; the upper breccia deposit is clast-supported, indicative of a lower energy emplacement regime, whereas the underlying unit is a vesiculated mudflow, which may represent a steam-rich, mud-rich fraction of the original hydrothermal explosion breccia (Fig. 17, site 1).

Energy Considerations for Large Hydrothermal Explosions in Yellowstone

If all the thermal energy released in a hydrothermal explosion were converted to kinetic energy, then ejecta from hydrothermal explosions might achieve velocities up to 670 m/s; however, other geologic influences probably limit velocities to about <200–400 m/s (Mastin, 1995, 2001). Initial energy releases involve decompression; Mastin (1995) assumes decompression occurs adiabatically and isentropically.

Ballistic trajectories can be calculated for various fragment sizes, initial velocity, ejection angle, topography, wind, temperature, and elevation using the principles and the program EJECT developed by Mastin (2001). Using observed fragment sizes and distributions of fragments in the Mary Bay explosion breccia deposits, EJECT was used to simulate ballistic processes. Along the bluffs on the northern shore of Yellowstone Lake 1100–1350 m from the center of the Mary Bay crater, maximum fragment sizes are ~2 m. Assuming an initial velocity of 200 m/s, 2-m rounded fragments ejected at an angle around 80° from horizontal, with no tail wind would travel ~1350 m (horizontal distance) from source in ~40 s of flight. These fragments would reach a calculated height of 2000 m and would impact at 195 m/s (435 mph). Ejection angle seems to be the critical variable in the calculations. Two-m fragments ejected at an angle of 45° travel nearly 4 km and reach a height of 1 km. Fragments this size, however, 4 km from the Mary Bay crater are unknown. Consequently most fragments ejected during explosions follow trajectories between 45° and near-vertical. Steep ejection angles are also consistent with the nature of the deposit: thick debris ramparts near crater rims and thinner, sheetlike deposits further away (Fig. 7).

Tail winds also can have a significant effect on fragment distributions and can produce an asymmetrically distributed deposit, characteristic of many of the explosion breccia deposits. For example, for 2-m fragments ejected at an 80° angle, a 10 m/s (22.4 mph) tail wind increases fragment travel distance ~300 m, to 1650 m. Smaller particles which travel shorter distances are even more strongly affected by wind. For example, calculations indicate that 10-cm fragments travel ~680 m with no tail wind, 985 m with a 10 m/s tail wind, and 1290 m with a 20 m/s (~45 mph) tail wind. One-cm particles travel only 90 m with no wind; with strong (20 m/s) tail winds, 1-cm-diam particles travel ~350 m. Both the Mary Bay and Indian Pond explosion deposits are asymmetrically distributed, perhaps a consequence of wind having been an important factor. EJECT is not designed for hydrothermal explosions that occur beneath lakes, but perhaps after the explosion starts, water above the crater ceases to be a factor and explosions proceed as if subaerial. However, sublacustrine settings do appear to strongly affect the distribution of near-crater fall-back material; debris aprons are poorly developed around subaqueous craters.

The distribution of deposits presumed to be from Elliott's crater on the floor of Yellowstone Lake (Figs. 7 and 8B) seem to be strongly asymmetric (Johnson et al., 2003). These deposits extend ~3 km south-southeast from the crater center (Fig. 7). Calculations made using EJECT (Mastin, 2001) suggest that a shallow ejection angle would be necessary to produce such a distribution of explosion breccia. The crater also is somewhat asymmetric in a south-southeast direction, which may indicate a south-southeast–oriented force.

Recent Hydrothermal Explosions: Examples of Smaller Events in Yellowstone

Recent smaller hydrothermal explosion events are instructive in understanding the large prehistoric explosion events. A spectrum of recent events ranging from new geysers to violent geyser eruptions to small hydrothermal explosions have been described first-hand in recent and historic times. An excellent example of a historic hydrothermal explosion is Excelsior Geyser in Midway Geyser Basin, which occupies a crater that is 45–75-m wide and 107-m long, and has near-vertical 4-m-high walls composed of layered sinter. This crater tripled its size during hydrothermal explosions in 1878 and 1881 and produced a rim deposit 1- to 2-m high. Hot water erupted upwards to ~100 m

as a muddy geyser that engulfed the full area of the craters; rock fragments weighing up to 20 kg also were ejected (Marler and White, 1975). No evidence exists today of the explosion debris ejected from Excelsior nearly 120 yr ago. Currently, Excelsior is a boiling pool that last erupted as an 8–25-m-high geyser in 1985 (Fournier et al., 1994a).

Another example is a fairly large recent explosion crater of unknown age that formed near the gap in the Back Basin of Norris Geyser Basin (Figs. 39). A lake now occupies this young large hydrothermal explosion crater. The crater is rimmed by steep, inward-dipping slopes that are breached on the western side of the lake. The lake is hot (39 °C), acidic (pH = 1.6), and ~4- to 5-m deep (sampled on Sept. 9, 2002; Gemery-Hill et al., 2007); the bottom is covered by a gelatinous, tan-yellow, fine-grained sediment. A brief description of the related breccia deposits is included in White et al. (1988); they refer to the deposits as not abundant and ranging from scattered fragments to deposits <3 m thick. Dense woods on the crater rim now largely conceal deposits of the crater rim.

Biscuit Basin, on the north margin of Upper Geyser Basin along Firehole River (Fig. 1), contains several small (15–30 m diameter) thermal pools that formed by hydrothermal explosions in 1925, 1931, and 1932. One of these, Sapphire Geyser, exploded violently 4 days after the M 7.5 Hebgen Lake earthquake in 1959, enlarging its pool and ejecting a surge of hot water and large ejecta blocks (Fournier et al., 1994a). Between 2006 and 2008, at least three small hydrothermal explosions or "forceful eruptions" of Wall Pool occurred and included the explosion of very hot water mixed with darker debris. On July 24, 2008, another pool, Black Diamond, experienced a "forceful eruption" which witnesses described as starting with a loud noise and had an eruption lasting 5–10 s that produced a water column 7–8 m high. The erupted water was described as very black containing apparent mud and gravel. The pool changed from being semiclear prior to the eruption to being very milky, opaque, and discolored after erupting. Black Diamond hosted forceful geyser eruptions also in 2006, 2007, and 2009 (Henry Heasler, 2009, personal commun.). A forceful eruption of Black Diamond on May 17, 2009, observed by a group of scientists, was a violent geyser eruption where water, black mud, and rocks were ejected in a 12–15 m high column, but there was no apparent enlargement of the existing crater. Witnesses described the event as sudden and without precursory signals. The event consisted of a sudden, loud thump followed by four pulses over about 10 s (Wade Johnson, 2009, personal commun.). Rock fragments comprised 10% of total ejecta; maximum size fragments were ~20–25 cm.

More recently, "forceful venting" has been described in the upper Pelican Valley (Astringent Creek area) in August 2008 (Heasler et al., 2008) and "forceful eruptions" have occurred in the Bechler area in southwest YNP (Ferris Fork Hot Springs) in September 2008 (Heasler and Jaworowski, 2008). In the recent case of Astringent Creek, forceful venting in an active hydrothermal area resulted in the formation of two small vents and dusting of fine-grained material. At Ferris Fork Hot Springs, a "blowout" measuring ~1.2 m in diameter and 1.2 m in depth formed sometime between September 21–23, 2008.

The small hydrothermal explosion of Porkchop Geyser in September 1989 (Fig. 40) is particularly instructive because of the long program of monitoring, sampling, and analyses that were conducted during the 30 yr preceding the explosive event (Fournier et al., 1991). Porkchop has been studied periodically since the mid-1920s (Allen and Day, 1935) and was carefully documented from 1960 until present (Hutchinson et al., 1990; Fournier et al., 1991; Ball et al., 2001; Gemery-Hill et al., 2007). From 1960 to 1971 Porkchop was a quiescent, gently overflowing thermal pool, but in late 1971 it began to produce infrequent geyser eruptions. By 1985, Porkchop had gone from a 2.5- to 3.0-cm triangular vent in 1984 to a perpetual spouter (Fig. 40). In 1989 geyser height increased from 6–9 m to 20–30 m just prior to the hydrothermal explosion that occurred on September 5. The explosion, which was observed by eight YNP visitors, ejected sinter blocks nearly 2 m long and produced a crater roughly 12 m × 14 m. Ejected fragments traveled a maximum horizontal distance of 66 m (Fournier et al., 1991).

Several features of the Porkchop explosion are pertinent: (1) geysering activity at this site increased significantly over nearly 2 decades preceding the explosion; (2) fluid-chemical geothermometer temperatures increased for several years prior to the explosion event (Fig. 41A); (3) the explosion crater formed is many times larger than the surface expression of the geyser prior to explosion (Fig. 41B), which indicates a broader area of near subsurface fluid flow connectivity; (4) the presumed triggering mechanism was a relatively subtle event related to the annual fall water table level decrease, which is often associated with increased Norris Geyser Basin hot spring activity (Fournier et al., 2002); and (5) the most recent geothermometer calculations (Fig. 41A) indicate less variable and lower maximum temperatures than those prevailing just before the explosion.

Calculated subsurface temperatures documented by Fournier et al. (1991) are unique in providing a time-series characterized by increasing enthalpy with time at the Porkchop vent. Fluid-chemical geothermometry indicates that subsurface temperatures increased from 215 to 240 °C in 1960–1962 and 275–310 °C in 1989. This temperature increase could reflect tapping a hotter fluid reservoir or a variation in the mixing ratio between two reservoirs with different temperature but similar chemistry. More importantly, Fournier et al. (1991) established a temporal relationship between the explosion and periodic water-table decline, which causes increased steam production, sharply reduced pH, and onset of geysering in some hot springs. Consequently, these data suggest that careful monitoring of geyser or hot spring fluid geochemistry and chemical geothermometry may enable predicting the onset of hydrothermal explosions.

Porkchop was in an active and energetic perpetual spouter stage, which suggests that hydrothermal systems need not be completely sealed, but just constricted, to produce an explosion. In the case of Porkchop, only a minor system perturbation was required to trigger a significant explosion.

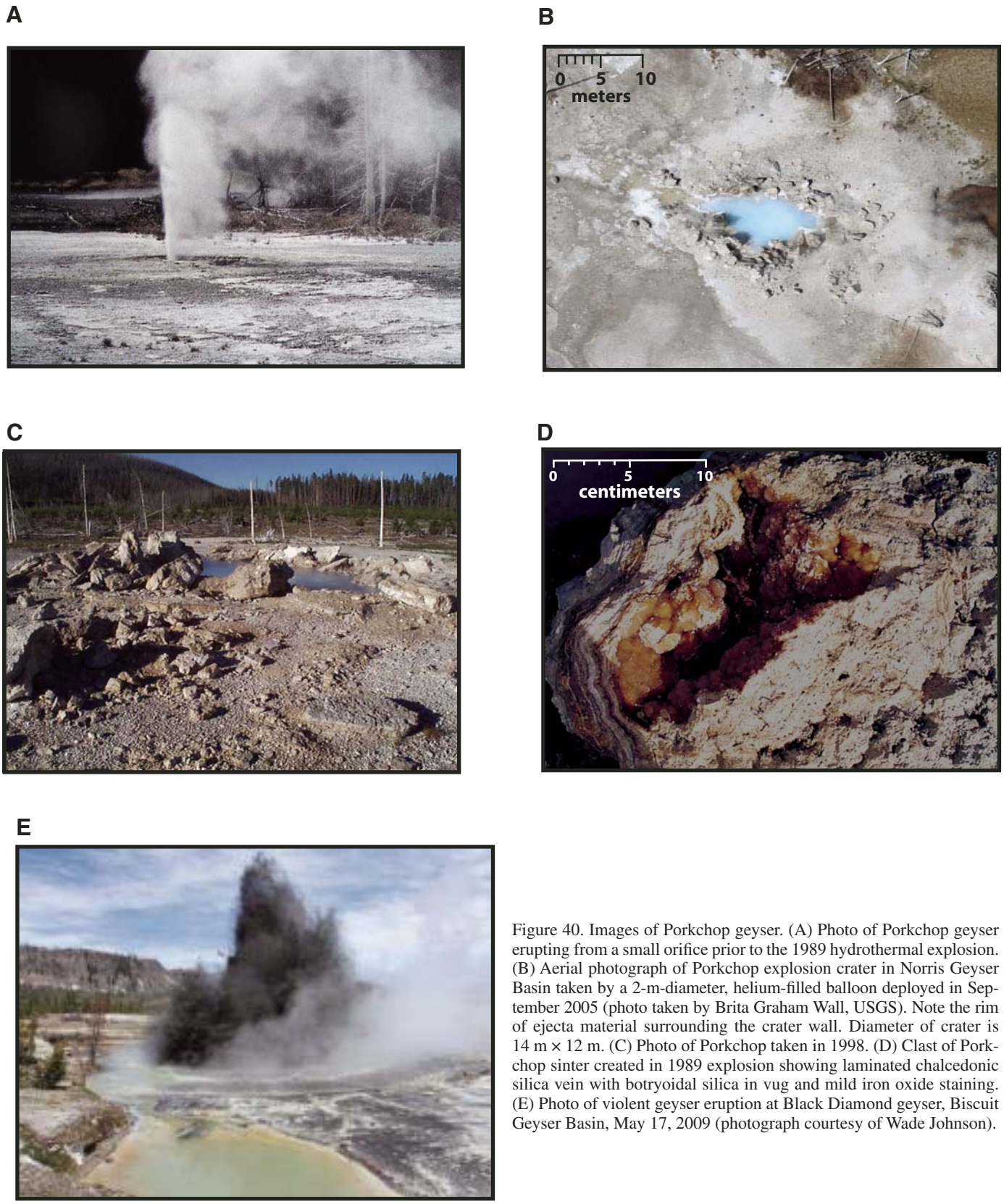

Figure 40. Images of Porkchop geyser. (A) Photo of Porkchop geyser erupting from a small orifice prior to the 1989 hydrothermal explosion. (B) Aerial photograph of Porkchop explosion crater in Norris Geyser Basin taken by a 2-m-diameter, helium-filled balloon deployed in September 2005 (photo taken by Brita Graham Wall, USGS). Note the rim of ejecta material surrounding the crater wall. Diameter of crater is 14 m × 12 m. (C) Photo of Porkchop taken in 1998. (D) Clast of Porkchop sinter created in 1989 explosion showing laminated chalcedonic silica vein with botryoidal silica in vug and mild iron oxide staining. (E) Photo of violent geyser eruption at Black Diamond geyser, Biscuit Geyser Basin, May 17, 2009 (photograph courtesy of Wade Johnson).

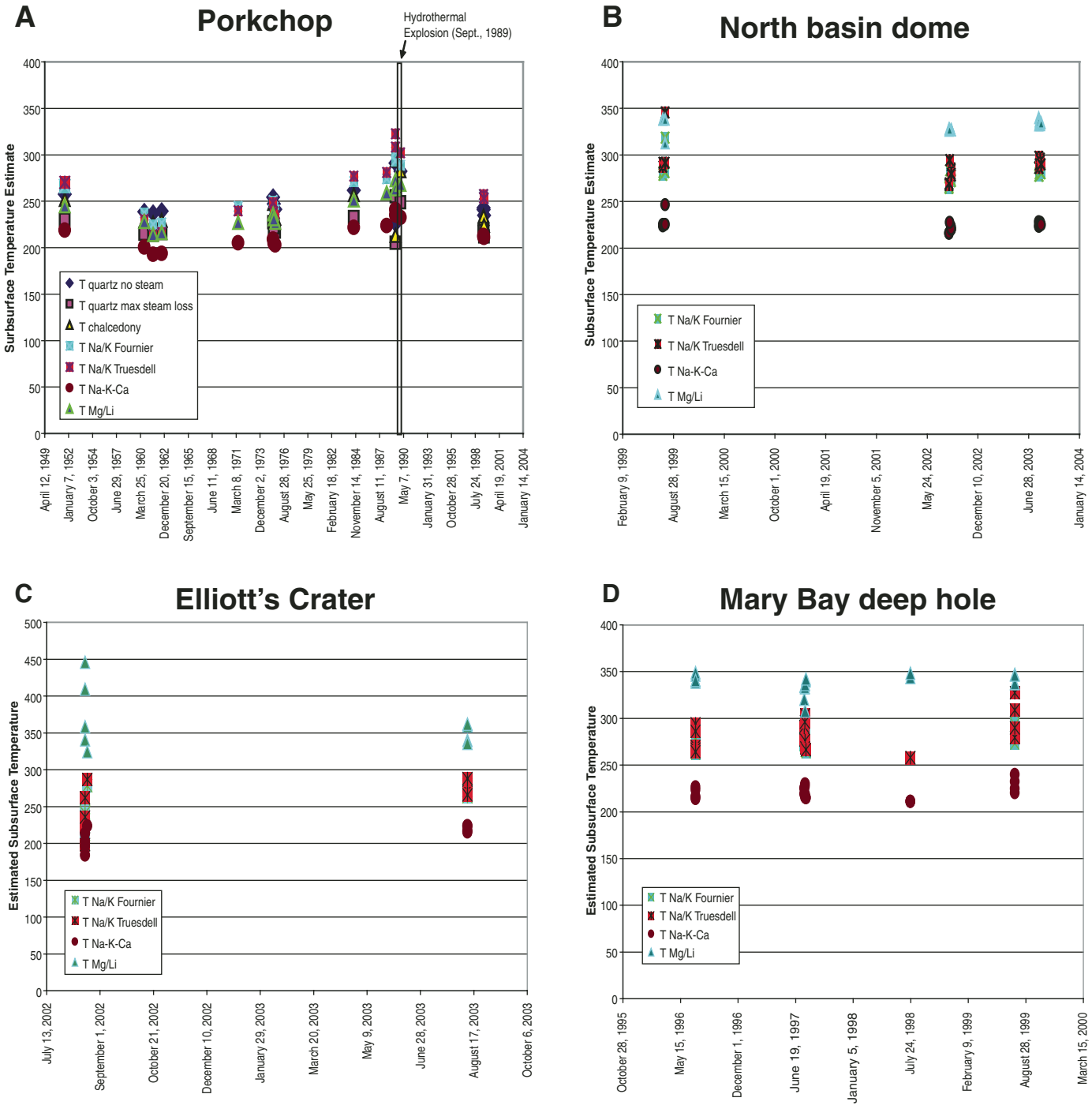

Figure 41. Fluid chemical geothermometer estimates for various thermal areas and vents in Yellowstone National Park. (A) Porkchop Geyser in Norris Geyser Basin, showing a sharp increase in estimated subsurface fluid temperatures just before the 1989 hydrothermal explosion that enlarged the geyser orifice to a 4-m-diam pool (Fournier et al., 1991). (B) North Basin hydrothermal dome from the northern basin of Yellowstone Lake, showing steady estimated temperatures since 1999. (C) Elliott's crater in the northern basin of Yellowstone Lake, showing steady estimated temperatures since 2002. (D) Deep active hydrothermal vent in Mary Bay explosion crater in the northern basin of Yellowstone Lake, showing steady estimated temperatures since 1996.

Potential Hazards Associated with Hydrothermal Explosions in Yellowstone

Considering the frequency, lack of obvious precursory manifestations, and mix of boiling water, steam, mud, and large rock fragments, hydrothermal explosions constitute a significant potential hazard to visitors and facilities in Yellowstone. Earthquakes, active deformation of the Yellowstone caldera, high heat flow, extensive and active thermal geyser basins, sudden lake or hydrothermal reservoir level changes, sustained climate changes, and generation of large waves, collapse craters, and landslides are important factors which may contribute to the initiation of hydrothermal explosions. Compared to the smaller counterparts with craters up to 10 m in diameter, large hydrothermal explosions constitute a greater potential hazard because the area affected is significantly larger (up to hundreds to over 1000 m in diameter), they can produce extremely large deep craters and involve ejection of large volumes of potentially hot ejecta. In addition, ejected material associated with large events may fall some distance from source thereby impacting a greater area. Finally, hydrothermal explosions may be associated with other hazardous events including earthquakes, landslides, flood events due to sudden lake drainage, and large waves.

Although magma at Yellowstone is at relatively shallow depths, large hydrothermal explosions are not directly associated with volcanic activity. Inflation of ~10 cm over a 3 yr period north of Norris Geyser Basin culminated in 2003 and was modeled by Wicks et al. (2006) as an intrusion of a 0.07 km^3 basaltic dike at 14-km depth. This deep intrusion contributed heat to the system and may have contributed in a general way to the development of a new north-trending linear hydrothermal field north of Norris along a preexisting fault. Inflation of 10 cm, such as at Norris, might also be the result of confined geothermal fluid inflation. Several hydrothermal explosions in New Zealand (e.g., Nairn et al., 2005), Indonesia, and Greece (Marini et al., 1993; LeGuern et al., 1982) have been associated with new intrusive and (or) extrusive activity; however, fragments ejected with these explosions are composed of relatively fresh rock derived from an area not previously subjected to hydrothermal alteration (Simmons et al., 1993). In contrast, the last volcanic event at Yellowstone occurred at ~70 ka (Obradovich, 1992, Christiansen, 2001). Much younger, nonvolcanically induced hydrothermal explosion deposits contain fragments that are extensively hydrothermally altered, which reflects existence of a preexisting hydrothermal system. The ongoing activity of hydrothermal springs and fumaroles in many of the large explosion craters suggests that these craters may pose continued potential hydrothermal explosion hazards.

Do Large Hydrothermal Domes Pose a Hazard in Yellowstone?

Large, only recently recognized, hydrothermal domes in Yellowstone are less common than large hydrothermal explosion craters (Morgan et al., 1999; Pierce et al., 2002a, 2007a; Morgan et al., 2003; Johnson et al., 2003). Hydrothermal domes appear to be structural features, whose flanks dip away from the centers and may be partially covered by caprock or have reduced permeability due to pore space sealing; caprock and (or) sealing may contribute to hydrothermal inflation and doming. These large hydrothermal domes have as much as 30–40 m of positive relief above the surrounding terrain, cover an area up to ~1 km^2, and are associated with active hydrothermal vents.

Whether hydrothermal domes in Yellowstone pose a hazard is difficult to assess because the life cycle of processes responsible for their development is not well-known; those domes that have been identified in Yellowstone appear to be stable at present. Whether development of these features represents precursors to hydrothermal explosions is not known. Hydrothermal dome formation has been proposed as a possible mechanism that allows for creation of volume in a developing massive sulfide deposit environment. Barriga and Fyfe (1988) suggest that hot, less dense ore-forming fluids may concentrate below and buoy upward a capping silica gel with a higher specific gravity. They propose the silica gel may act as an elastic barrier to rising hydrothermal fluids that become trapped below and inflate the cap rock (Barriga and Fyfe, 1988). Some hydrothermal domes could potentially evolve into explosive systems if seismic events were to result in a sudden pressure reduction due to rapid lake-level changes.

Surficial sediment samples and acoustic backscatter data suggest that much of the surface of the north basin dome is at least partially lithified due to hydrothermal mineralization. If the Porkchop model is diagnostic for explosion precursors (Fournier et al., 1994a), then sampling of hydrothermal fluids from the north basin dome and other hydrothermal areas in the park on a regular basis may help identify changes in temperature, pH, and chemistry, as well as changes in morphology. Regular geochemical fluid sampling on the lake floor and documentation of changes in vent activity requires use of a submersible ROV or autonomous underwater vehicle (AUV). Physical changes in the domal structures could be monitored by deployment of tilt meters, laser ranging devices, or by resurveying. The use of an AUV with mapping capabilities might provide data that allow detection of short-term deformation. In addition, deployment of lake-bottom seismometers might allow real-time monitoring of the hydrothermal system.

In 2004 (late August–early September), a series of seismic swarms were documented during a 2-week period; seismicity was focused less than 1 km southeast of the north basin dome where a small new hydrothermal vent had been observed with the ROV only 2 weeks earlier (Fig. 7). Seismicity also appeared to be focused near the edge of rhyolite lava flow and on a possible extension of the Lake Hotel graben. The largest seismic event had a Richter magnitude less than 2.5. Although low-magnitude seismic events are common in this part of the lake basin (Fig. 9), dozens of low-magnitude seismic events occurred during the 14-day period.

Another swarm of earthquakes in the northern basin of Yellowstone Lake occurred between December 27, 2008 and Janu-

ary 8, 2009 and was the second largest seismic swarm recorded in Yellowstone's history. Over 900 earthquakes were recorded; of these, 111 had greater than M2.0 and 18 were greater than M3.0. The largest earthquake was M3.9. Energy from all of the analyzed earthquakes for this swarm at Yellowstone Lake, referred to as the cumulative seismic moment, is equivalent to the energy of a single magnitude 4.5 earthquake (http://volcanoes.usgs.gov/yvo/publications/2009/09swarm.php). The most intense swarms occurred on December 27; at least 70 events had magnitudes between 2 and 3 whereas at least 16 events had magnitudes between 3 and 3.9. The swarms originated south and southeast of Stevenson Island in the northern basin of Yellowstone Lake and appeared to be focused parallel to and along north–northwest-trending fractures. Several of these fissures are quite prominent (Fig. 7) and are defined by the presence of dozens of active hydrothermal vents, including the deepest part of Yellowstone Lake where a 200-m-wide active hydrothermal system is located in the northern-most northwest-trending fissure at its southeast point.

Depths of earthquakes are difficult to determine but it is estimated that hypocenter depths ranged from 3 to 10 km for the 2008–2009 swarm (http://volcanoes.usgs.gov/yvo/publications/2009/09swarm.php). The earthquake hypocenters migrated and became shallower with time northward from southeast of Stevenson Island past the area of earthquake swarms in 2004 and the north basin dome, northwest toward the young Fishing Bridge fault and finally to Elephant Back Mountain. The areas of seismicity appear to be associated with areas of extension or dilation. Some visitors and employees in the vicinity reported feeling the largest of the events, but no damage was reported.

Earthquake swarms with magnitudes occasionally >4.0 are typical within the Yellowstone caldera yet none in historic time have resulted in a major activity. While the recent set of earthquake swarms in Yellowstone Lake in late 2008 to early 2009 was noteworthy, Yellowstone has experienced other similar large earthquake swarms without these events triggering either a hydrothermal explosion or volcanic activity (Lowenstern et al., 2005; http://volcanoes.usgs.gov/yvo/publications/2009/09swarm.php). A combination of three geologic factors contributes to earthquakes at Yellowstone: 1) normal faulting related to regional stress; 2) migration or introduction of magma at >7 km depth; and 3) migration of hydrothermal fluids (http://volcanoes.usgs.gov/yvo/publications/2009/09swarm.php; Waite and Smith, 2005; Pierce et al., 2007a).

Effects of Seasonal Lake Level Variations on Hydrothermal Venting in Yellowstone Lake

Yellowstone is a wet system with snowmelt providing an abundance of meteoric groundwater. Changes in climate and subsequent variations in meteoric water supply to the circulating hydrothermal systems also are important factors affecting long-term continental hydrothermal systems (Sturchio et al., 1993; Hurwitz et al., 2008) and may be important relative to the occurrence of hydrothermal explosions. Sturchio et al. (1993) found that ages of sinter deposits in Quaternary hydrothermal systems in the northern Kenya rift valley correspond with periods of higher lake levels within the rift. They concluded that an elevated water table and associated increases in available meteoric water contributed to enhanced heat transfer from deep sources to the surface.

In late September 2002, the following phenomena were observed above the north basin dome: a strong scent of H_2S, a 30–50-m-diameter plume of fine sediment in the shallow water column, and large concentrations of rising bubbles, many of them quite vigorous. These phenomena were not obvious in surveys conducted in late June and July. The fine-sediment plume, observed in the single channel echo-sound profile as an above-bottom reflector ~3 m below the lake surface originated from active hydrothermal vents on the north basin dome. In subsequent years (2003–2005), the sediment plume, gas, and bubbles were observed in late summer and early fall (Fig. 42). The timing of these events coincides with relatively rapid changes in lake level; levels are high in June and July and quickly decrease by 50 to > 100 cm in late August and September (Fig. 42).

In order to evaluate whether H_2S venting represented a substantial change in hydrothermal characteristics, fluids collected from active vents on the north basin dome from 1999, 2002, 2003, and 2004 were analyzed and compared (Figs. 41B and 43). All vent fluid samples are enriched in Cl, H_2S, and trace elements (As, B, Li, Cs, Mo, Sb, and W); however, mixing with cold, dilute, oxygenated lake water occurs just below the lake bottom and (or) as fluids vent on the lake bottom (Balistrieri et al., 2007; Shanks et al., 2005). Bulk chemistry of such rapidly evolving fluids can be normalized to Cl, which is a conservative element (does not precipitate) and can be used to account for variable dilution of individual samples. In addition, H_2S oxidation impacts vent fluid pH by creating acid, as follows:

$$H_2S(aq) + O_2(aq) = SO_4^{2-} + 2H^+ \quad (1)$$

Arrays on SO_4/Cl versus pH plot (Fig. 43) account for the bulk composition of venting fluids. Similar arrays for different north basin dome sample years (Fig. 43) suggest little or no fundamental change to the hydrothermal system between 1999 and 2004. These results are consistent with geothermometer calculations for these samples (Fig. 41B), which show no discernible subsurface temperature change.

The observed phenomena in late summer and fall seem to be associated with a drop in lake level significant enough to lower the hydrostatic head on active hydrothermal vent systems. On the north basin dome, this results in release of H_2S-rich gas bubbles and entrainment of fine-grained sediment in upwelling hydrothermal vent fluids. Field observations and annual lake level curves (Fig. 42) suggest that these seasonal phenomena are typical of this system.

At Norris Geyser Basin (White et al., 1988), Fournier et al. (2002) have documented potential causes of the long-known "annual disturbance" that commonly occurs in the fall and produces

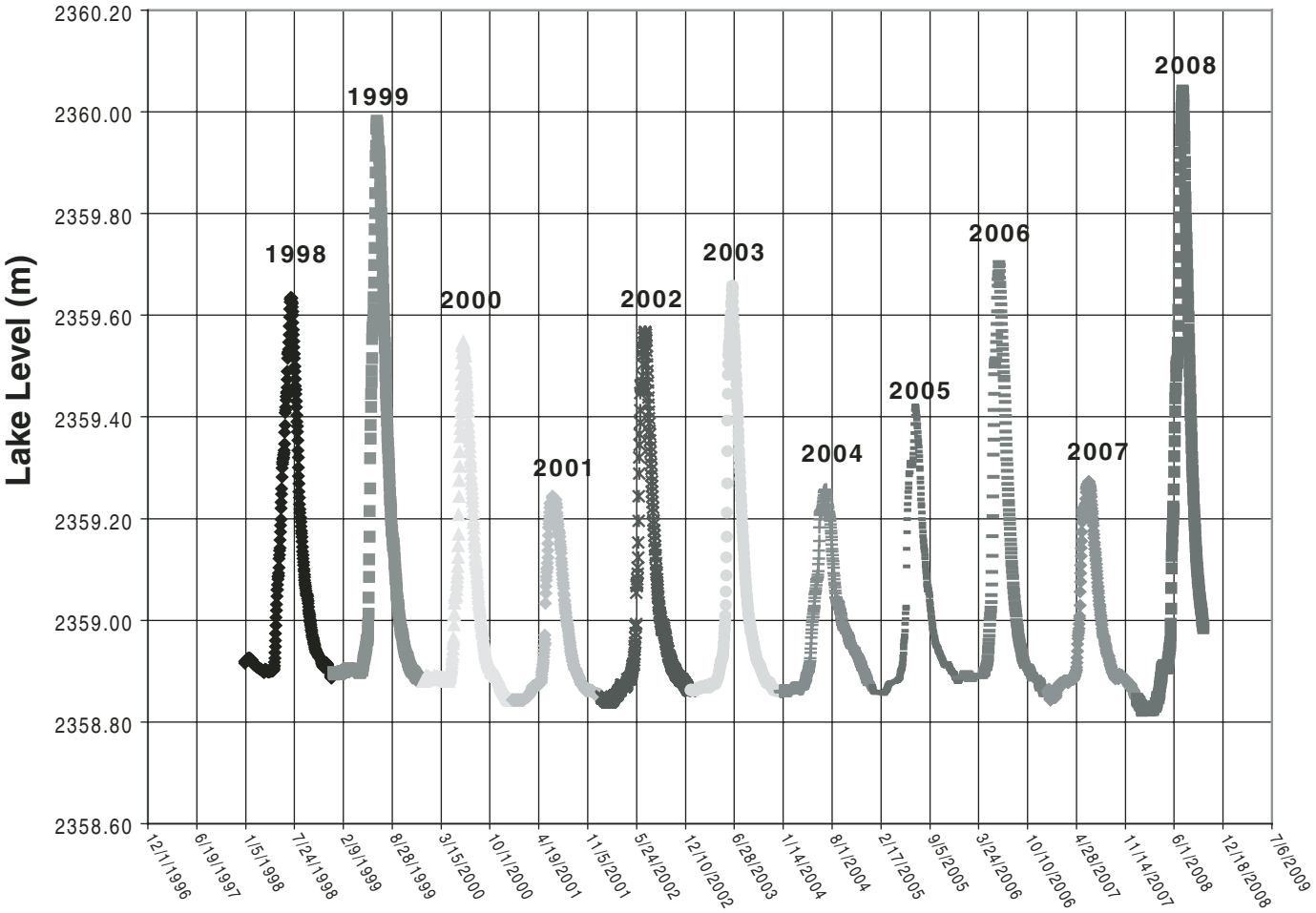

Figure 42. Yellowstone Lake level data and discharge data for the U.S. Geological Survey Fishing Bridge gauging station, downloaded from the National Water Information System (NWIS, http://nwis.waterdata.usgs.gov/wy/nwis/discharge/?site_no = 06186500), were fit to a power series regression, enabling calculation of lake level data from the daily discharge data available for the period from 1998 to 2004.

sudden changes in some thermal springs at Norris. These changes include turbid, sediment-rich fluid, sudden fluctuations in temperature and steam generation, and variations in pH, SO_4, and Cl that indicate mixing with shallow acid-sulfate waters. Fournier et al. (2002) suggest that the disturbance is due to a slight but critical drop in water table that lowers pressure sufficiently that fluids flash to steam in shallow subsurface parts of these systems. Because host rocks also are hot and do not adjust to temperature changes as rapidly as fluids, these systems fluctuate strongly and hydrothermal fluid from shallow parts of the reservoir become entrained. Turbidity is probably derived from clay minerals produced in acid-sulfate alteration zones. These conclusions, when applied to the north basin dome, imply that there may be a zone of acid sulfate water present in the shallow subsurface.

Recent research documents a strong correlation between Yellowstone Lake level variations in Yellowstone Lake and seismicity near the lake (Christiansen et al., 2005). Specifically, seismicity appears to increase and correspond with decreasing lake levels on a seasonal basis (Christiansen et al., 2005).

Role of Seismicity

Thousands of low-magnitude seismic events occur each year in Yellowstone (Fig. 9) and occasionally large events occur. No large seismic event in historic time, however, has triggered a large hydrothermal explosion. No hydrothermal explosions were associated with the 1975 M 7.5 earthquake within the northwestern part of the Yellowstone caldera (Pitt et al., 1979), the M 6.1 Hebgen earthquake in 1959 (Marler, 1964; Trimble and Smith, 1975), or the M 7.9 Borah Peak, Idaho earthquake in 1983 (Hutchinson, 1985). While these events and others (Pitt and Hutchinson, 1982) had a profound effect on the plumbing system of thermal basins and significantly affected geyser behavior and may have triggered very small explosions (e.g., Sapphire Geyser in Upper Geyser Basin [Marler, 1964; Muffler et al., 1971]), they did not result in any large-scale (>100 m diameter) hydrothermal explosions. Seismic events well away from Yellowstone also have been shown to affect the hydrothermal systems (cf., Husen et al., 2004b) but also have not triggered major hydrothermal explosions.

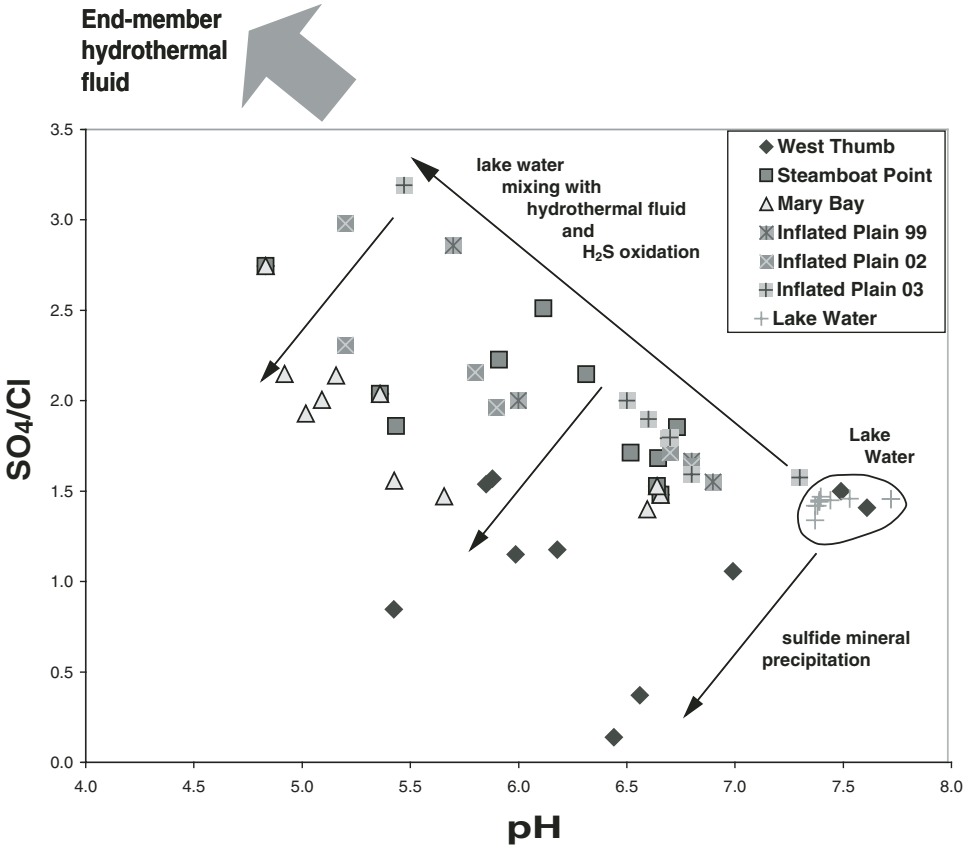

Figure 43. SO_4/Cl plotted against pH for hydrothermal fluids sampled from sublacustrine vents in Yellowstone Lake between 1996 and 2003. Fluid samples collected at the inflated plain between 1999 and 2003 show no significant change in chemistry over the 4 yr period, except that three of the 2002 samples show lower pH, perhaps due to entrainment of acid-sulfate fluids during a sublacustrine "fall disturbance."

CONCLUSIONS

The Yellowstone Plateau hosts an unparalleled large and active magmatic-hydrothermal system (Christiansen, 2001). Draped over this ever-changing landscape is a broad spectrum of structures and landforms related to the convection and circulation of fluids above an active magma reservoir (Eaton et al., 1975; Miller and Smith, 1999). The landforms and structures range from very large (more than 2.5 km in diameter) hydrothermal explosion craters and well-established thermal fields with complex histories to the most basic of hydrothermal structures such as joints, pipes, and thermal springs. The hydrothermal systems of Yellowstone (Fournier, 1989, 1999; White et al., 1988; White et al., 1971) constitute a natural laboratory to gain insights into the physical and chemical processes affecting different levels in the uppermost crust and shallowest part of an evolving caldera system (Fig. 2A).

Whereas hydrothermal explosions of the large magnitude described in this paper have not been witnessed in Yellowstone or elsewhere, geological evidence suggests: (1) that the model proposed by Smith and McKibbin (2000) and Browne and Lawless (2001) for development of hydrothermal explosions as the downward expansion of a steam front is reasonable and applies well to large Yellowstone events as identified in the stratigraphy of the deposits; (2) that at least a partial silicified cap rock included as clasts in the breccia deposit may have contributed to constriction of the hydrothermal system; (3) that hydrothermal breccia deposits contain lithic clasts reflective of the local stratigraphic section through which the explosion occurred, including lithified and silicified near-surface sediments (beach sediment, fluvial gravel, and lake sediment), and chalcedonic hydrothermal breccias of various types, and hydrothermally altered volcanic rocks from deeper in the system; (4) that depths of hydrothermal mineralization range from 180–540 m based on fluid inclusion analyses in mineralized veins in Mary Bay breccia; (5) that significant preexplosive hydrothermal activity was prevalent and well-established, as indicated by the character of breccia lithic clasts and extent of alteration of both the lithic clasts and fine-grained matrix; (6) that smaller craters nested within large explosion craters due to multiple explosions and secondary hydrothermal dissolution; and (7) that localization of large explosion craters occurs in areas that were extensively altered and fractured such as thermal geyser basins.

While hydrothermal explosions do not require either cap rock or a sealed reservoir in which pressure greatly exceeds hydrostatic (Browne and Lawless, 2001; Smith and McKibbin, 2000; McKibbin, 1990), a partial cap rock might contribute to explosions and might define conditions that "prime" an area for future explosion. An explosion will not occur unless some event reduces confining pressure and allows near-boiling fluids to flash into steam, which initiates a series of instantaneous and cascad-

ing explosions that result in the expulsion of large amounts of fractured rock, altered clay, boiling mud, water, and steam, and production of a crater. An integrated network of interconnected fractures and channelways is a necessary precondition to this type of event (Fig. 44). Factors that control the size of the eruption include the extent of existing alteration, the extent of interconnected fluid-filled voids and fractures, host rock lithology, and amount of readily available boiling water.

A major conclusion of this paper pertains to the triggering mechanism for the large, complex Mary Bay explosion that produced the largest hydrothermal explosion crater yet recognized. Approximate synchronicity of significant movement on the Lake Hotel graben, deposition of a dark, faulted sand (interpreted as a large wave deposit), and deposition of the Mary Bay hydrothermal explosion breccia suggest a genetic relationship between these events. The explosion may have been initiated by faulting caused by seismicity, a pressure drop related to passage of a large wave, or both. Bathymetric evidence from the Mary Bay crater and stratigraphic evidence from the breccia deposit suggests multiple explosive events during a relatively short period of time.

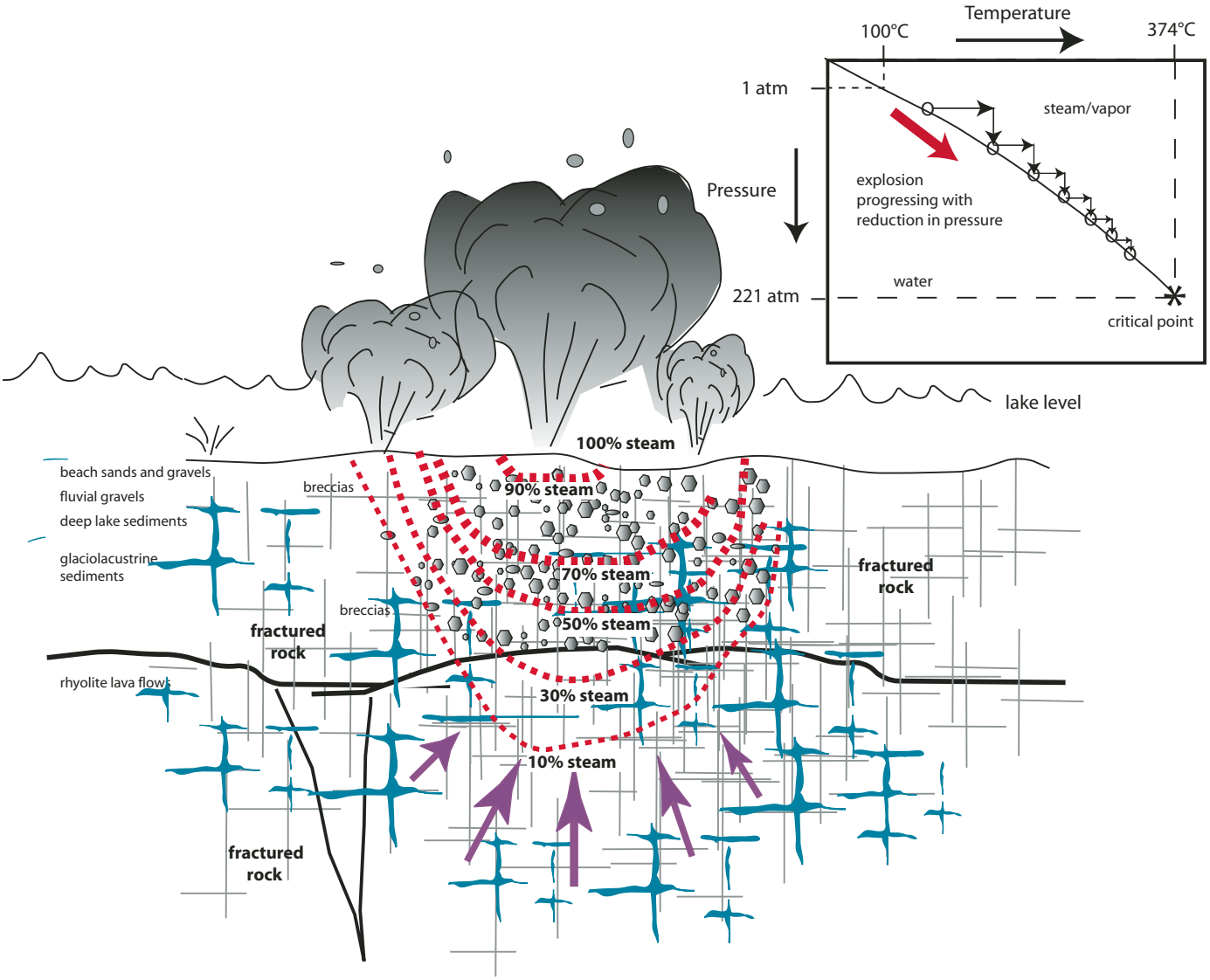

Figure 44. Schematic diagram illustrating a large hydrothermal explosion generated by a sudden pressure drop at the surface, which allows water to flash to steam. This pressure drop is transmitted downward through hydraulically connected fractures, starting a series of instantaneous and cascading explosions that result in the expulsion of large amounts of fractured rock, altered clay, boiling muds, and water and steam, and production of a large crater. As the pressure drop propagates to depth, a progressive decrease in the amount of steam is produced until, at some depth, no steam is produced. The water phase diagram (inset) shows this schematically as a series of pressure drops that shifts the fluid off the boiling curve into the steam field. This shift causes instantaneous boiling and the latent heat of vaporization causes cooling back to the two-phase boundary. The magnitude of the pressure drop relative to the boiling curve determines the percent steam produced.

Lithic clasts in the breccia deposit include lithologies from near surface and much deeper units, including a previously unknown rhyolite unit (Fig. 44). Nearly all lithic clasts are hydrothermally altered; fluid inclusion and stable isotope studies suggest conditions of ~230–300 °C at depths of 180–540 m below lake level. Complex hydrothermal breccias and veins in lithic clasts indicate a long-lived and well-developed subsurface hydrothermal system prior to explosion.

A large area of focused hydrothermal activity is currently present in the northern basin of Yellowstone Lake. Factors such as high heat flow, significant ongoing seismicity, active deformation associated with inflation/deflation of the Yellowstone caldera, an extensive system of parallel and orthogonal joints that affect permeability and fluid flow, and active fissure zones along which hydrothermal fluids circulate indicate a potential for additional, large hydrothermal explosion events in the future.

The northeast-trending Weasel Creek-Storm Point linear trend, which lies on the 450-mm contour of caldera uplift between 1927 and 1985 (Pelton and Smith, 1979, 1982; Dzurisin et al., 1994) may represent an active extensional fissure that has repeatedly cracked and opened to allow circulation of hydrothermal fluids. The Indian Pond hydrothermal explosion crater, the Storm Point hydrothermal dome, and the north basin dome are young features (<16 ka) with recently or presently active hydrothermal vents aligned along the Weasel Creek-Storm Point linear trend.

Sudden changes in Yellowstone Lake level, resulting in a small drop in pressure over an active hydrothermal feature, could occur due to seismic events and lake-bottom fault movement, which may create large "tsunami-like" waves (Morgan et al., 2003; Shanks et al., 2005, 2007). As in observed tsunamis, water withdrawal on the trough side of the wave would, in a matter of seconds, reduce the hydrostatic pressure (by perhaps 2–4 m water depth) on the thermal area beneath the present Mary Bay, where, if the thermal system was at the pressure boiling point, it would result in the thermal fluids flashing to steam and the Mary Bay hydrothermal explosion. Hydrothermal systems also may be affected by seasonal changes such as the hydrothermal disturbance that may have triggered the Porkchop explosion; similar changes also have been observed on the north basin dome in Yellowstone Lake (Fournier et al., 2002).

Similarly, active deformation, high heat flow, fractured rock, extensive and pervasive hydrothermally altered host rock, long-lived hydrothermal systems, susceptibility of hydrothermal systems to changes in water level, and recharge are all characteristics of the situation in the Norris Geyser Basin (Fournier et al., 1994a). The Norris Geyser Basin as well as the rest of YNP is being carefully monitored for changes in hydrothermal activity (Ingebritsen et al., 2001) and for potential large hydrothermal explosions by the Yellowstone Volcano Observatory (Christiansen et al., 2007; Friedman et al., 2007; Friedman and Norton, 2007; Clor et al., 2007; Lowenstern et al., 2005; Lowenstern and Hurwitz, 2008).

Radiometric dating and stratigraphic analyses of large hydrothermal explosion deposits indicate a spectrum of ages from late glacial to historic (Table 2). These ages clearly indicate that large hydrothermal explosions have been an ongoing phenomenon for the past 16 ka. For Yellowstone, our knowledge of hydrothermal craters and ejecta is generally limited to the period after the Yellowstone Plateau emerged from beneath a late Pleistocene icecap that was roughly a kilometer thick (Pierce, 1979; Good and Pierce, 1996; Licciardi and Pierce, 2007). Evidence of large explosion craters may have been removed by glacial processes; however, large explosions must have occurred earlier, and are indicated by multiple episodes of cementation and brecciation commonly observed in hydrothermal ejecta clasts. Mechanisms responsible for triggering explosion events are varied; causes range from seismic activity to sudden changes in lake levels to drought associated with changes in climate (e.g., Christiansen et al., 2005; Morgan et al., 2003, 2007a; Hurwitz et al., 2008). Large hydrothermal explosions could recur in Yellowstone.

Hydrothermal explosions generate large volumes of debris emplaced as relatively hot flow and fall deposits. Flow deposits have been found as far as 3 to 4 km from source and possible fall deposits may be exposed kilometers away. The "spray of fine material" generated in a recent phreatic eruption at Volcan Poas was recorded several kilometers from its source (Observatorio Vulcanológico y Sismológico de Costa Rica press release, Sept. 28, 2006). Large hydrothermal explosion events in Yellowstone Lake have generated large waves and associated deposits and pose yet another potential and geologically frequent hazard. Monitoring of the possible harmful effects of hydrothermal explosions is continuing.

ACKNOWLEDGMENTS

This paper benefited substantially from the previous contributions of many researchers whose investigations into the hydrothermal systems of Yellowstone provided the foundation for our current work. The body of work produced by Don White, Patrick Muffler, George Marler, Robert Fournier, Irving Friendman, and Rick (Roderick) Hutchinson is significant, and we acknowledge the impact that work has had on our studies.

The work presented in this paper was supported by many individuals. Invaluable help in the field was capably provided by Steve Harlan, Jim Maki, Brenda Bietler, Julie Friedman, Stacie Gibbons, Ulana Fuller, Charles Ginsberg, Virginia Rodriguez, Scott Brinson, Eric Walston, Bill Seyfried, Kang Ding, and Erika Thompson. Paul Doss provided areal photographs, assisted in the field, and supported all phases of our work during his tenure as supervisory geologist of YNP. We acknowledge and thank Bill McIntosh and Jack McGeehan for the radiometric analyses; Boris Schultz for his contributions to sublacustrine mapping; and Greg Lee, Laurie Morath, and Mike Webring for GIS assistance. We thank David Lovalvo of Eastern Oceanics for insightful discussions and ideas, for piloting the R/V Cutthroat and the ROV, and for the many underlake photographs, videos, and samples included in this paper. We are grateful to Ann Rodman and Carrie

Guiles at the Yellowstone Center for Resources (YNP) for GIS data on individual hydrothermal vents and thermal areas in YNP and acknowledge the significant effort required to create such a comprehensive data set. We thank Ray Watts for the LIDAR image of Storm Point; Pam Gemery-Hill, Steve Sutley, and Greg Meeker for assistance with geochemical and mineralogical studies; Eric Wienckowski for preparing the bathymetric maps of Indian Pond and Turbid, Duck, and Fern Lakes; and Isabelle Brownfield for assistance with the SEM. The authors acknowledge fruitful discussions regarding hydrothermal systems and processes with Bob Fournier, Patrick Muffler, Hank Heasler, Paul Doss, Steve Harlan, Steve Bohlen, Bob Christiansen, Jake Lowenstern, Larry Mastin, Irving Friedman, Ron Keam, Tammy Smith, Bill Seyfriend, Kang Ding, Jeff Alt, Sam Johnson, Bill Stephenson, and J. David Love. We thank individuals at YNP including John Varley, Mike Finley, Frank Walker, Suzanne Lewis, Christie Hendrix, Ann Deutche, Lloyd Kortge, Harlan Credit, Tom Oliff, Henry Heasler, Rick Fey, and Susan Ross for logistical support. The authors are grateful to the thorough reviews provided by Ed DuBray, Larry Mastin, Henry Heasler, and Elisabeth Brouwers, which greatly improved the paper. This project was funded by the U.S. Geological Survey Mineral Resources and Volcano Hazards Programs.

REFERENCES CITED

Allen, E.T., and Day, A.L., 1935, Hot springs of the Yellowstone National Park: Carnegie Institution of Washington Publication No. 466, 525 p.

Allen, R.M., Xue, M., and Hung, S., 2008, Complex geological interations in the mantel beneath western USA: Eos Transactions, American Geophysical Union, v. 89, no. 53, Fall Meeting Supplement, Abstract S31D-02.

Andre, L., Rabemanana, V., and Vuataz, F.-D., 2006, Influence of water-rock interactions on fracture permeability of the deep reservoir at Soultz-sous-Forêts, France: Geothermics, v. 35, p. 507–531, doi: 10.1016/j.geothermics.2006.09.006.

Atwater, B.F., Nelson, A.R., Clague, J.J., Carver, G.A., Yamaguchi, D.K., Bobrowsky, P.T., Bourgeois, J., Darienzo, M.E., Grant, W.C., Hemphill-Haley, E., Kelsey, H.M., Jacoby, G.C., Nishenko, A.P., Palmer, S.P., Peterson, C.D., and Reinhart, M.A., 1995, Summary of coastal geological evidence for past great earthquakes at the Cascadia subduction zone: Earthquake Spectra, v. 11, p. 1–18, doi: 10.1193/1.1585800.

Balistrieri, L.S., Shanks, W.C., III, Cuhel, R.L., Aguilar, C., and Klump, J.V., 2007, The influence of sublacustrine hydrothermal vents on the geochemistry of Yellowstone Lake, *in* Morgan, L.A., ed., Integrated geoscience studies in the greater Yellowstone area: Volcanic, tectonic, and hydrothermal processes in the Yellowstone geoecosystem: U.S. Geological Survey Professional Paper 1717, p. 169–199.

Ball, J.W., Nordstrom, D.K., Cunningham, K.M., Schoonen, M.A., Xu, Y., and DeMonge, J.M., 1998, Water-chemistry and on-site sulfur-speciation data for selected springs in Yellowstone National Park, Wyoming, 1994–1995: U.S. Geological Survey, Open-File Report 98–574, 40 p.

Ball, J.W., Nordstrom, D.K., Cunningham, K.M., Schoonen, M.A., Xu, Y., and DeMonge, J.M., 2001, Water-chemistry and on-site sulfur speciation data for selected springs in Yellowstone National Park, Wyoming, 1996–1998: U.S. Geological Survey, Open-File Report 01–49, 47 p.

Bargar, K.E., and Muffler, L.J.P., 1975, Geologic map of the travertine deposits, Mammoth Hot Springs, Yellowstone National Park, Wyoming: U.S. Geological Survey Miscellaneous Field Studies Map, MF-0659, scale 1:62,500.

Bargar, K.E., and Beeson, M.H., 1980, Hydrothermal alteration in Yellowstone geyser basins: U.S. Geological Survey Professional Paper 1175, 59 p.

Bargar, K.E., and Beeson, M.H., 1981, Hydrothermal alteration in research drill hole Y-2, Lower Geyser Basin, Yellowstone National Park, Wyoming: The American Mineralogist, v. 66, no. 5–6, p. 473–490.

Bargar, K.E., and Muffler, L.J.P., 1982, Hydrothermal alteration in research drill hole Y-11 from a vapor-dominated geothermal system at Mud Volcano, Yellowstone National Park, Wyoming, *in* Reid, S.G., and Foote, D.J., eds., Wyoming Geological Association 33rd annual field conference; Geology of the Yellowstone Park area: Mammoth Hot Springs, WY, United States: Guidebook - Wyoming Geological Association, p. 139–152.

Bargar, K.E., and Beeson, M.H., 1984, Hydrothermal alteration in research drill hole Y-6, upper Firehole River, Yellowstone National Park, Wyoming: U.S. Geological Survey Professional Paper 1054-B, p. B1–B24.

Bargar, K.E., and Beeson, M.H., 1985, Hydrothermal alteration in research drill hole Y-3, Lower Geyser Basin, Yellowstone National Park, Wyoming: U.S. Geological Survey Professional Paper 1054-C, p. C1–C23.

Barriga, F.J.A.S., and Fyfe, W.S., 1988, Giant pyretic base-metal deposits: The example of Feitais (Aljustrel, Portugal): Chemical Geology, v. 69, p. 331–343.

Bird, D.K., Schiffman, P., Elders, W.A., Williams, A.E., and McDowell, S.D., 1984, Calc-silicate mineralization in active geothermal systems: Economic Geology and the Bulletin of the Society of Economic Geologists, v. 79, p. 671–695.

Bonnichsen, B., and Kauffman, D.F., 1987, Physical features of rhyolite lava flows in the Snake River Plain volcanic province, southwestern Idaho, *in* Fink, J.H., ed., The emplacement of silicic domes and lava flows: Geological Society of America Special Paper 212, p. 119–145.

Breitzke, M., 2000, Physical properties of marine sediments, *in* Shulz, H.D., and Zabel, M., eds., Marine Geochemistry: Berlin-Heidelberg, Springer-Verlag.

Browne, P.R.L., and Lawless, J.V., 2001, Characteristics of hydrothermal eruptions, with examples from New Zealand and elsewhere: Earth-Science Reviews, v. 52, p. 299–331, doi: 10.1016/S0012-8252(00)00030-1.

Bryan, T.S., 2001, The Geysers of Yellowstone (third edition): Boulder, University Press of Colorado, 472 p.

Camp, V.E., 1995, Mid-Miocene propagation of the Yellowstone mantel plume head beneath the Columbia River Basalt source region: Geology, v. 23, p. 435–438.

Camp, V.E., and Ross, M.E., 2004, Mantle dynamics and genesis of mafic magnetism in the intermontane Pacific Northwest: Journal of Geophysical Research, v. 109, 14 p., doi: 10.1029/2003JB002838.

Chague-Goff, C., Dawson, S., Goff, J.R., Zachariasen, J., Berryman, K.R., Garnett, D.L., Waldron, H.M., and Mildenhall, D.C., 2002, A tsunami (ca. 6300 years BP) and other Holocene environmental changes, northern Hawke's Bay, New Zealand: Sedimentary Geology, v. 150, p. 89–102, doi: 10.1016/S0037-0738(01)00269-X.

Christiansen, L.B., Hurwitz, S., Saar, M.O., Ingebretsen, S.E., and Hsieh, P.A., 2005, Seasonal seismicity at western United States volcanic centers: Earth and Planetary Science Letters, v. 240, p. 307–323, doi: 10.1016/j.epsl.2005.09.012.

Christiansen, R.L., 1974, Geologic map of the West Thumb Quadrangle, Yellowstone National Park, Wyoming: U.S. Geological Survey, Geological Quadrangle Map, GQ-1191, scale 1:62,500.

Christiansen, R.L., 1975, Geologic map of the Canyon Quadrangle, Yellowstone National Park, Wyoming: U.S. Geological Survey, Geological Quadrangle Map, GQ-1192, scale 1:62,500.

Christiansen, R.L., 2001, The Quaternary and Pliocene Yellowstone Plateau Volcanic Field of Wyoming, Idaho, and Montana: U.S. Geological Survey Professional Paper, v. 729-G, 145 p.

Christiansen, R.L., and Blank, H.R., Jr., 1974, Geologic map of the Madison Junction Quadrangle, Yellowstone National Park, Wyoming: U.S. Geological Survey Geological Quadrangle Map, GQ-1190, scale 1:62,500.

Christiansen, R.L., Lowenstern, J.B., Smith, R.B., Heasler, H., Morgan, L.A., Nathenson, M., Mastin, L.G., Muffler, L.J.P., and Robinson, J.E., 2007, Preliminary assessment of volcanic and hydrothermal hazards in Yellowstone National Park and vicinity: U.S. Geological Survey Open-File Report 2007–1071.

Clayton, R.N., and Mayeda, T.K., 1963, The use of bromine pentafluoride in the extraction of oxygen from oxides and silicates for isotopic analysis: Geochimica et Cosmochimica Acta, v. 27, p. 43–52, doi: 10.1016/0016-7037(63)90071-1.

Clayton, R.N., O'Neil, J.R., and Mayeda, T.K., 1972, Oxygen isotope exchange between quartz and water: Journal of Geophysical Research, v. 77, p. 3057–3067, doi: 10.1029/JB077i017p03057.

Clingenpeel, S.R., Gorby, Y.A., Inskeep, W.P., Kahn, J.J., Lovalvo, D., Macur, R.E., Mathur, E., McDermott, T.R., Mills, K., Morgan, L.A., Nealson,

K.H., Shanks, W.C.P., and Varley, J., 2008, Yellowstone Lake: Genetic diversity in an aquatic, vent-impacted systems, *in* 2008 Yellowstone National Park NSF Research Coordinated Network and Montana State University Thermal Biology Institute Workshop on "Geothermal Biology and Geochemistry in Yellowstone National Park," p. 21.

Clor, L.E., Lowenstern, J.B., and Heasler, H.P., 2007, Systematics of water temperature and flow at Tantalus Creek during calendar year 2005, Norris Geyser Basin, Yellowstone National Park, Wyoming: U.S. Geological Survey Scientific Investigations Report 2007–5234, 17 p., http://pubs.usgs.gov/sir/2007/5234/.

Dobson, P.F., Kneafsey, T.J., Hulen, J., and Simmons, A., 2003, Porosity, permeability, and fluid flow in the Yellowstone geothermal system, Wyoming: Journal of Volcanology and Geothermal Research, v. 123, no. 3–4, p. 313–324, doi: 10.1016/S0377-0273(03)00039-8.

Dobson, P.F., Salah, S., Spycher, N., and Sonnenthal, E.L., 2004, Simulation of water-rock interaction in the Yellowstone geothermal system using TOUGHREACT: Geothermics, v. 33, no. 4, p. 493–502, doi: 10.1016/j.geothermics.2003.10.002.

Dzurisin, D., Yamashita, K.M., and Kleinman, J.W., 1994, Mechanisms of crustal uplift and subsidence at the Yellowstone caldera, Wyoming: Bulletin of Volcanology, v. 56, p. 261–270, doi: 10.1007/BF00302079.

Eaton, G.P., Christiansen, R.L., Iyer, H.M., Pitt, A.M., Mabey, D.R., Blank, H.R., Jr., Zietz, I., and Gettings, M.E., 1975, Magma beneath Yellowstone National Park: Science, v. 188, no. 4190, p. 787–796, doi: 10.1126/science.188.4190.787.

Facca, G., and Tonani, F., 1967, The self-sealing geothermal field: Bulletin of Volcanology, v. 30, p. 271–273, doi: 10.1007/BF02597674.

Ferrill, D.A., Wyrick, D.Y., Morris, A.P., Sims, D.W., and Franklin, N.M., 2004, Dilational fault slip and pit chain formation on Mars: GSA Today, v. 14, no. 10, p. 4–11, doi: 10.1130/1052-5173(2004)014<4:DFSAPC>2.0.CO;2.

Finn, C.A., and Morgan, L.A., 2002, High-resolution aeromagnetic mapping of volcanic terrain, Yellowstone National Park: Journal of Volcanology and Geothermal Research, v. 115, p. 207–231, doi: 10.1016/S0377-0273(01)00317-1.

Fournier, R.O., 1989, Geochemistry and dynamics of the Yellowstone National Park hydrothermal system: Annual Review of Earth and Planetary Sciences, v. 17, p. 13–53, doi: 10.1146/annurev.ea.17.050189.000305.

Fournier, R.O., 1999, Hydrothermal processes related to movement of fluid from plastic into brittle rock in the magmatic-epithermal environment: Economic Geology and the Bulletin of the Society of Economic Geologists, v. 94, p. 1193–1212.

Fournier, R.O., and Rowe, J.J., 1966, Estimation of underground temperatures from the silica content of water of hot springs and wet-steam wells: American Journal of Science, v. 264, p. 685–697.

Fournier, R.O., White, D.E., and Truesdell, A.H., 1976, Convective heat flow in Yellowstone National Park, *in* Second U.N. Symposium on the Development and Use of Geothermal Resources, Proceedings: Washington, D.C., U.S. Government Printing Office, v. 1, p. 731–739.

Fournier, R.O., Thompson, J.M., Cunningham, C.G., and Hutchinson, R.A., 1991, Conditions leading to a recent small hydrothermal explosion at Yellowstone National Park: Geological Society of America Bulletin, v. 103, p. 1114–1120.

Fournier, R.O., Christiansen, R.L., Hutchinson, R.A., and Pierce, K.L., 1994a, A field-trip guide to Yellowstone National Park, Wyoming, Montana, and Idaho; volcanic, hydrothermal, and glacial activity in the region: U.S. Geological Survey B 2099.

Fournier, R.O., Kennedy, B.M., Aoki, M., and Thompson, J.M., 1994b, Correlation of gold in siliceous sinters with $^{3}He/^{4}He$ in hot spring waters of Yellowstone National Park: Geochimica et Cosmochimica Acta, v. 58, no. 24, p. 5401–5419, doi: 10.1016/0016-7037(94)90238-0.

Fournier, R.O., Weltman, U., Counce, D., White, L.D., and Janik, C.J., 2002, Results of weekly chemical and isotopic monitoring of selected springs in Norris Geyser Basin, Yellowstone National Park during June-September, 1995: U.S. Geological Survey, Open-File Report 02–344, 50 p.

Friedman, I., and Norton, D.R., 2007, Is Yellowstone losing its steam?: Chloride flux out of YNP, *in* Morgan, L.A. ed., Integrated geoscience studies in the greater Yellowstone area: Volcanic, tectonic, and hydrothermal processes in the Yellowstone geoecosystem: U.S. Geological Survey Professional Paper 1717, p. 271–297.

Friedman, I., 2007, Monitoring by satellite telemetry of changes in geothermal activity at Norris Geyser Basin, Yellowstone National Park, Wyoming, *in* Morgan, L.A., ed., Integrated geoscience studies in the greater Yellowstone area: Volcanic, tectonic, and hydrothermal processes in the Yellowstone geoecosystem: U.S. Geological Survey Professional Paper 1717, p. 509–532.

Fujiwara, O., 2008, Bedforms and sedimentary structures characterizing tsunami deposits, *in* Shiki, T., Tsuji, Y., Yamazaki, T., and Minoura, K., eds., Tsunamiites: Features and implications: New York, Elsevier; p. 51–62.

Gemery-Hill, Pamela A., Shanks, Wayne C. III, Balistrieri, Laurie S., and Lee, Gregory K., 2007, Geochemical data for selected rivers, lake waters, hydrothermal vents, and subaerial geysers in Yellowstone National Park, *in* Morgan, L.A., ed., Integrated geoscience studies in the greater Yellowstone area: Volcanic, tectonic, and hydrothermal processes in the Yellowstone geoecosystem: U.S. Geological Survey Professional Paper 1717, p. 365–426.

Germanovich, L., and Astakhov, D.K., 2004, Stress-dependent permeability and fluid flow through parallel joints: Journal of Geophysical Research, v. 109, B09203, p. 1–18.

Hamilton, W.L., 1987, Water level records used to evaluate deformation within the Yellowstone Caldera, Yellowstone National Park: Journal of Volcanology and Geothermal Research, v. 31, no. 3–4, p. 205–215, doi: 10.1016/0377-0273(87)90068-0.

Hawkes, A.D., Bird, M., Cowie, S., Grundy-Warr, C., Horton, B.P., Hwai, A.T.S., Law, L., Macgregor, C., Nott, J., Ong, J.E., Rigg, J., Robinson, R., Tan-Mullins, M., Sa, T.T., Yasin, Z., and Aik, L.W., 2007, Sediments deposited by the 2004 Indian Ocean Tsunami along the Malaysia–Thailand Peninsula: Marine Geology, v. 242, p. 169–190, doi: 10.1016/j.margeo.2007.02.017.

Heasler, H., and Jaworowski, C., 2008, Preliminary analysis of hydrothermal activity at Ferris Fork Hot Springs, southwestern Yellowstone National Park: Yellowstone National Park Internal Report, 20 p.

Heasler, H., Jaworowski, C., and Foley, C., 2008, Aerial reconnaissance of a forceful hydrothermal vent, pelican Creek, Yellowstone National Park: Yellowstone National Park Internal Report, 6 p.

Hedenquist, J.W., and Henley, R.W., 1985, The importance of CO_2 on freezing point measurements of fluid inclusions: Evidence from active geothermal systems and implications for epithermal ore deposition: Economic Geology and the Bulletin of the Society of Economic Geologists, v. 80, p. 1379–1406.

Henley, R.W., Truesdell, A.H., Barton, P.B., Jr., and Whitney, J.A., 1984, Fluid-mineral equilibria in hydrothermal systems: Reviews in Economic Geology, Society of Economic Geologists, v. 1, 268 p.

Hildreth, W., 1981, Gradients in silicic magma chambers: Implications for lithospheric magmatism: Journal of Geophysical Research, v. 86, p. 10,153–10,192, doi: 10.1029/JB086iB11p10153.

Hurwitz, S., Kumar, A., Taylor, R., and Heasler, H., 2008, Climate-induced variations of geyser periodicity in Yellowstone National Park, USA: Geology, v. 36, no. 6, p. 451–454, doi: 10.1130/G24723A.1.

Husen, S., Smith, R.B., and Waite, G.P., 2004a, Evidence for gas and magmatic sources beneath the Yellowstone volcanic field from seismic tomographic imaging: Journal of Volcanology and Geothermal Research, v. 131, no. 3–4, p. 397–410, doi: 10.1016/S0377-0273(03)00416-5.

Husen, S., Taylor, R., Smith, R.B., and Heasler, H., 2004b, Changes in geyser eruption behavior and remotely triggered seismicity in Yellowstone National Park produced by the 2002 M 7.9 Denali Fault earthquake, Alaska: Geology, v. 32, no. 6, p. 537–540, doi: 10.1130/G20381.1.

Hutchinson, R.A., 1985, Hydrothermal changes in the upper Geyser Basin, Yellowstone National Park, after the1983 Borah Peak, Idaho, earthquake: U.S. Geological Survey Open-File Report 85–0290-A, p. 612–624.

Hutchinson, R.A., Fournier, R.O., and Thompson, J.M., 1990, Changes preceding the 1989 hydrothermal explosion of Porkchop Geyser, Yellowstone National Park, AGU 1990 fall meeting: Washington, American Geophysical Union, Eos, p. 1694.

Hutchinson, R., 1996, The on-going thermal evolution at Astringent Creek: Yellowstone Science, v. 4, no. 3, p. 11–13.

Ingebritsen, S.E., Galloway, D.L., Colvard, E.M., Sorey, M.L., and Mariner, R.H., 2001, Time-variation of hydrothermal discharge at selected sites in the western United States: Implications for monitoring: Journal of Volcanology and Geothermal Research, v. 111, p. 1–23, doi: 10.1016/S0377-0273(01)00207-4.

Jaworowski, C., Heasler, H.P., Hardy, C.C., and Queen, L.P., 2006, Control of hydrothermal fluids by natural fractures at Norris Geyser Basin: Yellowstone Science, v. 14, no. 4, p. 13–23.

Johnson, S.Y., Stephenson, W.J., Morgan, L.A., Shanks, W.C., III, and Pierce, K.L., 2003, Hydrothermal and tectonic activity in northern Yellowstone

Lake, Wyoming: Geological Society of America Bulletin, v. 115, no. 8, p. 954–971, doi: 10.1130/B25111.1.

Jones, B., de Ronde, C.E.J., Renault, W., and Owen, R.B., 2007, Siliceous sublacustrine spring deposits around hydrothermal vents in Lake Taupo, New Zealand: Journal of Geological Society, London, V. 164, p. 227–242.

Kaplinski, M.A., 1991, Geomorphology and geology of Yellowstone Lake, Yellowstone National Park, Wyoming [M.Sc. thesis]: Flagstaff, Arizona, Northern Arizona University, 82 p.

Keith, T.E.C., White, D.E., and Beeson, M.H., 1978, Hydrothermal alteration and self-sealing in Y-7 and Y-8 drill holes in northern part of upper Geyser Basin, Yellowstone National Park, Wyoming: U.S. Geological Survey P 1054-A.

Keith, T.E.C., and Bargar, K.E., 1993, Hydrothermal zeolite mineralization in U.S. Geological Survey research drill holes in Yellowstone National Park, Wyoming: International Conference on the Occurrence, Properties, and Utilization of Natural Zeolites, p. 132–133.

Kennedy, K.R., and Crock, J.G., 1987, Determination of mercury in geological materials by continuous-flow, cold-vapor, atomic absorption spectrophotometery: Analytical Letters, v. 20, p. 899–908.

Lamothe, P.J., Meier, A.L., and Wilson, S.A., 1999, The determination of forty-four elements in aqueous samples by inductively coupled plasma-mass spectrometry: U.S. Geological Survey Open-File Report 99–151, 14 p.

Lay, T., ed., 2009, Seismological Grand Challenges in Understanding Earth's Dynamic Systems: Report to the National Science Foundation, IRIS Consortium, 76 p.

Le Guern, F., Tazieff, H., and Pierret, R.F., 1982, An example of health hazard: People killed by gas during a phreatic eruption: Dieng Plateau (Java, Indonesia), February 20th 1979: Bulletin of Volcanology, v. 45, p. 153–157, doi: 10.1007/BF02600430.

Lehman, J.A., Smith, R.B., Schilly, M.M., and Braile, L.W., 1982, Upper crustal structure of the Yellowstone caldera from delay time analyses and gravity correlations: Journal of Geophysical Research, v. 87, p. 2713–2730, doi: 10.1029/JB087iB04p02713.

Locke, W.W., and Meyer, G.A., 1994, A 12,000 year record of vertical deformation across the Yellowstone caldera margin—The shorelines of Yellowstone Lake: Journal of Geophysical Research, v. 99, p. 20,079–20,094, doi: 10.1029/94JB00243.

Love, J.D., Good, J.M., and Browne, D.G., 2007, Lithology, fossils, and tectonic significance of Pleistocene lake deposits in and near ancestral Yellowstone Lake, *in* Morgan, L.A., ed., Integrated geoscience studies in the greater Yellowstone area: Volcanic, tectonic, and hydrothermal processes in the Yellowstone geoecosystem: U.S. Geological Survey Professional Paper 1717.

Lowenstern, J.B., Christiansen, R.L., Smith, R.B., Morgan, L.A., and Heasler, H., 2005, Steam explosions, earthquakes, and volcanic eruptions—What's in Yellowstone's future?: U.S. Geological Survey Fact Sheet 2005–3024.

Lowenstern, J.B., Smith, R.B., and Hill, D.P., 2006, Monitoring supervolcanoes: Geophysical and geochemical signals at Yellowstone and other large caldera systems: Philosophical Transactions of the Royal Society of London, Series A, v. 364, p. 2055–2072, doi: 10.1098/rsta.2006.1813.

Lowenstern, J.B., and Hurwitz, S., 2008, Monitoring a supervolcano in repose: Heat and volatile flux at the Yellowstone Caldera: Elements, v. 4, p. 35–40.

Marini, L., Principe, C., Chiodini, G., Cioni, R., Fytikas, M., and Marinelli, G., 1993, Hydrothermal eruptions of Nisyros (Dodecanese, Greece): Past events and present hazard: Journal of Volcanology and Geothermal Research, v. 56, p. 71–94, doi: 10.1016/0377-0273(93)90051-R.

Marler, G.D., 1964, Effects of the Hebgen Lake earthquake of August 17, 1959, on the hot springs of the Firehole Geyser basins, Yellowstone National Park: U.S. Geological Survey Professional Paper 0435, p. 185–197.

Marler, G.D., and White, D.E., 1975, Seismic Geyser and its bearing on the origin and evolution of geysers and hot springs of Yellowstone National Park: Geological Society of America Bulletin, v. 86, no. 6, p. 749–759, doi: 10.1130/0016-7606(1975)86<749:SGAIBO>2.0.CO;2.

Mason, B.G., Pyle, D.M., and Oppenheimer, C., 2004, The size and frequency of the largest explosive eruptions on Earth: Bulletin of Volcanology, v. 66, p. 735–748, doi: 10.1007/s00445-004-0355-9.

Mastin, L.G., 1991, The roles of magma and groundwater in the ephreatic eruptions at Inyo Crates, Long Valley Caldera, California: Bull. Volcanol., v. 53, p. 579–596.

Mastin, L.G., 1995, Thermodynamics of gas and steam-blast eruptions: Bulletin of Volcanology, v. 57, no. 2, p. 85–98.

Mastin, L., 2001, A simple calculator of ballistic trajectories for blocks ejected during volcanic eruptions: U.S. Geological Survey Open-File Report 01–45, Version 1.1, 18 p.

McIntosh, W.C., and Chamberlin, R.M., 1994, $^{40}Ar/^{39}Ar$ geochronology of Middle to Late Cenozoic ignimbrites, mafic lavas, and volcaniclastic rocks in the Quemado Region, New Mexico: New Mexico Geological Society Guidebook, v. 45, p. 165–185.

McKibbin, R., 1990, Mathematical modelling of hydrothermal eruptions, 1990 International Symposium on Geothermal Energy: Geothermal Resources Council Transactions, v. 14, pp. 1309–1316.

Meyer, G.A., 1993, Holocene and modern geomorphic response to forest fires and climate change in Yellowstone National Park [PhD dissertation]: Albuquerque, New Mexico, University of New Mexico.

Meyer, G.A., and Locke, W.W., 1986, Origin and deformation of Holocene shoreline terraces, Yellowstone Lake, Wyoming: Geology, v. 14, p. 699–702, doi: 10.1130/0091-7613(1986)14<699:OADOHS>2.0.CO;2.

Miller, D.S., and Smith, R.B., 1999, P and S velocity structure of the Yellowstone volcanic field from local earthquake and controlled-source tomography: Journal of Geophysical Research, v. 104, p. 15,105–15,121, doi: 10.1029/1998JB900095.

Morgan, L.A., Shanks, W.C., Pierce, K.L., and Rye, R.O., 1998, Hydrothermal explosion deposits in Yellowstone National Park—Links to hydrothermal processes [abs.]: Eos (Transactions, American Geophysical Union), fall annual meeting, v. 79, p. F964.

Morgan, L.A., Shanks, W.C., Lovalvo, D., Johnson, S.Y., Stephenson, W.J., Harlan, S.S., White, E.A., Waples, J., and Klump, J.V., 1999, New discoveries from the floor of Yellowstone Lake: Results from sonar imaging, seismic reflection, and magnetic surveys: Geological Society of America Abstracts with Programs, v. 31, no. 7, p. A-207.

Morgan, L.A., Shanks, W.C., III, and Pierce, K.L., 2002, Possible earthquake-generated wave deposits near Yellowstone Lake: Clues into triggering mechanisms of a large hydrothermal explosion crater: Eos (Transactions, American Geophysical Union), v. 83, no. 47, p. F1423.

Morgan, L.A., Shanks, W.C., III, Lovalvo, D.A., Johnson, S.Y., Stephenson, W.J., Pierce, K.L., Harlan, S.S., Finn, C.A., Lee, G., Webring, M., Schulze, B., Duehn, J., Sweeney, R.E., and Balistrieri, L.S., 2003, Exploration and discovery in Yellowstone Lake; results from high-resolution sonar imaging, seismic reflection profiling, and submersible studies: Journal of Volcanology and Geothermal Research, v. 122, no. 3–4, p. 221–242, doi: 10.1016/S0377-0273(02)00503-6.

Morgan, L.A., and Shanks, W.C., III, 2005, Influences of rhyolitic lava flows on hydrothermal processes in Yellowstone Lake and on the Yellowstone Plateau, *in* Inskeep, W.P., and McDermott, T.R., eds., Geothermal Biology and Geochemistry in Yellowstone National Park: Bozeman, Montana, Thermal Biology Institute, Montana State University, p. 31–52.

Morgan, L.A., Shanks, W.C., and Pierce, K.L., 2006, "Super" eruption environments make for "super" hydrothermal explosions: Extreme hydrothermal explosions in Yellowstone National Park: EOS (Transactions, American Geophysical Union) v. 87, no. 52, abstract V33C–0689.

Morgan, L.A., Shanks, W.C., Pierce, K.L., Lovalvo, D.A., Lee, G.K., Webring, M.W., Stephenson, W.J., Johnson, S.Y., Harlan, S.S., Schulze, B., and Finn, C.A., 2007a, The floor of Yellowstone Lake is anything but quiet: New discoveries from high-resolution sonar imaging, seismic reflection profiling, and submersible studies, *in* Morgan, L.A., ed., Integrated geoscience studies in the greater Yellowstone area: Volcanic, hydrothermal and tectonic processes in the Yellowstone geoecosystem: U.S. Geological Survey Professional Paper 1717, p. 91–126.

Morgan, L.A., Shanks, W.C., Lee, G., and Webring, M., 2007b, Bathymetry and geology of the floor of Yellowstone Lake, Yellowstone National Park, Wyoming, Idaho, and Montana: U.S. Geological Survey Scientific Maps Investigations Series 2973, 2 plates.

Morgan, P., Blackwell, D.D., Spafford, R.E., and Smith, R.B., 1977, Heat flow measurements in Yellowstone Lake and the thermal structure of the Yellowstone caldera: Journal of Geophysical Research, v. 82, p. 3719–3732, doi: 10.1029/JB082i026p03719.

Muffler, L.J.P., White, D.E., Truesdell, A.H., and Fournier, R.O., 1968, Violent late Pleistocene hydrothermal explosions in Yellowstone National Park (abstract): Boulder, Colorado, Geological Society of America Special Paper 115, p.158.

Muffler, L.J.P., White, D.E., and Truesdell, A.H., 1971, Hydrothermal explosion craters in Yellowstone National Park: Geological Society of America Bulletin, v. 82, p. 723–740, doi: 10.1130/0016-7606(1971)82[723:HECIYN]2.0.CO;2.

Muffler, L.J.P., White, D.E., Truesdell, A.H., and Fournier, R.O., 1982a, Geologic map of lower Geyser Basin, Yellowstone National Park, Wyoming: U.S. Geological Survey I-1373.

Muffler, L.J.P., White, D.E., Beeson, M.H., and Truesdell, A.H., 1982b, Geological map of Upper Geyser Basin, Yellowstone National Park, Wyoming: U.S. Geological Survey Miscellaneous Investigations Map I-1371, scale 1:4,800.

Nairn, I.A., Hedenquist, J.W., Villamor, Pilar, Berryman, Kelvin R., and Shane, Phil A., 2005, The ~AD1315 Tarawera and Waiotapu eruptions, New Zealand: Contemporaneous rhyolite and hydrothermal eruptions driven by an arrested basalt dike system?: Bulletin of Volcanology, v. 67, p. 186–193.

Nairn, I.A., and Wiradiradja, S., 1980, Late Quaternary hydrothermal explosion breccias at Kawerau geothermal field, New Zealand: Bulletin of Volcanologique, v. 43, no. 1, p. 1–13, doi: 10.1007/BF02597607.

Nelson, C.E., and Giles, D.L., 1985, Hydrothermal eruption mechanisms and hot spring gold deposits: Economic Geology and the Bulletin of the Society of Economic Geologists, v. 89, p. 1633–1639.

Nordstrom, D. K., Ball, J. W., and McCleskey, R. B., 2005, Ground water to surface water: Chemistry of thermal outflows in Yellowstone National Park, *in* Inskeep, W. P., and McDermott, T.R., eds., Geothermal Biology and Geochemistry in Yellowstone National Park: Bozeman, Montana, Montana State University Publications, Thermal Biology Institute, p. 73–94.

Norris, P.W., 1881, Fifth Annual Report of the Superintendent of the Yellowstone National Park: Washington, D.C., Government Printing Office.

Obradovich, J.D., 1992, Geochronology of the late Cenozoic volcanism of Yellowstone National Park and adjoining areas, Wyoming and Idaho: Open File Report 92–408, 45 p.

Observatorio Vulcanológico y Sismológico de Costa Rica, OVSICORI-UNA, 2006, New phreatic eruption from Poas Volcano: Press Bulletin, September 28.

O'Neil, J.R., Clayton, R.N., and Mayeda, T.K., 1969, Oxygen isotope fractionation in divalent metal carbonates: The Journal of Chemical Physics, v. 51, p. 5547–5558, doi: 10.1063/1.1671982.

Otis, R.M., 1975, Interpretation and digital processing of seismic reflection and refraction data from Yellowstone Lake, Wyoming [Ph.D. dissertation]: Salt Lake City, University of Utah, 223 p.

Otis, R.M., Smith, R.B., and Wold, R.J., 1977, Geophysical surveys of Yellowstone Lake, Wyoming: Journal of Geophysical Research, v. 82, p. 3705–3717, doi: 10.1029/JB082i026p03705.

Pelton, J.R., and Smith, R.B., 1979, Recent crustal uplift in Yellowstone National Park: Science, v. 206, p. 1179–1182, doi: 10.1126/science.206.4423.1179.

Pelton, J.R., and Smith, R.B., 1982, Contemporary vertical surface displacements in Yellowstone National Park: Journal of Geophysical Research, v. 87, p. 2745–2751, doi: 10.1029/JB087iB04p02745.

Pierce, K.L., 1973, Surficial geologic map of the Mammoth quadrangle and part of the Gardiner quadrangle, Yellowstone National Park, Wyoming and Montana: U.S. Geological Miscellaneous Geologic Investigations Map I-641, scale 1:62,500.

Pierce, K.L., 1979, History and dynamics of glaciation in the northern Yellowstone National Park area: U.S. Geological Survey Professional Paper 729-F, 89 p.

Pierce, K.L., 2004, Pleistocene glaciations of the Rocky Mountains, *in* Gillespie, A.R., Porter, S.C., and Atwater, B.F., eds., The Quaternary Period in the United States: Developments in Quaternary Science, v. 1: Amsterdam, Elsevier, p. 63–76.

Pierce, K.L., and Morgan, L.A., 1990, The track of the Yellowstone hotspot: Volcanism, faulting, and uplift: U.S. Geological Survey Open-File Report 90–413, 85 p.

Pierce, K.L., and Morgan, L.A., 1992, The track of the Yellowstone hot spot; volcanism, faulting, and uplift, *in* Link, P.K., Kuntz, M.A., and Platt, L.B., eds., Regional geology of eastern Idaho and western Wyoming, Geological Society of America, Memoir 179, p. 1–53.

Pierce, K.L., Adams, K.D., and Sturchio, N.C., 1991, Geologic setting of the Corwin Springs Known Geothermal Resource Area—Mammoth Hot Springs area in and adjacent to Yellowstone National Park, *in* Sorey, M.L., ed., Effects of potential geothermal development in the Corwin Springs Known Geothermal Resource Area, Montana, on the thermal features of Yellowstone national park: U.S. Geological Survey Water Resources Investigations Report 91-4052, p. C-1–C-37.

Pierce, K.L., Cannon, K.P., Meyer, G.A., Trebesch, M.J., and Watts, R., 2002a, Post-glacial inflation-deflation cycles, tilting, and faulting in the Yellowstone caldera based on Yellowstone Lake shorelines: U.S. Geological Survey Open-File Report 02–142.

Pierce, K.L., Morgan, L.A., and Saltus, R., 2002b, Yellowstone Plume Head: Postulated relations to the Vancouver slab, continental boundaries, and climate, *in* Bonnichsen, Bill, White, C.M., and McCurry, Michael, eds., Tectonic and magmatic evolution of the Snake River Plain Volcanic Province: Idaho: Geological Bulletin 30, p. 5–33.

Pierce, K.L., Despain, D.G., Whitlock, C., Cannon, K.P., Meyer, G., Morgan, L., and Licciardi, J.M., 2003, Quaternary geology and ecology of the Greater Yellowstone area, in Easterbrook, D.J., ed., Quaternary Geology of the United States: Reno, Nevada, Desert Research Institute, INQUA 2003 Field Guide Volume, p. 313–344.

Pierce, K.L., Cannon, K.P., Meyer, G.A., Trebesch, M.J., and Watts, R., 2007a, Post-glacial inflation-deflation cycles, tilting, and faulting in the Yellowstone caldera based on Yellowstone Lake shorelines, *in* Morgan, L. A., ed., Integrated geoscience studies in the greater Yellowstone area: Volcanic, hydrothermal and tectonic processes in the Yellowstone geoecosystem: U.S. Geological Survey Professional Paper 1717, p. 131–168.

Pierce, K.L., Despain, D., Morgan, L.A., and Good, J., 2007b, Effects of hotspot-related volcanism, faulting, and uplift on the greater Yellowstone ecosystem and human geography, *in* Morgan, L.A. ed., Integrated geoscience studies in the greater Yellowstone area: Volcanic, tectonic, and hydrothermal processes in the Yellowstone geoecosystem: U.S. Geological Survey Professional Paper 1717, p. 1–39.

Pitt, A.M., Weaver, C.S., and Spence, W., 1979, The Yellowstone Park earthquake of June 30, 1975: Seismological Society of America Bulletin, v. 69, p. 187–205.

Pitt, A.M., and Hutchinson, R.A., 1982, Hydrothermal changes related to earthquake activity at Mud Volcano, Yellowstone National Park, Wyoming: Journal of Geophysical Research, v. 87, p. 2762–2766, doi: 10.1029/JB087iB04p02762.

Potter, R.W., Clynne, M.A., and Brown, D.L., 1978, Freezing point depression of aqueous sodium chloride solutions: Economic Geology and the Bulletin of the Society of Economic Geologists, v. 66, p. 940–946.

Prostka, H.J., Smedes, H.W., and Christiansen, R.L., 1975, Geologic map of the Pelican Cone Quadrangle, Yellowstone National Park and vicinity, Wyoming: U.S. Geological Survey, Miscellaneous Geologic Investigations Map I-643, scale 1:62,500.

Richmond, G.M., 1973, Surficial geologic map of the West Thumb quadrangle, Yellowstone National Park, Wyoming: U.S. Geological Survey, Miscellaneous Geologic Quadrangle Map GQ-1243, scale 1:62,500.

Richmond, G.M., 1974, Surficial geologic map of the Frank Island Quadrangle, Yellowstone National Park, Wyoming: Miscellaneous Geologic Investigations Map I-0642, scale 1:62,500.

Richmond, G.M., 1976, Surficial geologic history of the Canyon Village Quadrangle, Yellowstone National Park, Wyoming: U.S. Geological Survey Bulletin 1427, 35 p, for use with map I-652.

Richmond, G.M., 1977, Surficial geologic map of the Canyon Village Quadrangle, Yellowstone National Park, Wyoming: U.S. Geological Survey Miscellaneous Geologic Investigations Map I-0652, scale 1:62,500.

Ruppel, E.T., 1972, Geology of pre-Tertiary rocks in the northern part of Yellowstone National Park, Wyoming, in Geology of Yellowstone National Park: U.S. Geological Survey Professional Paper 729-A, 66 p.

Rye, R.O., and Truesdell, A.H., 1993, The question of recharge to the geysers and hot springs of Yellowstone National Park: Open File Report 93–384, 40 p.

Shanks, W.C., III, Morgan, L.A., Balistrieri, L., and Alt, J.C., 2005, Hydrothermal vent fluids, siliceous hydrothermal deposits, and hydrothermally altered sediments in Yellowstone Lake, *in* Innskeep, W.P., and McDermott, T.R., eds., Geothermal Biology and Geochemistry in Yellowstone National Park: Bozeman, Montana, Thermal Biology Institute, p. 53–72.

Shanks, W.C., III, Alt, Jeffrey C., and Morgan, L. A., 2007, Geochemistry of sublacustrine hydrothermal deposits in Yellowstone Lake: Hydrothermal reactions, stable isotope systematics, sinter deposition, and spire growth, *in* Morgan, L.A., ed., Integrated geoscience studies in the greater Yellowstone area: Volcanic, tectonic, and hydrothermal processes in the Yellowstone geoecosystem: U.S. Geological Survey Professional Paper 1717, p. 201–234.

Shervais, J.W., and Hanan, B.B., 2008, Lithospheric topography, tilted plumes, and the track of the Snake River—Yellowstone hot spot: Tectonics, v. 27, 17 p., doi: 10.1029/2007/TC002181.

Shiki, T., Tsuji, Y., Yamazaki, T., and Minoura, K., eds., 2008, Tsunamiites: Features and implications: Amsterdam, Elsevier, 411 p.

Silberman, M.L., and Berger, B.R., 1985, Relationship of trace-element patterns to alteration and morphology of epithermal precious-metal deposits,

in Berger, B.R., and Bethke, P.M., eds., Geology and geochemistry of epithermal systems: Reviews in Economic Geology, v. 2, p. 202–232.

Sillitoe, R.H., 1985, Ore-related breccias in volcanoplutonic arcs: Economic Geology and the Bulletin of the Society of Economic Geologists, v. 80, p. 1467–1514.

Sillitoe, R.H., Baker, E.M., and Brook, W.A., 1984, Gold deposits and hydrothermal eruption breccias associated with a maar volcano at Wau, Papua New Guinea: Economic Geology and the Bulletin of the Society of Economic Geologists, v. 79, p. 655–683.

Simmons, S.F., Keywood, M., Scott, B.J., and Keam, R.F., 1993, Irreversible change of the Rotomahana-Waimangu hydrothermal system (New Zealand) as a consequence of a volcanic eruption: Geology, v. 21, p. 643–646, doi: 10.1130/0091-7613(1993)021<0643:ICOTRW>2.3.CO;2.

Smith, R.B., 1991, Earthquake and geodetic surveillance of Yellowstone: Seismological Research Letters, v. 62, p. 27.

Smith, R.B., and Braile, L.W., 1994, The Yellowstone hotspot, *in* Hill, D.P., Gasparini, P., McNutt, S., and Rymer, H., eds., Internal structure of volcanoes and geophysical precursors of eruptions: Amsterdam, Elsevier, p. 121–187.

Smith, T., and McKibbin, R., 2000, An investigation of boiling processes in hydrothermal eruptions, *in* Proceedings of the World Geothermal Congress, v. 1, Kyushu, Japan, May 28–June 10, 2000: Auckland, New Zealand, International Geothermal Association, p. 699–704.

Sorey, M.L., and Colvard, E.M., 1997, Hydrologic conditions in the Mammoth corridor, Yellowstone National Park and Vicinity, U.S.A: Geothermics, v. 26, no. 2, p. 221–249, doi: 10.1016/S0375-6505(96)00041-7.

Stanley, W.D., Hoover, D.B., Sorey, M.L., Rodriguez, B.D., and Heran, W.D., 1991, Electrical geophysical investigations in the Norris-Mammoth corridor, Yellowstone National Park, and the adjacent Corwin Springs Known Geothermal Resources Area: U.S. Geological Survey Water Resources Investigations, v. 91–4052, p. D1–D18.

Stout, R.G., and Al-Niemi, T.S., 2002, Heat-tolerant flowering plants of active geothermal areas in Yellowstone National Park: Annals of Botany, v. 90, p. 259–267, doi: 10.1093/aob/mcf174.

Stuiver, M., and Polach, H.A., 1977, Discussion reporting of ^{14}C data: Radiocarbon, v. 19, p. 355–363.

Sturchio, N.C., Muehlenbachs, K., and Seitz, M.G., 1986, Element redistribution during hydrothermal alteration of rhyolite in an active geothermal system; Yellowstone drill cores Y-7 and Y-8: Geochimica et Cosmochimica Acta, v. 50, no. 8, p. 1619–1631, doi: 10.1016/0016-7037(86)90125-0.

Sturchio, N.C., Keith, T.E.C., and Muehlenbachs, K., 1988, The dynamics of silica deposition in fractures; oxygen isotope ratios in hydrothermal silica from Yellowstone drill core Y-13: Transactions - Geothermal Resources Council, v. 12, p. 305–312.

Sturchio, N.C., Keith, T.E.C., and Muehlenbachs, K., 1990, Oxygen and carbon isotope ratios of hydrothermal minerals from Yellowstone drill cores: Journal of Volcanology and Geothermal Research, v. 40, no. 1, p. 23–37, doi: 10.1016/0377-0273(90)90104-N.

Sturchio, N.C., Dunkley, P.N., and Smith, M., 1993, Climate-driven variations in geothermal activity in the northern Kenya rift valley: Nature, v. 362, p. 233–234, doi: 10.1038/362233a0.

Sturchio, N.C., Murrell, M.T., Pierce, K.L., and Sorey, M.L., 1992, Yellowstone travertines; U-series ages and isotope ratios (C, O, Sr, U): Proceedings, International Symposium on Water Rock Interaction, v. 7, p. 1427–1430.

Sturchio, N.C., Pierce, K.L., Murrell, M.T., and Sorey, M.L., 1994, Uranium-series ages of travertines and timing of the last glaciation in the northern Yellowstone area, Wyoming-Montana: Quaternary Research (New York), v. 41, no. 3, p. 265–277.

Taggart, J.E., Jr., 2002, Analytical methods for chemical analysis of geologic and other materials: U.S. Geological Survey Open-File Report 02–223.

Thompson, J.M., and DeMonge, J.M., 1996, Chemical analyses of hot springs, pools, and geysers from Yellowstone National Park, Wyoming, and vicinity, 1980–1993: U.S. Geological Survey Open-File Report 96–0068, 66 p.

Trimble, A.B., and Smith, R.B., 1975, Seismicity and contemporary tectonics of the Hebgen Lake-Yellowstone Park region: Journal of Geophysical Research, v. 80, no. 5, p. 733–741, doi: 10.1029/JB080i005p00733.

Truesdell, A.H., Nathenson, M., and Rye, R.O., 1977, The effect of subsurface boiling and dilution on the isotopic compositions of the Yellowstone thermal waters: Journal of Geophysical Research, v. 82, p. 3694–3704, doi: 10.1029/JB082i026p03694.

U.S. Geological Survey, 1972, Geologic map of Yellowstone National Park: U.S. Geological Survey Miscellaneous Investigations Series Map I-711, scale 1:125,000.

Vikre, P.G., 1985, Precious metal vein systems in the National District, Humboldt County, Nevada: Economic Geology and the Bulletin of the Society of Economic Geologists, v. 80, p. 360–393.

Waite, G.P., and Smith, R.B., 2002, Seismic evidence for fluid migration accompanying subsidence of the Yellowstone caldera: Journal of Geophysical Research, v. 107, p. 2177, doi: 10.1029/2001JB000586.

Waite, G.P., and Smith, R.B., 2004, Seismotectonics and stress field of the Yellowstone volcanic plateau from earthquake first-motions and other indicators: Journal of Geophysical Research, v. 109, doi: 10.1029/2003JB002675.

Weed, W.H., and Pirsson, L.V., 1891, Occurrence of sulfur, orpiment, and realgar in the Yellowstone National Park: American Journal of Science, v. 42, p. 401–405.

Werner, C., Brantley, S.L., and Boomer, K., 2000, CO_2 emissions related to the Yellowstone volcanic system; 2, Statistical sampling, total degassing, and transport mechanisms: Journal of Geophysical Research, B, Solid Earth and Planets, v. 105, p. 10,831–10,846, doi: 10.1029/1999JB900331.

Werner, C., and Brantley, S., 2003, CO_2 emissions from the Yellowstone volcanic system: Geochemistry Geophysics Geosystems, v. 4, no. 7, doi: 10.1029/2002GC000473.

Werre, R.W., Bodnar, R.J., Bethke, P.M., and Barton, P.B., 1979, A novel gas-flow fluid inclusion heating/freezing stage: Geological Society of America Abstracts with Programs, v. 11, p. 539.

White, D.E., 1957, Thermal waters of volcanic origin: Geological Society of America Bulletin, v. 68, p. 1637–1658, doi: 10.1130/0016-7606(1957)68[1637:TWOVO]2.0.CO;2.

White, D.E., 1967, Some principles of geyser activity, mainly from Steamboat Springs, Nevada: American Journal of Science, v. 265, p. 641–684.

White, D.E., 1968, Hydrology, activity and heat flow of the Steamboat Springs thermal system, Washoe County, Nevada: U.S. Geological Survey Professional Paper 458-C, 109 p.

White, D.E., Muffler, L.J.P., and Truesdell, A.H., 1971, Vapor-dominated hydrothermal systems compared with hot-water systems: Economic Geology and the Bulletin of the Society of Economic Geologists, v. 66, no. 1, p. 75–97.

White, D.E., Fournier, R.O., Muffler, L.J.P., and Truesdell, A.H., 1975, Physical results of research drilling in thermal areas of Yellowstone National Park, Wyoming: U.S. Geological Survey Professional Paper 892, 70 p.

White, D.E., Hutchinson, R.A., and Keith, T.E.C., 1988, The geology and remarkable thermal activity of Norris Geyser Basin, Yellowstone National Park, Wyoming: U.S. Geological Survey Professional Paper 1456, 84 p.

White, D.E., Heropoulos, C., and Fournier, R.O., 1991, Gold and other minor elements associated with the hot springs and geysers of Yellowstone National Park, Wyoming, supplemented with data from Steamboat Springs, Nevada: U.S. Geological Survey Bulletin 2001, 19 p.

Whittlesey, L.H., 1988, Yellowstone place names: Helena, Montana Historical Society Press, 178 p.

Wicks, C.W., Jr., Thatcher, W.R., and Dzurisin, D., 1998, Migration of fluids beneath Yellowstone caldera inferred from satellite radar interferometry: Science, v. 282, no. 5388, p. 458–462, doi: 10.1126/science.282.5388.458.

Wicks, C.W., Thatcher, W., Dzurisin, D., and Svarc, J., 2006, Uplift, thermal unrest and magma intrusion at Yellowstone caldera: Nature, v. 440, p. 72–75, doi: 10.1038/nature04507.

Wold, R.J., Mayhew, M.A., and Smith, R.B., 1977, Bathymetric and geophysical evidence for a hydrothermal explosion crater in Mary Bay, Yellowstone Lake, Wyoming: Journal of Geophysical Research, v. 82, no. 26, p. 3733–3738, doi: 10.1029/JB082i026p03733.

Xu, T., and Pruess, K., 2001, On fluid flow and mineral alteration in fractured caprock of magmatic hydrothermal systems: Journal of Geophysical Research, v. 106, no. B2, p. 2121–2138, doi: 10.1029/2000JB900356.

Yellowstone National Park, 1966–1975, Low resolution bathymetric maps: Unpublished report, Yellowstone Center for Resources, Mammoth, Yellowstone National Park, Wyoming.

Yuan, H., and Dueker, K., 2005, Teleseismic P-wave tomogram of the Yellowstone plume: Geophysical Research Letters, v. 32, no. 7, p. L07304, doi: 10.1029/2004GL022056.

Manuscript Accepted by the Society 8 April 2009

Printed in the USA